PhD Thesis Entitled

Development of a New Heterogeneous Catalyst for Selective Production of 1,3-propanediol from Glycerol

Submitted in partial fulfillment of the requirements of the degree of

Doctorate of Philosophy

of the

Indian Institute of Technology Bombay, India

and

Monash University, Australia

By

MOHAMMAD KHAN SALABAT KHAN

UNDER THE GUIDANCE OF

PROF. A. K. SURESH (IIT Bombay)

PROF. S. M. MAHAJANI (IIT Bombay)

PROF. S. J. GHARPURE (IIT Bombay)

PROF. HUANTING WANG (MONASH U.)

The course of study for this award was developed jointly by

Monash University, Australia and the Indian Institute of Technology Bombay, India

and was given academic recognition by each of them.

The program was administrated by the IITB-Monash Research Academy

(Year 2021)

Dedicated to my family

Approval Sheet

The thesis entitled "Development of a New Heterogeneous Catalyst for Selective Production of 1,3-propanediol from Glycerol" by **Mohammad Khan Salabat Khan** is approved for the degree of **Doctor of Philosophy**.

(Prof. P. Selvam)
External Examiner

(Prof. Vinay A. Juvekar)
Internal Examiner

(Prof. A. K. Suresh)
IITB Supervisor

(Prof. Huanting Wang)
Monash Supervisor

(Prof. Debabrata Maiti)
Chairperson

Date: 22/12/2021

Place: Zoom

DECLARATION

I declare that this written submission represents my ideas in my own words and where others' ideas or words have been included, I have adequately cited and referenced the original sources. I also declare that I have adhered to all principles of academic honesty and integrity and have not misrepresented or fabricated or falsified any idea/data/fact/source in my submission. I understand that any violation of the above will be cause for disciplinary action by the Institute and can also evoke penal action from the sources which have thus not been properly cited or from whom proper permission has not been taken when needed.

Notice 1

Notice 2

Mohammad Khan

IITB ID: 144024004

Monash ID: 26857081

Abstract

As a renewable, bio-based alternative to fossil fuels in meeting the emerging energy demands in the world, biodiesel is expected to increase in importance in the coming years. During biodiesel synthesis, glycerol (1,2,3-propanetriol) forms as a by-product with an approximate yield of 10 wt%. It is reported that about 62% (≈2/3rd) of the world's glycerol supply comes from the biodiesel industry, the rest mostly coming from the oleochemical industry. This surplus supply of glycerol has considerably reduced the price of glycerol, and it is necessary to valorize glycerol for the sustainability of oleochemical and biodiesel industries. In this context, this thesis is concerned with the possible conversion of glycerol to 1,3-propanediol (1,3-PDO) by hydrogenolysis. 1,3-PDO is widely used in synthesizing poly-trimethylene terephthalate (PTT), a biodegradable polymer with several applications due to its unique features. It is reported that nearly 90% of 1,3-PDO is consumed in the making of PTT. The demand for 1,3-PDO is increasing rapidly and nearing 100 million pounds (£) annually. Selective synthesis of 1,3-PDO from glycerol suffers from low rate and low selectivity due to the difference in the reactivities of terminal and central hydroxyl groups of glycerol. This work studied the hydrogenolysis of glycerol to 1,3-PDO over a newly designed heteropolyacid promoted Pt-β-zeolite catalyst.

The thesis is broadly divided into two parts; the first part focuses on the catalysts reported in the literature for glycerol hydrogenolysis, attempting to understand the critical features of a catalyst in the selective conversion of glycerol to 1,3-PDO. Based on the literature search, a suitable catalyst formulation for the glycerol hydrogenolysis reaction was identified, and the role of its individual constituents was studied. We have prepared a novel series of heteropolyacid promoted Pt-β-zeolite catalysts with a high Si/Al ratio (Si/Al = 300) β-zeolite. Glycerol hydrogenolysis reaction was performed over a catalyst containing heteropolyacids like silicotungstic acid, phosphotungstic, and phosphomolybdic acid is evaluated. The silicotungstic acid (STA) was found to be the most effective promoter among the HPAs tried. The combination of Pt, STA, and β-zeolite was therefore studied in detail, with a series of catalysts Pt-xSTA/β-zeolite being synthesized with different ratios of STA to β-zeolite, in the range (x) from 0 to 100% STA. The prepared catalysts were characterized by different methods

such as N_2 physisorption, spectroscopy, and X-Ray diffraction (XRD). In particular, catalyst acidity was characterized by multiple techniques employing different probe molecules to identify the role of different types of acid sites on catalyst performance like Fourier transform infrared spectroscopy (FTIR) of adsorbed pyridine, temperature-programmed desorption of ammonia (NH_3–TPD), thermogravimetric analysis (TGA) of adsorbed 2,6-di-tert-butyl pyridine/pyridine, etc. Additionally, selected catalysts were also analyzed using CO-chemisorption and H_2 temperature-programmed reduction (H_2-TPR). Through an analysis of the performance of these catalysts in the hydrogenolysis of glycerol, the best performing catalyst was identified and further subjected to X-ray photoelectronic spectroscopy (XPS) and transmission electron microscopy (TEM) analysis. The catalyst parameters such as surface area, pore-volume, acidity, particularly Brønsted acidity, particle size, particle dispersion, etc., were estimated.

In the second part, the catalyst performance was studied in detail for the glycerol hydrogenolysis reaction in a batch slurry reactor at 200-220^oC and 30-50 bar H_2 pressure, 80 ml of 5 wt% glycerol aqueous solution, 2 g of prepared catalyst (2.5 wt% of the reaction mixture). The effect of different reaction parameters like reaction temperature, hydrogen pressure, glycerol concentration, platinum loading, catalyst loading, and reaction time on the glycerol hydrogenolysis is evaluated. The stability of hydrogenolysis products like 1,3-PDO, 1,2-propanediol (1,2-PDO), 1-propanol (1-PrOH) is also estimated. The experimental performance is related to characterization results. The catalyst re-usability was studied over 4 cycles. Lastly, based on observed kinetics and product stability, a plausible reaction mechanism over a Pt-STA/β-zeolite catalyst is proposed.

Lastly, the study concludes with modeling of reaction kinetics for glycerol hydrogenolysis based on the proposed reaction mechanism. The results have shown good agreement between the experimental data and model prediction for the Pt-0.3STA/β-zeolite catalyst. The values of the rate constants and the activation energies were evaluated as per the Arrhenius plot. The results show that low temperature favors 1,2-PDO formation, while high temperature seems to favor 1-PrOH formation. The effect of hydrogen pressure on reaction parameters was also studied. The results show that the H_2 pressure affects both rate and selectivity of the reaction, and it is found to be favorable for 1,3-PDO synthesis.

An experimental study on the conversion of glycerol to 1,3-PDO via glycerol's terminal hydroxyl group protection using aldehydes is performed, and the observed results were discussed.

The main contributions of the work are coming out to be the synthesis of a new series of catalysts for glycerol hydrogenolysis to 1,3-PDO. Furthermore, mechanistic investigations through extensive characterization and performance studies are carried out, leading to an understanding of the precise role of the various constituents of the catalyst and, hence, an optimized formulation of the catalyst. Additionally, detailed kinetic studies on one of the most promising catalysts in the series synthesized and a kinetic model over the temperature range of 200 to 220 ^{o}C and pressure range of 10 to 50 bar H_2 is given.

Keywords: *Glycerol, hydrogenolysis, 1,3-propanediol, 1,2-propanediol, Brønsted acidity.*

Contents

DECLARATION iv

Abstract v

Contents viii

List of Figures xiii

List of Tables xix

Nomenclature xxi

Chapter 1: INTRODUCTION 1

1.1 Introduction 1

1.2 Aim and Focus 11

1.3 Organization of report 12

Chapter 2: LITERATURE REVIEW 13

2.1 Homogeneous Catalysts 13

2.2 Heterogeneous Catalysts 14

2.2.1 Catalysts for 1,2-PDO synthesis 15

2.2.2 Catalysts for 1,3-PDO synthesis 16

2.3 New approaches to converting glycerol to 1,3-PDO 32

2.4 Conclusion 34

Chapter 3: EXPERIMENTATION 35

3.1 Materials 35

3.2 Catalyst preparation 36

3.3 Apparatus and Procedure 37

3.4 Analysis 39

3.5 Catalyst Characterization 39

3.5.1 Catalyst surface area and pore size distribution 40
3.5.2 X-ray powder diffraction (XRD) 40
3.5.3 Pulse chemisorption and TPR 41
3.5.4 Crystallite size by transmission electron microscopy (TEM) 41
3.5.5 X-ray photoelectron spectroscopy (XPS) 42
3.5.6 Acidic characteristics of catalysts 43
3.6 Conversion, yield, and Activity 46
Chapter 4: CATALYST CHARACTERIZATION RESULTS 47
4.1 Catalyst characterization 47
4.1.1 Surface area and pore size distribution 47
4.1.2 XRD results: Detection of H_xWO_3 species 51
4.1.3 Temperature-Programmed Desorption of Ammonia (NH_3-TPD) 53
4.1.4 Acidity determination through Thermogravimetry Analysis (TGA) 56
4.1.5 FTIR of adsorbed pyridine (Py-FTIR) 57
4.1.6 Pulse chemisorption 59
4.1.7 Reducibility property (Temperature programmed reduction) 61
4.1.8 Crystallite size by transmission electron microscopy (TEM) 62
4.1.9 X-ray photoelectron spectroscopy (XPS) 64
4.2 Heteropolyacid promoted catalyst 65
4.3 Physico-chemical properties of heteropolyacid promoted catalysts 66
4.4 Platinum dispersion and acidic properties of HPA/β-zeolite catalysts 68
4.5 Conclusion 70
Chapter 5: RESULTS AND DISCUSSION 71
5.1 Results and discussion 71
5.1.1 Performance evaluation: Role of catalyst constituents 71
5.1.2 Optimizing STA loading 74

5.1.3 Effect of total and Brønsted acidity 82

5.1.4 Performance evaluation of heteropolyacids promoted catalyst 86

a) Catalysts with HPA to β-zeolite 86

b) Catalysts with HPA to β-zeolite 88

5.1.5 Hydrogenolysis of different substrates (PDOs or 1-PrOH) 90

5.1.6 Mechanism of glycerol hydrogenolysis over Pt-HPA/β-zeolite catalyst 92

5.1.7 Comparison of observed glycerol hydrogenolysis results with reported results 96

5.1.8 Tabulated glycerol hydrogenolysis reaction results over all synthesized catalysts 97

5.2 Conclusion 98

Chapter 6: EFFECT OF REACTION PARAMETER/CONDITION ON THE KINETICS 100

6.1 Summary results of parametric study over Pt-0.3STA/β-zeolite catalyst 100

6.2 Summary results of parametric study over Pt-0.7STA/β-zeolite catalyst 103

6.3 Detailed parametric study over Pt-0.3STA/β-zeolite and Pt-0.7STA/β-zeolite catalysts 106

6.3.1 Effect of reaction temperature on glycerol hydrogenolysis over Pt-0.3STA/β-zeolite and Pt-0.7STA/β-zeolite catalysts 106

6.3.2 Effect of initial hydrogen pressure on glycerol hydrogenolysis over Pt-0.3STA/β-zeolite and Pt-0.7STA/β-zeolite catalysts 110

6.3.3 Effect of Platinum (Pt) loading on glycerol hydrogenolysis over Pt-0.3STA/β-zeolite and Pt-0.7STA/β-zeolite catalysts 113

6.3.4 Effect of catalyst amount on glycerol hydrogenolysis over Pt-0.3STA/β-zeolite and Pt-0.7STA/β-zeolite catalysts 116

6.3.5 Effect of glycerol concentration on glycerol hydrogenolysis over Pt-0.3STA/β-zeolite and Pt-0.7STA/β-zeolite catalysts 120

6.3.6 Glycerol hydrogenolysis products after 16 h of reaction 124

6.4 Conclusion 125

Chapter 7: KINETIC MODELING 126

7.1 Introduction 126
7.2 Kinetic modeling 128
7.2.1 Validation of absence mass transport limitations 128
7.2.2 Kinetic equations 131
7.2.3 Methodology of parameter estimation 132
7.3 Results and Discussion 133
7.3.1 Effect of hydrogen pressure on kinetic parameters 133
7.3.2 Arrhenius dependence study 136
7.4 Conclusions 142
Chapter 8: NEW APPROACHES: Conversion of glycerol to 1,3-PDO via protection of terminal hydroxyl groups 144
8.1 Introduction 144
8.2 Process Concept 145
8.3 Experimental 147
8.3.1 Materials and Methods 147
8.3.2 Product Analysis 147
8.3.3 Experimental Setup 147
8.3.4 Acetalization in Dean-Stark Apparatus 149
8.3.5 Acetalization in Cylindrical Reactor 150
8.3.6 Dehydration and hydrogenolysis of benzylidene acetal 150
8.4 Results and discussion 150
8.4.1 Acetalization of glycerol with aldehydes 150
8.4.2 Acetalization kinetics 151
8.5 Conclusion 155
Chapter 9: CONCLUSION & FUTURE SCOPE 156
9.1 Conclusion 156

9.1.1 Hydrogenolysis of glycerol with Pt-STA/β-zeolite catalysts 156
9.1.2 Kinetic Modeling and Simulation 158
9.1.3 New approach for 1,3-PDO synthesis 159
9.2 Future Work 159
9.2.1 Catalysts 159
9.2.2 Reaction Engineering studies 160
Appendix-A 161
References 181
List of Publications 206
Acknowledgments 207

List of Figures

Figure 1.1. Formation of glycerol from trans esterification process (R representing hydrocarbon chain containing 15-21 carbon atoms) 3

Figure 1.2. Formation of glycerol from saponification or biodiesel processes. 3

Figure 1.3. Global crude glycerol supply by different industries, the year 2018 [19] 5

Figure 1.4. Glycerol transformation to different chemicals through various processes 6

Figure 1.5. 1,3-PDO and other value-added products synthesis from glycerol metabolism (reproduced with permission, [32]) 8

Figure 1.6. General mechanism of glycerol hydrogenolysis to propanediols (1,2 or 1,3) 10

Figure 2.1. Selective formation of propanediols directed by the nature of acid sites 15

Figure 2.2. Structure of Ir–ReOx/SiO_2 catalyst under reductive conditions (reproduced with permission, [65]). 17

Figure 2.3. Direct hydrogenolysis of glycerol to propanediols over Ir–MOx/SiO_2 catalyst (reproduced with permission, [67]) 18

Figure 2.4. Effects of tungsten compounds addition on Pd/Pt-based catalysts. Conditions: active metal (5 mmol), 100 mM aqueous glycerol (5 mL), additive (HCl, pH 1.5; H_2WO_4, 40 mM; polyacid: 3.5 mM), H_2 (40 bar), 200 ^oC, 18 h (reproduced with permission, [85]). 20

Figure 2.5. Raman spectra of fresh and spent Pt–HSiW/ZrO_2 catalysts (reproduced with permission, [117]). 23

Figure 2.6. Influence of WO_3 (A) and TiO_2 (B) loadings on Pt/WO_3/TiO_2/SiO_2 catalysts (reproduced with permission, [105]) 25

Figure 2.7. Conversion of glycerol to 1,3-PDO via new approach (reproduced with permission, [26]) 33

Figure 3.1. (A) Catalyst preparation setup and (B) Calcination and reduction setup 36

Figure 3.2. Schematic of the experimental setup for hydrogenolysis of glycerol 37

Figure 4.1. N_2 physisorption isotherm and pore size distribution for synthesized catalysts ... 49

Figure 4.2. XRD patterns of prepared catalyst samples.....52

Figure 4.3. NH_3-TPD profiles for the prepared catalysts.....53

Figure 4.4. Py-FTIR spectra for the prepared catalyst: - (a) Pt/β-Zeolite, (b) Pt/0.07STA/β-Zeolite (c) Pt/0.1STA/β-Zeolite, (d) Pt/0.2STA/β-Zeolite, (e) Pt/0.3STA/β-Zeolite, (f) Pt/0.4STA/β-Zeolite (g) Pt/0.5STA/β-Zeolite, (h) Pt/0.6STA/β-Zeolite, (i) Pt/0.7STA/β-Zeolite, (j) Pt/0.8STA/β-Zeolite, (k) Pt/1.0STA/β-Zeolite 57

Figure 4.5. Observed platinum dispersion on prepared catalysts 59

Figure 4.6. H_2-TPR profiles of the prepared catalysts up to Pt-1.0STA/β-zeolite 61

Figure 4.7. TEM images of the catalyst Pt/0.3STA/β-zeolite, the particle size distribution, and the average particle diameter. 62

Figure 4.8. TEM images of the catalyst Pt/0.7STA/β-zeolite, the particle size distribution and the average particle diameter. 63

Figure 4.9. W 4f (A) and Pt 4d (B) XPS photoemission peaks of Pt/0.3STA/β-zeolite catalyst 64

Figure 4.10. W4f (A) and Pt 4d (B) XPS photoemission peaks of Pt/0.7STA/β-zeolite catalyst. 65

Figure 4.11. N_2 physisorption isotherm (A) and XRD spectra (B) of heteropoly promoted catalyst 67

Figure 5.1. Glycerol hydrogenolysis reactant and product profiles for different catalyst formulations: (a)β-zeolite, (b) Pt/β-zeolite, (c) 0.3STA/β-zeolite, (d) Pt/0.1STA/β-zeolite ...72

Figure 5.2. Glycerol hydrogenolysis reactant and product profiles for catalysts with different STA loadings: (a) Pt/0.07STA/β-zeolite, (b) Pt/0.2STA/β-zeolite, (c) Pt/0.3STA/β-zeolite (d) Pt/0.4STA/β-zeolite, (e) Pt/0.5STA/β-zeolite.....75

Figure 5.3. Glycerol hydrogenolysis reactant and product profiles for catalysts with different STA loadings: (a) Pt/0.6STA/β-zeolite, (b) Pt/0.7STA/β-zeolite, (c) Pt/0.8STA/β-zeolite (d) Pt/1.0STA/β-zeolite 77

Figure 5.4. Glycerol hydrogenolysis reactant and product profiles for catalysts with different STA loadings: (a) Pt/1.5STA/β-zeolite, (b) Pt/2.33STA/β-zeolite, (c) Pt/4.0STA/β-zeolite (d) Pt/9.0STA/β-zeolite (e) Pt/β-zeolite 81

Figure 5.5. (a) Surface coverage, Total & Brønsted acidity vs. catalyst (b) TOF, $P_{1,3\text{-PDO}}$, $S_{1,3\text{-PDO}}$ vs. surface coverage (c) glycerol conversion vs. total acidity (d) 1,3-PDO yield vs. Brønsted acidity.....83

Figure 5.6. (a) Surface coverage, Total & Brønsted acidity vs. catalyst (b) TOF, $P_{1,3\text{-PDO}}$, $S_{1,3\text{-PDO}}$ vs. surface coverage (c) glycerol conversion vs. catalyst (d) 1,3-PDO yield vs. Brønsted acidity.....85

Figure 5.7. Glycerol hydrogenolysis reactant and product profiles: (a)- Pt/β-zeolite, (b)- 5%Pt/0.3PMA/β-zeolite, (c)- Pt/0.3STA/β-zeolite, (d)- 5%Pt/0.3PTA/β-zeolite.....87

Figure 5.8. Glycerol hydrogenolysis reactant and product profiles: (a)- Pt/0.7PMA/β-zeolite, (b)- Pt/0.7STA/β-zeolite, (c)- Pt/0.7PTA/β-zeolite 89

Figure 5.9. 1,3-PDO, 1,2-PDO, and 1-PrOH hydrogenolysis profiles: (a)- 1,3-PDO, (b)- 1-PrOH, (c)- 1,2-PDO 90

Figure 5.10. 1,3-PDO, 1,2-PDO, and 1-PrOH hydrogenolysis profiles: (a)- 1,3-PDO, (b)- 1-PrOH, (c)- 1,2-PDO. 91

Figure 5.11. Complete reaction mechanism of glycerol hydrogenolysis over Pt-HPA/β-zeolite 94

Figure 5.12. The detailed reaction mechanism on the transformation of glycerol to 1,3-PDO over Pt-HPA/β-zeolite.....95

Figure 6.1. Effect of reaction temperature on: (I) glycerol conversion, (II) 1,3-PDO selectivity, (III) 1,2-PDO selectivity, (IV) 1-PrOH selectivity, (V) others selectivity, (VI) gaseous products selectivity vs. time/conversion over Pt-0.3STA/β-zeolite. Here, (a) 200 ^{o}C, (b) 210 ^{o}C, (c) 210 ^{o}C, (d) 240 ^{o}C. 107

Figure 6.2. Effect of reaction temperature on: (I) glycerol conversion, (II) 1,3-PDO selectivity, (III) 1,2-PDO selectivity, (IV) 1-PrOH selectivity, (V) others selectivity, (VI) gaseous products selectivity vs. time/conversion over Pt-0.7STA/β-zeolite. Here, (a) 200 ^{o}C, (b) 210 ^{o}C, (c) 210 ^{o}C, (d) 240 ^{o}C. 108

Figure 6.3. Effect of initial hydrogen (H_2) pressure on: (I) glycerol conversion, (II) 1,3-PDO selectivity, (III) 1,2-PDO selectivity, (IV) 1-PrOH selectivity, (V) others selectivity, (VI) gaseous products selectivity vs. time/conversion over Pt-0.3STA/β-zeolite, where (a) 10 bar, (b) 40 bar, (c) 50 bar. 111

Figure 6.4. Effect of initial hydrogen (H_2) pressure on: (I) glycerol conversion, (II) 1,3-PDO selectivity (III) 1,2-PDO selectivity, (IV) 1-PrOH selectivity, (V) others selectivity, (VI) gaseous products selectivity vs. time/conversion over Pt-0.7STA/β-zeolite, where (a) is 10 bar, (b) is 40 bar, (c) is 50 bar. 112

Figure 6.5. Effect of catalyst platinum loading on: (I) glycerol conversion, (II) 1,3-PDO selectivity, (III) 1,2-PDO selectivity, (IV) 1-PrOH selectivity, (V) others selectivity, (VI) gaseous products selectivity vs. time/conversion over Pt-0.3STA/β-zeolite. (a) – 2.5 wt%, (b) – 5 wt%, (c) – 10 wt%. 114

Figure 6.6. Effect of catalyst platinum loading on: (I) glycerol conversion, (II) 1,3-PDO selectivity, (III) 1,2-PDO selectivity, (IV) 1-PrOH selectivity, (V) others selectivity, (VI) gaseous products selectivity vs. time/conversion over Pt-0.7STA/β-zeolite. (a) – 2.5 wt%, (b) – 5 wt%, (c) – 10 wt%. 115

Figure 6.7. Effect of catalyst amount in reaction on: (I) glycerol conversion, (II) 1,3-PDO selectivity, (III) 1,2-PDO selectivity, (IV) 1-PrOH selectivity, (V) others selectivity, (VI) gaseous products selectivity vs. time/conversion over Pt-0.3STA/β-zeolite. Here, catalyst to glycerol ratio: (a) 0.25, (b) 0.5, (c) 0.75. 117

Figure 6.8. Effect of catalyst amount in reaction on: (I) glycerol conversion, (II) 1,3-PDO selectivity, (III) 1,2-PDO selectivity, (IV) 1-PrOH selectivity, (V) others selectivity, (VI) gaseous products selectivity vs. time/conversion over Pt-0.7STA/β-zeolite. Here, catalyst to glycerol ratio: (a) 0.25, (b) 0.5, (c) 0.75. 119

Figure 6.9. Effect of initial glycerol concentration on: (I) glycerol conversion, (II) 1,3-PDO selectivity, (III) 1,2-PDO selectivity, (IV) 1-PrOH selectivity, (V) others selectivity, (VI) gaseous products selectivity vs. time/conversion over Pt-0.3STA/β-zeolite. Here, (a) – 5 wt% glycerol, (b) – 10 wt% glycerol, (c) – 20 wt% glycerol, (d) – 30 wt% glycerol. 121

Figure 6.10. Effect of initial glycerol concentration on: (I) glycerol conversion, (II) 1,3-PDO selectivity, (III) 1,2-PDO selectivity, (IV) 1-PrOH selectivity, (V) others selectivity, (VI) gaseous products selectivity vs. time/conversion over Pt-0.7STA/β-zeolite. Here, (a) – 5 wt% glycerol, (b) – 10 wt% glycerol, (c) – 20 wt% glycerol, (d) – 30 wt% glycerol. 122

Figure 7.1. Effect of catalyst to glycerol ratio on the initial rate of glycerol hydrogenolysis, T = 220 ºC, 40 bar H_2. 129

Figure 7.2. Proposed kinetic pathways of glycerol hydrogenolysis for kinetic modeling..... 130

Figure 7.3. Updated kinetic pathways of glycerol hydrogenolysis for kinetic modeling 130

Figure 7.4. Concentration versus time (C/t) profiles for (I) glycerol at different pressures, (II) products at 10 bar, (III) products at 40 bar, (IV) products at 50 bar. Here, experimental data are shown by markers (dot) & simulated data are shown by lines. Reaction conditions: 80 mL of a 5 wt% glycerol solution, 2 g Pt-0.3STA/β-zeolite catalyst, reaction temperature = 220 ºC, 5 h of reaction time, stirring speed = 800 RPM. 135

Figure 7.5. Concentration versus time (C/t) profiles for (I) glycerol at different temperatures, (II) products at 200 ºC, (III) products at 210 ºC, (IV) products at 220 ºC. Here, experimental data are shown by markers (dot) & simulated data are shown by lines. Reaction conditions: 80 mL of a 5 wt% glycerol solution, 2 g Pt-0.3STA/β-zeolite catalyst, H_2 pressure = 40 bar, 5 h of reaction time, stirring speed = 800 RPM. 138

Figure 7.6. Arrhenius plot for rate constants 140

Figure 8.1. Representation of the new approach to glycerol conversion with benzaldehyde. 145

Figure 8.2. Representation of the new approach to glycerol conversion with formaldehyde146

Figure 8.3. (A) Dean-Stark apparatus and (B) cylindrical reactor.....148

Figure 8.4. Side-products observed during the acetalization of glycerol with benzaldehyde152

Figure 8.5. Concentration vs. time profiles for acetalization of glycerol with benzaldehyde: -(I) Effect of RPM, (II) Effect of catalyst loading, (III) Effect of reaction temperature, (IV) Effect of reactant mole ratio 153

Figure A.1. Calibration curve for key product(s) and reactant of glycerol hydrogenolysis ..161

Figure A.2. Correlation between 1,2-PDO yield and Lewis acidity using Py-FTIR 163

Figure A.3. Correlation between the product yield and amount of acid sites measured using TGA 163

Figure A.4. Glycerol conversion vs. time profiles for glycerol hydrogenolysis at different RPM. 164

Figure A.5. Bar chart representing the effect of reaction or catalyst parameters on glycerol conversion and product selectivities. 172

Figure A.6. A rough process flow sheet of the 1,3-propanediol production route 177

List of Tables

Table 1.1. Composition of pure and impure glycerol [14] 4

Table 1.2. Applications of pure glycerol with different grades [18] 5

Table 2.1. Pt-WOx/supported and Pt-WOx catalysts for glycerol hydrogenolysis to 1,3-PDO 21

Table 2.2. Hydrogenolysis of glycerol results observed on reported and new catalysts 31

Table 3.1. Different catalyst prepared with variable STA to β-zeolite ratio.....38

Table 4.1. Textural properties, surface coverage, and surface W density of the prepared catalyst 48

Table 4.2. Acidic sites of prepared catalysts measured using different techniques.....55

Table 4.3. Tabulated Pt dispersion and Pt size of prepared catalysts 60

Table 4.4. Textural properties and Pt dispersion of heteropolyacid promoted catalysts 68

Table 4.5. Acidic sites of heteropolyacid promoted catalysts using different techniques.....69

Table 5.1. Comparison of Pt/xSTA/β-zeolite catalytic performance with those reported in literature 96

Table 5.2. Glycerol hydrogenolysis reaction results over different catalysts (synthesized)....97

Table 6.1. Reaction parameter study for glycerol hydrogenolysis reaction over Pt-0.3STA/β-zeolite (quantitative) 101

Table 6.2: - Summarized results from a parametric study of glycerol hydrogenolysis reaction over Pt-0.7STA/β-zeolite catalyst.....103

Table 6.3. Glycerol conversion and product selectivities after 16 h of reaction 124

Table 7.1 Values of rate constant after solving and optimizing the kinetic model at three different hydrogen pressures.....134

Table 7.2. Correlation coefficients (R^2) values for all the components fitted using optimized model parameters for reaction under three different hydrogen pressures.....136

Table 7.3. Values of rate constant after solving and optimizing the kinetic model at three different temperatures. 137

Table 7.4. Correlation coefficients (R^2) values for all the components fitted using optimized model parameters for reaction under three different temperatures. 139

Table 7.5. Results of parameter estimation (for Pt-0.3STA/β-zeolite catalyzed reaction) 141

Table A.1. Values of CI bound for 200 ^oC 166

Table A.2. Values of CI bound for 210 ^oC 167

Table A. 3. Values of CI bound for 220 ^oC 167

Table A. 4. Values of CI bound for 10 bar H_2 168

Table A.5. Values of CI bound for at 50 bar H_2 168

Table A.6. Reaction parameter study for glycerol hydrogenolysis reaction over Pt-0.3STA/β-zeolite (qualitative) 169

Table A.7. Product stream composition from the reactor 174

Table A.8. Plant details for 200 kilotons of biodiesel produced per year (glycerol produced 20 kilotons per year) 176

Table A.9. Stream composition from each equipment 177

Nomenclature

Acronyms

1,2-PDO	1,2-propanediol
1,3-PDO	1,3-propanediol
1-PrOH	1-propanol
E_j	Activation energy for the j^{th} reaction, kJ/mol
C_i	Concentration of i^{th} species in bulk liquid, mmol/L
k_0	Frequency factor, min^{-1} for first order
Gly/gly	glycerol
ΔHrxn	Heat of reaction
HPA	Heteropoly acid
PMA	Phosphomolybdic acid
PTA	Phosphotungstic acid
Pt	Platinum
k_i	rate constant for i^{th} species in bulk liquid, min^{-1} for first order
r_i	rate of reaction, mmol/L/h
STA	Silicotungstic acid
W	Tungsten
$HxWO_3$	Tungsten bronze
WOx	Tungsten oxide

Abbreviations

2,6-dTbPy	2,6-di-tert-butylpyridine.
BET	Brunauer Emmett Teller
FTIR	Fourier Transformed Infra-Red Spectroscopy

XPS	photoelectron spectroscopy
Py	Pyridine
NH_3–TPD	Temperature- programmed desorption of ammonia
TPR	Temperature-programmed reduction
TGA	Thermo Gravimetric Analysis
TEM	Transmission Electron Microscopy
XRD	X-ray diffraction

Chapter 1: INTRODUCTION

1.1 Introduction

In today's world, our dependence on energy from non-regenerative resources like fossil or petroleum fuels, coal, and methane is proving a challenge to the sustainability of our energy production methods. Energy plays a vital role in a nation's economic growth. It is an essential feedstock for the modern society for its need for power, housing, clothing, and agriculture. Moreover, fossil resources are also the origins of multiple synthetic materials and chemicals. From 1970 to 2015, the world's energy supply has increased from 6 Gtoe (Gigatons of Oil Equivalent) to 15 Gtoe, and fossil resources continued to be the primary source of energy supply. In 1973, fossil fuel usage was about to 86% for producing direct energy, and in 2015, it was around 78% [1].

Moreover, Oil production could reach a maximum limit by 2020, and its usage will continue to rise, driven mainly by India and China. The fossil reservoirs are depleting due to increased use and rapid industrialization [2] and influencing the energy and chemical industries. The tight supply of fossil fuels and chemicals is becoming a grave concern day by day. The main drawbacks of fossil fuels are, they are limited and non-renewable. The current consumption of crude oil globally is over 11 billion tonnes per year. The annual rate of crude oil reserves diminution is 4 billion tonnes per year. If crude oil usage continues at the same rate globally, then the remaining oil reserves will be over by 2052 [3].

Petroleum, coal, wind, solar, nuclear, etc., resources generate the energy utilized by various sectors like industrial, agricultural, transport, etc. [4–6]. The energy from oil usage for these sectors in the year 1973 was 42%, remaining energy comes from other sources. In the year 2014, the oil usage of these sectors increased to 64.5% of global oil usage. The use of fossil fuels in the last 45 years is increased by 43.3% [7]. Apart from sustainability considerations, intensive usage of fossil fuels increases CO_2 emissions, a severe threat to the climate since the accumulation of CO_2 and other gases is responsible for climate change [8]. The level of CO_2 from the year 2007 to the year 2030 is expected to rise by approximately 80% [1]. Due to the issues associated with the fossil fuels like decreasing reservoirs, increasing demands, unsteady supply, fluctuating prices, and rising global warming from its usage, researchers focus on

finding alternative energy sources to fossil fuels. Any alternative to fossil fuel should have some features like easy availability, economic feasibility, environmental friendliness. Biofuels seem to possess all these features. Biodiesel is a renewable biofuel that is biodegradable, less toxic, and environmentally friendly and is attracting attention worldwide [9,10]. Converting available biomass into renewable fuels and chemicals can thus ease the stress on fossil resources. Moreover, the solution to the energy crisis without adversely affecting the environment and society can be found by using renewable energy resources with social engineering.

With the increasing global population, energy demands are also increasing. Biofuels grab much attention from researchers as an alternative fuel to fulfill the rising energy demands [11,12]. Biomass is a broadly available and renewable resource, which can be obtained from animals and plants. The biomass needs to be converted into the platform molecules before their utilization. In the transport sector, biodiesel can similarly contribute to the conservation of fossil resources. Biodiesel is either employed alone or mixed with the conventional diesel fuel during the combustion process inside the engine. It has lower exhaust emission of dust, hydrocarbon, carbon dioxide or carbon monoxide, and smoke. Rudolf Diesel (inventor of diesel engine) had also tested the peanut oil in diesel engines as a fuel initially and found that vegetable oils can be employed directly in diesel engines [1]. Biodiesel represents one of the crucial attempts to replace fossil sources of energy with renewable sources. Global biodiesel production is projected to attain a 39.3 bln L (billion liters) value by 2027, with a 9% increase compared to the 2017 level. Region policies will continue to influence biodiesel production in addition to market forces. European Union is likely to become a key producer of biodiesel, and the production should reach 12.9 bln L by 2027. United States will be the second-largest biodiesel producer with a predicted value of 6.7 bln L by 2027. The other chief biodiesel producers include Brazil, Indonesia, Argentina, and Thailand, etc.

Biodiesel use is expected to increase steadily in developing countries. Biodiesel use in Indonesia, Argentina, and Brazil is expected to rise by 2027, given increases in domestic mandates. Due to biodiesel blending obligations, countries like India, Malaysia, Colombia, the Philippines, Thailand, and Paraguay are predicted to see an increase in biodiesel use; the biodiesel consumption in most countries is projected to start from minimal levels, and their biodiesel content in diesel fuels will remain in between 1% to 3% by volume, except Colombia where the blend is expected to remain about 6.5% by volume [13].

Biodiesel is derived by trans-esterification of triglycerides with methanol in the presence of an acid catalyst. The stoichiometry of biodiesel production is shown as follows: -

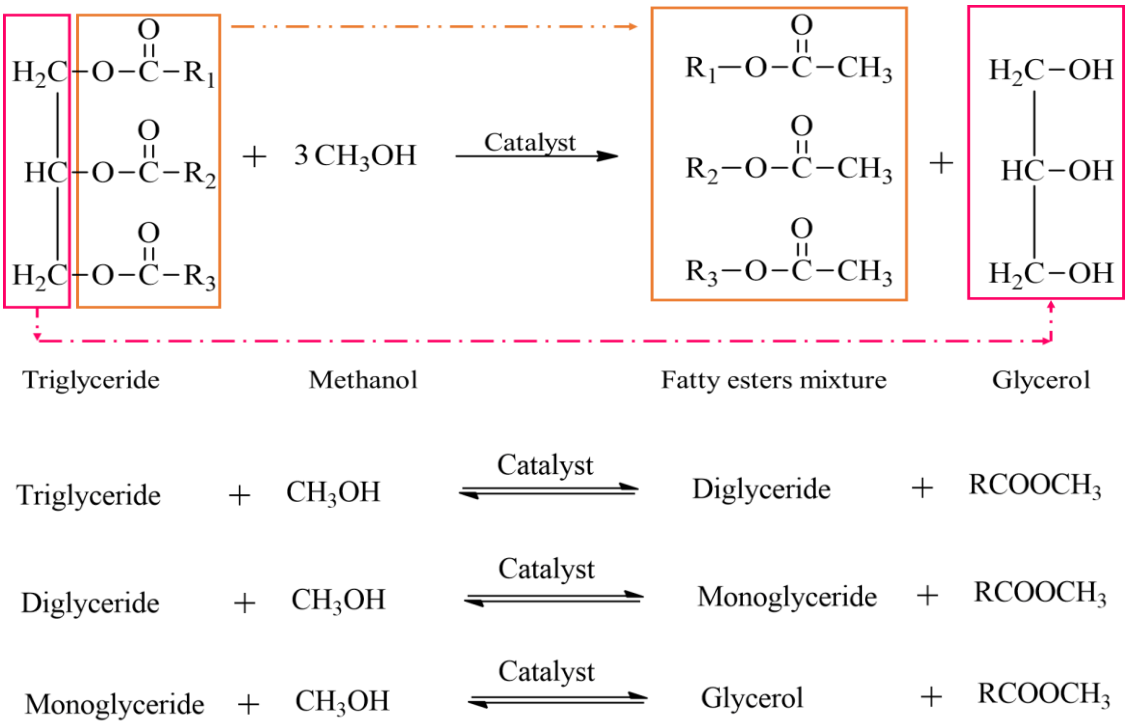

Figure 1.1. Formation of glycerol from trans esterification process (R representing hydrocarbon chain containing 15-21 carbon atoms)

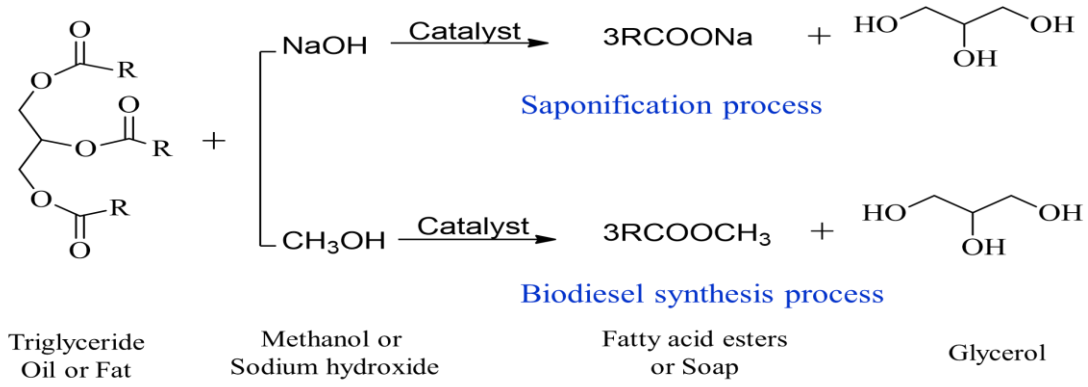

Figure 1.2. Formation of glycerol from saponification or biodiesel processes.

As shown in Figure 1.1, biodiesel is produced either from transesterification or alcoholysis of edible vegetable oils. When vegetable oil undergoes the transesterification process to form biodiesel, glycerol forms as a by-product. The transesterification process produces three moles of fatty acid methyl esters along with one mole of glycerol. The approximate yield of glycerol in this process is around 10% by weight. Lately, glycerol has been obtained through the

transesterification of soybean, sunflower, rapeseed, or palm oils during biodiesel production [14,15].

Moreover, glycerol is an industrial by-product in other processes as well, such as soap synthesis (see Figure 1.2), microbial fermentation, hydrogenolysis of glucose in the mixture of fatty ester, polyols, and fatty acid processes. It is reported that 62% (≈2/3rd) of the world's glycerol supply comes from the biodiesel industry (See Figure 1.3). The glycerol obtained from the biodiesel industry contains around 14–50% of methanol. Hence the glycerol obtained through this process is crude with 60–80% purity. The crude glycerol is impure and unsuitable for pharmaceutical applications, and it requires purification for its sell-off. Only pure glycerol with a concentration of more than 99% is commercially valuable. Table 1.1 shows the chemical compositions of impure and pure glycerol. Table 1.2 represents the application of pure glycerol based on purity/grades.

Table 1.1. Composition of pure and impure glycerol [14]

Contents	**Impure glycerol**	**Pure glycerol**
Glycerol (%)	60–80	99.1–99.8
Moisture (%)	1.5–6.5	0.11–0.8
Ash (%)	1.5–2.5	0.054
Soap (%)	3.0–5.0	0.56
Acidity (pH)	0.7–1.3	0.10–0.16
Chloride (ppm)	ND	1
Colour (APHA)	Dark	34–45

Therefore, to make pure glycerol, a huge cost is involved to remove methanol, making the process uneconomical for small and medium capacity plants [15,16]. Over the years, the price of pure glycerol globally varied from Rs 80/kg to Rs 250/kg, which is much higher than impure glycerol Rs 3/kg to Rs 25/kg [16]. Additionally, the global production of biodiesel increased

significantly, with an average growth of 42% [17]. This rapid increase in biodiesel production has increased the crude glycerol amount in the market. The oversupply of glycerol from biodiesel and oleochemical industries has made crude glycerol worthless.

Table 1.2. Applications of pure glycerol with different grades [18]

Grade	Type of glycerol	Usage
Grade I	Technical grade ≈ 99.5%	Intermediate compound for various chemicals however not applied to food or drug formulation
Grade II	*USP grade 96–99.5%	Food products, pharmaceuticals and cosmetics
Grade III	Kosher or USP/**FCC grade 99.5–99.7%	Kosher foods and drinks

*USP—United States pharmacopeia. **FCC—Food chemical codex.

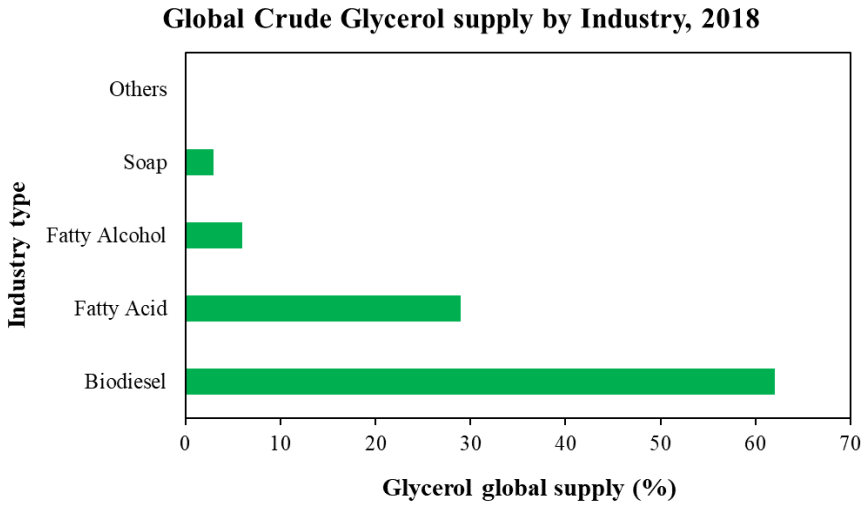

Figure 1.3. Global crude glycerol supply by different industries, the year 2018 [19]

Moreover, the price of pure glycerol also went down, it was Rs 110/kg (before the rapid growth of biodiesel) to Rs 50/kg, and that of crude glycerol price dropped from Rs 40/kg to Rs 8/kg in

the year 2007 [20]. Hence, biodiesel producers are forced to invest a heavy amount of money in removing the unwanted glycerol away from their plants [21]. Therefore, it is essential to develop the processes for glycerol valorization, which is necessary for the sustainability of oleochemical and biodiesel industries.

Glycerol (1,2,3-propanetriol) is a colorless, odorless, viscous liquid with a sweet taste widely used in the production of pharmaceuticals, cosmetic products, foods, etc. It was reported that glycerol could be converted to many valuable chemicals. Figure 1.4 represents the various processes through which glycerol can be converted to different value-added products. The processes include etherification, acetalization, esterification, oxidation, reduction, dehydration, hydrogenolysis, reforming, halogenation, oligomerization, etc.

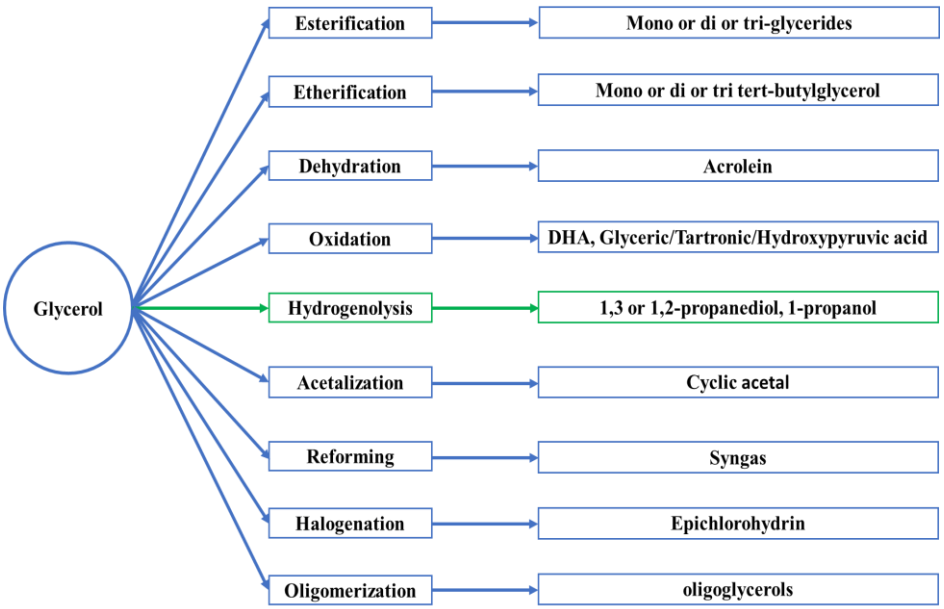

Figure 1.4. Glycerol transformation to different chemicals through various processes

The products obtained from glycerol include lactic acid, dihydroxyacetone, succinic acid, citric acid, propionic acid, DCP, ethanol, hydrogen, and so on [21–23]. Alternatively, glycerol can also be converted to propanediol. Mainly 1,3-propanediol (1,3-PDO), which has several applications such as in food, perfumes, coatings, paints, adhesives, fragrances, laminates, cosmetics, pharmaceuticals, personal care products, and lab grade chemicals. Additionally, 1,3-PDO is used to manufacture polyesters, polyethers, polyurethanes, heterocyclic compounds, and biocides [21,23,24]. The most important application of 1,3-PDO is a synthesis of poly-trimethylene terephthalate (PTT) [21,23]. PTT is a biodegradable polymer and has several applications due to its unique features. According to a market report, nearly 90% of 1,3-PDO

is consumed in the making of PTT [25]. 1,3-PDO is suitable for making PTT because it does not impart the ethylene glycol stiffness and avoids the floppiness of 1,6-hexanediol and 1,4-butanediol [26]. The PTT derived from 1,3-PDO has a zig-zag or coil-like or shape with superior characteristics during stretching and stretch regaining. Additionally, polymers obtained from 1,3-PDO have higher UV resistance, better wash-fastness, and lower dyeing temperature than commercially available polyesters [27]. The common trademarks of PTT found in the market are CDP Nature works (from Dow Chemical), Dupont's Soronam (from Dupont), and Shell Chemical's CorterraTM (from Shell) [28]. It shows 1,3 PDO can relieve the stress on petroleum derivatives in the global polyester market to a significant extent.

The global production of 1,3-PDO is increasing rapidly and gaining over 100 million pounds yearly [27]. The increase in 1,3-PDO production is attributed to the rise in market demands of its high-valued derivatives. According to a market report, in the year 2014, the global market demand for 1,3-PDO was 146 kilotons and is expected to reach 225.9 kilotons by 2022 with a CAGR of 5.8% from 2015 to 2022 [29]. Based on another market report, the price of 1,3-PDO is expected to grow from $million 490 in 2019 to $ million 870 by 2024, at a 12.2 % CAGR from 2019 to 2024 [30]. Therefore, the conversion of glycerol to 1,3-PDO looks like an attractive route for its valorization.

Currently, the traditional processes synthesizing 1,3-PDO are acrolein hydration, ethylene oxide hydroformylation. More recently, the 1,3-PDO is synthesized from the glycerol via enzymatic transformation [31,32]. Many methods have been developed to produce 1,3-PDO from crude and pure glycerol.

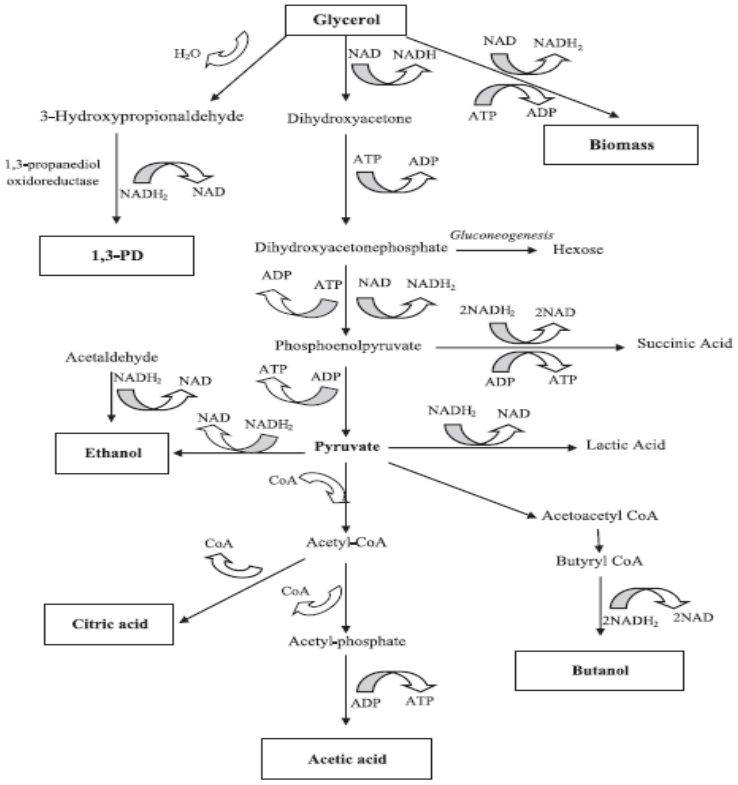

Figure 1.5. 1,3-PDO and other value-added products synthesis from glycerol metabolism (reproduced with permission, [32]**).**

Different microorganisms like Klebsiella pneumonia, or Citrobacter freudii, or Clostridium butyricum, have been reported to convert glycerol to 1,3-PDO effectively. The synthesis of 1,3-PDO from glycerol via fermentation is mainly achieved using either the micro-aerobic or anaerobic bacteria fermentation process [33–35]. Figure 1.5 shows the mechanism through which 1,3-PDO is produced from glycerol via the fermentation route. It was reported that in an ideal anaerobic condition, the maximum possible theoretical yield of 1,3-PDO is 0.875 mol/mol glycerol. Zhang et al. [36] reported the yield of 1,3-PDO up to 0.7 mol/mol glycerol using Klebsiella pneumoniae catalyst by inactivating the gene which produces ethanol via acetaldehyde. In another study, the author was able to achieve a 0.52 mol/mol yield of 1,3-PDO by suppressing the lactate formation [37].

Though the biological pathway looks attractive and straightforward, however, this process contains a few significant drawbacks. This fermentation process requires pure microbial cultures like Lactobacillus, Enterobacter, Pelobacter, Clostridium, Klebsiella, and Citrobacter for 1,3-PDO synthesis from glycerol. Pure microbial cultures require expensive equipment and complicated procedures. The by-products formed during the process, such as butyrate, ethanol, and acetate, reduce the 1,3-PDO selectivity. The bacteria stop functioning if the glycerol

concentration is more than 17%. Therefore, chemical methods have attracted much interest in glycerol conversion to 1,3-PDO.

The commercial production of 1,3-PDO via chemical route is done from the petroleum derivatives such as acrolein (Degussa-DuPont route) or hydroformylation of ethylene oxide (Shell route). The synthesis of 1,3-PDO from acrolein occurs via its hydration to 3-HyPA, followed by 1,3-PDO synthesis from catalytic hydrogenation. During hydrolysis, acrolein forms polymer via self-condensation. This makes 1,3-PDO yield suffer because hydration reaction has to compete with acrolein self-condensation reaction. Moreover, hydroformylation of ethylene oxide was carried out over cobalt-ruthenium homogeneous catalysts. The yield of the process is around 90%. However, the impurity level in this process is almost 10 times compared to the fermentation process [27]. The hazardous nature and low conversion efficiency of the acrolein process.

Moreover, an impure product of the ethylene oxide process has spurred a large amount of interest in producing 1,3-PDO from other chemical sources such as glycerol. The decreased price of glycerol and its increased production makes glycerol the best candidate for 1,3-PDO synthesis. Several chemical processes have been reported for converting glycerol to 1,3-PDO via catalytic hydrogenolysis. All these catalysts and processes will be discussed in detail in the literature review (chapter 2).

Glycerol hydrogenolysis is a catalytic process that involves the fission of either chemical bond between carbon-carbon or carbon-oxygen in glycerol followed by the simultaneous addition of hydrogen atom to form a molecular fragment [38]. Figure 1.6 represents the general pathway of the hydrogenolysis process. The glycerol hydrogenolysis is a complex reaction and it can lead to 1,2-propanediol (1,2-PDO) or 1,3-PDO. However, 1,3-PDO being most valuable, its formation from glycerol seems attractive. But, the selectivity towards 1,3-PDO or 1,2-PDO is mainly dependent on the catalyst used and reaction conditions. Therefore, this work aims to synthesize a catalyst that will be active towards 1,3-PDO and perform the allied studies to come up with suitable catalytic and reaction principles so that the reaction may be carried out with facility.

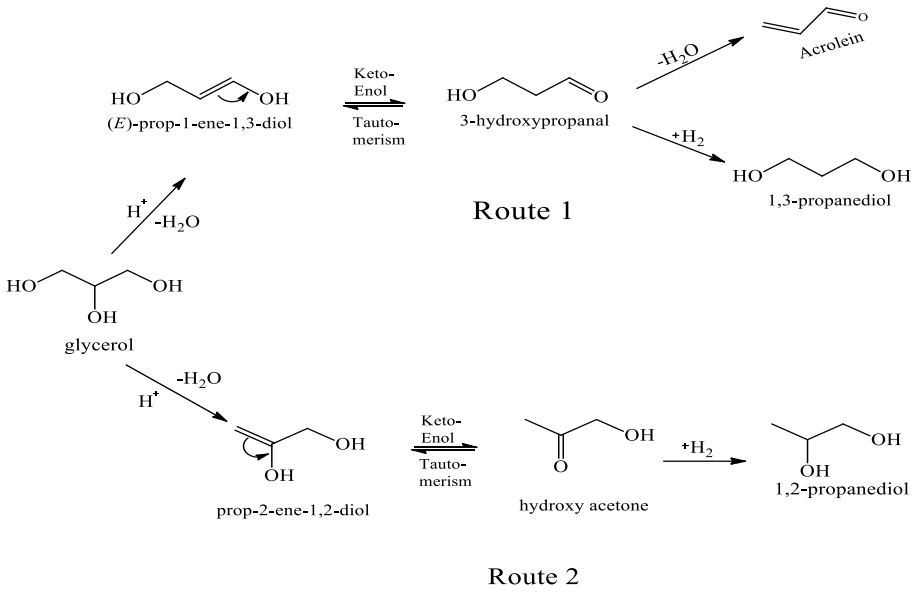

Figure 1.6. General mechanism of glycerol hydrogenolysis to propanediols (1,2 or 1,3)

There has been considerable research on homogeneous and heterogeneous catalysts for glycerol hydrogenolysis to 1,3-PDO. The catalyst needs to have both the acid and metal sites for the selective conversion of glycerol to propanediols. The use of simple catalysts with acid and metal sites will result in the formation of 1,2-PDO. The difference between the market value of glycerol and 1,2-PDO is minimum. However, 1,2–PDO can be used as a monomer for polyester resin, as an antifreeze agent, in paints, etc. Most of the catalytic systems have resulted in higher yields of 1,2-PDO, using a bifunctional catalyst having hydrogenation metal and an acidic or basic co-catalyst or support [39,40]. It is because of the different reactivity of glycerol's hydroxyl (–OH) groups. The 2º –OH group has more steric hindrance than the 1º –OH group; this makes the 2º –OH group inaccessible to the active sites of the catalysts.

Additionally, Nimlos et al. [41] reported that the dehydration energy barriers for both the –OH groups of neutral glycerol are nearly equal (73.2 kcal mol^{-1} for 1º –OH group and 70.9 kcal mol−1 for 2º –OH group), and their proton affinities are also roughly equal (194.8 kcal mol^{-1} for 1° –OH group and 195.4 kcal mol^{-1} for the 2° –OH group). Hence, these tiny discrepancies in reactivity of the –OH groups make the selective transformation of glycerol to 1,3-PDO very difficult. Furthermore, the selectivity issues are further compounded by the fact that glycerol dehydration to acrolein and glycerol hydrogenolysis to 1,3-PDO have the same intermediate 3-HyPA, acrolein on hydrogenation leads to 1-propanol. Therefore, glycerol hydrogenolysis needs the development and understanding of the reaction parameters, including catalyst selection, so that more valued 1,3-PDO can be obtained.

From the former discussion, it is clear that 1,3-PDO has various applications, and its demand is increasing continuously. On the other hand, glycerol production is also growing due to increased biodiesel production, which has increased glycerol availability at cheaper rates. Conversion of glycerol to 1,3-PDO via fermentation route has its limitations; however, catalytic hydrogenolysis seems attractive. Glycerol hydrogenolysis is a complex reaction with multiple series and parallel reactions. These side reactions make the 1,3-PDO synthesis reaction non-selective. A good understanding of the catalyst used in a reaction and favorable reaction parameters may lead to a good 1,3-PDO selectivity and reduce the environmental load.

With this motive, the thesis broadly addresses the issues at the level of both catalyst design and reaction engineering (see section 1.3- organization of report).

1.2 Aim and Focus

In this work, the focus is to study the catalysts proposed in the literature for glycerol hydrogenolysis to 1,3-propanediol and, based on the understanding thus gained, design an improved catalyst. The activity and selectivity issues at micro and macro (reaction engineering) levels are addressed. The former (catalysis research) is the one that holds great potential in making 1,3-PDO from glycerol. The catalyst search should not only consider its effects on rates and selectivity; it should also consider the impact and role of each component of the catalyst on performance.

With this objective, the available catalysts were studied and understood which features a catalyst should have in order to convert glycerol to 1,3-PDO. We have designed a new catalyst based on this understanding, studied the characterization and performance of a synthesized catalyst in order to optimize its formulation, and finally obtained the detailed kinetics to enable reactor design for the hydrogenolysis.

The role of each constituent of catalyst and its effect on reaction acidity and selectivity is addressed. The amendment in the catalyst structure is performed to improve its acidic characteristics, especially Brønsted acidic sites. The dependence of 1,3-PDO yield over catalysts Brønsted acidic sites is addressed.

Considering the reaction's multiphase complexity effect of each parameter, *viz.* temperature, pressure, concentration, catalyst loadings, etc., are addressed. Literature shows only a few

groups have discussed the effect of these parameters, and hence the interpretation of the data obtained becomes difficult. A detailed study is required to fill this gap.

1.3 Organization of report

Chapter 1 gives general information on the resource scene for petrochemicals and energy and provides the motivation for the present studies, leading up to broad study objectives.

In **Chapter 2,** a detailed literature review on the reaction of interest, glycerol hydrogenolysis to 1,3-propanediol, is reported together with what is known about the reaction mechanism, homogeneous/heterogeneous catalysts reported, and the current level of understanding of how they function. The chapter concludes with a summary of gaps in the literature, based on which the present study is planned.

Chapter 3 describes the experimental setups and procedures employed for characterization of the synthesized catalysts, glycerol acetalization and hydrogenolysis reaction, product analysis, and calculations.

Chapter 4 details the catalyst structure, characterization studies and attempts to correlate the catalyst composition with characteristics essential for the desired function.

In **Chapter 5,** the kinetic studies on different synthesized catalysts are described.

Chapter 6 discusses the effect of different reaction parameters on glycerol hydrogenolysis over best-performing catalysts.

Chapter 7 presents the kinetic modeling and parameter estimation for the Pt-0.3STA/β-zeolite catalyst.

Chapter 8 emphasizes the new approaches for converting glycerol to 1,3-PDO via glycerol's terminal hydroxyl group protection.

Chapter 9 summarizes the conclusion of the present work and future directions.

Chapter 2: LITERATURE REVIEW

It is clear from the introduction that glycerol hydrogenolysis is a complex reaction. The reaction contains at least two steps, which are dehydration and hydrogenation, for making propanediols. In the case of catalytic hydrogenolysis, a catalyst should therefore have bifunctionality, like sites for dehydration and sites for hydrogenation. There has been considerable research on homogeneous and heterogeneous catalysts for glycerol hydrogenolysis to 1,3-PDO. In this review, we will study which are the factors responsible for converting glycerol to 1,3-PDO from catalyst design and reaction aspects. This will help us in designing a new catalyst for glycerol hydrogenolysis. Simultaneously, reaction conditions will help us perform a reaction with higher selectivity towards 1,3-PDO. The following section shows the various catalyst used for glycerol hydrogenolysis to 1,3-PDO, their limitations, and scope for improvement.

2.1 Homogeneous Catalysts

Some homogeneous catalysts appear to possess some activity towards the conversion of glycerol to 1,3-PDO. As the catalyst should have both the functionalities (metal for hydrogenation and acid for dehydration), a single species may not be effective; hence, many researchers have used homogeneous catalyst complexes. Researchers from Celanese Corporation patented the use of a homogeneous catalyst for the hydrogenolysis of glycerol in 1985. The authors developed a reaction with a homogeneous rhodium complex [$Rh(CO)_2(acac)$] catalyst in a 1-methyl-2-pyrrolidinone solvent with tungstic acid (H_2WO_4) as a promoter at 200 °C and 320 bar syngas pressure. The obtained yield of 1,3-PDO was 21.0% [42]. When syngas was replaced by hydrogen gas, then the yield of 1,3-PDO dropped slightly. Further, when H_2SO_4 replaced H_2WO_4, then no propanediols or propanols were detected. It indicates that H_2WO_4 plays an important role than just being a protic acid. Moreover, the catalytic performance depends on the amount of H_2WO_4 used. If its amount is doubled, it significantly reduces the catalyst activity, and the observed yield is reduced by $1/3^{rd}$.

Shell oil company patented a homogeneous Pd complex as a catalyst with water or sulfolane as a solvent in 1998. The reaction conditions were 140 °C and 60 bar syngas pressure. After 10 hr of reaction, the selectivity of 1,3-propanediol was 30.8% [43]. Schlaf et al. has reported the

deoxygenation reaction of glycerol on homogeneous ruthenium complex catalyst in sulfolane solvent at 110 °C temperature and 52 bar H_2 pressure. The yield of 1,3-PDO in this process was less than 5% [44].

The reported catalytic systems may have converted glycerol to 1,3-PDO. However, the use of a homogeneous catalyst is not viable from an economic or industrial perspective. Moreover, the use of organic solvents like sulfolane or 1-methyl-2-pyrrolidinone is undesirable from an environmental perspective. Therefore, the emphasis has shifted towards designing a heterogeneous catalyst for glycerol hydrogenolysis. The following section describes the literature on heterogeneous catalysts which are active for glycerol hydrogenolysis to propanediols.

2.2 Heterogeneous Catalysts

Before discussing different heterogeneous catalysts reported for glycerol hydrogenolysis, it is important to understand the reaction mechanism on a catalyst surface to convert glycerol to 1,3-PDO or 1,2-PDO. This will narrow down the literature search and help us focus only on those catalysts that possess features crucial to 1,3-PDO synthesis.

The most widely reported reaction mechanism for glycerol hydrogenolysis to propanediols is dehydration, followed by the hydrogenation reaction mechanism, as shown in Figure 2.1. In this reaction mechanism, the nature of acidic sites on the catalyst's surface decides the product selectivity among propanediols. This is interesting and important as well while designing a catalytic material. In this mechanism, a Brønsted acidic site can protonate either 1° or 2° ―OH group of glycerol; 2° ―OH group of glycerol possesses higher steric hindrance. The protonation of the 2° ―OH group of glycerol generates 2° carbocation, which is more stable than the 1° carbocation. The 2° carbocation will lead to 3-hydroxypropanal (3-HyPA). Here, it should be noted that 3-HyPA is thermodynamically unstable; however, its formation is kinetically favored over the formation of hydroxyacetone. Hence, the reaction proceeds via 2° ―OH group protonation followed by dehydration to form a highly unstable 3-HyPA intermediate which will be hydrogenated on metallic sites to 1,3-PDO. On the other hand, Lewis acid sites of a catalyst contain empty orbital to accommodate the lone pair of electrons either from 1° or 2° ―OH group of glycerol by covalent bond coordination. However, the covalent bond forms with less steric hindered 1° ―OH group rather than with 2° ―OH group.

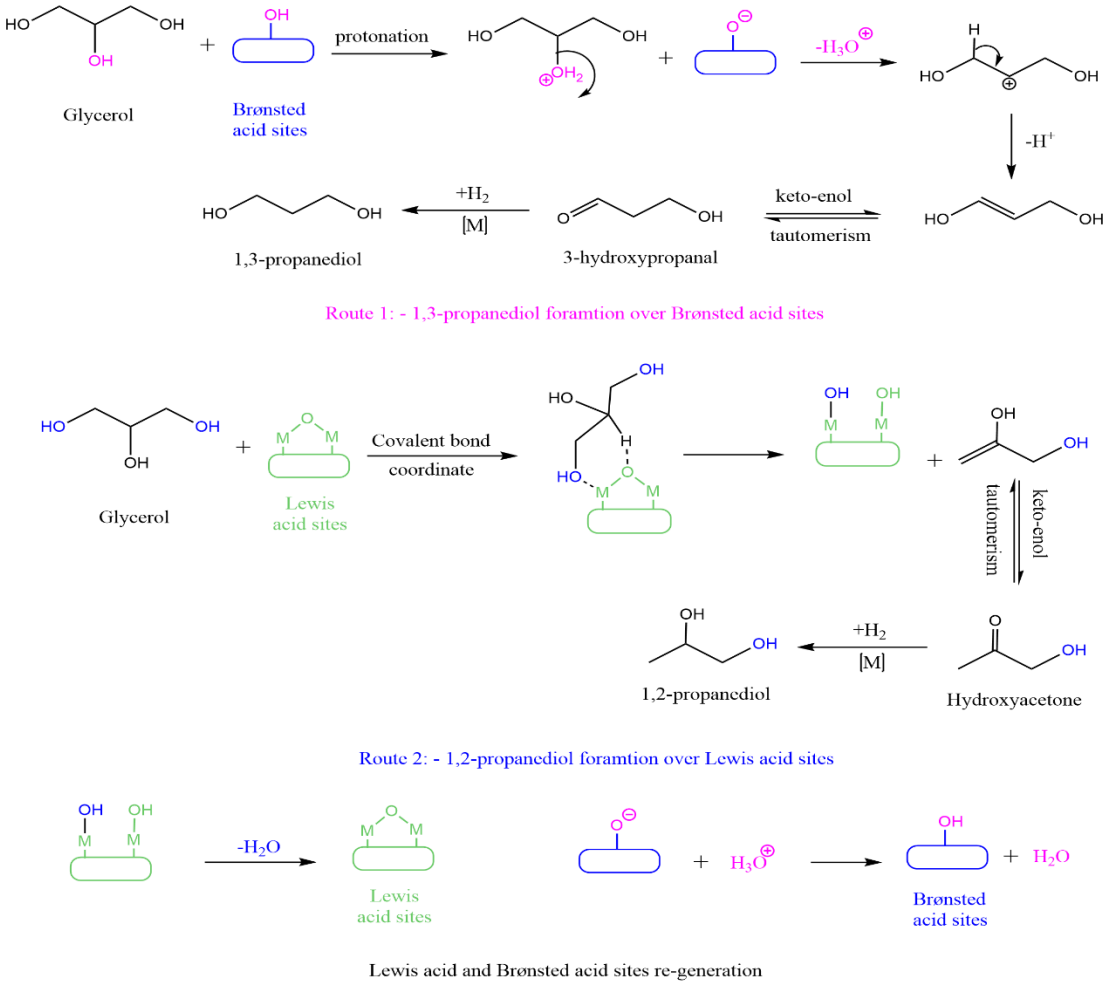

Figure 2.1. Selective formation of propanediols directed by the nature of acid sites

Hence, the covalent bond with the 1° —OH group continues, followed by dehydration, which results in acetol or hydroxyacetone forming 1,2-PDO on hydrogenation (Figure 2.1). Finally, the Lewis and Brønsted acid sites will be re-generated. The re-generation of the Brønsted acid site occurs via the interaction of H_3O^+ ions with its conjugate base. In contrast, the regeneration of Lewis acid sites occurs via thermal dehydration of their hydrated forms [45]. This mechanism shows that a catalyst should have a Brønsted acidic site to form 1,3-PDO from glycerol. Moreover, heterogeneous catalysts have their advantages over homogeneous catalysts. There has been considerable research on heterogeneous catalysts for glycerol hydrogenolysis. We will briefly describe them in the following section.

2.2.1 Catalysts for 1,2-PDO synthesis

Supported catalysts with Noble metals (Pt, Pd, Rh, Ir, Re) and non-noble metals (Zr, Zn, Cu, Ni) have been studied extensively for the hydrogenolysis of glycerol [46–50]. The non-noble

metals were found to be selective for the hydrogenolysis of glycerol to 1,2-PDO [22,39,51]. The copper (Cu) and nickel (Ni) metals were reported to be more active and selective towards 1,2-PDO synthesis from glycerol. Cu based catalytic system yielded nearly 90% 1,2-PDO [52,53]. However, Ni-based catalysts were a little less selective towards 1,2-PDO due to affinity towards ethylene glycol formation via C–C dissociation [54,55]. Cu and Ni-containing catalysts can be used either in batch mode or continuous mode. The continuous mode is superior from a practical point of view. Now the catalyst development for 1,2-PDO synthesis from glycerol has been shifted from high yield to long catalyst life and the resistance to the impurity of glycerol [56] because glycerol purification is a costly process [57]. The better support and Cu interaction or use of a good promotor can increase the life of Cu in a catalyst.

The use of a non-aqueous reaction medium is also found to be effective in increasing catalyst life [58]. In one case, it was found that the use of rare-earth metal additives helped increase the catalyst performance [59]. In another case, catalyst Cu/SiO_2 prepared via hydrothermal method was reported to have a longer life, here stronger interaction between Cu and SiO_2 support increases the catalyst life [60].

While the 1,2-PDO formation from glycerol is easy and doesn't require any special catalytic material/metal for its synthesis, the synthesis of 1,3-PDO from glycerol is complicated and challenging. Moreover, it also requires the catalyst to possess some unique features like a high ratio of Brønsted to Lewis acidity, sufficient surface area, non-leaching catalytic components, etc. As stated earlier, various noble metals were reported to be active for the hydrogenolysis of glycerol to 1,3-PDO. However, only two catalytic systems have effectively converted glycerol to 1,3-PDO. Those are catalysts containing Ir-ReOx and containing Pt-WOx catalytic systems. We will briefly discuss the results observed over these catalysts together with some other catalysts.

2.2.2 Catalysts for 1,3-PDO synthesis

Chaminand et al. [46] have used Rh/C catalyst together with H_2WO_4 in water or sulfolane, or dioxane. Their best results were with sulfolane as a 4% 1,3-PDO yield. Oh et al. [47] have reported a 55.6% yield of 1,3-PDO over Pt-sulfated ZrO_2 catalyst in DMI solvent. Despite the good yield of 1,3-PDO reported by Oh, the use of organic solvents can be a problem. Moreover, Gong et al. [61] reported that protic solvents like water and ethanol favor the formation of 1,3-PDO compared to aprotic solvents like DMI and sulfolane during glycerol hydrogenolysis. Ethanol and/or methanol are the organic products of glycerol hydrogenolysis;

hence choosing them as a solvent may affect the analysis of the reaction. Water is the most common protic solvent, and it doesn't affect the reaction analysis. Therefore, glycerol hydrogenolysis in water over a heterogeneous catalyst would be preferable industrially and environmentally.

a) Ir-ReOx containing catalytic systems

Tomishige's group has reported the broadest work over a catalyst containing Ir and ReOx [48,62–66]. Nakagawa et al. [48] first reported work on Ir–ReOx/SiO_2 catalyst in 2010. The work shows that the catalyst is most effective for glycerol hydrogenolysis to 1,3-PDO over Re-containing catalysts. The authors tried different noble metals like Ir, Pd, Pt, Ru, and Rh catalysts. Ir–ReOx/SiO_2 catalyst showed the highest selectivity for 1,3-PDO. The maximum yield of 1,3-PDO was 38% with 81% glycerol conversion after 36 h. Moreover, Rh–ReOx/SiO_2 catalyst showed comparable activity, and the rest showed lower activity. However, Rh–ReOx/SiO_2 showed lower selectivity for 1,3-PDO. Furthermore, monometallic catalysts like Ir/SiO_2 or ReOx/SiO_2 were totally inactive for glycerol hydrogenolysis. Here, the reaction conditions used were: catalyst 150 mg, 31 µmol Ir, 4 g glycerol, 1 g water, sulfuric acid (H^+/Ir = 1), 80 bar H_2, and 120 °C. In the other study from the same group over Ir–ReOx/SiO_2 catalyst [63], the authors varied the catalyst's Re/Ir mole ratio. The results show, with no Re in the catalyst (Ir/SiO2 the glycerol conversion is zero. With an increase in Re amount in the catalyst, the glycerol conversion was increased till Re/Ir ratio 2; beyond this ratio, the glycerol conversion drops. However, the selectivity of 1,3-PDO remains unchanged except for high Re amounts, where it slightly decreased. The results show a decrease in average Ir particle size with an increase in Re amount. Moreover, the characterization results suggest that the ReOx cluster partially covers the Ir surface, and the Re amount increases the number of Ir–Re pairs (see Figure 2.2). The authors claim that these pairs may be acting as an active site for glycerol hydrogenolysis.

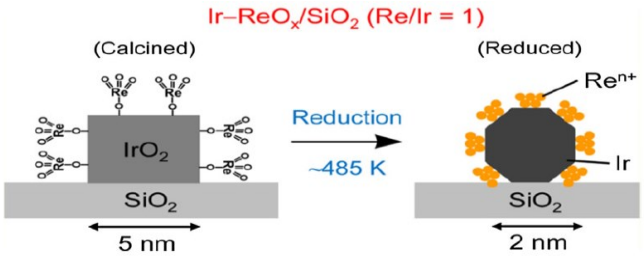

Figure 2.2. Structure of Ir–ReOx/SiO_2 catalyst under reductive conditions (reproduced with permission, [65]**).**

This was the first group that proposed the direct hydrogenolysis of glycerol [65] reaction mechanism over the Ir-ReOx/SiO_2 catalyst (see Figure 2.3). Here, a molecule of glycerol adsorbs over the surface of ReOx and forms metal alkoxide. Meanwhile, the hydride-like species get activated on the Ir metal, which attacks the 2-position of the alkoxide and breaks the C–O bond. The hydrolysis of this reduced alkoxide releases the product.

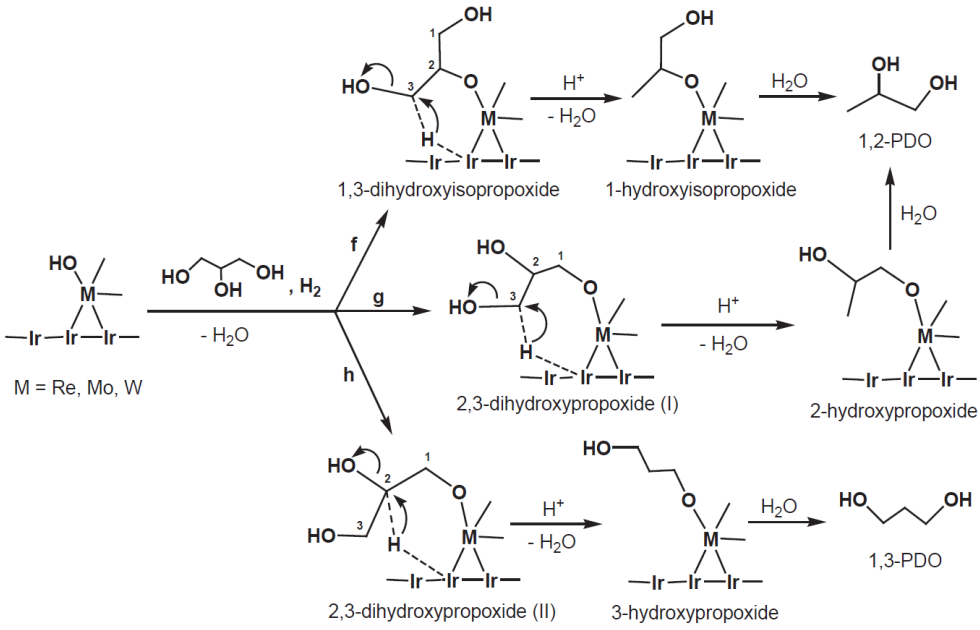

Figure 2.3. Direct hydrogenolysis of glycerol to propanediols over Ir–MOx/SiO_2 catalyst (reproduced with permission, [67]**).**

In this process, the adsorption of glycerol can result in two types of alkoxides, *viz.* 2,3-dihydroxypropoxide (the terminal alkoxide) or 1,3-dihydroxyisopropoxide (the internal alkoxide). If 1,3-dihydroxyisopropoxide or 2,3-dihydroxypropoxide (I) (7 membered-ring) structure forms, it will lead to 1,2-PDO. Whereas, if 2,3-dihydroxypropoxide (II) (6 membered-ring) forms, then it will produce 1,3-PDO. Here, the cleavage of the 2° C–O bond is favored over 1° because 6-membered-ring transition states are more stable than 7-membered-ring transition states. This reaction mechanism appears more plausible than the dehydration-hydrogenation reaction mechanism (see Figure 2.1) because it combines the oxophilic nature of Re and the interface with Ir (Re-Ir bonding). However, the 6-membered-ring transitional structure is difficult to detect by experiment. Similarly, the catalyst Rh–ReOx/SiO_2 is also active for C–O hydrogenolysis. It is similar in many aspects to Ir–ReOx/SiO_2 like kinetics, suitable reaction conditions, catalyst structure, substrate, and proposed reaction mechanism [64,68,69]. However, it largely produces 1,2-PDO than 1,3-PDO from glycerol [70–72].

Though the catalyst looks attractive and produces 1,3-PDO with high selectivity, the leaching of active metals like Ir and Re compromises the stability of these catalysts [48,62]. Therefore, a robust and stronger Pt-WO_x based catalytic system appears to be a better option for glycerol hydrogenolysis to 1,3-PDO [73–75].

b) Pt-WOx containing catalytic systems

In comparison to Ir-ReOx based catalytic system, the Pt-WOx based catalytic system seems more attractive from a practical point of view, perhaps due to the low cost of W, being active without adding any liquid acid (e.g., H_2SO_4), as well as tunability by using a variety of supports. Moreover, Ir-ReOx and Pt-WOx based catalysts have different structures. Ir-ReOx is featured with 3D ReOx clusters decorated on the surface of Ir NPs, while the Pt-WOx is typically in the form of Pt NPs on the 2D WOx sub-monolayers. Moreover, the Ir-ReOx catalysts are active at lower temperatures (120 ºC) than Pt-WOx catalysts (160–180 °C). Table 2.1 summarizes the yield of 1,3-PDO reported over different catalysts; moreover, the following section briefly discussed the various Pt-WOx catalytic systems for glycerol hydrogenolysis to 1,3-PDO.

c) Polyoxometalates containing catalysts

The polyoxometalates (POMs) are a polyatomic ion, mostly an anion, consisting of 3 or more transition metal oxyanions linked by shared oxygen atoms to form closed 3-D frameworks. POMs are widely preferred in catalysis due to their chemical properties like acidities, redox potentials, and solubility, which can be adjusted by selecting the elemental composition and counter cations [76,77]. Acid-type POMs are soluble in polar solvents or water; hence they can be used as homogeneous catalysts. Heteropolyacids (HPAs), also known as POMs, are early transition metal-oxygen anion clusters that exhibit a broad range of compositions, molecular sizes, and architectures [78]. HPAs with Keggin type structures are known to be environment-friendly and economically feasible solid acids [79]. Various types of HPAs were used as catalysts, among them phosphotungstic acid (HPW), silicotungstic acid (HSiW), and phosphomolybdic acid (HPMo) was widely used because of their high catalytic activity [45,80–84].

Dam et al. [85] studied the effect of acidic additives over commercially available Pd/SiO_2, Pd/Al_2O_3, Pt/SiO_2, and Pt/Al_2O_3 catalysts in water at 40 bar H_2 and 200 °C. The acidic additives were phosphotungstic acid (HPW), silicotungstic acid (HSiW), tungstic acid (H_2WO_4), and hydrochloric acid. The results (see Figure 2.4) show that the Pt-based catalyst and tungstic additives were active for producing 1,3-PDO with 20 to 40% selectivity, and hydrochloric acid

was less active. When Pd was used as an active metal, the main products were 1-PrOH or/and 1,2-PDO. The types of tungstic additive or catalyst support showed limited influence on the selectivity trend.

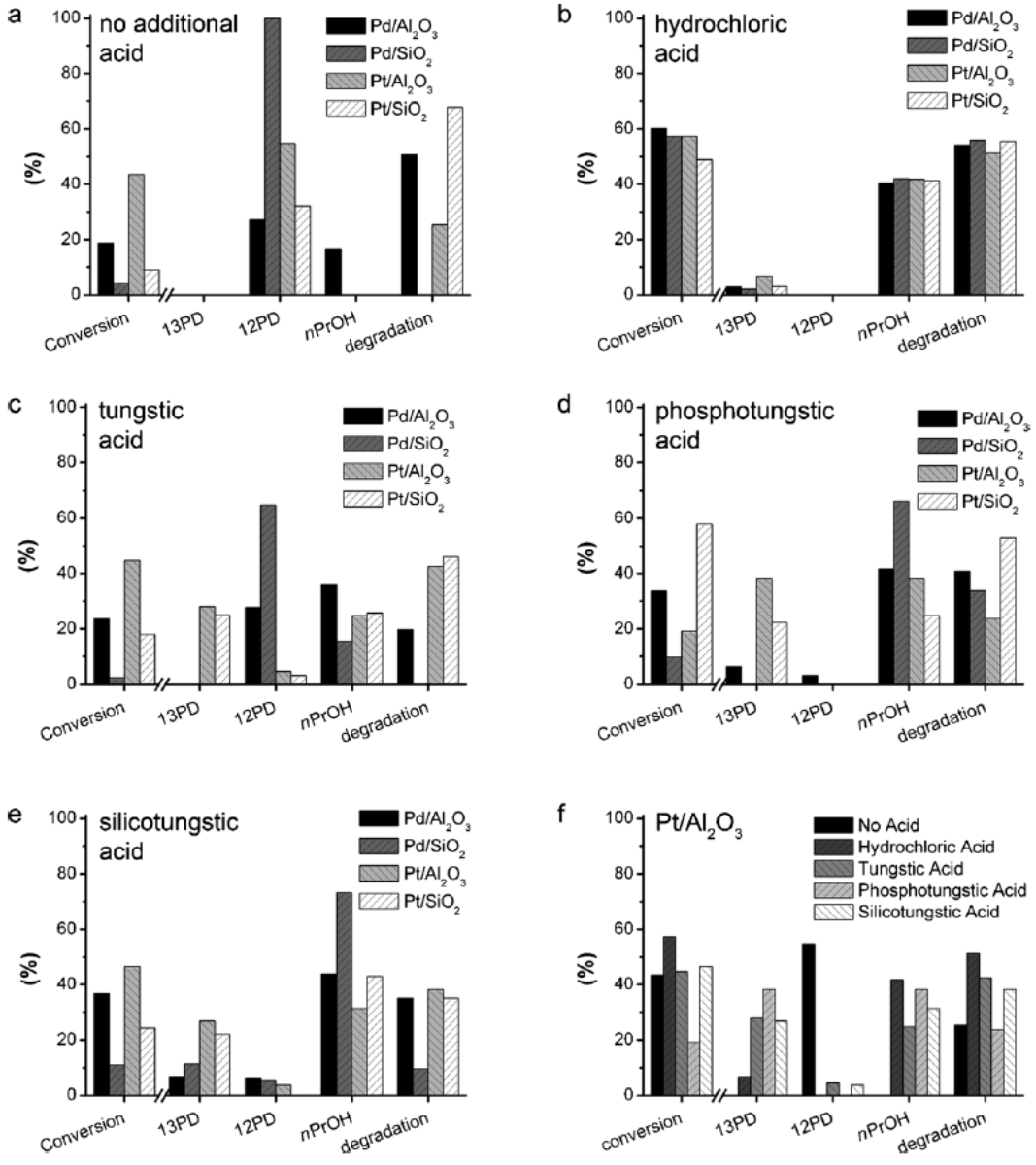

Figure 2.4. Effects of tungsten compounds addition on Pd/Pt-based catalysts. Conditions: active metal (5 mmol), 100 mM aqueous glycerol (5 mL), additive (HCl, pH 1.5; H_2WO_4, 40 mM; polyacid: 3.5 mM), H_2 (40 bar), 200 °C, 18 h (reproduced with permission, [85]**).**

Table 2.1. Pt-WOx/supported and Pt-WOx catalysts for glycerol hydrogenolysis to 1,3-PDO

S.N.	Catalyst	T [°C]	P [bar]	Time / WHSV	X (%)	$S_{1,3\text{-PDO}}$ [%]	$Y_{1,3\text{-PDO}}$ [%]	Reference
1	$Rh/C+H_2WO_4$	180	80	168 h	32	12	3.8	[46]
2	$Pt/m\text{-}WO_3$	180	55	12 h	18	39.2	7.1	[86]
3	Pt/WOx	140	10	12 h	59.8	36.3	21.7	[87]
4	AuPt/WOx	140	10	12 h	81.4	51.6	42	[75]
5	La/Pt/WOx	140	10	1 h^{-1}	39.9	41.3	16.5	[88]
6	$Pt/Au/WO_3$	155	55	7.5 h	30.7	54.3	16.7	[89]
7	Pt/Nb-WOx	160	50	12 h	40.3	27.5	11.1	[90]
8	$Pt/H\text{-}WO_3$	160	50	12 h	63.8	43.1	27.5	[91]
9	Pt/Al_2O_3+HSiW	200	40	18 h	49	28	13.7	[85]
10	$Pt\text{-}HSiW/SiO_2$	200	60	0.045 h^{-1}	81.2	38.7	31.4	[92]
11	$Pt\text{-}HSiW/ZrO_2$	180	50	0.09 h^{-1}	24.1	48.1	11.3	[93]
12	$Pt\text{-}LiHSiW/ZrO_2$	180	50	0.09 h^{-1}	43.5	53.6	23.3	[94]
13	$Pt\text{-}HSiW/mAl_2O_3$	200	40	15 h	60.5	33.3	20.1	[95]
14	$Cu\text{-}HSiW/SiO_2$	210	5.4	0.08 h^{-1}	83.4	32.1	26.8	[96]
15	Pt/W-SBA-15	150	40	30 h	86.8	70.8	61.5	[97]
16	$Pt/WO_3\text{-}Al_2O_3\text{-}SiO_2$	160	60	12 h	48	56	27	[98]
17	$Pt\text{-}WO_3$/SBA-15	210	1	1.02 h^{-1}	86	42	36	[99]
18	$Pt\text{-}WOx/SiO_2$	210	--	50 h	42.6	25.8	11	[100]
19	$Pt\text{-}WOx/SiO_2$	140	80	30 h	100	57	57	[101]
20	WPt/SiO_2	160	80	18 h	64.2	57.2	36.7	[102]
21	Pt-WOx/SAPO-34	210	1	50 h	48	18.8	9	[103]
22	$Pt\text{-}WOx/SiO_2\text{-}Al_2O_3$	210	1	50 h	53	24.3	12.8	[104]
23	$Pt/WO_3/TiO_2/SiO_2$	180	55	12 h	15.3	50.5	7.7	[105]
24	$Pt/WO_3/ZrO_2$	170	80	18 h	85.8	28.2	24.2	[73]
25	$Pt/WO_3/ZrO_2$	170	55	12 h	31.6	34.9	11	[61]
26	$Pt/WO_3/ZrO_2$	130	40	24 h	70.2	45.6	32	[106]
27	$Pt/WO_3/ZrO_2$	180	80	50 h	77.7	21.9	23.1	[107]
28	$Pt\text{-}WOx/t\text{-}ZrO_2$	140	80	24 h	78.3	64.8	49.4	[108]
29	$Pt/WOx/SiO_2\text{-}ZrO_2$	180	50	1 to 3 h^{-1}	54.3	52	28.2	[109]
30	$Pt/WO_3/Al_2O_3$	180	50	1 h^{-1}	57.5	40.4	23.2	[110]
31	$Pt/WOx/Al_2O_3$	220	45	24 h	60.3	31.2	18.8	[111]
32	$Pt/WOx/Al_2O_3$	260	1	0.14 h^{-1}	>99	14	14	[112]
33	$Pt/WOx/Al_2O_3$	200	45	16 h	80.3	38.5	30.9	[113]
34	Pt/WOx/AlOOH	180	50	12 h	100	66	66	[74]
35	$Pt\text{-}WOx/Al_2O_3$	160	50	0.09 h^{-1}	64.2	66.1	42.4	[114]

36	Pt-WOx/Al_2O_3	200	25	16 h	59.4	55.9	33	[115]
37	Pt/ZrW38Mn3	180	55	18 h	56.2	45	25.3	[116]

This work showed the mixture of noble metal and tungsten species is effective in forming 1,3-PDO from glycerol. However, the use of homogeneous additives in the reaction mixture is not preferred practically. Moreover, it is easy to find the interaction between HPAs and active metals in heterogeneous catalytic systems. Therefore, heterogeneous catalysts containing both POMs and active metals have been studied by various researchers.

d) Heterogeneous catalysts with active metal and POMs

Zhu et al. [96] studied the vapor-phase glycerol hydrogenolysis over a Cu-HSiW/SiO_2 catalyst prepared via incipient wetness impregnation in a fixed-bed reactor. The glycerol conversion and product selectivities showed dependence on the reaction temperature, H_2 pressure, initial water content, and space velocity. The presence of water showed a decrease in both activities and 1,3-PDO selectivity over Cu–HSiW/SiO_2 catalyst. At optimized conditions (210 °C, 5.4 bar H_2, and no water), the conversion and 1,3PDO selectivity reached 83.4% and 32.1%, respectively. Afterward, the same group reported a study using aqueous phase glycerol on Pt–HSiW/SiO_2 catalyst [92]. The catalyst was prepared using the same technique, and the reaction was studied with the same conditions and reactor. The characterization results, like Raman spectroscopy, showed the presence of Keggin structure, XRD patterns showed a reduction in the Pt peaks with an increase in HSiW amount in a catalyst. CO chemisorption result shows an increasing and decreasing trend in Pt dispersion with the increase in HSiW amount. Py-FTIR results show an increase in acid sites, especially Brønsted acid sites in a catalyst with an increase in HSiW amount. Under the reaction condition where Cu–HSiW/SiO_2 catalyst showed 9.1% glycerol conversion with 8.9% 1,3-PDO selectivity, the Pt–HSiW/SiO_2 catalyst showed 81.2% conversion and 38.7% selectivity. The maximum glycerol conversion and 1,3-PDO selectivity were observed at 15% HSiW loading. Here, the glycerol conversion and 1,3-PDO selectivity significantly depended on temperature, H_2 pressure, and space velocity. The same group published a study on glycerol hydrogenolysis to propanols (1 and 2) over Pt–HSiW/ZrO_2. Under the optimized condition (200 °C, 50 bar H_2), the maximum yield of propanol was 94.1%. The catalyst showed 160 h long performance. Although the study focuses on synthesizing propanols, 1,3-PDO selectivity and glycerol conversion were 40% and 60%, respectively, at 160 °C. The Raman spectra of fresh and spent catalyst showed $SiW_{12}O_{40}^{4-}$

(950–1020 cm^{-1}) bands, signifying that the Keggin structure was remained intact even after the reaction run (see Figure 2.5). Moreover, the XRD and CO adsorption results of fresh and spent catalysts verified that the Pt particles on ZrO_2 support had no remarkable agglomeration. The strong interaction between acidic sites HSiW and weakly basic sites of the ZrO_2 support would be the reason for the good stability of Pt–HSiW/ZrO_2 catalyst. The catalyst Pt–HSiW/ZrO_2 performance was further improved by modifying it with alkali metals [94]. Alkali metals like K, Li, Cs, and Rb were doped into Pt–HSiW/ZrO_2 catalyst using an alkali nitrate precursor by an ion-exchange technique. The ratio of alkali metal to HPAs was set to 2. The Pt–LiHSiW/ZrO_2 catalyst showed 43.5% glycerol conversion with 53.6% 1,3-PDO selectivity at 180 °C. The authors stressed that the modification effect with Li includes adjusting the acidity and improving the tolerance to water solvent.

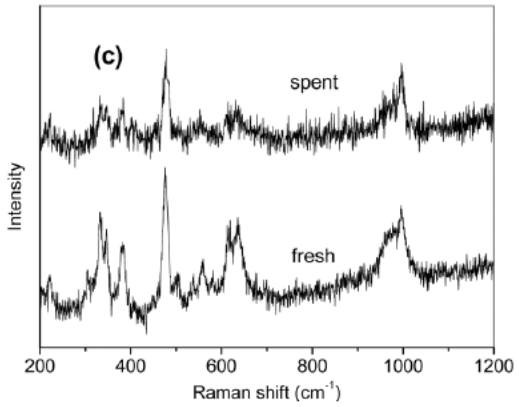

Figure 2.5. Raman spectra of fresh and spent Pt–HSiW/ZrO_2 catalysts (reproduced with permission, [117]**).**

Alhanash et al. [117] reported the use of acid-type polyoxometalate for glycerol hydrogenolysis. The author prepared Rh and Ru supported $Cs_{2.5}H_{0.5}PW_{12}O_{40}$ (CsPW) catalyst. CsPW is a well-known water-insoluble strong Brønsted acid salt with a large surface area (~100 m^2 g^{-1}) and good thermal stability. The catalysts were prepared using the impregnation technique with CsPW and metal chloride solution. The results show high selectivity for 1,2-PDO, while 1,3-PDO was observed only over Rh/CsPW catalyst with 7.1% selectivity. Rapid catalyst deactivation was also observed, which was explained by loss of acidity from tungsten (VI) reduction in the POMs. The authors claim that the deactivation of catalyst can be overcome by using a more stable polyoxometalate such as $SiW_{12}O_{40}^{4-}$.

From the preceding discussion, it is clear that both H_2WO_4 and tungsten HPAs can convert glycerol to 1,3-PDO. However, HPAs as a constituent of heterogeneous catalysts can yield

more 1,3-PDO than soluble tungsten catalysts. In addition to the HPAs acidity, the ratio of active metal like Ru, Rh, Pt to W atom is overlooked. This is one of the key parameters which affects the 1,3-PDO formation rates. Furthermore, the homogeneous mixture of tungstic acid or tungsten HPAs is difficult to recover and reuse. Even if HPAs were supported over some oxide supports, a risk of HPA leaching remains during the hydrothermal reactions. Good interaction between support and HPAs is required, or more robust Pt-WOx catalysts are required.

e) Supported Pt-WOx catalysts

A broad range of supported Pt-WOx catalysts has been reported for glycerol hydrogenolysis due to their robustness, tunable acidity, and improved Pt-WOx interactions. Kurosaka et al. [73] studied the glycerol hydrogenolysis over Pt/WO_3 supported on different oxide supports, including SiO_2-Al_2O_3, Al-MCM-41, Al_2O_3, HY zeolite, anatase TiO_2, and ZrO_2 in 1,3-dimethyl-2-imidazolidinone (DMI) solvent. The $Pt/WO_3/ZrO_2$ catalyst showed the highest 1,3-PDO yield (24.2%) and glycerol conversion (85.8%). The superior performance of $Pt/WO_3/ZrO_2$ catalyst over other catalysts does not seem conclusive due to the absence of in-depth characterizations of the catalyst. Qin et al. [118] investigated $Pt/WO_3/ZrO_2$ performance for aqueous phase glycerol hydrogenolysis. Their results showed glycerol conversion of 70.2% with 45.6% 1,3-PDO selectivity at 130 °C and 40 bar H_2 pressure over a catalyst with 10 wt% W and 3 wt% Pt loadings. Therefore, the two studies discussed above show a considerable difference in the performances of the same catalyst $Pt/WO_3/ZrO_2$. This is partly because of the solvent effect; the two groups in their studies used different solvents. Gong et al. [61] studied the effect of different solvents for glycerol hydrogenolysis over $Pt/WO_3/ZrO_2$ catalyst. Their results show that the selectivity of 1,3-PDO was higher in water than in DMI solvent. More interestingly, when a 1:1 water:DMI mixture was used as a solvent, the yield of 1,3-PDO almost doubled compared to using a single solvent by doubling the amount. Other reasons for the difference in the behavior of the 'same' catalyst in different studies could also be differences in catalyst synthesis technique and the loading of Pt and WOx, both of which were different in the two studies on $Pt/WO3/ZrO_2$ mentioned above. The different loading of the active metals would have resulted in differences in dispersion and interfacial structure. This ultimately leads to variations in activity and selectivity. However, the better performance in protic solvent compared to aprotic solvent cannot be ignored. Gong et al. [105] have also published a study on a series of $Pt/WO_3/TiO_2/SiO_2$ catalysts with different loadings in the hydrogenolysis of aqueous glycerol. The catalyst performance showed a volcano-curve type

dependence on the WO_3 and TiO_2 loading (see Figure 2.6). The acidity characterization results showed that the addition of WO_3 increases the acidity of catalyst in terms of both the number of acid sites (especially Brønsted acid sites) and its acid strength. XRD results of $Pt/WO_3/TiO_2/SiO_2$ catalyst showed no peaks corresponding to Pt, TiO_2, and WO_3, whereas $Pt/WO_3/SiO_2$ and Pt/SiO_2 showed the peaks representing Pt.

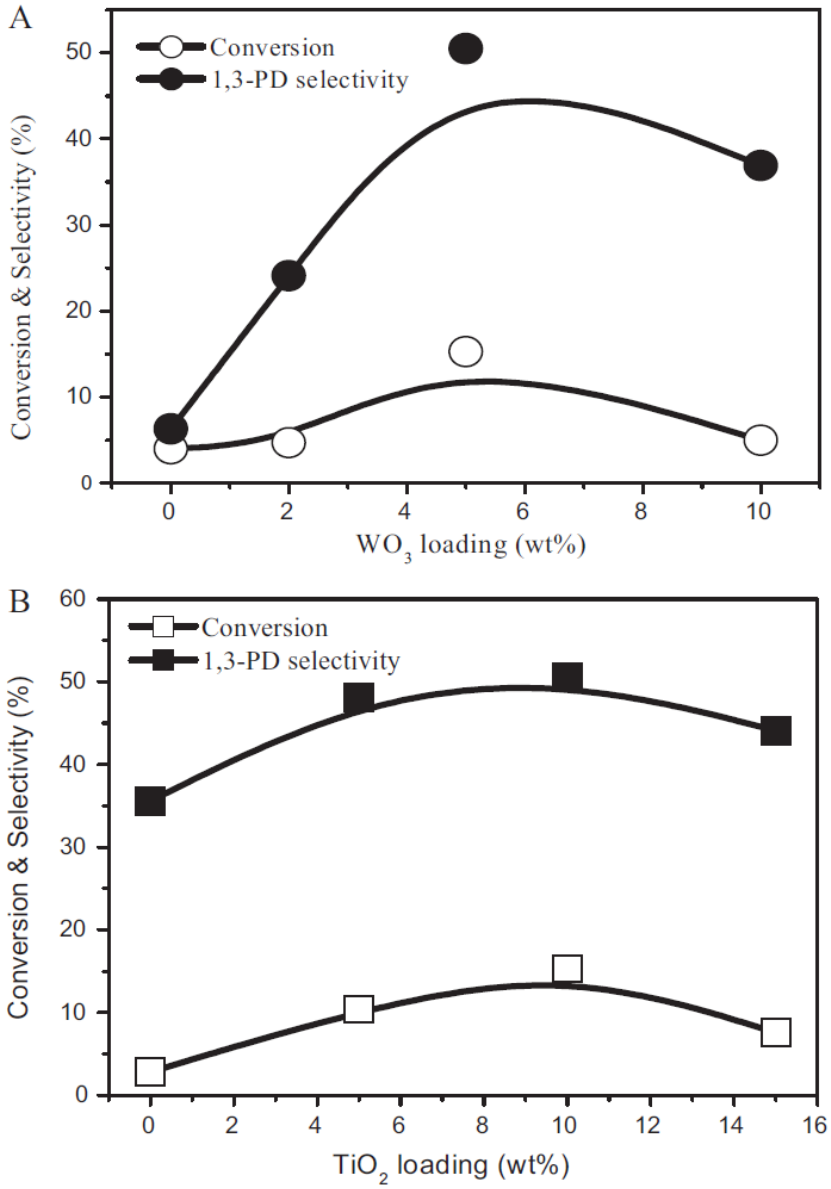

Figure 2.6. Influence of WO_3 (A) and TiO_2 (B) loadings on $Pt/WO_3/TiO_2/SiO_2$ catalysts (reproduced with permission, [105]**).**

Hence, it looks like one of the roles of TiO_2 is to improve the dispersion of Pt in a catalyst. The optimum loadings of WO_3 and TiO_2 were 5% and 10%, respectively. The results show 15.3% glycerol conversion and 50.5% 1,3-PDO selectivity. All the studies reported above show the

requirement of WOx in a catalyst for producing 1,3-PDO from glycerol. The formation of 1,3-PDO requires Brønsted acid sites, and this is closely related to the WOx loading in a catalyst.

Besides $Pt/WO_3/ZrO_2$ or $Pt/WO_3/TiO_2/SiO_2$ catalysts, the combination of Pt, WOx, and Al_2O_3 based supports has been explored extensively. They are found to be some of the most effective catalysts for the hydrogenolysis of glycerol to 1,3-PDO. Suzuki et al. of KAO corporation first patented the use of $5\%Pt\text{-}5\%W/Al_2O_3$ catalyst for glycerol hydrogenolysis [119]. Their result shows 23% conversion of glycerol with 67% 1,3-PDO selectivity at 160 °C and 55 bar H_2 pressure. Arundhathi et al. [74] from the Tomishige group reported the use of boehmite (AlOOH) supported Pt-W catalyst for glycerol hydrogenolysis. The loading of Pt and W was 1.8% and 8%, respectively. This catalyst has the highest glycerol conversion and 1,3-PDO selectivity; the observed glycerol conversion was 100% with 66% 1,3-PDO selectivity at 180 °C and 50 H_2. This is one of the best results reported; the AlOOH surface area was 180 $m^2\ g^{-1}$. When the catalyst was prepared using AlOOH support of lower surface area 56 $m^2\ g^{-1}$, the selectivity of 1,3-PDO was reduced to 37%. The authors have also compared $Pt/WO_3/AlOOH$ catalyst performance with $Pt/WO_3/Al_2O_3$. AlOOH and $\gamma\text{-}Al_2O_3$ were used with the same surface area. The activity and 1,3-PDO selectivity were much lower over $Pt/WO_3/Al_2O_3$ catalyst. However, Uttraporn et al. [120] have reported poor performance of boehmite supported ($Pt/WOx/AlOOH$) catalyst compared to Al_2O_3 supported ($Pt/WOx/\gamma\text{-}Al_2O_3$) catalysts. The authors credited the superior performance of $Pt/WO_3/AlOOH$ catalyst to the number of surface Al-OH species in the catalyst, which was, however, not supported by the data provided; the XRD results contradict the statement. Moreover, the reaction mixture used for the reaction is very small 1 mmol of glycerol (92 mg or 0.073 ml) in 3 ml of water, and the reactor volume was 50 ml. We wonder how the reaction mixture was stirred.

Zhu et al. [114] investigated glycerol hydrogenolysis to 1,3-PDO over $Pt/WOx/Al_2O_3$ catalyst in a fixed-bed reactor. They have studied the effect of an increase in WOx loading from 5 to 20 wt%. The loading of platinum was fixed at 2 wt%. The result shows that when the loading of WOx reached 10 wt%, the catalyst showed maximum activity and selectivity as 64.2% glycerol conversion with 66.1% 1,3-PDO selectivity. The characterization results showed that the increase in WOx content of catalyst increases platinum dispersion, acidity, both Lewis and Brønsted acidity up to 10 wt% WOx. However, a further increase in WOx content slightly reduces the dispersion of Pt and acidity. The authors claim that the 10 wt% loading is the dispersion threshold of WOx. Because at this loading, the WOx would have reached the sub-monolayer coverage. Furthermore, the addition of WOx significantly reduced the reduction

temperature of PtOx, due to the strong electronic interaction between PtOx and WOx species. From the XPS results, it is clear that with the addition of WOx metallic Pt species on the surface had been reduced to zero-valent (Pt^0). The authors claim that over the surface of Al_2O_3 exists an electron donor-acceptor interaction between WOx and Pt^0, where electrons were easily transferred from Pt^0 to WOx species. The high performance of the catalyst was credited to the higher amount of Brønsted acid sites and strong electronic interaction between Pt and WOx species. Over the $Pt/WOx/Al_2O_3$ catalyst, Lei et al. [121] reported the glycerol hydrogenolysis in a fixed-bed reactor and achieved the highest space-time yield of 1,3-PDO (191.7 $mg_{1,3\text{-}PDO}/g_{Cat}.h$) at 180 °C and 50 bar H_2. The glycerol conversion and 1,3-PDO selectivity showed strong dependence on W and Pt loadings. Moreover, the appropriate molar ratio of Pt/W was in the range of 1/2–1/4. The optimum loading of Pt was around 5 wt%, and for W, it was between 10–15 wt%. The authors claim that on the surface of Al_2O_3, the WOx existed as sub-monolayer polytungstates, and metallic Pt was highly dispersed (dispersion > 50%) on WOx, which promoted the in-situ generation of strong Brønsted acid sites *via.* hydrogen dissociation and spillover. This will help in getting 1,3-PDO from glycerol selectively.

García-Fernández et al. [111] showed that the tungsten surface density (W atoms nm^{-2}) could also affect the glycerol hydrogenolysis over $Pt/WO_3/Al_2O_3$ catalyst. The authors claim that the maximum selectivity of 1,3-PDO was achieved at a W loading where highly dispersed highest polytungstate species can be formed. They have found that the tungsten density could control the type of WOx species present on the catalyst, namely monotungstates (coordinated structure: WO_4), polytungstates (coordinated structure: WO_5/WO_6), and WO_3 crystalline nanoparticles. The presence of polytungstates generated a relatively low amount of weak/medium Brønsted sites, which was beneficial for the selective formation of 1,3-PDO from glycerol. The maximum selectivity of 1,3-PDO was obtained as 51.9% with 53.1% glycerol conversion at 200 °C temperature and 45 bar H_2 over 9%Pt-8%WOx/Al_2O_3 catalyst.

Very recently, Liu et al. [101] from the Tomishige group prepared $Pt\text{-}WOx/SiO_2$ catalyst and applied it for glycerol hydrogenolysis. The authors reported the 1,3-PDO yield of 57% at 140 °C at 80 bar H_2 over $Pt\text{-}WOx/SiO_2$ (Pt: 4 wt% and W: 0.94 wt%) catalyst, which was in the highest yield among the reported tungsten-containing catalysts. On the other hand, the use of a similar catalyst with different WOx loading at 210 °C was reported by Shi et al. [122]. However, their results (18.4% conversion with 19.4% 1,3-PDO selectivity) are totally different from what is reported by Liu. Moreover, Liu et al. used 5.1 g of the reaction mixture in 190 ml of the autoclave. We were surprised how the reaction mixture would have been stirred.

f) Mesoporous WOx supported Pt catalysts

WOx usually has a low surface area and is therefore not suitable as support by itself. However, the use of WOx as support leads to direct interaction between WOx and active metal. Longjie et al. [86] prepared a catalyst Pt supported on mesoporous WO_3 (m-WO_3) and studied glycerol hydrogenolysis over it. The m-WO_3 catalyst was prepared using WCl_6 as the precursor and triblock P123 ($EO_{20}PO_{70}EO_{20}$) as the structure-guiding agent. The m-WO_3 has a surface area of 22 m^2 g^{-1}. The XRD and TEM results showed highly dispersed Pt particles on m-WO_3. For comparison, when the catalyst was prepared using commercial WO_3 (c-WO_3), the Pt size of a larger diameter (>10 nm) was observed. The glycerol hydrogenolysis result over Pt/ m-WO_3 was 18% glycerol conversion with 39.3% 1,3-PDO selectivity, whereas the Pt/ c-WO_3 catalyst gave 4.5% glycerol conversion with 29.9% selectivity. The difference in activity and selectivity were credited to high Pt dispersion and good reducibility of Pt/m- WO_3 catalyst. Later the same research group reported a Pt catalyst supported on mesoporous Ti–W oxides [123]. However, the results for activity and 1,3-PDO selectivity of Pt/Ti–W oxide catalyst were similar to those of Pt/m-WO_3 catalyst.

Wang et al. [75,124] developed mesoporous WOx supported Pt and Pt-Au bimetallic catalysts. The mesoporous WOx was prepared with a large surface area (126 m^2g^{-1}) and abundant oxygen vacancies (x = 2.8), which favored the Pt dispersion as pseudo-single atoms. Such high dispersion of Pt gave rise to 37.4% glycerol conversion with 35.1% 1,3-PDO selectivity at 140 °C and 10 bar H_2 [124]. When a small amount of Au was added to the catalyst (Au-Pt/WOx), it has increased the catalytic performance by a great extent in identical conditions [75]. Characterization results showed that the addition of Au facilitated the reduction of WOx species and increased the in-situ generated Brønsted acid sites, thereby improving the catalytic activity and selectivity. Under identical conditions, the glycerol conversion reached 52% glycerol conversion with 56.3% 1,3-PDO selectivity.

g) Zeolite catalyzed glycerol dehydration

Zeolites are microporous aluminosilicate minerals with a negatively charged honeycomb structure. Zeolites are commonly used as industrial catalysts or adsorbents; they occur naturally; however, they are also produced industrially on a large scale. They are expensive compared to metal oxides; however, they possess unique features and a large surface area, which will be very useful in catalytic applications. Protonic zeolite represents the most important family of solid acid catalysts used in the industry [125]. Their unique properties

include thermal stability, high Brønsted acidity, shape selectivity, facile regeneration, and tunable acidity [126,127]. Zeolites were found to be effective for glycerol dehydration and hydrogenolysis due to their versatility.

Kim et al. [128] studied the gas-phase dehydration of glycerol over various H-zeolites in a fixed bed reactor at 315 ºC and atmospheric pressure. The various H-zeolites like H-βzeolite, H-ferrierite, H-mordenite, H-Y, and H- ZSM-5 with variable SiO_2/Al_2O_3 ratio. The results showed that all the zeolites were active for the glycerol dehydration to acrolein. The glycerol conversion was decreased in the following order: silica-alumina > H-β (Si/Al–25) > H-β (Si/Al–27) > γ-Al_2O_3 > H-mordenite (Si/Al–20) > H-ferrierite (Si/Al–55) > H-ferrierite (Si/Al–20) > H-ZSM-5 (Si/Al–23) ~ H-β (Si/Al–350) > H-β (Si/Al–38) ~ H-Y (Si/Al–5.1). Almost all the catalysts produce acrolein in the first 2 h of reaction with a selectivity greater than 40% except for H-Y (29.7%), H-β-38 (33.1%), and H-β-350 (38.8%) zeolites (numbers in parenthesis show acrolein selectivity). H-ferrierite (Si/Al–55) showed the highest selectivity for acrolein as 59%, and H-βzeolite (Si/Al–25) showed the highest glycerol conversion as 76.4%. Despite showing the lowest surface acidity, catalyst H-β (Si/Al–350) (0.08 mmol NH_3/gcat) has shown the higher conversion and higher acrolein selectivity than H-β (Si/Al–38) (0.50 mmol NH_3/gcat) and H-Y (Si/Al–5.1) (0.58 mmol NH_3/gcat). The authors credit the performance of H-β (Si/Al–350) to its higher external surface area (699 m^2g^{-1}) than the H-β (Si/Al–38) catalyst (578 m^2g^{-1}). Authors claim that the external surface area is one of the key factors affecting the glycerol dehydration activity other than the surface acidic sites. Corma et al. [129] reported a study on glycerol dehydration in a moving bed reactor over a ZSM-5 catalyst. Their best acrolein yield was 55–61% at 350ºC. Hoang et al. [130] used the zeolites (H-ZSM-5, H-Y, H-Mordenite, and H-ZSM-22) to convert glycerol to gasoline range alkyl-aromatics. The highest yield of acrolein was observed over HZSM-22 as 86% yield with 100% glycerol conversion at 400 ºC and atmospheric pressure.

h) Different metal-supported zeolite for glycerol hydrogenolysis

The zeolites supported metals like Ni, Ru, Cu, Pt, Zn, Zr, etc., were used as a bifunctional catalyst for glycerol hydrogenolysis to yield valuable products.

Jin et al. [131] have used H-Y zeolite-supported Ru catalysts for glycerol hydrogenolysis. The main product observed was 1,2-PDO with 81.3% selectivity, and the glycerol conversion was 60.1% at 220 ºC and 30 bar H_2. Gallegos-Suarez et al. [132] have used KL-zeolite supported Ru catalysts for glycerol hydrogenolysis at 180 ºC and 80 bar H_2. Their main product was

ethylene glycol with 48% selectivity and 1,2-PDO with 32% selectivity; however, the glycerol conversion was only 7.5%. Lin et al. [133] have used commercial H-β-zeolite (Si/Al = 15.8) and Ni/Al_2O_3 catalyst combinations for glycerol hydrogenolysis to 1-PrOH in a fixed-bed reactor. The glycerol conversion obtained was 89.9%, and the selectivity of 1-PrOH was 60.3% at 220 ºC, 20 bar H_2. Additionally, the selectivity of 1,3-PDO and 1,2-PDO was 2.6% and 3.7%, respectively. The glycerol conversion obtained over Ni/Al_2O_3 catalyst was 60.5%, and the 1-PrOH selectivity was only 0.2%. The addition of βzeolite externally to the Ni/Al_2O_3 catalyst has increased the selectivity of 1-PrOH. Wan et al. [134] have studied the hydrogenolysis of glycerol to 1,3-PDO over IrOx promoted different zeolites at 180 ºC and 80 bar H_2 pressure. Out of them, IrOx/H-ZSM-5 showed the highest selectivity for 1,3-PDO as 55%, followed by SiO_2-Al_2O_3 catalyst with 36.8% selectivity; H-Mordenite has shown 16% 1,3-PDO selectivity.

Kant et al. [50] have studied the glycerol hydrogenolysis over Ni, Cu, Zn, and Zr supported on H-β-zeolite (Si/Al = 25) and over H-β-zeolite catalysts at 200 ºC and 41.4 bar H_2 pressure. The results over the H-β-zeolite catalyst showed glycerol conversion of 85% with 0.2% 1,3-PDO selectivity and 85% 1-PrOH selectivity after 10 h of reaction. The H-β-zeolite has largely converted glycerol to 1-PrOH. When the Zr/H-β-zeolite catalyst was used with similar conditions, the 1-PrOH selectivity was reduced to 64% with 68% glycerol conversion and 4% 1,3-PDO selectivity. When bimetallic Ni-Zr/Hβ-zeolite catalyst was used for glycerol hydrogenolysis, the 1-PrOH selectivity was further reduced to 51% with 77% glycerol conversion, and 1,3-PDO selectivity was increased to 14%. The authors claim that the reduction in the glycerol conversion and 1-PrOH selectivity over Zr/H-β-zeolite or Ni-Zr/H-β-zeolite was due to agglomeration of Zr or Ni-Zr crystallites over H-β-zeolite, which reduces available acid sites (acidity). The reduction in acidity reduces the over hydrogenolysis of propanediols to 1-PrOH and thereby increases the propanediols selectivity.

Priya et al. [135] investigated the vapor phase glycerol hydrogenolysis over H-mordenite supported Pt catalyst at 215 ºC and atmospheric pressure. Their results shows 94.9% glycerol conversion with 48.6% 1,3-PDO selectivity [135]. Later in their other study, the authors prepared Pt-Cu bimetal catalyst supported on H-mordenite and studied the glycerol hydrogenolysis at 210 ºC and 1 bar H_2. The results showed the glycerol conversion of 90% with 58.5% 1,3-PDO selectivity [136]. The other groups have also used H-mordenite for glycerol dehydration [128] and glycerol hydrogenolysis [134]. However, their results show a poorer performance of H-mordenite compared to other catalysts. Moreover, the glycerol

hydrogenolysis to 1,3-PDO is favorable at higher hydrogen pressures [92,96]; at such low pressure getting such a high selectivity of 1,3-PDO is surprising.

i) Zeolite supported Pt-WOx catalysts

Shi et al. [103] reported the hydrogenolysis of glycerol over Pt-WOx/SAPO-34 catalyst at 210 ^{o}C, 60 bar H_2. They have varied WOx loading from 0 to 40 wt%; the best results were observed at a WOx loading of 20 wt%, Pt loading was fixed to 2 wt%. The results showed that after 50 h, the glycerol conversion was reached 48% with 18.8% 1,3-PDO selectivity and 44.1% 1-PrOH selectivity. García-Fernández et al. [115] reported a study on Pt-WOx promoted HZSM-5 catalyst. They have varied WOx loadings as 5%, 15%, 25%, and Pt loading was fixed to 2 wt%. The best results were observed over Pt-15%WOx/H-ZSM5 as 17.3% glycerol conversion with 20.6% 1,3-PDO selectivity and 65% combined selectivity of 1-PrOH and propane.

The literature shows different catalytic systems which are active for glycerol hydrogenolysis to 1,3-PDO. When we tried to reproduce the results reported in the literature, we have not observed any similarities between the reported results and our results (see Table 2.2).

Table 2.2. Hydrogenolysis of glycerol results observed on reported and new catalysts

Catalyst	Reaction Condition	Time (h)	Gly. Conver. (%)	Selectivity (%)			
				1,3-PDO	1,2-PDO	1-PrOH	Others
Pt/WOx	10 bar H_2, 140 ^{o}C	12	3.5	3.21	2.67	47.51	46.61
2Pt-10WOx-γAl_2O_3	50 bar H_2, 180 ^{o}C	16	21.9	0	23.3	6.33	67.24
2Pt-8WOx-AlOOH	40 bar H_2, 180 ^{o}C	12	32	0	45.2	37.83	11.1
2Pt-10WOx-SiO_2	40 bar H_2, 180 ^{o}C	12	28.7	2.4	39.7	41.3	16.6
2Pt-10WOx-ZrO_2	50 bar H_2, 170 ^{o}C	12	29.3	2.9	35.8	44.3	17
3Pt-HZSM5 (30)	40 bar H_2, 215 ^{o}C	12	6.3	0	24.8	59.7	15.5
3Pt-10WOx-HZSM5 (30)	40 bar H_2, 215 ^{o}C	12	9.7	3.7	26.7	50.3	19.3
3Pt-Bzeolite (40)	40 bar H_2, 220 ^{o}C	12	7.3	1.6	18.05	49.1	31.3
3Pt-10WOx-Bzeolite (40)	40 bar H_2, 220 ^{o}C	12	11.4	7.6	16.3	45.7	30.4

2.3 New approaches to converting glycerol to 1,3-PDO

The glycerol hydrogenolysis to 1,3-PDO reaction is complex and leads in general to a mix of different products that necessitate complex product work-up and hence affect the process economics. The catalytic systems look unselective towards 1,3-PDO from glycerol and make several products because of the variable reactivity of –OH groups in glycerol. Hence, protecting the terminal hydroxyl groups of glycerol and performing hydrogenolysis over the protected group looks encouraging.

Wang et al. [26] have introduced a new approach (see Figure 2.7) to increase the selectivity of the glycerol conversion process via selective dehydroxylation. In this method, the glycerol is converted to 1,3–PDO through acetalization of glycerol, tosylation of acetal, and detosyloxylation (detosylation and hydrogenation). The authors mentioned that to increase the selectivity of 1,3–PDO, the terminal hydroxyl group (–OH) was protected (acetal), and the middle hydroxyl group was converted to a strong leaving group (tosylation) followed by removal of tosyl group via catalytic hydrogenolysis (detosyloxylation). The catalyst used for hydrogenolysis was Raney–Ni, and the reaction conditions were H_2 pressure 30 bar and temperature 160 ºC for 24 h. The yield of 1,3–PDO in this process was at most 72%. The authors also provided the economics of the process, considering a 74 % yield of 1,3–PDO. Out of the total raw material cost, 76% results from the cost of tosyl chloride. The major disadvantage of the process is the high raw material cost. This is mainly because of the tosyl chloride. For every kg of 1,3–PDO produced, 3.61 kg of tosyl chloride is required. The reaction time of hydrogenation is relatively high, that is 24 h.

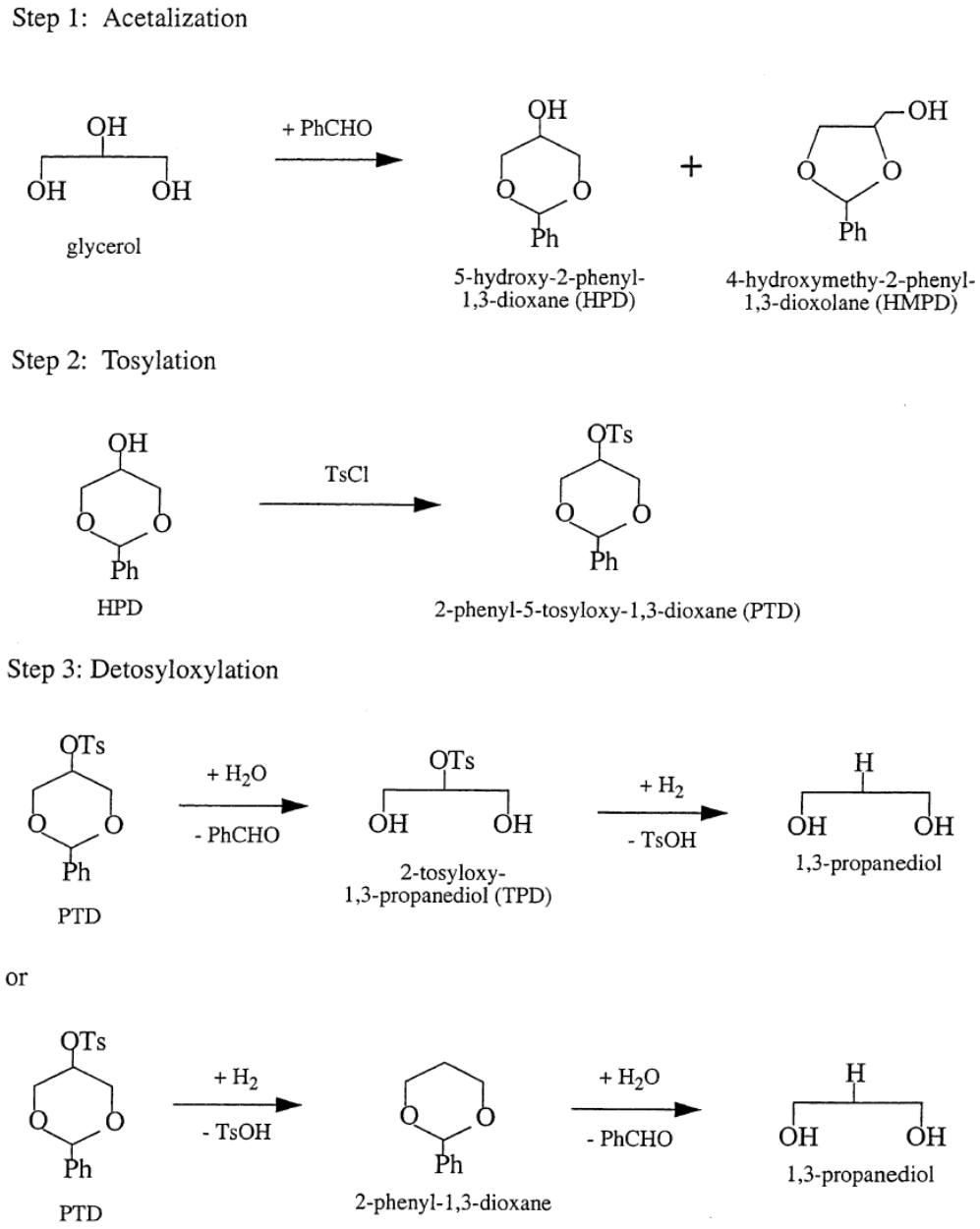

Figure 2.7. Conversion of glycerol to 1,3-PDO via new approach (reproduced with permission, [26]**).**

2.4 Conclusion

The literature shows different catalytic systems which are active for glycerol hydrogenolysis to 1,3-PDO. However, the different group reports different results over the same catalysts, which looks like difficulties in reproducibility from one lab to the other. In most cases, the characterization result contradicts with claims offered by authors. Moreover, in many studies, inadequate characterization of the catalysts was reported. Many studies are on very small scales, and this being a heterogeneous reaction, good mixing is essential to ensure that the results are reproducible and reliable. Furthermore, in most of the cases, adequate details of the reaction apparatus are not provided. The reaction time in most cases is relatively high, which increases the risk of over hydrogenolysis of propanediols. Most studies report a single-point conversion and/or selectivity. It is not clear if what is reported is the best that can be achieved since the reaction network is complex with several series/parallel steps. The catalyst activities were not reported as TOF, which would have allowed a realistic comparison between different catalysts.

Moreover, it is also got cleared from the literature that the catalyst containing simple metals or non-noble metals combined with acid supports (mainly Lewis acid) led to the formation of 1,2–Propanediol. The conversion of glycerol to 1,3–PDO is challenging and requires the presence of Brønsted acid sites. Here, the catalyst acidity is essential for activity (glycerol conversion), whereas Brønsted acidity of a catalyst is important for 1,3-PDO selectivity. Certain elements seem to confer the desired features on the catalyst, such as noble metal (Pt and Ir) combined with WOx, ReOx, SnOx, etc. Heteropolyacids catalysts are considered to be Brønsted acid-type catalysts. Heteropolyacids are always supported on metal oxide to improve their dispersion and surface area. The catalyst support probably has a role in catalysis as well.

On the other hand, literature broadly reports the Pt-WOx catalysts supported on metal oxides. Whereas, very few literature reports are available on the zeolite-supported Pt-WOx catalysts, especially low acidity zeolite (high Si/Al ratio). Therefore, a glycerol hydrogenolysis study over a catalyst containing noble metal Pt, heteropolyacids, and a low acidity zeolite (β-zeolite-300) seems worth investigating.

Chapter 3: EXPERIMENTATION

It is well understood from the literature study (chapter 2) that glycerol hydrogenolysis is a complex reaction with the combination of various series and parallel reactions. Furthermore, the reaction mechanism has provided more insight into the hydrogenolysis of the process, and it is clear that the product selectivity of this reaction is acid sites driven. A catalyst with Lewis acid sites was found to be effective for 1,2-PDO production, whereas 1,3-PDO synthesis requires a catalyst with Brønsted acid sites. Also, noble metals were found to be active for 1,3-PDO, while simple or non-noble metals have produced 1,2-PDO. Therefore, a catalyst with high Brønsted acidity, sufficient total acidity, good surface area, well-dispersed noble metal particles would be useful for 1,3-PDO synthesis. This chapter describes the details of these materials and procedures followed for preparing the effective catalysts. Hence, the catalytic materials and synthesis of catalyst were planned based on these insights. Further, the catalysts prepared were characterized using various techniques, and their performance was assessed in a suitable reactor. The details about catalyst synthesis procedure and catalyst characterization techniques will be discussed in the following sections.

3.1 Materials

Glycerol (99.5%) was supplied by Merck Ltd. India. While, molecular hydrogen of 99.999% purity was sourced from Sunlight Gas, India. The chemicals used in catalyst preparation -- Chloroplatinic acid hexahydrate (99.9%), Tungsten Oxide (99.9%), Ammonium paratungstate (99.99%), Phosphomolybdic acid hydrate (99.9%), Phosphotungstic acid hydrate (RG), Silicotungstic acid hydrate (99.9%) – were all obtained from Sigma-Aldrich USA. The H-beta zeolite (SiO_2/Al_2O_3 = 300), used as catalyst support, was obtained from Zeolyst International USA. Analytical standards and reagents such as n-butanol, 1,3-Propanediol, 1,2-Propanediol, 1-Propanol, 2-Propanol, Ethanol, Methanol, Hydroxyacetone, Acetone, Acrolein, Ethylene glycol, etc. were obtained from Merck Ltd. India.

3.2 Catalyst preparation

The Pt-STA/β-zeolite catalysts were prepared by using the sequential impregnation method; Figure 3.1 A shows the setup used. The obtained β-zeolite powder was calcined in static air with a temperature ramp of 5 °C/min and held for 4 h at 550 ºC. The calcined β-zeolite was impregnated with aqueous solutions containing the desired amounts of silicotungstic acid (STA) *viz.* We have made 0.1 STA to β-zeolite ratio using 5 g β-zeolite and 0.5 g of STA in 50 ml water followed by evaporation at 100 ºC. The formed xSTA/β-zeolite samples were dried at 110ºC for 12 h and further calcined at 450ºC in static air for 4 h.

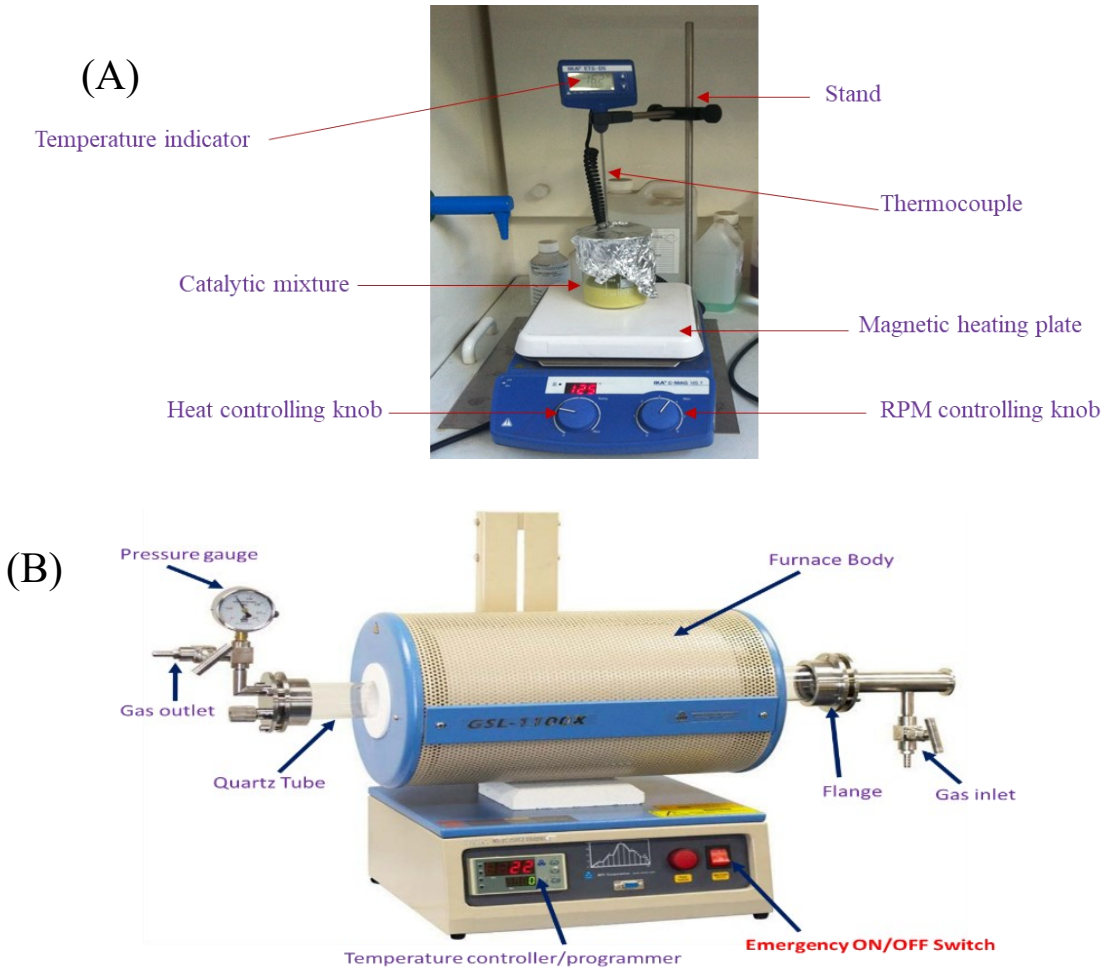

Figure 3.1. (A) Catalyst preparation setup and (B) Calcination and reduction setup

They were then impregnated with an aqueous solution of hexachloroplatinic acid ($H_2PtCl_6 \cdot 6H_2O$). Here, 5 g of 0.3STA/β-zeolite was impregnated with 3.2 ml of 8 wt% hexachloroplatinic acid aqueous solution followed by evaporation at 100 ºC. The impregnated samples were dried at 110ºC for 12 h followed by calcination in static air at 400ºC for 4 h. The

final catalyst was designated as Pt/xSTA/β-zeolite, where x stands for STA to β-zeolite ratio. Table 3.1 represents different catalysts prepared with various STA/HPA to β-zeolite ratios. For comparison, Pt/β-zeolite samples without STA were also prepared by impregnating the calcined β-zeolite with an aqueous solution of $H_2PtCl_6 \cdot 6H_2O$ as per the procedure mentioned before. The loading of platinum (Pt) was fixed at 5wt% in all the catalysts (Entry 1 to 20 in Table 3.1) except for four catalysts, which were prepared with 2.5 and 10 wt% Pt loading to investigate the effect of platinum loading (Entry 21 to 24 in Table 3.1). All the prepared catalysts were reduced in flowing hydrogen at 100 ml/min, at 400°C for 3 h. Figure 3.2 (B) shows the setup used for catalyst reduction.

3.3 Apparatus and Procedure

The experimental setup is shown in Figure 3.2. Glycerol hydrogenolysis was performed in a 100 ml capacity stainless steel batch reactor (Amar Equipment Pvt. Ltd.). The reactor is equipped with a magnetic drive and a thermocouple attached to a temperature controller. The stirring speed was set, and the controller controlled the reaction temperature according to the given set point. The autoclave is equipped with a pressure relief valve and a ruptured disc for safety against any pressure surges during the reaction. The outlets of the relief valve and rupture disc were safely directed to the exhaust through steel tubing. The gas line to the autoclave is equipped with a non-return valve to avoid any backflow from the autoclave. The autoclave temperature is controlled by circulating water in a submerged cooling coil as and when required.

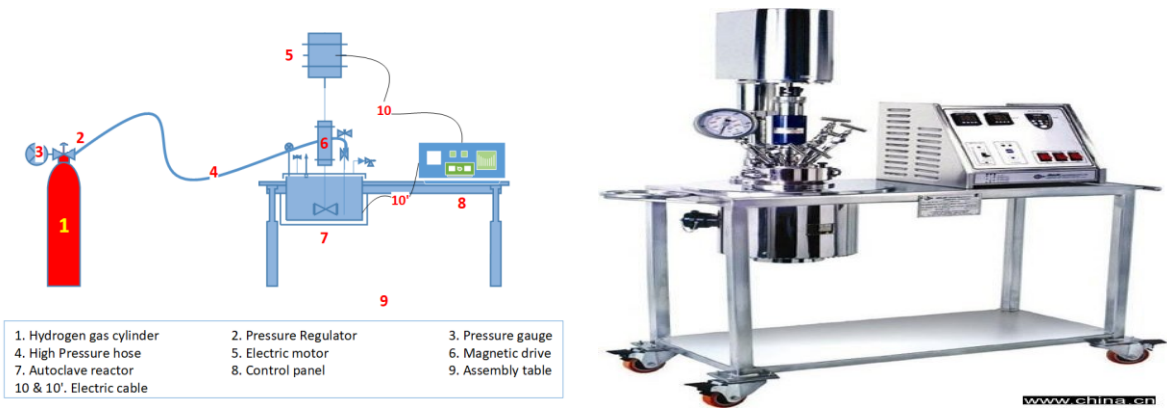

Figure 3.2. Schematic of the experimental setup for hydrogenolysis of glycerol

Table 3.1. Different catalyst prepared with variable STA to β-zeolite ratio

Entry	Catalysts (Pt/*x*STA/βzeolite)	STA/HPA to βzeolite ratio (*x*)
1	Pt/β-Zeolite	0
2	Pt/0.07STA/β-Zeolite	0.07
3	Pt/0.1STA/β-Zeolite	0.1
4	Pt/0.2STA/β-Zeolite	0.2
5	Pt/0.3STA/β-Zeolite	0.3
6	Pt/0.4STA/β-Zeolite	0.4
7	Pt/0.5STA/β-Zeolite	0.5
8	Pt/0.6STA/β-Zeolite	0.6
9	Pt/0.7STA/β-Zeolite	0.7
10	Pt/0.8STA/β-Zeolite	0.8
11	Pt/1.0STA/β-Zeolite	1
12	Pt/1.5STA/β-Zeolite	1.5
13	Pt/2.3STA/β-Zeolite	2.3
14	Pt/4.0STA/β-Zeolite	4
15	Pt/9.0STA/β-Zeolite	9
16	Pt/STA	--
17	Pt/0.3PTA/β-Zeolite	0.3
18	Pt/0.3PMA/β-Zeolite	0.3
19	Pt/0.7PTA/β-Zeolite	0.7
20	Pt/0.7PMA/β-Zeolite	0.7
21	2.5%Pt/0.3STA/β-Zeolite	0.3
22	10%Pt/0.3STA/β-Zeolite	0.3
23	2.5%Pt/0.7STA/β-Zeolite	0.7
24	10%Pt/0.7STA/β-Zeolite	0.7

In a typical run, the reactor (100 ml) was charged with 2.0 g of synthesized catalyst (2.5 wt% of the reaction mixture) and 80 ml of 5 wt% aqueous solutions of glycerol. The reactor was then sealed and purged 5 times with 10 bar N_2 gas, then pressurized with H_2 gas to the desired

level. Heating was started, and once the reactor reached the required temperature, the stirrer was switched on. This time (20–25 min) was considered as the "zero-reaction time." Reaction samples were collected intermittently over the period in a bomb and immediately cooled down. The reactor was then repressured to the original pressure.

In several cases, the experiments were repeated two times to check reproducibility and get an idea of the standard error of measurements, and in all such instances, the reproducibility was found to be satisfactory. Error bars in the figures discussed in the coming sections show the spread of results from repeat experiments.

3.4 Analysis

The liquid samples were filtered through a 0.2 μm syringe filter and then analyzed on a gas chromatograph (Mak Analytica, India) equipped with a ZB-WAX capillary column (30 m long, 0.25 mm inner diameter, and 0.25 μm thickness) from Phenomenex. N_2 was used as a carrier with a flowrate of 30 ml min^{-1} with 1-butanol as an internal standard on the flame ionization detector (FID). Injector and detector were kept at 230^o C temperature. The oven was programmed as follows: - Hold at 80^o C for 4 min followed by a heating ramp of 20 ^{o}C/min up to 180^o C; hold for 2 min, followed by a heating ramp of 10 ^{o}C/min up to 230 ^{o}C; hold for 4 min followed by cooling to 80 ^{o}C. Standard samples are used for calibration of the instrument in the experimentation range. The identified compounds are glycerol, 1,3-PDO, 1,2-PDO, 1-propanol (1-PrOH), 2-propanol (2-PrOH), ethanol (EtOH), hydroxyacetone, ethylene glycol, acetone, methanol (MtOH), and acrolein.

3.5 Catalyst Characterization

In the chemical/catalyst industry, noble metal-containing catalysts are preferably prepared by dispersing them onto high surface area solids. For any metal-supported catalysts, their metal crystallite size, catalyst porosity, and surface chemistry can affect the catalytic activity and product selectivity. The role of the support in a catalytic reaction is still a matter being investigated, and it is widely reported in the literature that the nature of supports and dispersion of noble-metal nanoparticles can influence the reactions [137–139]. The catalyst preparation technique used or the nature of catalyst support can induce electronic perturbation resulting in

a metal-support interaction [140]. Physico-chemical characterization methods for catalysts are important to understand the different aspects of the catalysts to explain the outcomes of experimental data.

In this thesis, various catalyst characterization techniques have been used. These include - N_2 physisorption for surface area (Brunauer–Emmett–Teller (BET) method) and pore size distribution analysis. X-ray diffraction (XRD) for phase analysis, Transmission electron microscopy (TEM), Electron Spectroscopy for Chemical Analysis (ESCA)/ photoelectron spectroscopy (XPS) for the oxidation state of tungsten, and to understand other electronic interactions. Temperature- programmed desorption of ammonia (NH_3–TPD), temperature-programmed reduction (TPR), and pulse-chemisorption. As understood from the literature reviewed in Chapter 2, Brønsted/Lewis acidity seems to be an important factor in directing the reaction. These were therefore characterized by several methods such as FT-IR with pyridine as probe (Py-IR) thermogravimetric analysis (TGA) after adsorbing pyridine and 2,6-di-tert-butylpyridine.

3.5.1 Catalyst surface area and pore size distribution

It is essential to know the total surface area, pore size, and pore size distribution of the catalysts, especially those supported on porous materials. The N_2 physisorption analysis is performed to measure all the stated properties. Measurements for N_2 physisorption were performed using a Micromeritics 3Flex instrument. Before doing the measurements, the samples were degassed at 300 ^oC for 8 h. The specific surface area, pore volumes, and size distribution were calculated from the collected isotherm data for nitrogen physisorption at -196 ^oC. Surface areas were calculated using the BET/t-plot method, and the pore volumes were calculated using the BJH method. The total surface area for each catalyst was obtained from the BET method. The micropore surface areas and micropore volumes were determined by the t-plot method. The pore size distribution was obtained by applying the BJH model to the adsorption isotherm.

3.5.2 X-ray powder diffraction (XRD)

X-ray diffraction (XRD) is commonly used to determine the bulk structure and composition of heterogeneous catalysts with crystalline structures [141,142]. Because most catalysts are in the form of polycrystalline powders, the XRD analysis is typically limited to the identification of specific lattice planes that produce peaks at their corresponding angular positions 2θ, determined by Bragg's law, $2d \sin\theta = n\lambda$. In spite of this limitation, the characteristic patterns

associated with individual solids make XRD quite useful for identifying the bulk crystalline components of solid catalysts. The powder X-ray diffraction (XRD) patterns were collected using a Philips X'-pert diffractometer instrument for the prepared catalyst and support. The data were collected over a 2θ range of 5–90º at a scan rate of 2° min^{-1} using Cu Kα radiation (k = 1.5418 Å) at 40 kV and 40 mA.

3.5.3 Pulse chemisorption and TPR

To determine the metal-support interaction (via H_2-TPR), dispersion, and acidity/alkalinity, temperature program (CO-TPD, TPR) and pulse-chemisorption techniques were used (TPDRO 1100, Thermo Scientific). The analysis involves three steps- pre-treatment, Pulse chemisorption, and temperature-programmed desorption (TPD). In a typical pre-treatment procedure, the first step is cleaning the gas line with inert gas (such as Argon). The second step is pre-treatment with 5% O_2/He followed by 5% H_2/Ar to ensure that the exposed catalyst surface is oxidized and reduced completely. Finally, high-temperature desorption is carried out by the inert gas argon. Thus, it is ensured that the catalyst's active metal surface is at zero oxidation state, and the catalyst is free from impurities.

For the H_2 temperature-programmed reduction (TPR) run, about 100 mg of non-reduced catalyst samples were initially pre-treated in Ar at 160 ºC for 90 min and then cooled to room temperature. Subsequently, 10%H_2–90%Ar mixture was added to the apparatus. Afterward, the sample was heated at a ramp rate of 10 ºC/min up to 900 ºC, and at the same time, the readings from the thermal conductivity detector were recorded.

For every run of CO chemisorption analysis, about 100 mg of reduced catalyst sample (reduced priorly at 400 ºC, 3 h) was initially pre-treated in Ar at 160 ºC for 90 min and then cooled to room temperature. The catalyst sample was then saturated by pure CO at room temperature by providing the known amount of calibrated pulses of pure CO followed by desorption at the same temperature, which was recorded against time. To determine the Pt particle size, the stoichiometry factor for adsorbed CO to platinum atom was taken as 1 [143,144].

3.5.4 Crystallite size by transmission electron microscopy (TEM)

Transmission electron microscopy (TEM) resembles optical microscopy, except those electromagnetic lenses instead of optical lenses are used to focus an electron beam on the sample. Two modes are available in TEM, a bright-field mode where the intensity of the

transmitted beam provides a two-dimensional image of the density or thickness of the sample and a dark-field mode where the electron diffraction pattern is recorded. A combination of topographic and crystallographic information, including particle size distributions, can be obtained in this way [145]. Since TEM has a higher resolution than SEM (down to 0.1 nm), it is often used to image nanosized catalysts such as metal oxide particles, supported metals, and catalysts with nanopores. TEM analyses were used to obtain the platinum crystallite size and size distribution. The requirement for thin specimens containing no volatile components limits the range.

To measure the crystallite size of the active phase of the catalyst, first, catalysts were suspended in the water, followed by sonication for 80–90 min. Further, the prepared solution was dispersed onto a 3 mm diameter TEM grid (a thickness of approximately 0.3 mm in such a way that in the center of the disc, the material is fully etched away). Usually, around this hole, there will be sufficiently thin areas (approximately 100 nm) to permit electrons to pass through. Finally, the grid is dried under IR-lamp for 30–35 minutes before subjecting to the analysis. The TEM analysis of the best performing catalysts was performed on a high-resolution field emission transmission electron microscope (HR-TEM, JEOL-2100F) using an accelerating voltage of 200 kV.

3.5.5 X-ray photoelectron spectroscopy (XPS)

X-ray photoelectron spectroscopy (XPS or ESCA) can analyze the surface's chemical state and electronic state (top surface: - 0-10 nm). XPS is based on the photoelectric effect arising when a high-energy photon hits a material. During the process, the kinetic energy and number of electrons that escape from the material's surface are analyzed [146].

X-ray photoelectron spectroscopy (XPS) analysis was performed on VG Multi Lab 2000 spectrometer with Mg Kα radiation and multichannel detector to determine platinum and tungsten species' binding energies and state. The catalyst was reduced in flowing hydrogen at 400 ^{o}C for 3h before the measurement. Samples were prepared by dispersing the catalytic powders on the aluminum foil. The working pressure of Argon at the analysis chamber was less than 1.5 X 10^{-7} Pa. Kinetic energies were converted to binding energy (BE (eV) = (1486.6 - KE) + 0.5) for monochromatic Al Kα source, where 0.5 eV is used as a correction. The obtained binding energy values were calibrated by the C 1s peak at 284.8 eV.

3.5.6 Acidic characteristics of catalysts

Given the importance of different types of acid sites in the mechanism of glycerol hydrogenolysis, acidity was characterized in several different ways. The total acidity of the catalyst is often estimated using a temperature desorption technique with NH_3 or pyridine as a probe molecule, the former being preferred frequently [24,47,92–94,114,147]. We have employed NH_3 as the probe molecule in the present study. The reduced (at 400 ^oC) catalyst sample is heated to eliminate any impurities, followed by cooling. NH_3 is then adsorbed over the cooled catalyst, followed by its heating/desorption. Depending on the strength of the acid sites over which NH_3 molecules adsorb, *viz.* weak or medium or strong Lewis/Brønsted sites, ammonia desorption peaks occur at different temperatures. It has been reported that the (high temperature) peak representing the strong acid zone corresponds to Brønsted acid sites [148]. In contrast, the low-temperature peaks are due to contributions from weak Brønsted or Lewis acid sites. To separately estimate the Brønsted and Lewis acidity, the most preferred method is pyridine FTIR analysis [92–94,114,134,147]. We have used the Py-FTIR technique to measure the Brønsted and Lewis acidic sites in reduced (Pt-xSTA/β-zeolite) catalysts. The Brønsted and Lewis acid sites were measured from the peaks corresponding to pyridine ion at particular wavelengths. In addition to these peaks, the acid sites can also contribute to other peaks in combination or from bridging hydroxyl groups (Si–OH–Al), silanol groups (Si–OH), Al^{3+}, $Al(OH)^{2+}$, AlO^{+}, $Al(OH)_2^{+}$, AlO(OH), $Al(OH)_3$ [149]. As an additional technique, Brønsted and the total acidity of the reduced catalyst samples were also measured using thermogravimetric analysis (TGA). The total concentration of acid sites (total acidity, sites/m^2, or mol/g) was measured using temperature-programmed desorption of pyridine as a probe molecule using TGA as explained in literature [28,52]. Measurement of Brønsted acidity was done using temperature-programmed desorption of 2,6-di-tert-butylpyridine (dTBpy).

It is clear from the above description that the different techniques employed probe different aspects of acidity. It would be interesting to see which results correlate best with which aspects of performance. The procedure for acidity measurement using these techniques is described in the following sections.

a) Temperature-Programmed Desorption of Ammonia (NH_3-TPD)

When probes with specific adsorption characteristics are used, additional chemical information can be extracted from adsorption-desorption experiments. Temperature-programmed desorption (TPD), in particular, is often employed to obtain information about specific sites in

catalysts [151,152]. The temperature at which desorption occurs indicates the strength of adsorption. In contrast, the amount of gas consumed in the uptake or the amount of desorption upon heating suggests the concentration of the surface sites. The most common molecule used in TPD to probe acidic sites is NH_3.

Here, NH_3-TPD experiments were conducted using Micromeritics 3-Flex instrument equipped with a thermal conductivity detector (TCD). In a typical procedure, about 100 mg of sample was loaded in a U-model quartz tube and supported by quartz wool. Then, it was treated at 800 °C at a rate of 10 °C/min under a flow of He (50 cm^3 min^{-1}) for 1 h, and then the temperature was decreased to 50 °C. The sample was then saturated with the NH_3 under a 30 ml/min flow of NH_3 (10%)/He gas mixture, followed by purging with the highly purified He at 50 °C for an hour. Subsequently, the temperature increased from 50 to 800 °C at 10 °C/min in flowing He (30 cm^3 min^{-1}), and desorption of NH_3 was monitored.

b) Fourier-transform infrared spectroscopy (FTIR) of adsorbed pyridine

In catalysis, infrared (IR) spectroscopy is commonly used to characterize specific adsorbates. Because of the localized nature and particular chemical specificity of molecular vibrations, IR spectra are pretty rich in information. They can be used to extract or infer both structural and compositional information on the adsorbate itself and its coordination on the catalyst's surface. In some instances, IR spectroscopy is also suitable for directly characterizing solids, mainly if they can be probed in the far-IR region [153–155]. For example, the acid-base properties of specific surface sites can be tested by recording the ensuing vibrational perturbations and molecular symmetry lowering of either acidic (CO and CO_2) or basic (pyridine and ammonia) adsorbates.

FT-IR was carried out using Nexus 470 FT-IR made by Nicolet to figure out the functional group (qualitative analysis of Brønsted and Lewis acid sites) within the catalysts and obtained organic compounds. Highly pure potassium bromide (KBr) powder was dried at 110 °C overnight to remove the moisture and then mixed with 10 mg of solid catalyst to make the pellets (100 mg KBr). The pellet was then placed on the magnetic holder and then set in the FTIR sample chamber for the rest of the procedure. The quantification of Brønsted and Lewis acid sites was estimated from the integrated area of adsorption bands at ca. 1540 and 1450 cm^{-1}, respectively, described elaborately in previous reports [153,156].

c) Thermogravimetry Analysis (TGA) for Acidic sites measurement

In the case of Pt-xSTA/βzeolite catalyst, the STA forms tungsten bronze ($HxWO_3$) species after reduction, which is deep blue in color. As the ratio of STA/βzeolite increases, the color intensity of the final catalyst increases, and it becomes difficult to apply the IR technique to the colored catalyst. Hence, we have used the thermogravimetry analysis (TGA) technique to estimate all the catalysts' concentrations of acid sites.

The total number of acidic sites (sites m^{-2} or g^{-1}) over each catalyst was estimated using the temperature-programmed desorption of pyridine (TPD-pyridine) as the probe molecule. Similarly, the Brønsted acidity for all the catalysts was measured using the 2,6-Di-tert-butylpyridine (dTBPy) as a probe molecule. The typical procedure is thermogravimetry (TGA) was performed from ambient temperature to 600 ºC at a heating rate of 10 ºC/min, in a stream of dry N_2 flowing at 40 cm^3 min^{-1}, using a NETZSCH STA 449F3 thermogravimetric analyzer [150]. Changes in the mass of the sample were recorded during the ramping operation.

The analysis was performed using 50 mg of the catalyst after pre-treatment at 250 ºC for 3 h in the air before the exposure to the probe molecule. 15–20 mg of pyridine–covered samples were subjected to TG analysis on heating up to 600 ºC (at 20 ºC/min heating rate) in dry N_2 (flow rate = 40 ml/min). The mass loss due to desorption of pyridine from the acidic sites was determined as a function of total surface acidity as sites g^{-1} or m^{-2} of the catalyst. The equation used to calculate the acid density site is as follows:

$$Acid\ site\ density = \frac{moles\ of\ pyridine\ desorbed \times Avogadro\ number\left(\frac{site}{mole}\right)}{weight\ of\ the\ sample\ (g) \times BET\left(\frac{m^2}{g}\right)} \qquad \text{Eq 3.1}$$

A similar procedure was adopted for measuring the Brønsted acidity of the catalyst. Here, the 2,6-Di-tert-butylpyridine (dTBPy) was used as a probe molecule.

The loss due to the desorption of pyridine or dTBPy was used from the acidic sites, was measured as a function of both the total acidity and Brønsted acidity, respectively, in the catalysts. The Lewis acidity was estimated as a difference between total and Brønsted acidity.

3.6 Conversion, yield, and Activity

With standard samples, the relation between peak area/height from the gas-chromatograms and the weight of the components provide the calibration factors. These calibration curves give the mass/moles of every single component available in the reaction mixture. In this way, the time-dependencies of the glycerol hydrogenolysis are mapped by plotting the concentration of reactants and products.

The glycerol conversion and product selectivity or yield are estimated using the concentration of reactants and products obtained from gas-chromatogram calibration.

The glycerol conversion, product selectivity, product yield, and 1,3-PDO productivity are defined as in eq. 3.2-3.5 below.

$$Conversion\ (\%) = \frac{moles\ of\ glycerol\ reacted}{initial\ moles\ of\ glycerol} \times 100 \qquad \text{Eq 3.2}$$

$$Selectivity\ (\%) = \frac{moles\ of\ desired\ product\ formed}{moles\ of\ glycerol\ consumed} \times 100 \qquad \text{Eq 3.3}$$

$$Yield\ (\%) = fractional\ conversion\ \times fractional\ selectivity\ \times 100 \qquad \text{Eq 3.4}$$

$$\text{1,3-PDO productivity } (h^{-1}) = \frac{glycerol\ initial\ moles \times yield\ of\ 1{,}3{-}PDO \times 76\ (g\ mol^{-1})}{total\ Pt\ amount\ (g) \times reaction\ time\ (h)} \qquad \text{Eq 3.5}$$

Chapter 4:
CATALYST CHARACTERIZATION RESULTS

In Chapter 3**,** we have synthesized the Pt/β-zeolite and different STA promoted Pt/β-zeolite catalysts with STA loadings varying from 0 to 100% STA loadings. In addition, we have also synthesized PTA and PMA containing catalysts with PTA or PMA to β-zeolite ratios as 0.3 and 0.7. This chapter will discuss the results observed after the characterization of these catalysts using different catalyst characterization techniques discussed in chapter 3.

The effect of the addition of STA on Pt/β-zeolite catalyst properties like acidity, surface area, pore volume, dispersion, metal interaction, etc., will be observed in this chapter.

4.1 Catalyst characterization

4.1.1 Surface area and pore size distribution

The textural properties of the Pt–xSTA/β-zeolite catalysts were measured by nitrogen physisorption measurements at -196 ^{o}C. The corresponding results for the samples are listed in Table 4.1. Furthermore, the obtained nitrogen adsorption-desorption isotherms and the corresponding BJH pore size distribution are shown in Figure 4.1(I)-(II) and Figure 4.1(III)-(IV), respectively. The observed surface area for the parent β-zeolite (Si/Al = 300) sample was 580 m^2 g^{-1} with 0.462 cm^3 g^{-1} total pore volume. The results show that the addition of platinum (Pt) and silicotungstic acid (STA) have reduced the catalyst's surface area and pore volume.

The reduction in the surface area is attributed to the decrease in β-zeolite pore volume from 0.462 to 0.023 cm^3 g^{-1} after the addition of STA and Pt. The Pt-xSTA/β-zeolite catalyst samples generally gave the same type I isotherm (microporous) as the parent β-zeolite except for Pt-9.0STA/β-zeolite and Pt/STA catalysts which showed a mesoporous nature.

Table 4.1. Textural properties, surface coverage, and surface W density of the prepared catalyst

Catalyst	S_{BET} ($m^2\ g^{-1}$)	S_{micro} ($m^2\ g^{-1}$)	S_{meso} ($m^2\ g^{-1}$)	V_{total} ($cm^3\ g^{-1}$)	V_{micro} ($cm^3\ g^{-1}$)	Surface coverage	surface W density (W nm^{-2})
β-Zeolite	580	423	157	0.462	0.184	--	--
Pt/β-Zeolite	540	403	137	0.441	0.166	0.0	0.0
Pt/0.07STA/β-Zeolite	524	392	132	0.425	0.163	0.2	0.3
Pt/0.1STA/β-Zeolite	505	376	129	0.413	0.152	0.3	0.5
Pt/0.2STA/β-Zeolite	481	369	112	0.384	0.148	0.5	0.9
Pt/0.3STA/β-Zeolite	362	284	78	0.294	0.114	0.9	1.6
Pt/0.4STA/β-Zeolite	334	263	71	0.246	0.099	1.1	2.2
Pt/0.5STA/β-Zeolite	304	241	63	0.233	0.096	1.4	2.7
Pt/0.6STA/β-Zeolite	284	226	58	0.176	0.092	1.6	3.3
Pt/0.7STA/β-Zeolite	277	222	55	0.169	0.09	1.9	3.6
Pt/0.8STA/β-Zeolite	239	190	51	0.147	0.081	2.2	4.3
Pt/1.0STA/β-Zeolite	208	166	42	0.133	0.062	2.7	6.2
Pt/1.5STA/β-Zeolite	160	128	32	0.093	0.052	4.1	9.6
Pt/2.33STA/β-Zeolite	130	107	23	0.076	0.043	6.4	13.8
Pt/4.0STA/β-Zeolite	107	86	21	0.066	0.035	11.0	19.2
Pt/9.0STA/β-Zeolite	46	43	2	0.023	0.017	24.7	50.5
Pt/STA	8	7	1	0.005	0.003	--	286.5

The results suggested that the loaded amount of Pt and STA does not significantly affect the textural properties of the β-zeolite, as reported in the literature [50,157]. A hysteresis loop of type H3 was observed after $P/P^0 \approx 0.42$ in the sorption isotherm for the samples up to 0.5 STA to β-zeolite ratio, resulting from plate-like particles with slit-like pores, surface roughness, and external surface [158]. Beyond this, loading up to 4.0 STA to β-zeolite ratio type H4 hysteresis was observed, which arises due to narrow slit-like pores [158].

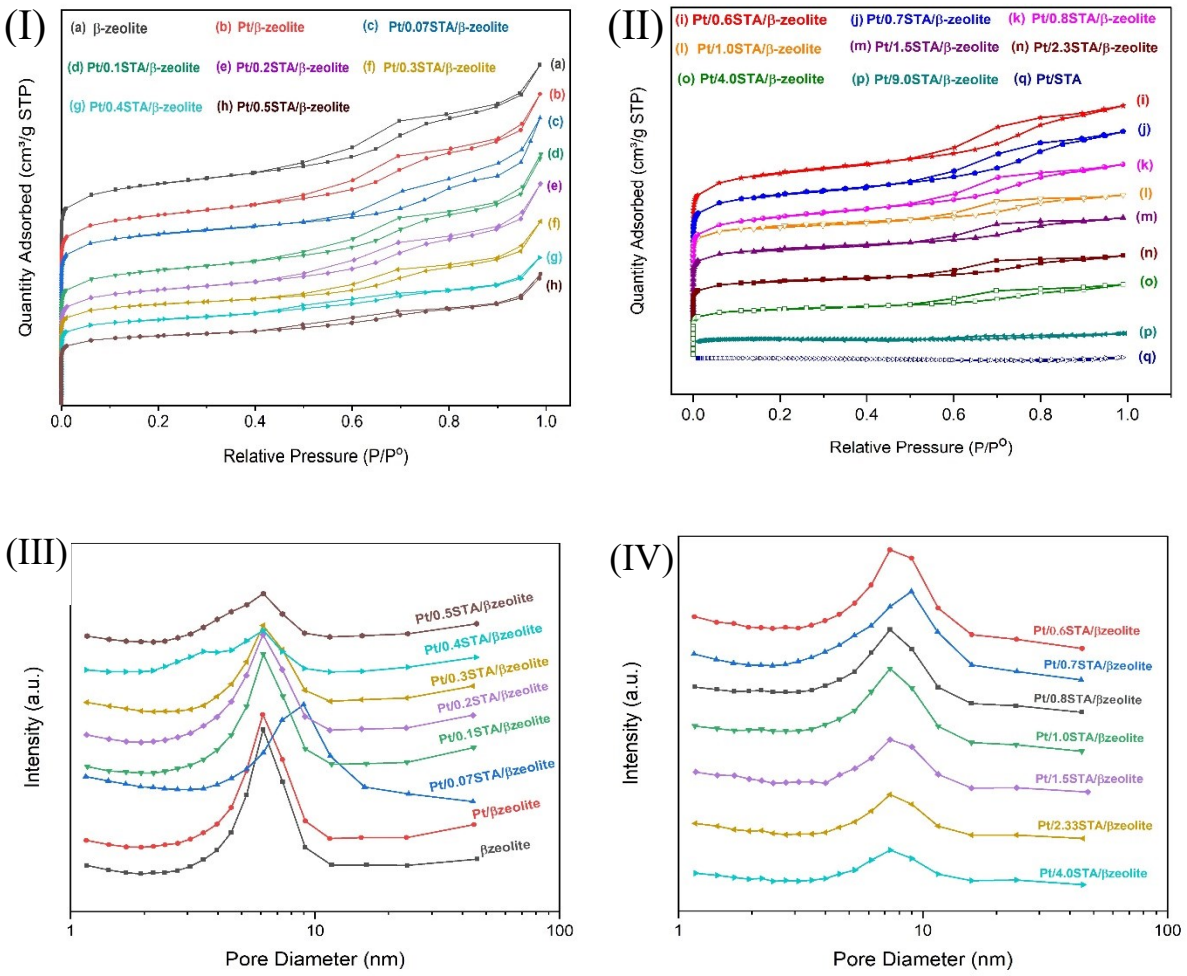

Figure 4.1. N_2 physisorption isotherm and pore size distribution for synthesized catalysts

However, micro-porosity was present in those samples. Finally, the catalysts Pt-9.0STA to β-zeolite and Pt/STA show an isotherm type IV, characteristic of mesoporous solids. The shifts in isotherms with increased STA to β-zeolite ratio are mainly due to the reduction in the amount of β-zeolite in the catalyst. The micro-porosity was mostly due to the β-zeolite in the catalysts.

The parent β-zeolite and various Pt-xSTA/β-zeolite catalyst samples showed a pore size distribution in the range of 1.1–10 nm, centered at ca. 7 nm except for Pt/0.07STA/β-Zeolite, for which the PSD is centered around ca. 10 nm. A similar pore size distribution for β-zeolite

catalyst was also reported elsewhere [157,159]. The parent β-zeolite catalyst showed the micropore volume of 0.184 cm^3 g^{-1}, which was reduced with the addition of Pt and STA species, probably due to the blockage of β-zeolite pores by the same species.

Additionally, we have estimated the surface/monolayer coverage capacity of WO_3 over the β-zeolite catalyst and the tungsten surface density using the formula given by Ketzer et al. [149] and Thomas et al. [160] (see Eq. A.1 and A.2 in Appendix-A), respectively (see Table 4.1). Costa et al. [161] reported that the WO_3 monolayer coverage capacity for USY zeolite catalyst with surface area 750 m^2/g lies near 32% WO_3 loading. Our results over the β-zeolite catalyst with a surface area of 580 m2/g showed that the STA to β-zeolite ratio of 0.3 or surface coverage value 0.9 reaches the sub-monolayer capacity or dispersion threshold. Moreover, the catalyst with STA to β-zeolite ratio of 0.4 or surface coverage value 1.1 goes beyond the monolayer capacity. Therefore, STA loadings (STA to β-zeolite ratio) equal to or higher than 0.4 would result in excess STA or STA multilayer formation.

Barton et al. [162] prepared a series of tungsten-promoted ZrO_2 catalysts. They reported three different zones based on the tungsten loadings or tungsten surface densities (W atoms per nm^2 of catalyst support). They are monotungstate (WO_4) species with tungsten surface density 0–4 W nm^{-2} known as the sub-monolayer region, polytugstate (WO_5/WO_6) species with tungsten surface density 4–8 W nm^{-2} known as a polytungstate growth region, and coexistence of polytungstate and crystalline WO_3 with tungsten surface density >8 W nm^{-2} known as polytungstate/crystalline WO_3 coexistence region. Moreover, Barton et al. [163] also reported that the sub-monolayer region on the ZrO_2 surface contains well dispersed distorted octahedral WOx species (tungsten species) with constant absorption edge energy as 3.49 eV. These species are difficult to reduce and contain fewer acidic sites. The optical absorption edge energy is defined as the minimum photon energy required to excite an electron from the highest occupied molecular orbital (HOMO, at the top of the valence band in semiconductor domains) to the lowest unoccupied molecular orbital (LUMO, at the bottom of the conduction band). At intermediate tungsten loadings (4–8 W nm^{-2}) or in the polytungstate growth region, the WOx species domain size rises. The absorption edge energy reduces from 3.49 to 3.16 eV, and their reduction becomes easier, which increases the reactant conversion rates with an increase in tungsten loadings. At higher tungsten loadings (tungsten surface density >8 W nm^{-2}), part of the WOx species polymerizes to tungsten trioxide (WO_3) and the polytungstate species coexists with crystalline monoclinic WO_3 (m-WO_3) species. In this region the absorption edge energy maintains at a constant value of 3.16 eV. Moreover, in this region, a second absorption edge

appears at 2.6 eV but the formation of crystalline m-WO_3 reduces the reactant conversion rates because the polytungstate species (WO_5/WO_6) becomes inaccessible to the reactants. It is worth noting that, Barton and co-workers reported maximum o-xylene iso-merization turnover rates over WOx–ZrO_2 catalysts at tungsten loading 12 wt% or WOx surface densities 10 W nm^{-2} that exceed the theoretical monolayer capacity of ZrO_2. Moreover, 12 wt% tungsten loading exist in the polytungstate/crystalline WO_3 coexistence region. This means the optimum loading of tungsten (W) in a catalyst lies above the monolayer coverage of W over a solid.

On the contrary, Zhu et al. [114] reported the glycerol hydrogenolysis over Pt-WOx/Al_2O_3 catalyst. Their best results were observed at a tungsten loading of 10 wt%, which reaches sub-monolayer coverage of the Al_2O_3 catalyst. They have reported, when WOx content reaches sub-monolayer coverage or dispersion threshold over WOx/Al_2O_3 catalyst, the polytungstate species became dominant and held the maximum acidity. Moreover, based on theoretical calculations, the authors also said the octahedral polytungstate species have the most abundant edge sites due to the condensation process at monolayer coverage. The edge sites are the most acidic units [164]. Therefore, the catalyst Pt–10WOx/Al_2O_3 possessed strong acid sites due to the generation of interconnected WOx species. Thus, according to Zhu et al. [114], the maximum acidity or optimum loading of tungsten (W) in a catalyst lies at the sub-monolayer coverage of W over a solid catalyst.

Both the reported studies above claim that tungsten-promoted catalyst/solids can give better results either at the sub-monolayer coverage region or at the polytungstate/crystalline WO_3 coexistence region. In search of finding the best results over STA or WOx promoted β-zeolite catalyst, we varied the STA loading from 0 to 100% STA and studied their properties and performance, which will be discussed in the coming sections. In our case, the monolayer coverage was observed beyond 0.3 STA to β-zeolite ratio loading.

4.1.2 XRD results: Detection of H_xWO_3 species

Figure 4.2 depicts the X-ray diffraction patterns of the β-zeolite and Pt–xSTA/β-zeolite catalysts. The parent β-zeolite catalyst showed diffraction peaks around 7.9° and 22.6° [159,165]. The intensities of these peaks were reduced with an increase in STA to β-zeolite ratio up to 0.7. Most of the STA (WOx) is likely to remain on the β-zeolite's external surface due to the catalyst preparation technique (wet impregnation) used. With a further increase in STA to β-zeolite ratio beyond 1.0, the peaks corresponding to β-zeolite have vanished. This may be because either the surface of β-zeolite is entirely occupied by the STA species or the

reduction in the percentage of β-zeolite (although it is still nearly 50%) in the catalysts is responsible for the disappearing β-zeolite peaks.

For catalysts with an STA to β-zeolite ratio less than or equal to 0.1, diffraction peaks corresponding to WOx species were not detected, indicating a homogeneous dispersion of WOx on the β-zeolite surface. At higher STA to β-zeolite ratios viz. 0.2 and 0.3, the peaks at 23.5° (coexisting with β-zeolite peak) and 33.5° (a new peak) were detected, which correspond to H_xWO_3 species, and the spectra resemble the $H_{0.53}WO_3$ (JCPDS: 01-072-1712) XRD spectra. Moreover, the formation of $H_{0.53}WO_3$ species can be clearly seen at a higher STA to β-zeolite ratio (2.33, 4.0, 9.0, and Pt/STA). Barton et al. [162] reported that H_2 could restore Brønsted acidity by reducing WOx species or forming the acidic H_xWO_3 species. Moreover, Baertsch et al. [166] said that the clusters of WO_x possessed the Brønsted acidity, possibly as H_xWO_3 species or as hydroxyls on monotungstate and polytungstate Zr-O-W linkages. Thus, we conclude that the presence of $H_{0.53}WO_3$ species in our synthesized catalyst indicates the existence of Brønsted acid sites, which are believed to help 1,3-PDO formation during the glycerol hydrogenolysis [105,123,145,150]. At higher STA loading, say 0.4, 0.5, or 0.6, we have observed peaks related to m-WO_3 species, which would have formed due to excess STA to β-zeolite ratio [163]. As discussed above, at 0.3 STA to β-zeolite ratio, the catalyst reaches the sub-monolayer capacity or dispersion threshold of β-zeolite. Therefore, loadings higher than 0.3 would have resulted in excess STA and thus started forming m-WO_3 species. Furthermore, at higher STA to β-zeolite ratios, say 2.33, 4.0, 9.0, and Pt/STA, the peaks corresponding to m-WO_3 were not visible/present.

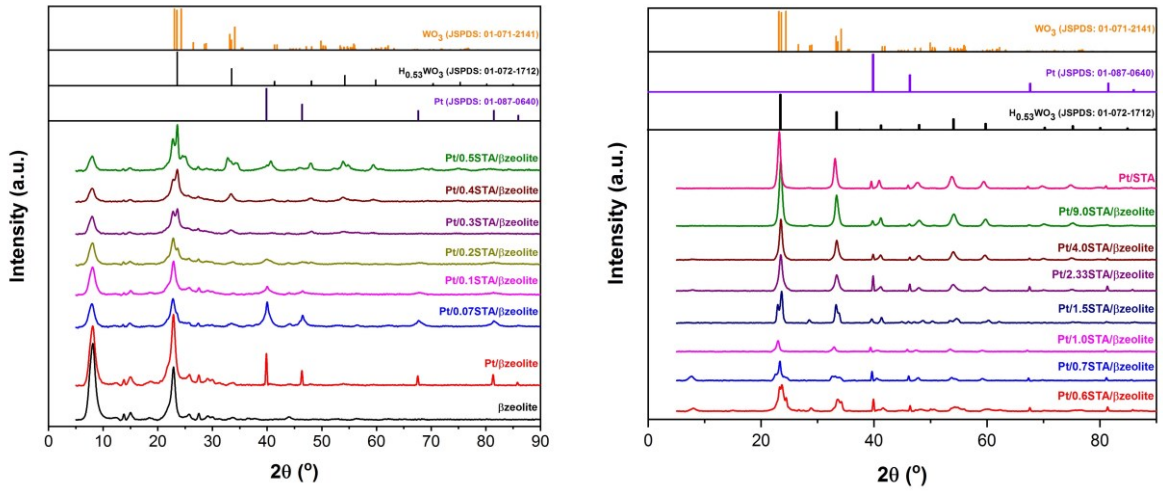

Figure 4.2. XRD patterns of prepared catalyst samples

This may be because at higher STA loadings, either the dominance of H_xWO_3 species is very high, because of which peaks related to m-WO_3 species are not distinguishable, or STA has wholly converted to H_xWO_3 species.

The diffraction peaks at 39.89, 46.4, 67.71, 81.57, and 86.04° corresponds to the 111 planes of Pt (fcc) structure, and the next (200), (220), (311), and (222), respectively. The intensity of Pt peaks was reduced with an increase in STA to β-zeolite ratio up to 0.4. Thus, it can be concluded that the increase in STA loading facilitates the dispersion of Pt particles in agreement with the previous reports [92,114]. With the further increase in STA to β-zeolite ratio (0.4 onwards), the Pt peaks become evident. However, the Pt peaks were less intense compared to the Pt peak intensity over Pt/β-zeolite catalyst for the same amount of Pt loading. This may be because excess STA loadings block the available pores of β-zeolite, making Pt peaks evident.

4.1.3 Temperature-Programmed Desorption of Ammonia (NH_3-TPD)

NH_3-TPD method was employed for Pt-xSTA/β-zeolite catalysts to probe the available surface acidic sites and determine their strength. The spectra obtained are shown in Figure 4.3. The catalyst Pt/β-zeolite showed well-resolved desorption peaks at two distinct temperature zones, *viz.* low-temperature zone (150–300°C) and medium temperature zone (300–500°C); no peak was observed in the high-temperature zone (500–650°C).

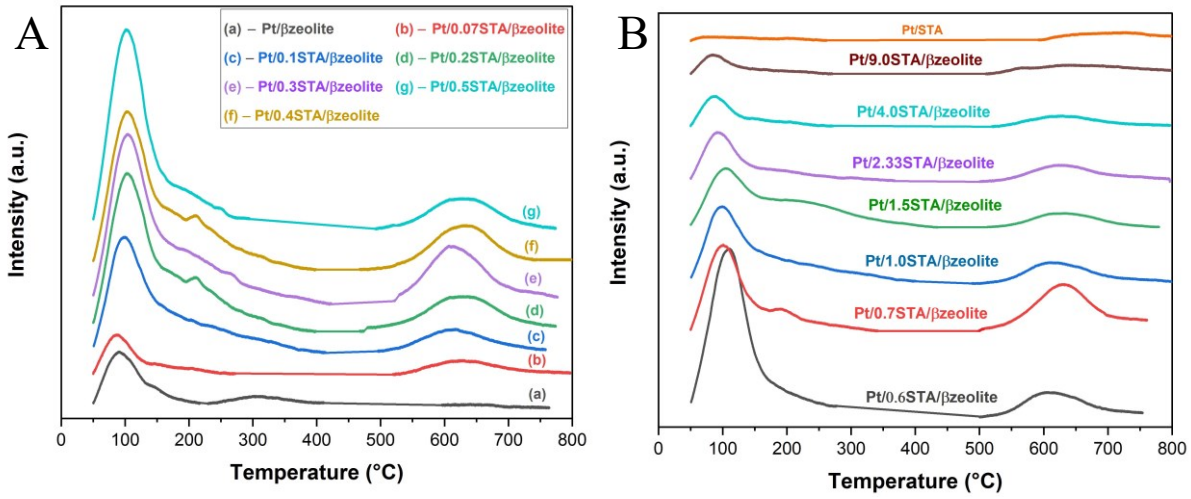

Figure 4.3. NH_3-TPD profiles for the prepared catalysts.

These temperature zones correspond to weak, moderate, and strong acid site strengths, respectively [82,147]. Wang et al. [167] reported the NH_3-TPD results for various β-zeolite

catalysts. Their work shows a decrease in catalyst acidity with an increase in SiO_2/Al_2O_3 ratio. The β-zeolite with SiO_2/Al_2O_3 ratio 350 has shown the lowest acidity. The β-zeolite used in our work has a SiO_2/Al_2O_3 ratio of 300. In the case of STA promoted catalysts, the peaks representing the strong acid sites were observed along with the peak corresponding to weak acid sites. It is worth noting that a separate peak representing moderate acid sites was absent in the case of STA promoted catalyst which was present in the Pt/β-zeolite catalyst (see spectra (a) from Figure 4.3A). However, after adding STA, the weak acid site peak got broader, and a shoulder peak at a temperature of more than 200°C appeared. It is attributed to the merging of peaks related to weak acid sites with moderate acid sites. Such broad peaks after the deposition of STA were also observed by Atia et al. [82] and Zhu et al. [93], and the broad peaks in the case of zeolites were observed by Wang et al. [167] and Kim et al. [128]. Moreover, the NH_3-TPD study for the STA catalyst was carried out by Raveendra et al. [168]. Their results show that STA catalyst contains only strong acidic sites.

The results show that the addition of STA to the Pt/β-zeolite catalyst improves its acid strength. The total acidity of the catalyst increased with an increase in STA to β-zeolite ratio from 0.07 to 0.5. With a further increase in STA to β-zeolite ratio beyond 0.6, the total acidity of the catalyst decreased. After catalyst calcination, the STA species converts into WOx species at lower STA loadings. However, at higher STA loadings, part of WOx species polymerizes to WO_3 species, and both co-exist in a catalyst. The higher STA to β-zeolite ratio increases the formation of both WOx and WO_3 species. Since WOx contributes largely to the acidity, its higher concentration increases the catalyst's acidity. However, the higher concentration of WO_3 species reduces the acidity by blocking the WOx species. The blocking of WOx species reduces their access with the reactant (here NH_3), and that's how acidity reduces. Our results show a decrease in total acidity after the STA to β-zeolite ratio of 0.6 due to the formation of higher amounts of WO_3 species. It is worth noting that the catalyst Pt-0.7STA/β-zeolite showed the highest strong acidic sites and less weak acidic sites. It may be because the excess WO_3 species would have blocked the weak acidic sites present over the Pt-0.7STA/β-zeolite catalyst (see NH_3-TPD profiles), and the WOx species have provided the strong acidic sites at this particular loading. Though the WO_3 species are less active, their concentration and dispersion alter the catalyst acidity. Therefore, the catalyst will give results in the way WO_3 species have changed the acidity.

Table 4.2. Acidic sites of prepared catalysts measured using different techniques

Catalyst	TGA (μmol $g_{cat.}^{-1}$)		NH_3-TPD (μmol $g_{cat.}^{-1}$)				Py-FTIR (μmol $g_{cat.}^{-1}$)	
	Brønsted[a]	Total[a]	weak[b]	medium[b]	strong[b]	Total[b]	Brønsted[c]	Lewis[c]
Pt/β-Zeolite	79.9	784.1	280.1	50.3	--	330.4	2.8	210.1
Pt/0.07STA/β-Zeolite	200.0	821.6	490.2	--	130.1	620.3	6.1	162.4
Pt/0.1STA/β-Zeolite	273.8	848.3	570	--	210.2	780.2	14.9	173.7
Pt/0.2STA/β-Zeolite	300.1	877.5	790.3	--	350.1	1140.4	35.2	188.6
Pt/0.3STA/β-Zeolite	390.5	915.0	850.1	--	440.4	1290.5	74.0	187.7
Pt/0.4STA/β-Zeolite	313.0	1000.6	1270	--	320.1	1590.1	40.5	201.5
Pt/0.5STA/β-Zeolite	330.3	1024.1	1430.4	--	280	1710.4	42.3	204.1
Pt/0.6STA/β-Zeolite	342.7	993.2	1244.2	--	392.1	1636.3	47.9	218.5
Pt/0.7STA/β-Zeolite	467.3	958.1	739.1	--	546.1	1325.2	87.9	157.7
Pt/0.8STA/β-Zeolite	354.7	831.7	813.3	--	380	1193.3	53.1	207.6
Pt/1.0STA/β-Zeolite	280.5	754.7	850	--	297.4	1147.4	37.2	138.8
Pt/1.5STA/β-Zeolite	202.8	595.7	900.3	--	214.1	1114.4	--	--
Pt/2.33STA/β-Zeolite	132.9	489.3	487.2	--	180.3	667.5	--	--
Pt/4.0STA/β-Zeolite	99.4	273.1	217.1	--	133.3	350.4	--	--
Pt/9.0STA/β-Zeolite	60.6	190.8	160.2	--	80.2	240.4	--	--
Pt/STA	50.2	107.4	40.1	--	60.4	100.5	--	--

[a] The amount of Total and Brønsted acid sites was determined by desorbed pyridine and 2,6-dTBpyridine respectively from TGA analysis. [b] The amount of weak, medium, strong, and Total acid sites was determined by desorbed ammonia (NH_3) using NH_3-TPD analysis. [c] The amount of Lewis and Brønsted acid sites were calculated from Py-FTIR band intensities using the molar extinction coefficients.

The total acidity of all the catalysts can be estimated based on ammonia injection calibration experiments, and the obtained results for the acidic sites are given in Table 4.2. The total acidity increased with the increase in STA to β-zeolite ratio up to 0.5. Increasing STA to β-zeolite ratio beyond 0.5 resulted in decreasing the total acidity of the catalyst. However, the strong acidity was highest over Pt-0.7STA/β-zeolite catalyst and second-highest over Pt-0.3STA/β-zeolite catalyst.

4.1.4 Acidity determination through Thermogravimetry Analysis (TGA)

The measurement total and Brønsted acidity of the catalysts was also performed using thermogravimetry analysis (TGA). The typical procedure is already explained in the experimental section (Chapter 3). The number of total acidic sites was calculated using pyridine as a probe molecule, as pyridine adsorbs over all the acidic sites present in the catalyst sample. In the tungsten-supported catalysts, W^{6+} Lewis centers coordinate with pyridine molecules, and pyridine molecules can also be protonated by Brønsted acid sites. Hence, pyridine as a probe molecule can estimate all types of acidic sites present in the catalyst sample [150].

The number of Brønsted acidic sites was estimated using 2,6-di-tert-butylpyridine as a probe molecule. 2,6-di-tert-butylpyridine is a good candidate to calculate the Brønsted acidity present in the catalyst. It only adsorbs over the Brønsted-acid sites because of its steric hindrance. Unlike the pyridine molecule, which adsorbs over all the acidic sites present in the catalyst, the 2,6-di-tert-butylpyridine does not coordinate with the Lewis acid centers, while its protonation by Brønsted acid sites is possible [166]. The Lewis acid sites can be estimated by the difference between total acidity and Brønsted acidity present in a particular catalyst.

The observed results are reported in Table 4.2. The results show that the total acidity of the Pt/β-zeolite catalyst increases with an increase in STA to β-zeolite ratio up to 0.5 followed by a decrease in the total acidity of the catalyst on further increase in STA to β-zeolite ratio. Brønsted acidity increases with an increase in STA to β-zeolite ratio up to 0.3, and decreases with further increase in STA to β-zeolite except for 0.7 STA to β-zeolite which showed the highest Brønsted acidity. The TGA results are consistent with NH_3-TPD results. In both cases, the total acidity was increased till 0.5 STA to β-zeolite ratio followed by a decrease in total acidity. Similarly, the catalyst Pt/0.7STA/β-zeolite showed the highest Brønsted acidity in TGA analysis, and in NH_3-TPD, it showed the highest strong acidity. The catalyst Pt/0.3STA/β-zeolite showed the second-highest Brønsted/strong acidity.

4.1.5 FTIR of adsorbed pyridine (Py-FTIR)

FTIR spectroscopy with adsorbed pyridine as a probe molecule was carried out to determine the Lewis and Brønsted acidity of the synthesized catalysts.

After catalyst reduction, the color of STA/WOx promoted catalysts became darker (deep blue) due to the formation of $HxWO_3$ species. The intensity of color increased with an increase in the STA to β-zeolite ratio. The FTIR technique's analysis of the darker samples is difficult as it affects the light absorption during analysis. Hence, we could only measure or study the Py-FTIR spectra of the catalyst up to STA to β-zeolite ratio 1.0 (Pt-1.0STA/β-zeolite). The results observed using this technique are discussed in the following section.

FTIR spectra of adsorbed pyridine for the prepared catalysts are shown in Figure 4.4. The catalyst samples show typical pyridine adsorption bands coordinated to Lewis sites centered at ca. 1450 cm^{-1} [94]. The bands at ca. 1540 cm^{-1} were attributed to the pyridine adsorbed at Brønsted acid sites. Moreover, adsorption bands around ca. 1489 cm^{-1} were assigned to the combined contribution of pyridine adsorbed over Lewis and Brønsted acid sites [169]. The amounts of Lewis and Brønsted acid sites were calculated from the adsorption band intensities at ca. 1450 and 1540 cm^{-1}, respectively, using molar extinction coefficients [170]. The calculated values for both the acidic sites are reported in Table 4.2.

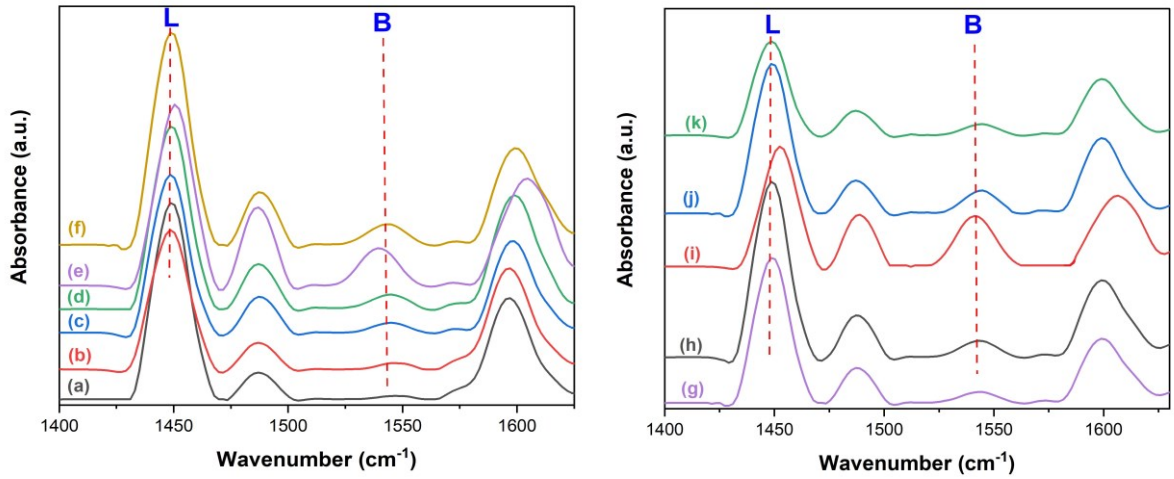

Figure 4.4. Py-FTIR spectra for the prepared catalyst: - (a) Pt/β-Zeolite, (b) Pt/0.07STA/β-Zeolite (c) Pt/0.1STA/β-Zeolite, (d) Pt/0.2STA/β-Zeolite, (e) Pt/0.3STA/β-Zeolite, (f) Pt/0.4STA/β-Zeolite (g) Pt/0.5STA/β-Zeolite, (h) Pt/0.6STA/β-Zeolite, (i) Pt/0.7STA/β-Zeolite, (j) Pt/0.8STA/β-Zeolite, (k) Pt/1.0STA/β-Zeolite

The Py-FTIR results show that the intensity of the adsorbed bands at ca. 1450 cm^{-1} was slightly reduced over the Pt/0.07STA/β-zeolite catalyst. This may be due to the partial pore blockage

of β-zeolite by STA species, which hinders the access to acidic sites for the pyridine molecules [147]. The result shows a reduction in the Lewis acid sites and the increase in Brønsted acid sites of Pt/0.07STA/β-zeolite catalyst. This could be due to the conversion of Lewis acid sites to Brønsted acid sites in the presence of Pt particles [171]. Further increase in the STA to β-zeolite ratio in the catalyst has increased the bands' intensities and amounts associated with Lewis and Brønsted acid sites. The band's intensity at ca. 1540 cm^{-1} increased continuously with the addition of STA up to Pt/0.3STA/β-zeolite catalyst followed by a slight decrease at 0.4 to 0.6 STA to β-zeolite ratio. The 1540 cm^{-1} band intensity increased further at a catalyst Pt/0.7STA/β-zeolite, which shows the highest intensity peak and contains the highest Brønsted acidic sites in the studied series. The catalyst Pt/0.7STA/β-zeolite has demonstrated the highest ratio for Brønsted to Lewis acidic sites. According to Triwahyono et al. [171], the Brønsted acid sites came from the surface OH groups located on the specific configuration of tungsten or well-dispersed WOx of WO_3/ZrO_2 catalyst. In contrast, the removal of the same surface OH groups produces Lewis acid sites.

Thus Py-FTIR results allow us to conclude, Pt–0.7STA/β-zeolite catalyst showed the highest Brønsted acidity (or contained well dispersed acidic H_xWO_3 sites) followed by Pt–0.3STA/β-zeolite catalyst, in agreement with TGA and NH_3–TPD results.

Barton et al. [11] and Zhu et al. [10] reported that with an increase in WOx or STA loading in the catalyst, its acidity increases. The former said at intermediate WOx loadings (4–8 W nm^{-2}), the reactant conversion rate increases (per W atom). Our results agree with them as the glycerol conversion increases up to Pt-0.5STA/β-zeolite catalyst. On the other hand, Zhu et al. [114] reported that when WOx content reached sub-monolayer coverage over WOx/Al_2O_3 catalyst, the polytungstate species became dominant and held the maximum acidity. Our result contradicts them. However, we observed that at sub-monolayer coverage, the catalyst possesses higher strong/Brønsted acidity, which reduces with an increase in STA loading beyond monolayer coverage due to the formation of WO_3 species (See XRD spectra of Pt-0.5STA/β-zeolite). However, the acidity is still increasing because the WOx species domain increases (WOx and WO_3 coexist) with an increase in the STA to β-zeolite ratio up to 0.5. Hence, loading up to 0.5 STA to β-zeolite ratio will provide one catalyst with higher Brønsted acidity at sub-monolayer coverage.

Further, increase in STA to β-zeolite ratio from 0.6 to 100% STA the total acidity was reduced due to the formation of excess WO_3 species. However, the catalyst Pt-0.7STA/β-zeolite showed the highest Brønsted acidic sites. This may be because with an increase in the STA to β-zeolite

ratio, the formation of both WOx and WO_3 species increases. The former is mainly responsible for the increase in acidity, while the latter is slightly helpful in acidity. Moreover, the latter blocks the acidic sites of the support, and in the case of the Pt-0.7STA/β-zeolite catalyst, it would have blocked weak acid sites as observed in the NH_3-TPD experiment (see Figure 4.3B). The strong acidic sites were increased due to an increase in the amount of WOx species. Moreover, the peak representing strong acid sites/high-temperature zone is reported to be attributed to NH_3 desorption from the Brønsted acid sites [148]. Hence, we suggest that the 0.7 STA to β-zeolite ratio is the optimum loading with the highest Brønsted acidity in a β-zeolite (Si/Al=300) supported catalytic system. Furthermore, the Brønsted acidity measured through TGA and FTIR also confirms the presence of the highest Brønsted acidity over a Pt-0.7STA/β-zeolite catalyst.

4.1.6 Pulse chemisorption

The particle size of Pt and its dispersion over the catalysts can be estimated using the quantity of CO adsorbed over the catalyst. Taylor et al. [33] reported that CO adsorbs over the surface of Pt atoms at room temperature preferentially over WOx species. Additionally, the stoichiometry of CO chemisorption will vary based on the type of adsorption sites available, and the adsorption stoichiometric ratio for CO/Pt typically varies in-between 1 and 2 [172], although the most commonly used CO/Pt adsorption stoichiometric ratio to estimate platinum dispersion and platinum size is 1 [143,144]. Here, the Pt particle dispersion and the Pt size were determined from the irreversible CO-chemisorption for synthesized catalysts Pt–xSTA/β-zeolite (x=0 to 1). The results are shown in Figure 4.5 and Table 4.3.

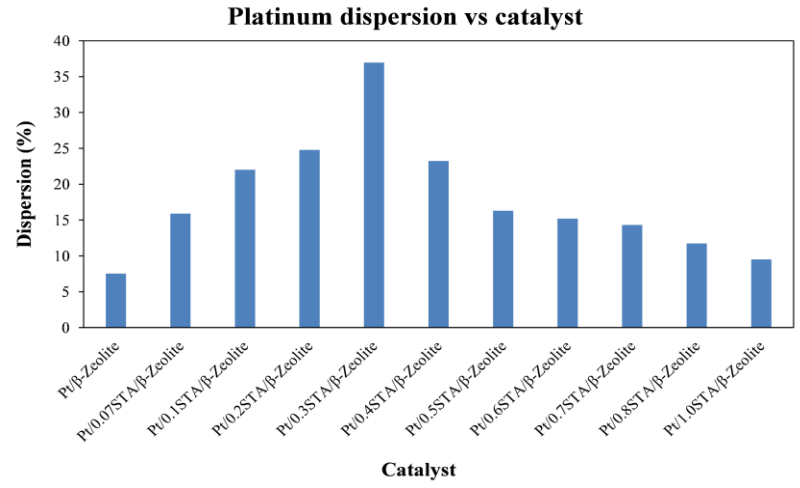

Figure 4.5. Observed platinum dispersion on prepared catalysts

The results show that the catalyst Pt/β-zeolite has the lowest dispersion of Pt (7.5%). The dispersion increased with an increase in STA to β-zeolite ratio up to 0.3. The catalyst Pt-0.3STA/β-zeolite shows the highest Pt dispersion (37.0%) (see also Table 4.3). Indicating that the STA addition has a favorable effect on the dispersion of Pt particles.

However, a further increase in STA to β-zeolite ratio reduces the Pt particle dispersion and increases the calculated Pt cluster size. Such behavior of decrease in Pt particle dispersion was not essentially due to the change in Pt particle sizes but may be due to the partial blockage of Pt particles by the excessive amount of STA species [114]. This can be assigned as the dual effect of STA particles, the dispersion effect, and the bimetallic coverage effect.

Table 4.3. Tabulated Pt dispersion and Pt size of prepared catalysts

Catalysts	Pt dispersion (%)	Pt size (nm)	Amount gas adsorbed (µmol/g)	Amount of metal reacted (µmol/g)
Pt/β-Zeolite	7.5	13.5	19.3	19.3
Pt/0.07STA/β-Zeolite	15.9	6.4	40.8	40.8
Pt/0.1STA/β-Zeolite	22.0	4.6	56.4	56.4
Pt/0.2STA/β-Zeolite	24.8	4.1	63.5	63.5
Pt/0.3STA/β-Zeolite	37.0	2.8	94.8	94.8
Pt/0.4STA/β-Zeolite	23.2	4.4	59.6	59.6
Pt/0.5STA/β-Zeolite	16.3	6.2	41.8	41.8
Pt/0.6STA/β-Zeolite	15.2	6.7	39.1	39.1
Pt/0.7STA/β-Zeolite	14.3	7.1	36.7	36.7
Pt/0.8STA/β-Zeolite	11.8	8.7	30.1	30.1
Pt/1.0STA/β-Zeolite	9.5	10.7	24.4	24.4

Similar effects of metal particles coverage by metal oxides species have been broadly explained for the catalysts like Ir-ReOx/SiO_2 [63], Pt-SnOx/Al_2O_3 [173], and Ru-MoOx/ZrO_2 [174]. Chen et al. [174] reported that in the case of Ru–MoOx/ZrO_2 catalyst, the small loadings of MoOx promote the dispersion of Ru particles. However, excessive loadings of MoOx species can cover the Ru particle sites and thereby reduce the Ru particle dispersion.

4.1.7 Reducibility property (Temperature programmed reduction)

Figure 4.6 shows the H_2–TPR profiles of Pt/β-zeolite and Pt–xSTA/β-zeolite catalysts (x = 0 to 1.0). It was anticipated that after calcination under an oxygen atmosphere, the platinum salt from the catalyst forms oxidic PtO and PtO_2 species. These PtO and PtO_2 undergo reduction at various temperatures based on their initial oxidation state and their location in the zeolite support (external surface, acid or basic sites, internal channels of the support, etc.) or on their initial oxidation state.

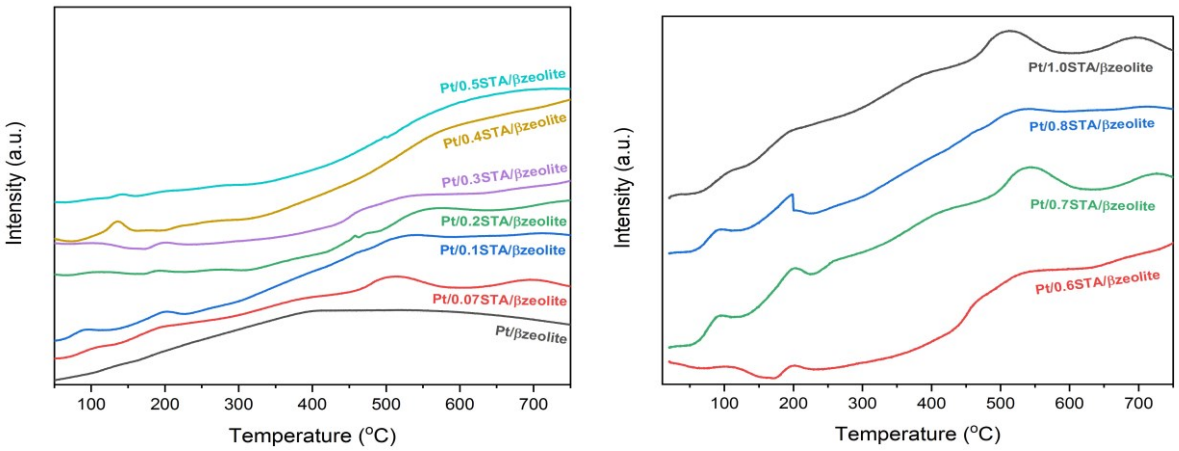

Figure 4.6. H_2-TPR profiles of the prepared catalysts up to Pt-1.0STA/β-zeolite

Pt on β-zeolite support can form five different species, which includes: PtO (80 °C) and PtO_2 (160 –180 °C) species located inside the zeolite channels; Pt^{2+} ions (250 °C) and Pt^{4+} ions (320–350 °C) located in the zeolite formed by ion-exchange process (by replacing H^+ ions which were generated from NH^{4+} ions after calcination of β-zeolite, which were present in the zeolite framework to balance a negative charge produced during Al^{3+} substitution in place of Si^{4+}) and lastly Pt^{2+} ions coordinated with silanol group as Pt–$(O–Si\equiv)_y^{2-y}$ species (400–550 °C) in the defects of β-zeolite [175,176]. In our case, the Pt/β-zeolite catalyst shows a broad reduction peak at a maximum temperature around 400 °C, which shows a strong interaction between Pt^{2+}

ions and β-zeolite support. These Pt^{2+} ions after reduction with H_2 give rise to protons (See Eq 4.1) of significant Brønsted acidity [175],

$$Pt^{2+} + H_2 \longrightarrow Pt^0 + 2H^+ \qquad \text{Eq 4.1}$$

The addition of STA to the Pt/β-zeolite catalyst considerably reduced the PtOx reduction temperature, perhaps due to the strong electronic interaction between WO_x (STA) and PtOx species [114]. The STA-loaded catalysts show the other peaks at higher temperatures which correspond to the reduction of WO_3 or WO_x species [114]. The reduction profiles for Pt-xSTA/β-zeolite catalysts are very broad and may contain multiple overlapping peaks. According to Barton et al. [162], the reduction profiles for WO_3 are broad and contain three overlapping peaks in three different temperature zones: at 300–500 ºC (WO_3 to $WO_{2.9}$) at 550–700 ºC ($WO_{2.9}$ to WO_2) and at 750–850 ºC (WO_2 to W). After reduction with H_2, the WO_3 or WOx species forms the $HxWO_3$ species, which has considerable acidity and is helpful in glycerol hydrogenolysis.

From the foregoing discussion of the catalyst characterization results, it is clear that the catalyst Pt–0.3STA/β-zeolite and Pt–0.7STA/β-zeolite exhibit sufficient surface area, good platinum dispersion, good reducibility, and high Brønsted acidity. Therefore, these catalysts were further subjected to chemical state and TEM analysis. The following section explains the obtained results.

4.1.8 Crystallite size by transmission electron microscopy (TEM)

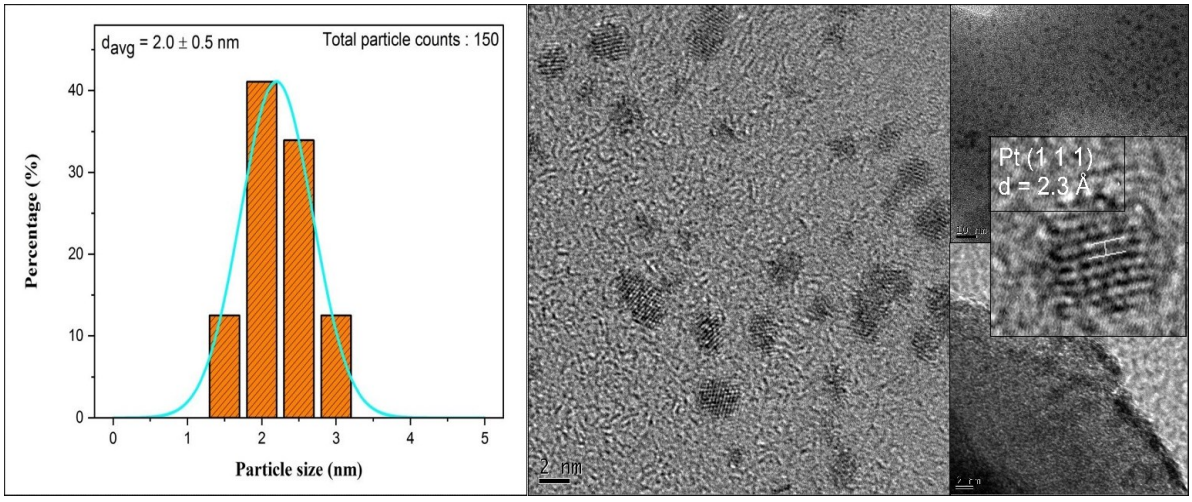

Figure 4.7. TEM images of the catalyst Pt/0.3STA/β-zeolite, the particle size distribution, and the average particle diameter.

The size and morphology of Pt–0.3STA/β-zeolite and Pt–0.7STA/β-zeolite catalysts were determined by high-resolution transmission electron microscopy (HRTEM). The obtained results are illustrated in Figure 4.7 and Figure 4.8, which show the HRTEM images of the reduced Pt/0.3STA/β-zeolite and Pt/0.7STA/β-zeolite catalysts, respectively.

The average particle size of Pt in both cases varies from 1 to 4 nm (see the histogram, particle count 150 to 250) with highly dispersed spherical platinum particles. It can be observed that the Pt particles were largely located on the external surface of the β-zeolite catalyst, and a small fraction of Pt might have been located within the β-zeolite channels. This result shows a good dispersion of the platinum particles on the 0.3STA/β-zeolite and 0.7STA/β-zeolite catalyst support, and there was not any noticeable agglomeration of Pt particles present.

The observed particles in the HRTEM images were confirmed as metallic platinum by means of the lattice fringes (d = 0.23 nm) of the Pt 111 plane. It was observed that the average particle size of metallic platinum on the Pt/xSTA/β-zeolite catalyst was totally dependent on the STA loading.

Here, for the Pt/0.3STA/β-zeolite catalyst, the average Pt particle size estimated from the TEM histogram is 2 ± 0.5 nm and from the CO-chemisorption is 2.8 nm which is slightly higher. Similarly, for the Pt/0.7STA/β-zeolite catalyst, the TEM histogram shows the average Pt particle size as 2.3 ± 0.5 nm, whereas CO-chemisorption estimated it to be 7.1 nm which is very large. Iglesia et al. [177] reported that the average particle sizes obtained by TEM are actual sizes and CO-chemisorption uptakes over predicts the particle sizes.

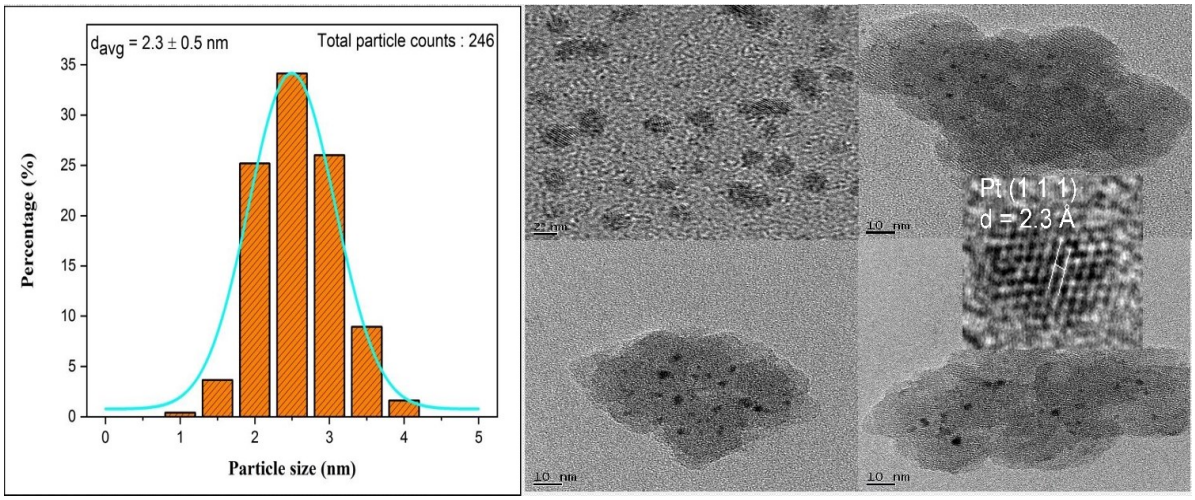

Figure 4.8. TEM images of the catalyst Pt/0.7STA/β-zeolite, the particle size distribution and the average particle diameter.

These results confirm that the reduction in Pt dispersion or increment in Pt size determined by CO-chemisorption is not due to an actual reduction in Pt size but due to blocking Pt particles by excess STA species.

4.1.9 X-ray photoelectron spectroscopy (XPS)

X-ray photoelectron spectroscopy (XPS) is a helpful method to probe the oxidation state, elemental composition, and the electronic environment of each component present on the catalyst surface [178–181]. In this work, XPS analysis has been used to identify the surface chemical states of the Pt-0.3STA/βzeolite and Pt-0.7STA/βzeolite catalysts after reduction at 400 ºC. Figure 4.9 (A) shows the W 4f spectra, and Figure 4.9 (B) shows the Pt 4d spectra of the Pt/0.3STA/βzeolite catalyst. The Pt 4d lines were analyzed instead of the most intense Pt 4f lines due to their serious overlapping with the strong Al 2p peaks [173]. The two peaks at ca. 315.2 and 331.5 eV were ascribed to Pt $4d_{5/2}$ and Pt $4d_{3/2}$ of metallic Pt, respectively. The obtained results suggest that the surface Pt species had been completely reduced to zero-valent Pt (Pt0) [46]. Figure 4.10 (B) consists of two spin-orbit components. In the W 4f region, the doublet at ca. 34.9 and 37.2 eV binding energies corresponded to W $4f_{7/2}$ and W $4f_{5/2}$ of W^{5+}. The binding energies at 35.9 and 38.1 eV were assigned to W $4f_{7/2}$ and W $4f_{5/2}$ of W^{6+}. The intensity ratio of $W^{5+}/(W^{5+} + W^{6+})$ is 0.12. The amount of W^{5+} formed corresponds to the density of Brønsted acid sites.

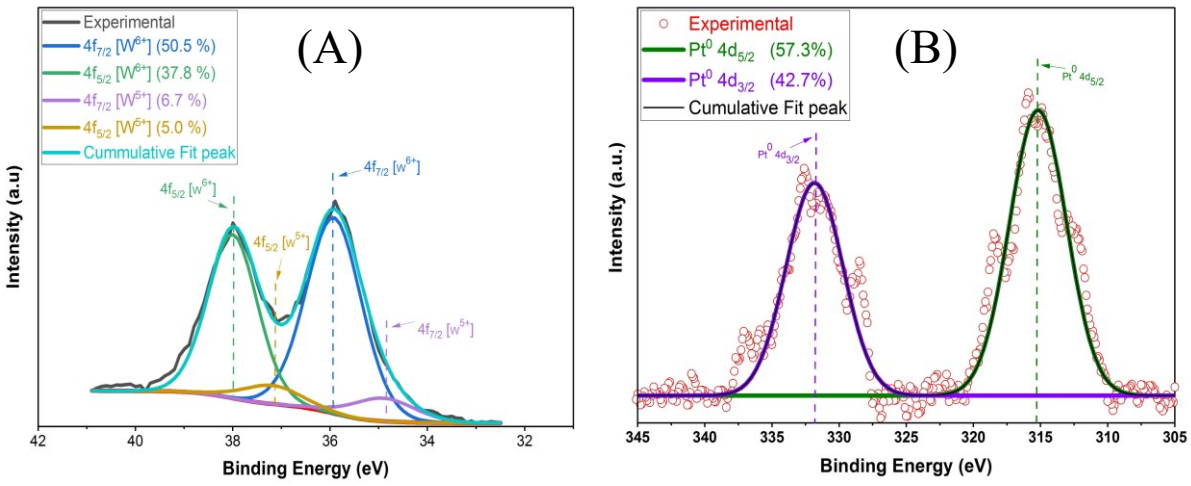

Figure 4.9. W 4f (A) and Pt 4d (B) XPS photoemission peaks of Pt/0.3STA/β-zeolite catalyst

Similarly, the Pt/0.7STA/β-zeolite catalyst was analyzed using the XPS technique. Figure 4.10 (A) shows the W 4f spectra, and Figure 4.10 (B) shows the Pt 4d spectra of the Pt/0.7STA/β-zeolite catalyst. In this case, the results show that the surface Pt particles were reduced to zero-

valent Pt (Pt^0) completely. The intensity ratio of $W^{5+}/(W^{5+} + W^{6+})$ was 0.14, slightly higher than the former catalyst. This could be attributed to the higher concentration of the Brønsted acid sites present in the Pt/0.7STA/β-zeolite catalyst, which would have formed after the reduction of W^{6+} ions to W^{5+} at a temperature of 400 °C. These results also confirm that the catalyst Pt/0.7STA/β-zeolite contains higher Brønsted acidity than Pt/0.3STA/β-zeolite catalyst in agreement with TGA and FTIR results.

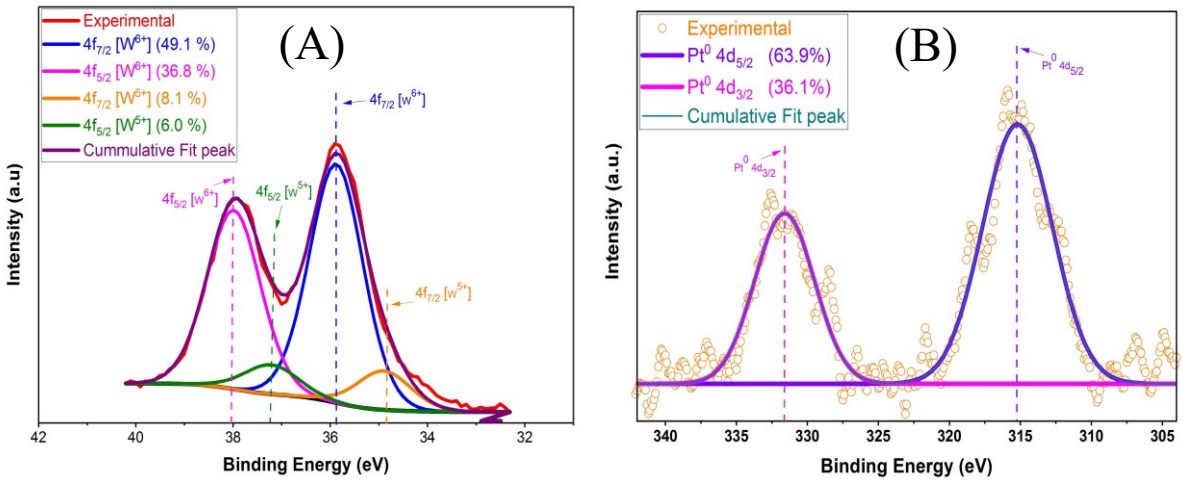

Figure 4.10. W4f (A) and Pt 4d (B) XPS photoemission peaks of Pt/0.7STA/β-zeolite catalyst.

Fan et al. [108] have reported a $W^{5+}/(W^{5+} + W^{6+})$ intensity ratio of 0.12 for Pt–WO_x/t-ZrO_2 catalyst, over which they found a considerable selectivity for 1,3-PDO (74%). Zhu et al. [114] reported the existence of strong electronic interaction between Pt^0 and WO_x species where the electron was likely to move from Pt^0 to WO_x species, which resulted in the formation of W^{5+} species. In our case, the presence of W^{5+} species clearly shows the hydrogen spillover from Pt to STA species. It helps in generating active hydrogen and W^{5+} species simultaneously, which greatly enhances the reaction rate of hydrogenation of intermediates (3-hydroxypropanal) in glycerol hydrogenolysis.

4.2 Heteropolyacid promoted catalyst

Heteropolyacids (HPAs) have shown excellent catalytic activity in homogeneous as well as heterogeneous acid-catalyzed reactions due to their unique features, such as adjustable acidity and well-organized structures [182,183]. HPAs have stronger Brønsted acidity, uniform acid sites, and acidity that is more easily tunable than that of metal oxides [184]. In addition to this,

HPAs are less toxic, relatively stable under humid conditions, easily soluble in polar solvents such as water, ketones, and lower alcohols [79,83]. HPAs are used as catalysts in different acid-catalyzed reactions, *viz.* glycerol dehydration, alcohol dehydration, hydration of olefins or esters, and alkene hydration [185,186]. It was reported by Micek-Ilnicka [187] that the tungsten-containing HPAs possess higher thermal stability, lower oxidation potential, and stronger acidity compared to molybdenum-containing HPAs. However, the main drawbacks of using unsupported HPAs as a catalyst in the reaction are their low surface area (<10 m^2/g), less thermal stability, and easy leaching in polar solvents affecting their performance in a long hour reaction under severe reaction conditions. To address this issue, HPAs are often supported over high surface area porous materials, *viz.* SiO_2, ZrO_2, Al_2O_3, AC, etc.

Moreover, the dehydration step involved in glycerol hydrogenolysis requires a strong acid; the use of supported HPAs would be promising. Furthermore, the high SiO_2 to Al_2O_3 ratio zeolites have low acidity but high surface area. Hence, supporting the HPAs on such zeolites will impart acidity to the zeolites and surface area to the HPAs. It is worth studying the HPAs promoted zeolites with a high SiO_2 to Al_2O_3 ratio as an acid catalyst for hydrogenolysis of glycerol to 1,3-PDO using Pt as an active metal.

Three HPAs, namely silicotungstic acid (STA), phosphotungstic acid (PTA), and phosphomolybdic acid (PMA), were supported on β-zeolite. The characterization results for STA promoted catalysts have already been discussed in the sections above. PTA and PMA supported on β-zeolite are compared with the earlier results here. The loading of PTA or PMA is chosen as 0.3 and 0.7 because over these loadings STA promoted catalysts have shown higher Brønsted acidity, which favors the formation of 1,3-PDO from glycerol.

The PTA and PMA promoted catalysts were characterized using similar techniques as discussed in the previous sections. The results are discussed in the following section.

4.3 Physico-chemical properties of heteropolyacid promoted catalysts

The textural properties of the Pt–xHPA/β-zeolite (x=0.3 and 0.7) catalysts are listed in Table 4.5. The nitrogen adsorption-desorption isotherms are shown in Figure 4.11 (A). The surface area of the Pt-0.3PTA/β-zeolite catalyst was 369 $m^2\ g^{-1}$, that of Pt-0.3PMA/β-zeolite catalyst

was 365 m^2 g^{-1}. In the case of Pt-0.7PTA/β-zeolite and Pt-0.3PMA/β-zeolite catalysts, the surface area was 287 and 284 m^2 g^{-1}. The surface area in both cases is nearly similar to STA promoted catalysts.

Figure 4.11 (A) shows that all catalysts with HPA to β-zeolite ratio 0.3 showed type I isotherm with type H3 hysteresis loop after $P/P^0 \approx 0.42$ as observed for β-zeolite [50,157] and also for Pt-0.3STA/β-zeolite catalyst (See Figure 4.1(I)). In the case of HPA to β-zeolite ratio 0.7 catalysts, the sorption isotherm was of type I with hysteresis loop of type H4 as observed in the case of Pt-0.7STA/β-zeolite catalyst (See Figure 4.1(II)). This confirms that the deposition of Pt and HPAs does not affect the qualitative aspects of the porous structure of the parent β-zeolite catalyst. The microporosity was retained in the prepared catalysts. The reduction in the micropore volume of β-zeolite (0.184 cm^3 g^{-1}) catalyst after the addition of HPA indicates HPA deposition in the pores of the β-zeolite catalyst.

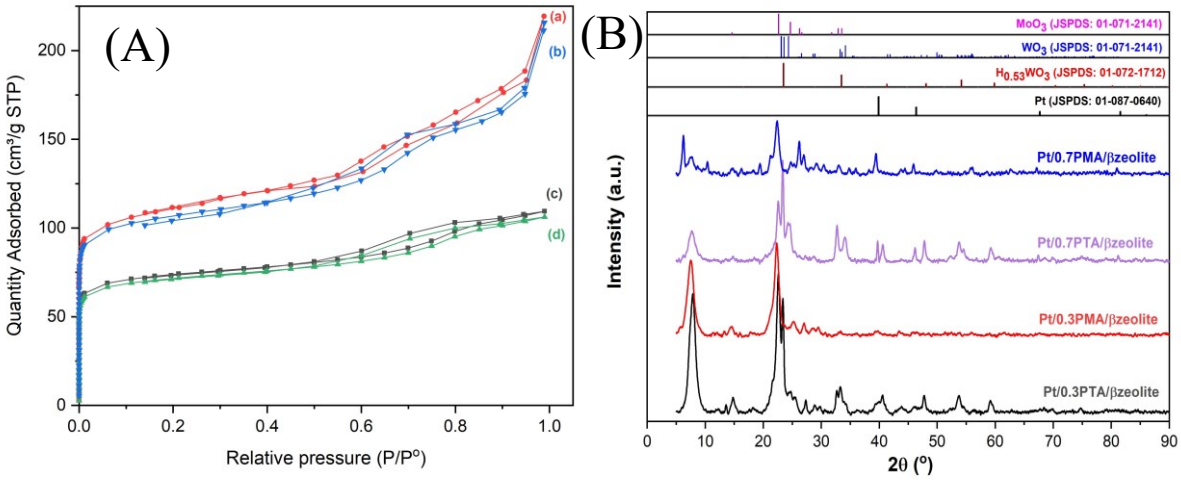

Figure 4.11. N_2 physisorption isotherm (A) and XRD spectra (B) of heteropoly promoted catalyst

Figure 4.11(B) shows the diffraction patterns of the Pt–HPAs/β-zeolite (HPA= PTA and PMA) catalysts with 0.3 and 0.7 HPA to β-zeolite ratio. The diffraction peaks for parent β-zeolite, Pt, WO_3, and H_xWO_3 were already discussed in the previous section (see section 4.1.2). In the case of Pt-0.3PMA/β-zeolite, the peaks correspond to neither the PMA keggin structure (JCPDS: 01-070-1705) nor the PMA decomposition products such as molybdenum phosphate/MoP_2O_7 (JCPDS: 00-039-0026) or molybdenum oxide/MoO_3 (JCPDS: 00-001-0706) was observed, most likely because of their good dispersion over the β-zeolite support. While in the case of Pt-0.7PMA/β-zeolite, the peaks corresponding to MoO_3 were observed. This may be because the

formation of MoO3 from PMA starts at a temperature of 350 ºC [82], and due to the excess amount of PMA in a catalyst, the formed MoO_3 is visible in XRD spectra.

On the other hand, Pt-xPTA/β-zeolite (x=0.3 and 0.7) has shown some peaks either corresponding to $HxWO_3$ or m-WO_3. However, the peaks representing keggin PTA were not present, indicating that either the tungsten-HPAs have fully decomposed to $H_{0.53}WO_3$/m-WO_3 or the keggin tungsten-HPAs were dispersed well over the β-zeolite surface. The peaks corresponding to m-WO_3 were present in both the catalysts and their intensity was increased in the case of the Pt-0.7PTA/β-zeolite catalyst. The $H_{0.53}WO_3$ possess the Brønsted acid sites which are essential for the selective conversion of glycerol to 1,3-PDO [150].

4.4 Platinum dispersion and acidic properties of HPA/β-zeolite catalysts

The platinum (Pt) particle dispersion over the Pt-xHPA/β-zeolite (x=0.3 and 0.7) catalysts was estimated using CO adsorbed quantity over it. The observed results of Pt dispersion are shown in Table 4.4.

Table 4.4. Textural properties and Pt dispersion of heteropolyacid promoted catalysts

Catalyst	S_{BET} ($m^2\ g^{-1}$)	S_{micro} ($m^2\ g^{-1}$)	S_{meso} ($m^2\ g^{-1}$)	V_{total} ($cm^3\ g^{-1}$)	V_{micro} ($cm^3\ g^{-1}$)	Pt dispersion (%)
Pt/0.3PTA/β-Zeolite	369	287	82	0.310	0.125	30.9
Pt/0.3PMA/β-Zeolite	365	285	80	0.295	0.115	22.8
Pt/0.7PTA/β-Zeolite	287	229	58	0.174	0.099	13.1
Pt/0.7PMA/β-Zeolite	284	227	57	0.170	0.094	11.9

The results show that the dispersion of Pt increased with the addition of HPA to Pt/β-zeolite catalyst. It shows the addition HPAs to the β-zeolite catalyst increases the metal dispersion due to increased interaction between HPAs and β-zeolite. For 0.3 HPA to β-zeolite ratio, the Pt dispersion was higher over Pt-0.3PTA/β-zeolite followed by Pt-0.3PMA/β-zeolite catalyst. For

0.7 HPA to β-zeolite ratio catalysts, the trend was similar; the Pt dispersion was higher over Pt-0.7PTA/β-zeolite and then Pt-0.7PMA/β-zeolite catalysts. The STA containing catalysts has given the highest Pt dispersion with both the loadings.

The total, Lewis, and Brønsted acidity of the xHPA/β-zeolite (x=0.3 and 0.7) catalysts were measured using different techniques. The observed results are shown in Table 4.5.

Table 4.5. Acidic sites of heteropolyacid promoted catalysts using different techniques

Catalyst	Py-FTIR[a] (μmol $g_{cat.}^{-1}$)		TGA[b] (μmol $g_{cat.}^{-1}$)		NH3-TPD[c] (μmol $g_{cat.}^{-1}$)		
	Brønsted	Lewis	Brønsted	Total	Weak	Strong	Total
Pt/0.3PTA/β-Zeolite	65.9	205.7	313.2	1017.4	945.1	403.2	1348.4
Pt/0.3PMA/β-Zeolite	9.2	223.6	70.0	836.5	897.7	312.5	1210.2
Pt/0.7PTA/β-Zeolite	78.2	189.9	403.5	1083.7	875.9	498.2	1374.1
Pt/0.7PMA/β-Zeolite	23.3	218.4	96.3	895.5	844.1	397.2	1241.3

The results show that the catalyst Pt-0.3PTA/β-zeolite showed the highest total acidity, whether by FTIR or by TGA (higher than Pt-0.3STA/β-zeolite catalyst). However, the Pt-0.3PTA/β-zeolite catalyst showed Brønsted acidity lower than Pt-0.3STA/β-zeolite catalyst but higher than the Pt-0.3PMA/β-zeolite catalyst. The 0.7 HPA to β-zeolite ratio containing catalysts followed the same fashion as the Pt-0.7PTA/β-zeolite catalyst showed the highest total acidity and second-highest Brønsted acidity. The catalyst Pt-0.7PMA/β-zeolite showed the lowest total and Brønsted acidity.

4.5 Conclusion

The characterization results of Pt-xHPA/β-zeolite catalysts showed how STA or HPA is beneficial in increasing the Brønsted acidity of the catalyst preferentially. This is relevant in view of the literature suggesting that Brønsted acidity is required to enhance the 1,3-PDO selectively in glycerol hydrogenolysis. The N_2 physisorption result shows the addition of STA doesn't affect the textural properties of β-zeolite, and micro-porosity was retained up to 4.0 STA to β-zeolite ratio. The XRD data revealed the existence of tungsten bronze phase ($H_{0.53}WO_3$) and crystalline m-WO_3 in STA or PTA promoted catalysts. In the case of PMA containing catalysts, peaks related to MoO_3 were observed at 0.7 PMA to β-zeolite ratio. The CO-chemisorption results revealed an increase in the dispersion of platinum with the increase in STA or HPA to β-zeolite ratio. The HRTEM analysis proves that the reduction in Pt dispersion or increase in Pt size at higher HPA to β-zeolite ratio was not due to size change but due to covering Pt particles by excess HPA species.

The TPR analysis shows a reduction in temperature due to increased interaction between Pt and WOx species and confirms the spillover of hydrogen from Pt to WOx species. The XPS analysis also revealed H_2 spillover and strong electronic interaction between Pt^0 and WO_x species. The acidity characterization study revealed that the addition of HPA increases the acidity of the catalyst. In the case of STA promoted catalyst, the Pt–0.7STA/β-zeolite catalyst showed the highest Brønsted acidity followed by Pt–0.3STA/β-zeolite catalyst, and Pt–0.5STA/β-zeolite catalyst showed the highest total acidity. The PTA-containing catalysts showed higher total acidity. However, their Brønsted acidity is still less than STA-containing catalysts.

The catalyst characterization results of this chapter will be helpful in relating the performance of glycerol hydrogenolysis over each catalyst in the coming chapters.

Chapter 5:
RESULTS AND DISCUSSION

5.1 Results and discussion

From the catalyst characterization results given in Chapter 4, it is clear that the addition of STA to Pt/β-zeolite catalyst increases catalyst acidity, dispersion, reducibility properties, etc. In this chapter, we will study the performance of STA promoted catalysts on glycerol hydrogenolysis reaction to relate the reaction performance to physicochemical characteristics of the catalysts and find the best performing catalyst from the series of catalysts. The effect of reaction parameters is then explored. The performance of the catalyst will be decided primarily by its 1,3-PDO selectivity.

The hydrogenolysis of glycerol was studied over the synthesized catalysts at standard reaction conditions, *viz.* 220 ^{o}C, 40 bar initial H_2 pressure, 2.0 g of synthesized catalyst (2.5 wt% of reaction mixture), 80 ml of 5 wt% glycerol aqueous solution and a reaction time of 5 h. In several cases, the experiments were repeated two times to check reproducibility, and in all cases, the reproducibility was found to be satisfactory. The results from repeat experiments have been shown by error bars in the figures discussed in the coming sections.

5.1.1 Performance evaluation: Role of catalyst constituents

The catalyst of interest is the combination of three species: platinum (Pt), silicotungstic acid (STA), and β-zeolite. Each of these species plays a role in the reaction, and we try to understand the same by conducting reactions with specific catalyst formulations. The hydrogenolysis of glycerol was studied over β-zeolite, Pt/β-zeolite, Pt/0.1STA/β-zeolite, and 0.3STA/β-zeolite, under otherwise similar conditions. Figure 5.1 compares the results. In All the figures (experiment results), the term "Others" represents a lumping of products such as 2-propanol, acetone, ethanol, methanol, hydroxyacetone, acrolein, ethylene glycol, etc.

The results show that the conversion of glycerol (see Figure 5.1 (I)) improved with the addition of Pt to β-zeolite catalyst. However, 1,2-PDO selectivity (see Figure 5.1 (III)) also increased, and Pt/β-zeolite catalyst has shown the highest selectivity towards the 1,2-PDO. It is probably due to the higher Lewis acid content of the catalyst. Zhu et al. [93] have observed a similar trend over Pt/ZrO_2 catalyst due to its larger Lewis acidity.

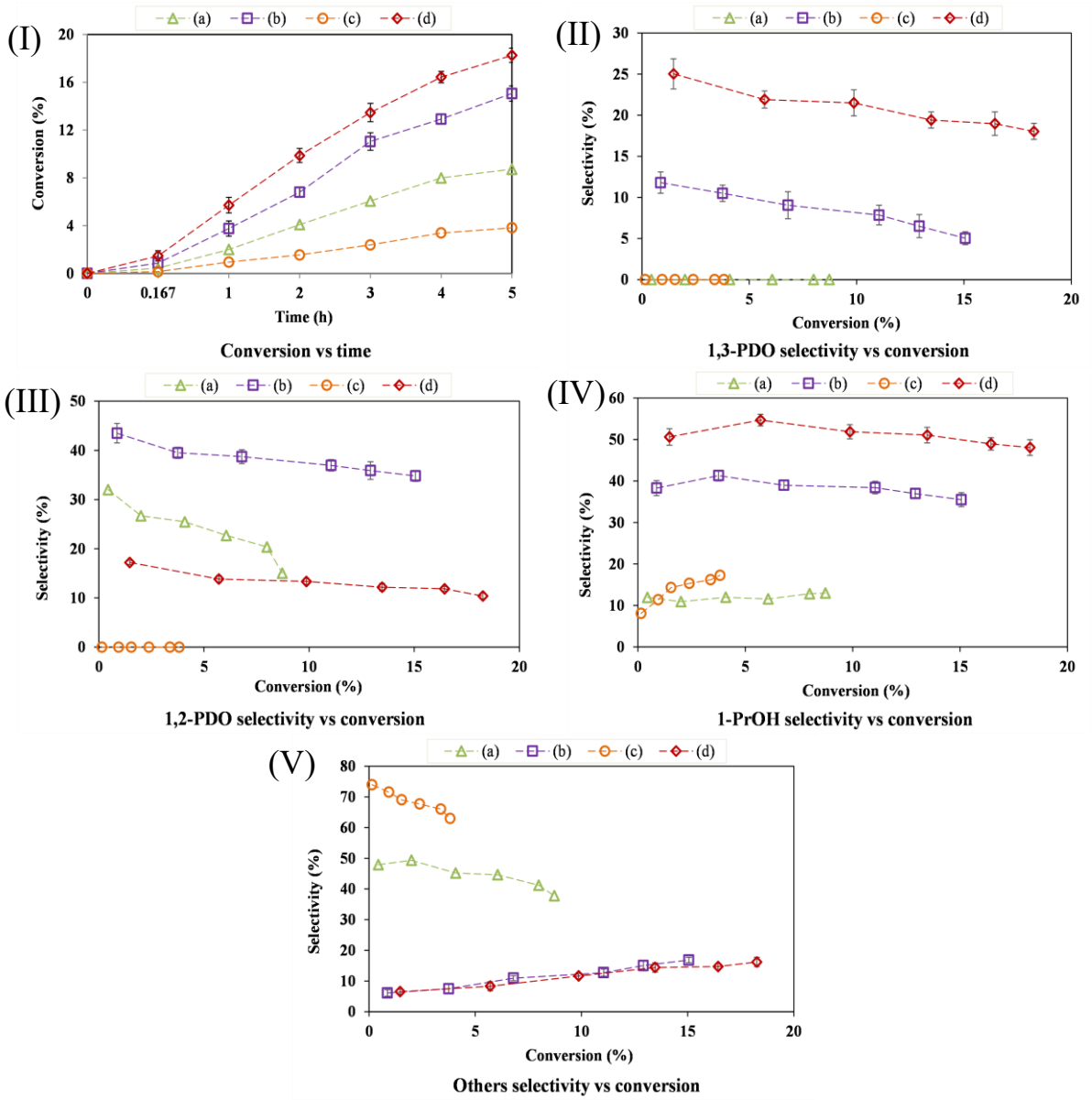

Figure 5.1. Glycerol hydrogenolysis reactant and product profiles for different catalyst formulations: (a)β-zeolite, (b) Pt/β-zeolite, (c) 0.3STA/β-zeolite, (d) Pt/0.1STA/β-zeolite

When we used β-zeolite as the catalyst, the main reaction product was ethanol, which would have formed *via* C–C cleavage of glycerol (ethylene glycol to ethanol). The addition of Pt reduced the ethanol formation but increased the 1-PrOH formation. This could be due to an increase in the hydrogenation of dehydrated glycerol to 1-PrOH by metal sites. Here, the reason

for the formation of higher 1-PrOH is the β-zeolite support itself. Many published studies on glycerol hydrogenolysis over zeolite catalysts have reported a higher selectivity to 1-PrOH [50,115,134]. Sometimes, even using a physical mixture of zeolites with other solid catalysts like Ni/Al_2O_3 or $Ir\text{-}ReO_x/SiO_2$ has resulted in high selectivity to 1-PrOH [62,133]. Thus, the obtained results and literature clearly show that 1-PrOH forms as one of the main products of glycerol hydrogenolysis over zeolite-supported catalysts.

A possible route through which 1-PrOH may form over Pt/β-zeolite catalyst is the over hydrogenolysis of propanediols [93]. While this is possible, Figure 5.1 (IV) clearly shows the formation of 1-PrOH from the very start of the reaction in all cases. This result indicates the existence of a possible parallel route to 1-PrOH directly from glycerol over Pt/β-zeolite catalyst. It could be via glycerol dehydration to acrolein over-acidic sites, followed by fast hydrogenation to 1-PrOH over metal sites [62]. The dehydration of glycerol to acrolein over different zeolites has already been proven [128]. Therefore, we hypothesize that the higher formation of 1-PrOH over Pt/β-zeolite catalyst is *via* acrolein through a dehydration-hydrogenation route. It is worth noting that we have not observed a noticeable amount of acrolein during the reaction (around 4-7% w/w), suggesting a high rate of hydrogenation of acrolein under the prevailing conditions [188]. 1-PrOH formation can thus be reduced either by blocking the active sites of β-zeolite, which promote the 1-PrOH or ethanol formation [50] or by reducing the surface area of β-zeolite because of which glycerol gets converted to acrolein despite the low acidity of β-zeolite [128].

On the other hand, as has been noted and it is widely reported [105,123,145,150] that the formation of 1,3-PDO from glycerol hydrogenolysis requires the presence of Brønsted acid sites. These sites are essential for the conversion of glycerol to 3-hydroxypropanal (3-HPA) (see Figure 2.1), which is an intermediate for the formation of 1,3-PDO [189]. It has also been reported that the addition of tungsten species (STA) increases the Brønsted acid sites or acidic protons of the catalyst [123,162]. Additionally, promoting the Pt-containing catalysts with STA may increase the hydrogen spillover, which increases the catalyst performance by increasing the hydrogenation of 3-HPA to 1,3-PDO [114]. Our results do indeed show that the presence of STA (WO_x) in the Pt/β-zeolite catalyst helps in improving the 1,3-PDO selectivity and glycerol conversion (see Figure 5.1 (II)) results related to Pt/0.1STA/β-zeolite).

Most importantly, the selectivity of 1,2-PDO was reduced by a great extent when STA was added. However, the 1-PrOH selectivity has further increased, probably due to the over hydrogenolysis of 1,2-PDO as 1-PrOH forms largely *via* 1,2-PDO, as discussed later. Hence,

while the addition of STA looks attractive, its amount needs to be optimized so that the formation of 1-PrOH via 1,2-PDO (on Lewis acid sites) is curtailed. Therefore, different catalysts with varying STA to β-zeolite ratios were prepared and investigated, as discussed in the next section.

In order to further investigate the role of Pt and the possible synergy between Pt and STA, we studied the glycerol hydrogenolysis over Pt-free 0.3STA/β-zeolite catalyst. The results show that the glycerol conversion dropped to only 3.82% (after 5 h). The main product of the reaction was acrolein with 63.96% selectivity (see Figure 5.1 (V)); acetol was also observed with 10.86% selectivity. Alhanash et al. [45] have reported that the Lewis acid sites predominantly produce acetol (an intermediate in the formation of 1,2-PDO) and the Brønsted acid sites are responsible for the formation of acrolein (which forms by the dehydration of 3-HPA) during the glycerol dehydration process. Our results clearly show that the addition of STA provides the Brønsted acidity to the catalyst, as the primary product of the reaction was acrolein, and hence, the results are in agreement with those of Alhanash and others [93]. However, it is worth noting that 1,3-PDO was not formed at all over the 0.3STA/β-zeolite catalyst and the glycerol conversion was also very low, which clearly indicates the importance of metal catalyst in the formation of 1,3-PDO from glycerol. The hydrogenation metal (Pt) activates the hydrogen molecule present in the reaction environment [47,93,94].

5.1.2 Optimizing STA loading

The STA to β-zeolite ratio was varied over the range 0.07-100% STA, and the hydrogenolysis of glycerol was studied under otherwise similar conditions. The characterization result showed an increase in acidity up to 0.5 STA to β-zeolite ratio followed by a decrease in acidity (see Table 4.2). Moreover, the catalyst with a 0.3 and 0.7 STA to β-zeolite ratio showed higher Brønsted acidity than others. In view of these results, the optimization of STA is carried out by dividing the catalysts into three groups on the basis of STA to β-zeolite ratio: from 0.07 to 0.5, 0.6 to 1.0, and from 1.5 to 100% STA. The results are discussed in the same sequence in the following subsections.

a) STA to β-zeolite ratio from 0.07 to 0.5

Figure 5.2 shows the reactant conversion and product selectivity profiles over Pt/β-zeolite catalysts with STA to β-zeolite from 0.07 to 0.5. The glycerol conversion increased continuously with an increase in STA to β-zeolite ratio (see Figure 5.2 (I)). This can be

attributed to the increase in total acidity of the catalyst with increased STA loading (see Table 4.2). The 1,3-PDO selectivity showed an increasing trend with an increase in STA loading up

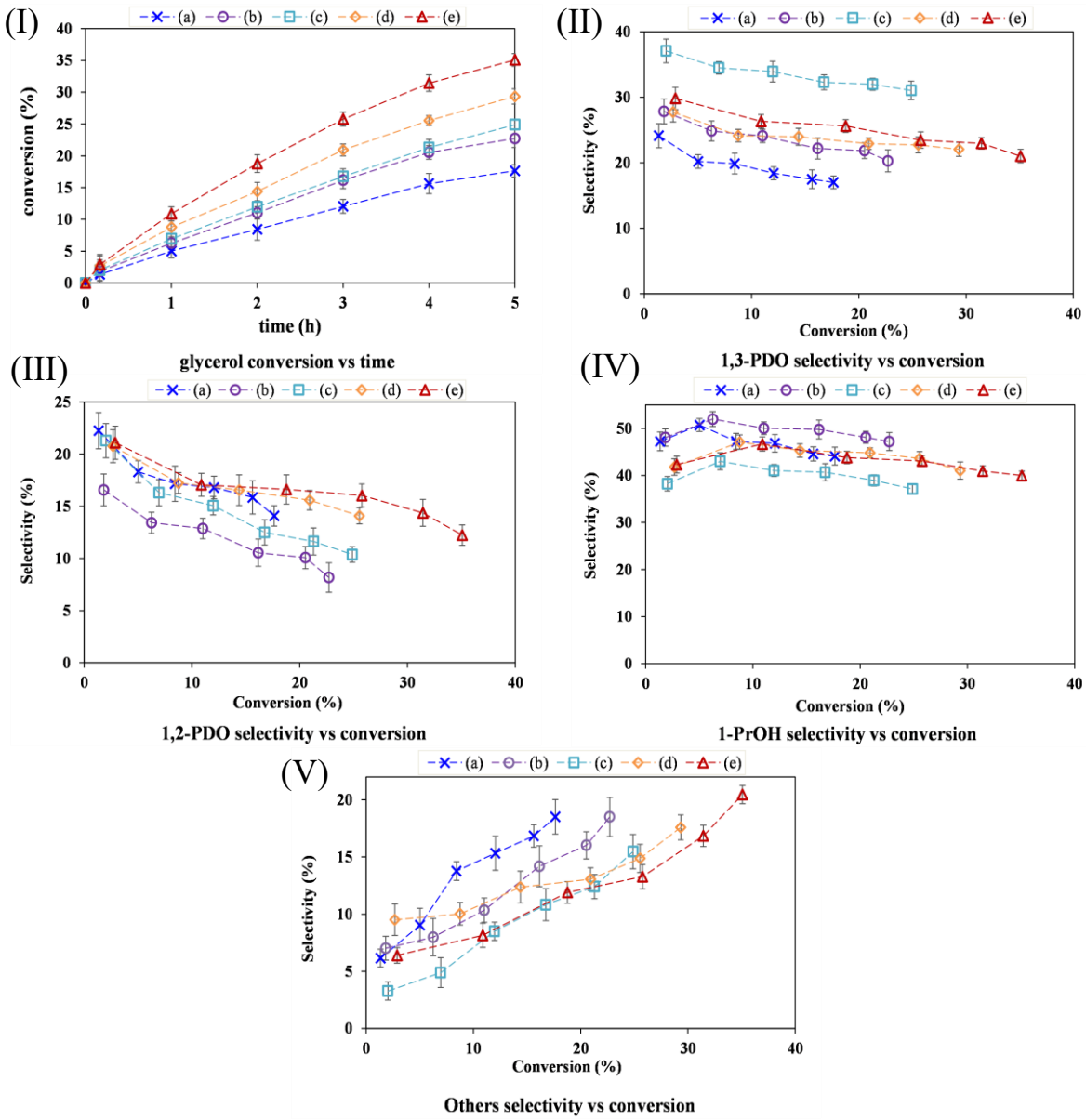

Figure 5.2. Glycerol hydrogenolysis reactant and product profiles for catalysts with different STA loadings: (a) Pt/0.07STA/β-zeolite, (b) Pt/0.2STA/β-zeolite, (c) Pt/0.3STA/β-zeolite (d) Pt/0.4STA/β-zeolite, (e) Pt/0.5STA/β-zeolite

to 0.3 (see Figure 5.2 (II)) but declined for higher loadings. The catalyst Pt-0.3STA/β-zeolite offered the higher 1,3-PDO selectivity as 31.04 ± 1.41% after 5 h, although an even higher selectivity was observed at higher STA loadings which will be discussed in the next section. As the characterization result showed, Brønsted acidity (see Table 4.2) was higher for this catalyst in the studied STA to β-zeolite ratio range (0.07 to 0.5), which helps in the selective formation of 1,3-PDO. It is also noteworthy that the catalyst has reached sub-monolayer coverage of STA at this loading (see Table 4.1). Similar results are reported by Zhu et al. [114]

for Pt–10WO_x/Al_2O_3 catalyst. Furthermore, 1,3-PDO is more stable compared to 1,2-PDO in the reaction environment, and its further conversion to 1-PrOH or other products is not that easy [93,190]. As expected, the selectivity of 1,2-PDO was also seen to be decreasing with an increase in STA to β-zeolite loading, but only up to 0.2 (see Figure 5.2 (III)). The catalysts with the higher STA loadings of 0.4 and 0.5 offered little higher selectivity (12 to 14%) for 1,2-PDO. The catalyst Pt-0.2STA/β-zeolite showed the lowest selectivity (8.17 ± 1.41% after 5 h) for 1,2-PDO, followed by Pt-0.2STA/β-zeolite (10.37 ± 0.75% after 5 h). As mentioned already, the 1-PrOH essentially forms from 1,2-PDO; we have observed the catalyst, which has shown the lowest 1,2-PDO selectivity, yielding the highest formation of 1-PrOH as seen in Figure 5.2 (IV). Here, most of the 1,2-PDO has been converted to 1-PrOH. Interestingly, the 1-PrOH selectivity seems to go through a maximum with conversion, the maximum occurring at about 10% conversion, but the formation of others increases continuously with the conversion. This indicates a need for careful optimization of the conversion target in the interest of the desired selectivity. We further observe that excessive acidity is also not favorable for this reaction as it may increase the over hydrogenolysis of PDOs to 1-PrOH.

The catalyst Pt-0.3STA/β-zeolite has shown the lowest value for 1-PrOH and others (see Figure 5.2 (IV) and (V)), and this is due to the highest Brønsted acidity, which converts glycerol to 1,3-PDO, and 1,3-PDO does not easily hydrogenolyse to subsequent products.

A catalyst reusability study for Pt-0.3STA/β-zeolite catalyst was also performed. For that, the catalyst of run 1 was washed with methanol 5 times, centrifuged, and then dried at 120 ^oC overnight. The dried catalyst was used for run 2, and the reaction was performed. The recovered catalyst of this run was used for run 3 and so on by following a similar procedure. The results of all of these reactions were consistent even after 4 runs. After the 4^{th} run (5-hour), the conversion of glycerol and 1,3-PDO selectivity were only lower by 1% and 0.88%, respectively.

b) STA to β-zeolite ratio from 0.6 to 1.0

This section shows the results of glycerol hydrogenolysis over the catalysts containing STA to β-zeolite ratios as 0.6, 0.7, 0.8, and 1.0. The hydrogenolysis of glycerol was studied under otherwise similar conditions. The results of this study are discussed in detail below.

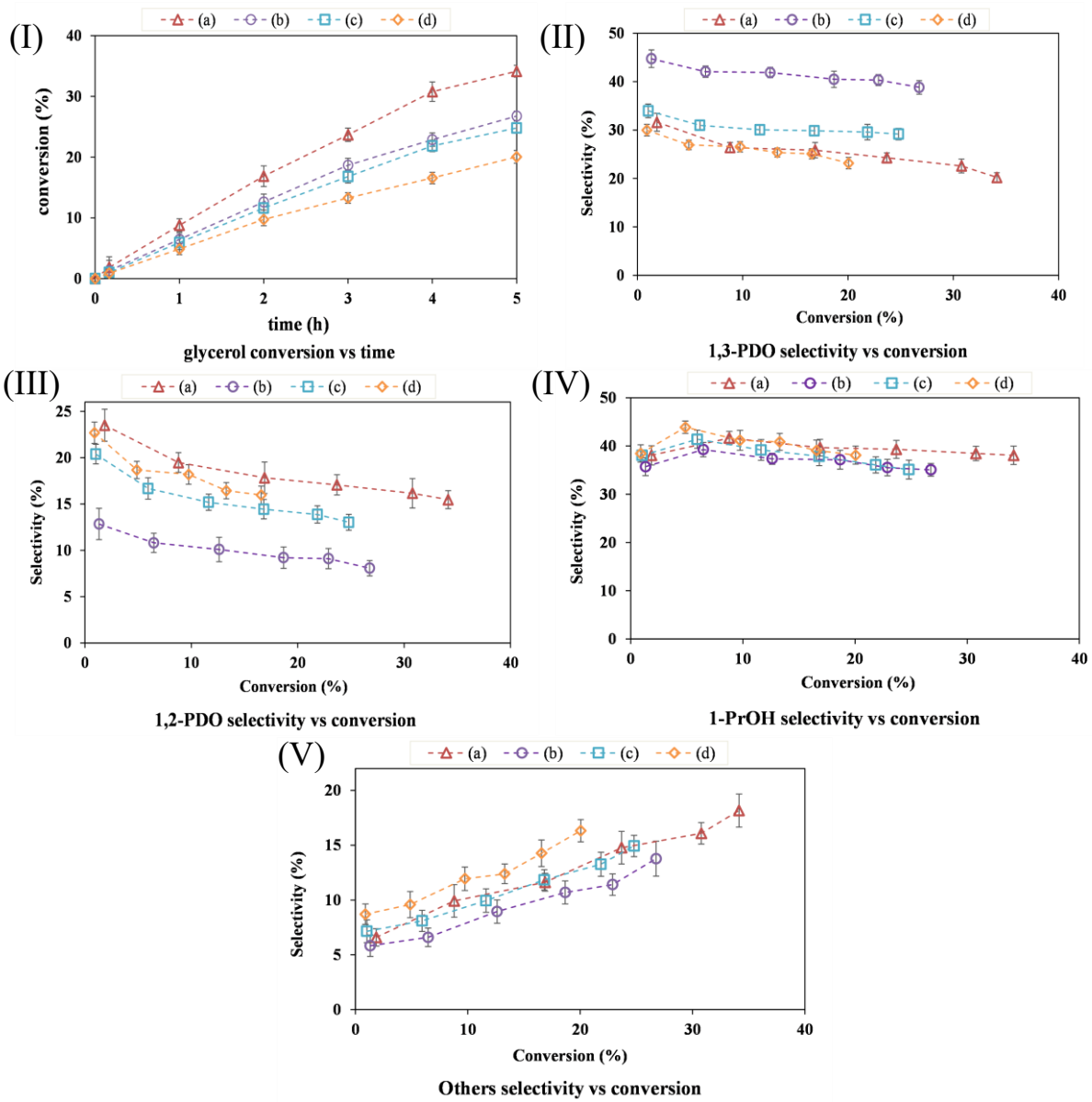

Figure 5.3. Glycerol hydrogenolysis reactant and product profiles for catalysts with different STA loadings: (a) Pt/0.6STA/β-zeolite, (b) Pt/0.7STA/β-zeolite, (c) Pt/0.8STA/β-zeolite (d) Pt/1.0STA/β-zeolite

The product selectivity and glycerol conversion profiles over Pt-xSTA/β-zeolite catalysts (x = 0.6 to 1.0) are shown in Figure 5.3. The results show that the catalyst Pt-0.6STA/β-zeolite gives the highest glycerol conversion as 34.14 ± 1.65%; beyond this, the glycerol conversion was reduced with an increase in STA to β-zeolite ratio as 26.76 ± 1.27% with 0.7, 24.8 ± 1.15% with 0.8, and 20.05 ± 1.04% with 1.0 STA to β-zeolite ratio (see Figure 5.3 (I)). The probable reason for the drop in glycerol conversion would be a decrease in the total acidity of catalysts (See Table 4.2) and surface area (See Table 4.1) with an increase in the STA to β-zeolite ratio 0.6 to 1.0. The 1,3-PDO selectivity was increased with an increase in STA to β-zeolite ratio from 0.6 to 0.7 (see Figure 5.3 (II)) but declined for higher ratios. The catalyst Pt-0.7STA/β-

zeolite shows the highest 5-hr selectivity to 1,3-PDO at 38.81 ± 1.39%. The highest selectivity of 1,3-PDO is attributed to the highest amount of Brønsted acid sites or the relatively high ratio of Brønsted to Lewis acid sites (see Figure 4.4 and Table 4.2). Moreover, this catalyst showed well-dispersed small Pt particles (See Figure 4.8 TEM results), good interaction between Pt and WOx species (see Figure 4.6 H_2-TPR and Figure 4.10 XPS results), and sufficient surface area (see Table 4.1). The catalyst with the highest Brønsted acidity (see Table 4.2) in the entire STA to β-zeolite ratio series has shown the lowest 1,2-PDO selectivity, the highest selectivity to 1,3-PDO and high rates of 1,2-PDO hydrogenolysis over it. The catalyst with higher Lewis acidity has shown the larger 1,2-PDO selectivity (see Figure 5.3 (III)). The observed 1,2-PDO selectivity over Pt-0.6STA/β-zeolite catalyst was 15.5 ± 1.15% and over Pt-0.7STA/β-zeolite catalyst was 8.07 ± 0.82%. The 1-PrOH selectivity is nearly constant in all the cases. However, the Pt-0.7STA/β-zeolite catalyst has the lowest value, as seen in Figure 5.3 (IV). This is probably due to the higher selectivity to 1,3-PDO, which is stable in the reaction environment, which will be discussed later. In all the STA promoted catalysts, it is only in the Pt-0.7STA/β-zeolite catalyst that the 1,3-PDO selectivity crosses the 1-PrOH selectivity. Due to the stability of 1,3-PDO in the reaction environment, it is more stable compared to 1,2-PDO, and its over hydrogenolysis to 1-PrOH or other products is not easy [15,16]. Hence, an increase in selectivity of 1,3-PDO decreases the selectivity of 1-PrOH. The formation of others increases continuously with the conversion over all the catalysts; however, catalyst Pt-0.7STA/β-zeolite (see Figure 5.3 (V)) shows the lower amounts.

A reusability study for the Pt-0.7STA/β-zeolite catalyst showed that the catalyst was reusable even after 5 cycles. After the 5^{th} run (5-hour), the conversion of glycerol and 1,3-PDO selectivity were only lower by 1.3% and 1.1%, respectively.

c) STA to β-zeolite ratio from 1.5 to 100% STA

This section shows the glycerol hydrogenolysis over the catalysts containing STA to β-zeolite ratios as 1.5, 2.3, 4.0, 9.0, and 100% STA (Pt/STA). The hydrogenolysis of glycerol was studied under otherwise similar conditions. The results of this study are discussed in detail below.

The product selectivity and glycerol conversion profiles over Pt-xSTA/β-zeolite catalysts (x = 1.5 to 9.0, and Pt/STA) are shown in Figure 5.4. The results show that the glycerol conversion was reduced with an increase in STA to β-zeolite ratio from 1.5 to 2.33, as observed over previous catalysts (0.6 to 1.0STA/β-zeolite). The catalyst Pt-1.5STA/β-zeolite showed 14.87%

and Pt-2.33STA/β-zeolite showed 12.46%. On the other hand, we observed a strange behavior in glycerol conversion over a further increase in STA to β-zeolite ratio from 4.0 to Pt/STA catalyst. The glycerol conversion increased with an increase in the STA to β-zeolite ratio: 13.6% at 4.0 STA to β-zeolite ratio, 16.4% at 9.0 STA to β-zeolite ratio, and 19.9% with Pt/STA catalyst (see Figure 5.4 (I)). The reason for an increase in the glycerol conversion at higher STA loadings despite the decrease in total acidity (see Table 4.2) is given by Tai et al. [191]. According to them, $HxWO_3$ species dissolve in hot water and act as a homogeneous catalyst. The catalyst again comes to $HxWO_3$ species on cooling.

Moreover, the catalyst was reusable at least 17 times without losing activity. In our case, the amount of $HxWO_3$ species increases with an increase in STA to β-zeolite ratio. These $HxWO_3$ species are responsible for the rise in conversion beyond STA to β-zeolite ratio 4.0. We haven't performed the reusability study over these catalysts because the selectivity of 1,3-PDO over them is less compared to other (previously studied) catalysts. In addition to $HxWO_3$ species, other factors also affect the rate of reaction, *viz.* surface area, acidity, Pt dispersion, etc. The Pt/STA catalyst has a very little surface area (SA) than the Pt-0.5STA/β-zeolite catalyst (its SA is 38 times more than Pt/STA). This could be the reason the latter catalyst has given higher glycerol conversion compared to the former, despite the high amount of $HxWO_3$ species and their dissolution in hot water in the case of the former (Pt/STA) catalyst.

On the other hand, it may be possible the platinum species would have leached in the solvent during $HxWO_3$ dissolution in hot water, but this study is out of our scope. This catalyst was prepared by impregnating STA and chloroplatinic acid at one time, followed by drying, calcination, and reduction.

It also needs to be emphasized that we have prepared the Pt/STA catalyst by calcining STA first, followed by Pt deposition (impregnation), then calcination and reduction of the formed catalyst. The observed glycerol conversion over this catalyst (prepared by separate calcination) was only 3.5%. This may be because prior calcination of STA will result in crystalline WO_3 species. These species are difficult to reduce, and only a small part will be able to convert to $HxWO_3$. Therefore, they possess less acidity and give low reactant conversion. However, using STA and Pt precursor together during synthesis will help it form $HxWO_3$ species during the reduction process, which possesses the Brønsted acidity as well as dissolves in hot water. Therefore, the conversion of the reactant is higher over a Pt/STA catalyst prepared via combined calcination than Pt/STA prepared via separate calcination.

The catalyst Pt/STA has shown the highest 1,3-PDO selectivity as 23.6% in this range of STA to β-zeolite ratio (1.5 to 100%STA), attributed to the higher concentration $HxWO_3$ species of Pt/STA catalyst which possesses the Brønsted acidity. All other catalysts showed 1,3-PDO selectivity in between 20 to 23% (See Figure 5.4 (II)).

The 1,2-PDO selectivity was lowest over a catalyst Pt-4.0STA/β-zeolite at 14.0%. All other catalysts showed 1,2-PDO selectivity in between 14.8 to 18% (See Figure 5.4 (III)). Moreover, this particular catalyst showed the highest selectivity for 1-PrOH as 40.2%, other catalysts showed 1-PrOH selectivity between 37 and 39% (See Figure 5.4 (IV)). As described previously, the 1-PrOH largely forms from 1,2-PDO and we have observed the catalyst which gives less 1,2-PDO is happened to give more 1-PrOH except for the highest Brønsted acidity catalyst (Pt-0.7STA/β-zeolite). Similar trends were also observed for Pt-0.2STA/β-zeolite and Pt-0.8STA/β-zeolite catalysts.

The selectivity to others was lowest over a Pt/STA catalyst as 14.7%, attributed to the highest selectivity of 1,3-PDO, which will not undergo over-hydrogenolysis easily. The other catalyst showed selectivity to others in between 15 to 17% (See Figure 5.4 (V)).

The selectivity to gaseous products, mainly propane, ethane, and methane, obtained through mass/carbon balance was in the range of 5 to 9% over all the catalysts.

To sum up, the best performing catalysts from the 1,3 PDO selectivity point of view in the entire STA to β-zeolite ratio range is Pt-0.7STA/β-zeolite, followed by Pt-0.3STA/β-zeolite catalyst.

The glycerol hydrogenolysis study over catalysts containing STA to β-zeolite ratio from 0 to 100% STA revealed that the addition of STA certainly affects the product distribution. Moreover, the interesting catalyst which offered higher 1,3-PDO selectivity and higher glycerol conversion lies in the range of 0 to 1.0 STA to β-zeolite ratio. In this ratio range, we have observed two regions. In region one, the glycerol conversion increases with an increase in STA to β-zeolite ratio up to 0.5. In another region, the glycerol conversion drops with an increase in STA to β-zeolite ratio beyond 0.5. On the other hand, we have observed higher 1,3-PDO selectivity in region one at sub-monolayer coverage and the highest 1,3-PDO selectivity in region 2 at STA to β-zeolite ratio 0.7. As our interest in the study is to focus on 1,3-PDO selectivity, and it was only higher in the STA to β-zeolite ratio range from 0 to 1.0. Therefore, we conclude that the interesting catalysts exist in the STA to β-zeolite ratio range from 0 to 1.0.

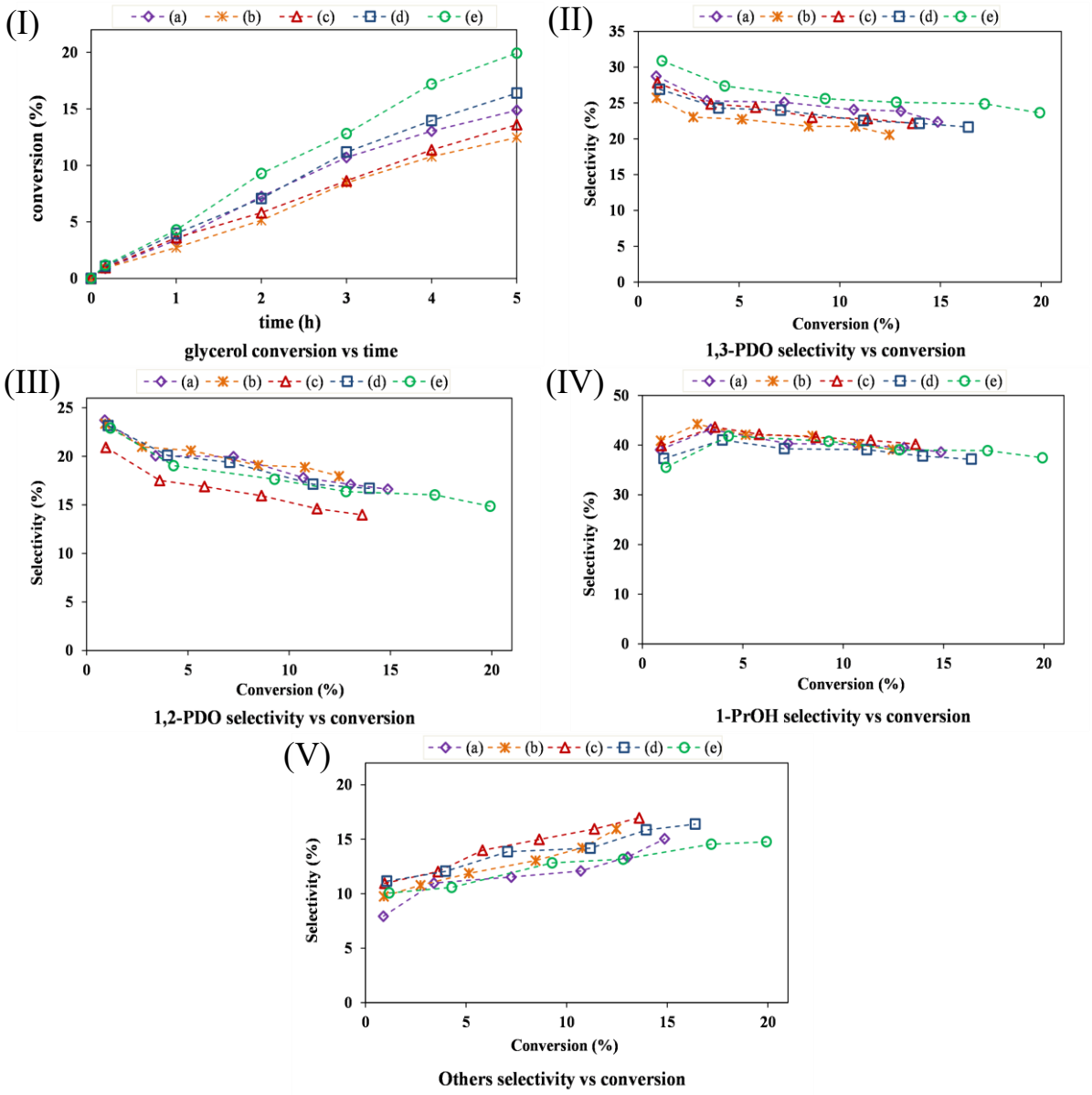

Figure 5.4. Glycerol hydrogenolysis reactant and product profiles for catalysts with different STA loadings: (a) Pt/1.5STA/β-zeolite, (b) Pt/2.33STA/β-zeolite, (c) Pt/4.0STA/β-zeolite (d) Pt/9.0STA/β-zeolite (e) Pt/β-zeolite

Moreover, total acidity is responsible for higher glycerol conversion and Brønsted acidity is responsible for 1,3-PDO selectivity. Therefore, we tried to relate the effect of total or Brønsted acidity with glycerol conversion or 1,3-PDO selectivity for these two regions, which will be discussed in the following section.

5.1.3 Effect of total and Brønsted acidity

a) Catalysts with STA to β-zeolite ratio in the range 0 to 0.5

Glycerol hydrogenolysis involves acid-catalyzed dehydration as an initial step to form the intermediates and subsequent hydrogenation on metal sites leading to the formation of several products. Hence, the presence of acid sites is extremely important for the initiation of glycerol hydrogenolysis [93,192,193]. Figure 5.5 (a) shows the total acidity, Brønsted acidity, and STA surface coverage of the catalysts synthesized. The total acidity was measured by NH_3-TPD technique, Brønsted acidity was measured by py-FTIR technique and surface coverage of STA was estimated using the formula given by Liu et al. [194]. The results show that the acidity of Pt/β-zeolite catalyst increases with the addition of STA continuously over the range of STA loadings studied, in line with the previous report [114]. The total acidity of the catalyst increased with an increase in STA to β-zeolite ratio up to 0.5.

On the other hand, the Brønsted acidity of the catalyst increases up to 0.3 STA to β-zeolite ratio and then decreases. It is seen that the surface coverage of STA on the Pt/β-zeolite catalyst increases continuously with the STA/β-zeolite ratio, achieving sub-monolayer coverage for 0.3 STA to β-zeolite ratio and then increasing further as the ratio is increased. The catalyst Pt-0.3STA/β-zeolite, with sub-monolayer coverage, has also shown the highest Brønsted acidity [114]. Further, we have also tried to correlate the 1,3-PDO selectivity ($S_{1,3\text{-PDO}}$), its productivity ($P_{1,3\text{-PDO}}$), and turnover frequencies TOF (since comparisons among catalysts for activity are best made in terms of TOF) with surface coverage as shown in Figure 5.5 (b). TOFs were calculated from the maximum reaction rate in each case, as determined from the concentration vs. time plot. The concentration of active sites of Pt per gram of the designed catalyst was determined using CO-chemisorption (See Table 4.3). It is seen that the catalyst Pt/0.5STA/β-zeolite shows the highest TOF; this may be attributed to its high total acidity (highest in the series, see Figure 5.5 (a)). On the other hand, the catalyst Pt/β-zeolite has shown the second highest TOF in the studied series despite its low Pt dispersion (see Table 4.3). This seems consistent with the finding of Koningsberger et al. [195]. According to them, the high value of TOF for Pt on zeolite catalyst system is due to the high Si/Al ratio, polyvalent cations, and the extra-framework Al, leading to an increase in the TOF even at low Pt dispersion. Both the catalysts however, show the lower 1,3-PDO selectivity/productivity, correlating with its lowest Brønsted acidity. The addition of STA has improved the values of $P_{1,3\text{-PDO}}$ and $S_{1,3\text{-PDO}}$ due to increased Pt dispersion and Brønsted acid sites (See Table 4.2 and Table 4.3). The catalyst Pt-

0.3STA/β-zeolite has shown the highest values for $P_{1,3\text{-PDO}}$ and $S_{1,3\text{-PDO}}$, attributed to the highest Pt dispersion and highest Brønsted acidity, which was observed at sub-monolayer coverage. Moreover, the higher surface coverage (multilayer) has increased the catalyst's total acidity, eventually increasing the glycerol conversion up to 0.5 STA to β-zeolite ratio, as shown in Figure 5.5 (c). The reason for the highest glycerol conversion at 0.5 STA to β-zeolite ratio can be attributed to the higher catalyst acidity.

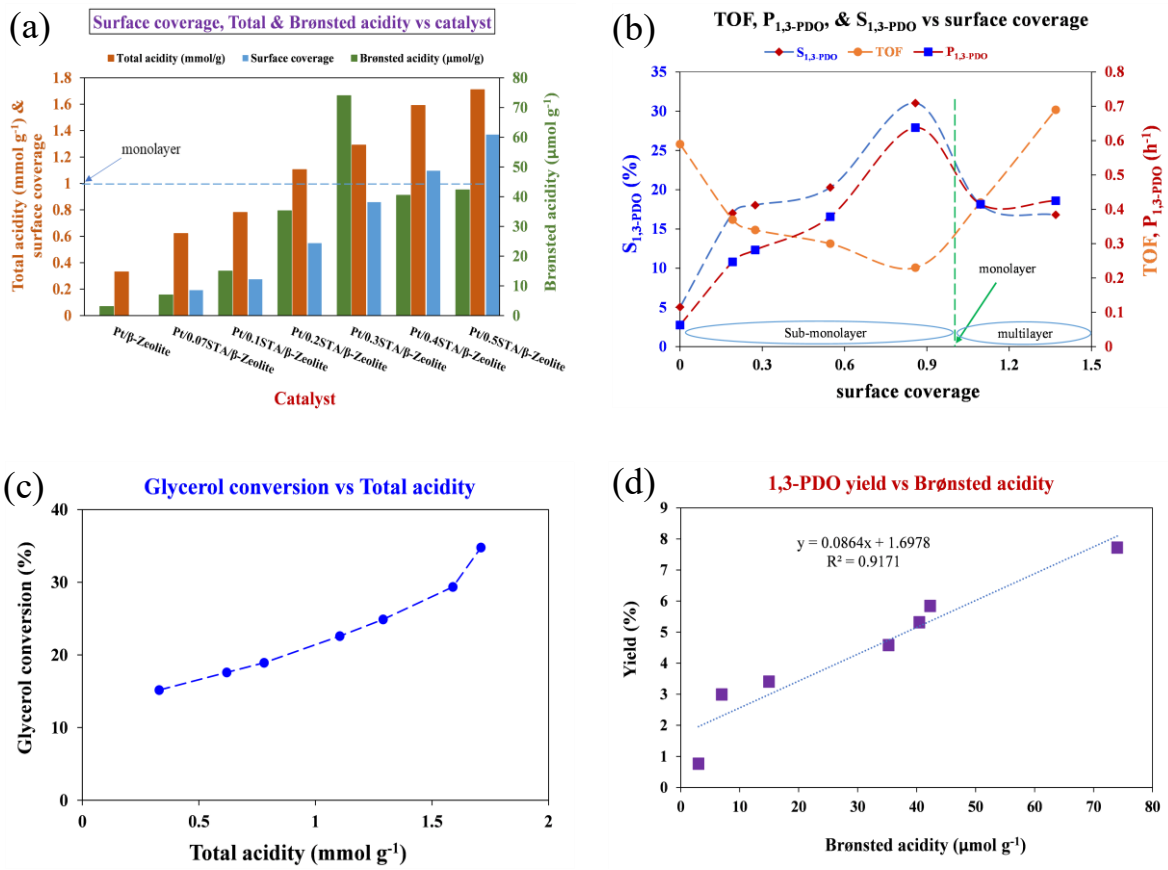

Figure 5.5. (a) Surface coverage, Total & Brønsted acidity vs. catalyst (b) TOF, $P_{1,3\text{-PDO}}$, $S_{1,3\text{-PDO}}$ vs. surface coverage (c) glycerol conversion vs. total acidity (d) 1,3-PDO yield vs. Brønsted acidity

As mentioned before, Brønsted acid sites are responsible more for the formation of 1,3-PDO by removing the middle –OH of glycerol [92,105,123,196]. Hence, we have attempted to relate the Brønsted acid sites obtained by the Py-FTIR technique over each catalyst with 1,3-PDO yield observed over that catalyst in Figure 5.5 (d) (see Figure A.3 in the Appendix-A for correlation using TGA technique). The results show that the yield of 1,3-PDO correlates nearly linearly with the amount of Brønsted acid sites. The catalyst (Pt-0.3STA/β-zeolite) with the higher Brønsted acid sites has shown the higher 1,3-PDO yield in this series of catalysts (0 to 0.5 STA/β-zeolite ratio). Similar results for higher 1,3-PDO yield over a higher Brønsted

acidity catalyst were also reported by Zhu et al. [94,114], Gong et al. [105], and Oh et al. [47]. The Brønsted acidity reduces beyond STA to β-zeolite ratio 0.3 because part of STA forms m-WO_3 as described under the discussion of XRD results.

It can thus be concluded that the addition of STA to the Pt/β-zeolite catalyst has enhanced the total acidic sites in the catalysts, leading to higher conversion of glycerol. Still, the selectivity decreases beyond sub-monolayer coverage, correlating with Brønsted acidity.

b) Catalysts with STA to β-zeolite ratio in the range 0.6 to 1.0

In this section, we tried to relate the effect of a further increase in STA to β-zeolite ratio from 0.6 to 1.0 on glycerol conversion and 1,3-PDO (product of interest) selectivity.

Figure 5.6(a) shows the amount of total and Brønsted acidity available over each catalyst. While Figure 5.6(b) shows the relationship between the total acidity (NH_3-TPD) of the Pt-xSTA/β-zeolite catalysts vs. glycerol conversion. The results show that the glycerol conversion was reduced with an increase in STA to β-zeolite ratio from 0.6 to 1.0. The Pt/0.6STA/β-zeolite catalyst showed the highest total acidity, followed by the catalyst Pt/0.7STA/β-zeolite. Likewise, the total acidity of the catalysts was reduced with an increase in STA to β-zeolite ratio, and therefore, the glycerol conversion was reduced with a reduction in acidity [114]. The catalyst Pt/0.6STA/β-zeolite showed the highest glycerol conversion in this STA to β-zeolite ratio range (0.6 to 1.0), and it is attributed to its highest acidity. However, this glycerol conversion is still less than the glycerol conversion observed over Pt/0.5STA/β-zeolite catalyst, which showed the highest glycerol conversion in the entire series of catalysts studied (0 to 100%STA) due to its highest acidity.

On the other hand, the catalyst Pt/0.7STA/β-zeolite showed the highest Brønsted acidity. The Brønsted acid sites of a catalyst favor the elimination of middle –OH of glycerol and eventually promote the formation of 1,3-PDO [92,105,123,196]. To prove this fact, we have tried to correlate the amount of Brønsted acid sites vs. 1,3-PDO yield obtained over each catalyst. Figure 5.6 (c) shows the correlation between 1,3-PDO yield and concentration of Brønsted acid sites over

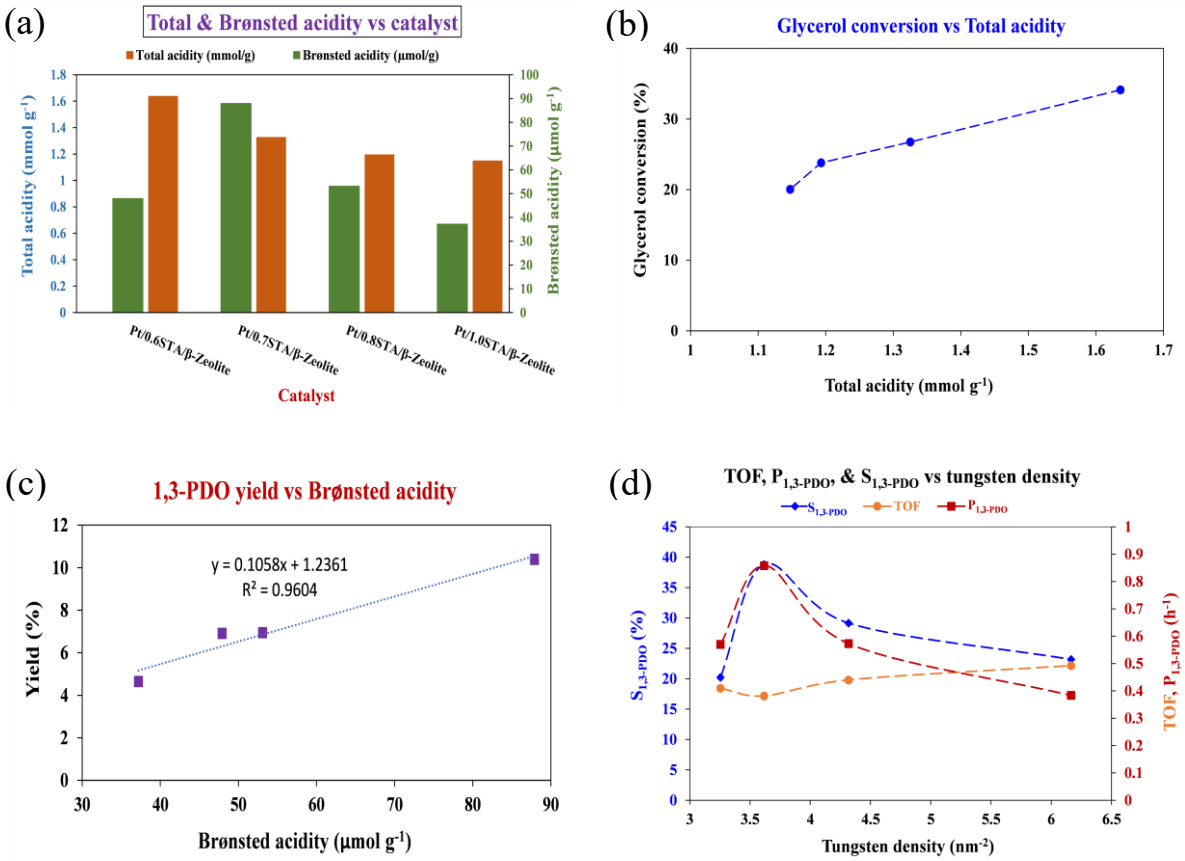

Figure 5.6. (a) Surface coverage, Total & Brønsted acidity vs. catalyst (b) TOF, $P_{1,3\text{-PDO}}$, $S_{1,3\text{-PDO}}$ vs. surface coverage (c) glycerol conversion vs. catalyst (d) 1,3-PDO yield vs. Brønsted acidity

different catalysts obtained using the Py-FTIR technique. The result shows that the yield of 1,3-PDO is strongly proportional to the Brønsted acid sites. The yield of 1,3-PDO was increased with an increase in catalysts Brønsted acidity. The catalyst Pt-0.7STA/β-zeolite has shown the highest 1,3-PDO yield and selectivity attributed to its highest concentration of Brønsted acidity confirmed by TGA and Py-FTIR techniques (See Table 4.2). It is worth noting that this catalyst has shown the highest 1,3-PDO yield in the entire catalyst series attributed to its highest Brønsted acidity; the results are in line with the reported results [47,94,105,114].

Additionally, we have also tried to correlate the 1,3-PDO productivity ($P_{1,3\text{-PDO}}$), its selectivity ($S_{1,3\text{-PDO}}$), and turnover frequencies TOF with tungsten density, as shown in Figure 5.6 (d). The results show that the values for TOFs were roughly equal in all the cases. However, the catalyst Pt-1.0STA/β-zeolite has shown the highest value. In contrast, the catalyst Pt-0.7STA/β-zeolite has shown the highest values for $P_{1,3\text{-PDO}}$ and $S_{1,3\text{-PDO}}$, attributed to its highest Brønsted acidity.

Furthermore, literature reports that 1,2-PDO preferentially forms over the Lewis acid sites [17,33]. However, its correlation with Lewis acid sites in both the zones (provided in

Appendix-A see Figure A.2) is unsatisfactory, probably due to its instability which will be discussed in detail in the coming section (see section 5.1.5).

5.1.4 Performance evaluation of heteropolyacids promoted catalyst

a) Catalysts with HPA to β-zeolite ratio 0.3

From the performance evaluation study of STA promoted catalysts, it is clear that the catalyst with STA to β-zeolite ratio 0.3 and 0.7 has performed better compared to catalysts other STA to β-zeolite ratio because of their higher Brønsted acidity. Heteropolyacids (HPAs) are known to have high Brønsted acidity. Therefore, we have studied the effect of HPAs addition to β-zeolite catalyst on glycerol hydrogenolysis. The HPA loading was kept as 0.3 and 0.7 for exploring this effect to facilitate comparison with STA catalysts because at this loading STA promoted catalyst showed better performance.

In this section, we have studied the glycerol hydrogenolysis over heteropolyacids (HPAs) promoted catalysts, namely catalysts containing phosphotungstic acid (PTA), phosphomolybdic acid (PMA), and silicotungstic acid (STA). The study on STA-containing catalysts has already been reported in the sections above. However, its results will be further used in this section for comparison.

Figure 5.7 shows the results of glycerol hydrogenolysis observed over Pt-0.3HPA/β-zeolite catalysts. The conversion of glycerol (see Figure 5.7(I)) increased with the addition of HPAs to the Pt/β-zeolite catalyst. The catalyst Pt-0.3PTA/β-zeolite showed the highest glycerol conversion as 26.90 ± 1.1%, attributed to its highest total acidity. The order of total acidity among the synthesized catalysts was Pt/β-zeolite < Pt-0.3PMA/β-zeolite < Pt-0.3STA/β-zeolite < Pt-0.3PTA/β-zeolite. Therefore, we have observed a similar trend in glycerol conversion. Moreover, the Brønsted acidity was highest over the Pt-0.3STA/β-zeolite catalyst, followed by Pt-0.3PTA/β-zeolite catalyst. Here, the 1,3-PDO selectivity (see Figure 5.7(II)) was highest over Pt-0.3STA/β-zeolite catalyst followed by Pt-0.3PTA/β-zeolite catalyst due to their Brønsted acidity. The Pt/β-zeolite catalyst has shown the highest 1,2-PDO selectivity (see Figure 5.7 (III)) due to its large Lewis acidity and lower total acidity. The former will help in glycerol conversion to 1,2-PDO and the latter will not allow over-hydrogenolysis of the formed 1,2-PDO [93,197]. Unsurprisingly, the selectivity of 1,2-PDO decreased after the deposition of HPAs to the Pt/β-zeolite catalyst. However, the catalyst Pt-0.3PMA/β-zeolite has shown

slightly higher selectivity for 1,2-PDO as 19.86 ± 1.60% after 5 h of reaction compared to catalyst with tungsten-HPAs (STA and PTA).

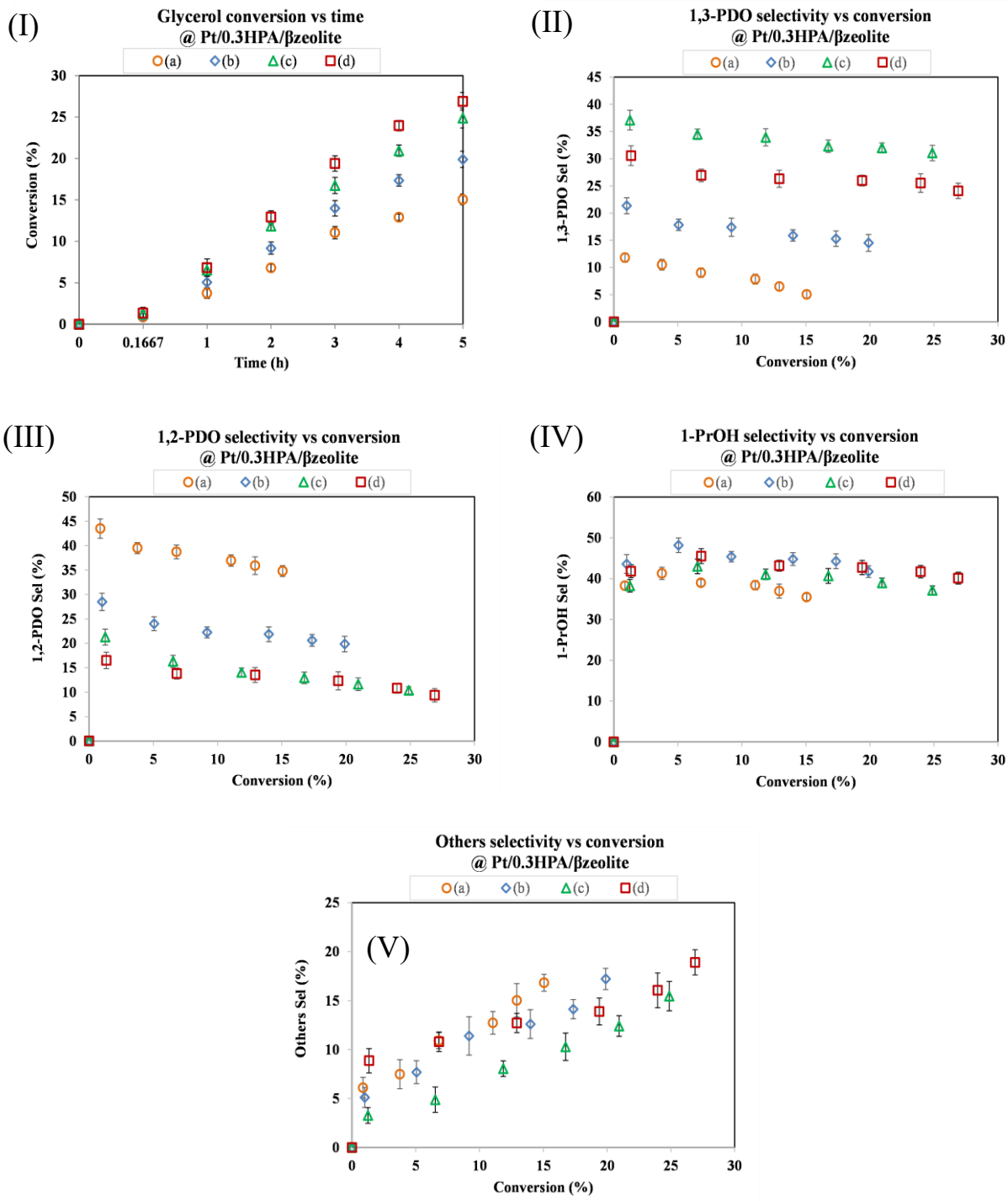

Figure 5.7. Glycerol hydrogenolysis reactant and product profiles: (a)- Pt/β-zeolite, (b)- 5%Pt/0.3PMA/β-zeolite, (c)- Pt/0.3STA/β-zeolite, (d)- 5%Pt/0.3PTA/β-zeolite

This was due to the formation of MoO_3 after the decomposition of PMA at 450 ^oC (calcination temperature), increasing the Lewis acid sites considerably than the Brønsted acid sites leading

to a rise in 1,2-PDO selectivity [93]. The selectivity of 1-PrOH (See Figure 5.7 (IV)) looks nearly the same in all the cases. However, the catalyst Pt/β-zeolite showed the lowest selectivity for 1-PrOH. The HPA containing catalysts showed higher selectivity for 1-PrOH compared to Pt/β-zeolite catalyst. It was attributed to their higher acidity and affinity towards the formation of 1,2-PDO. Higher acidity helps in the over-hydrogenolysis of PDOs. This is the reason Pt-0.3PMA/β-zeolite catalyst has shown lesser 1,2-PDO yield as compared to Pt/β-zeolite catalyst despite having the higher Lewis acidity [16]. Lewis acidity helps the formation of 1,2-PDO, but higher Lewis acidity promotes 1,2-PDO over hydrogenolysis to 1-PrOH. Hence, the catalysts Pt-0.3PTA/β-zeolite and Pt-0.3PMA/β-zeolite showed higher 1-PrOH selectivity because the former has a higher total acidity and the latter has the highest Lewis acidity. Furthermore, the selectivity of others (see Figure 5.7(V)) was lowest over Pt-0.3STA/β-zeolite catalyst because of the higher stability of 1,3-PDO in the reaction environment. It will be further discussed in detail in the hydrogenolysis of different substrate sections.

b) Catalysts with HPA to β-zeolite ratio 0.7

Figure 5.8 shows the glycerol hydrogenolysis result observed over Pt-0.7HPA/β-zeolite catalysts. The results show that catalyst Pt-0.7PTA/β-zeolite showed the highest glycerol conversion (see Figure 5.8 (I)), attributed to its highest total acidity. The trend of glycerol conversion over Pt-0.7HPA/β-zeolite catalysts was Pt-0.7PTA/β-zeolite > Pt-0.7STA/β-zeolite > Pt-0.7PMA/β-zeolite. The selectivity of 1,3-PDO (see Figure 5.8 (II)) was highest over Pt-0.7STA/β-zeolite catalyst followed by Pt-0.7PTA/β-zeolite catalyst and then Pt-0.7PMA/β-zeolite catalyst. This is attributed to the highest Brønsted acidic sites of STA promoted catalyst followed by PTA and PMA catalyst. The catalyst Pt-0.7PMA/β-zeolite showed the highest Lewis acidity, attributed to the formation of MoO_3 (see Figure 4.11), which will contribute to increases in Lewis acid sites [93]. Hence, the selectivity of 1,2-PDO (see Figure 5.8 (III)) was higher over Pt-0.7PMA/β-zeolite. Moreover, selectivity for 1-PrOH (see Figure 5.8 (IV)) was also highest over this catalyst attributed to its higher acidity, which will over-hydrogenolyse 1,2-PDO to 1-PrOH.

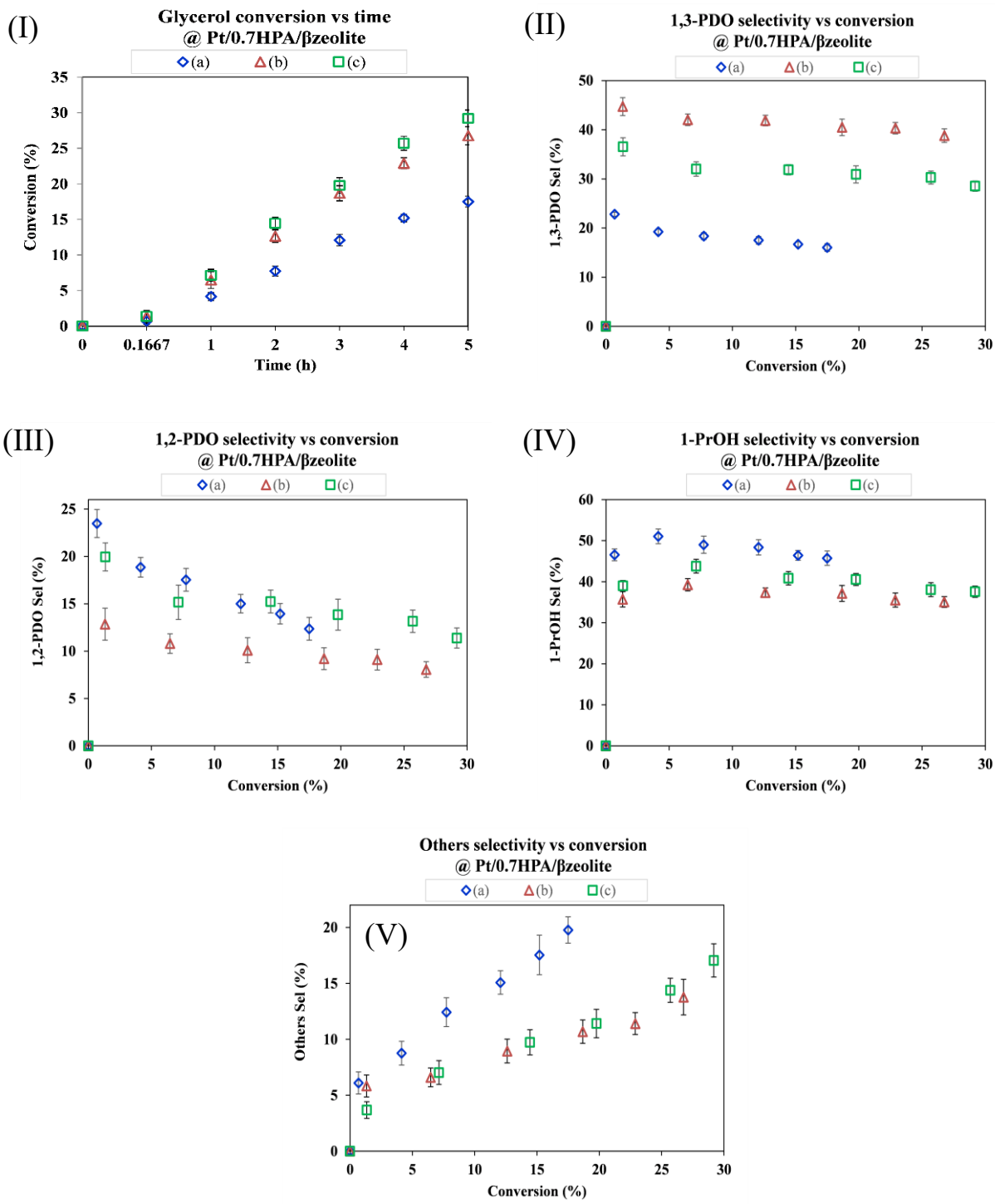

Figure 5.8. Glycerol hydrogenolysis reactant and product profiles: (a)- Pt/0.7PMA/β-zeolite, (b)- Pt/0.7STA/β-zeolite, (c)- Pt/0.7PTA/β-zeolite

5.1.5 Hydrogenolysis of different substrates (PDOs or 1-PrOH)

a) Hydrogenolysis using Pt-0.3STA/β-zeolite catalyst

The hydrogenolysis of substrates like 1,2-PDO, 1,3-PDO, and 1-PrOH over the Pt-0.3STA/β-zeolite catalyst was studied in a similar environment. Figure 5.9 (I) represents reactant conversion vs. time, Figure 5.9 (II) represents 1-PrOH selectivity vs. time, Figure 5.9 (III) shows others selectivity vs. time, Figure 5.9 (IV) shows the gaseous product selectivity vs. time.

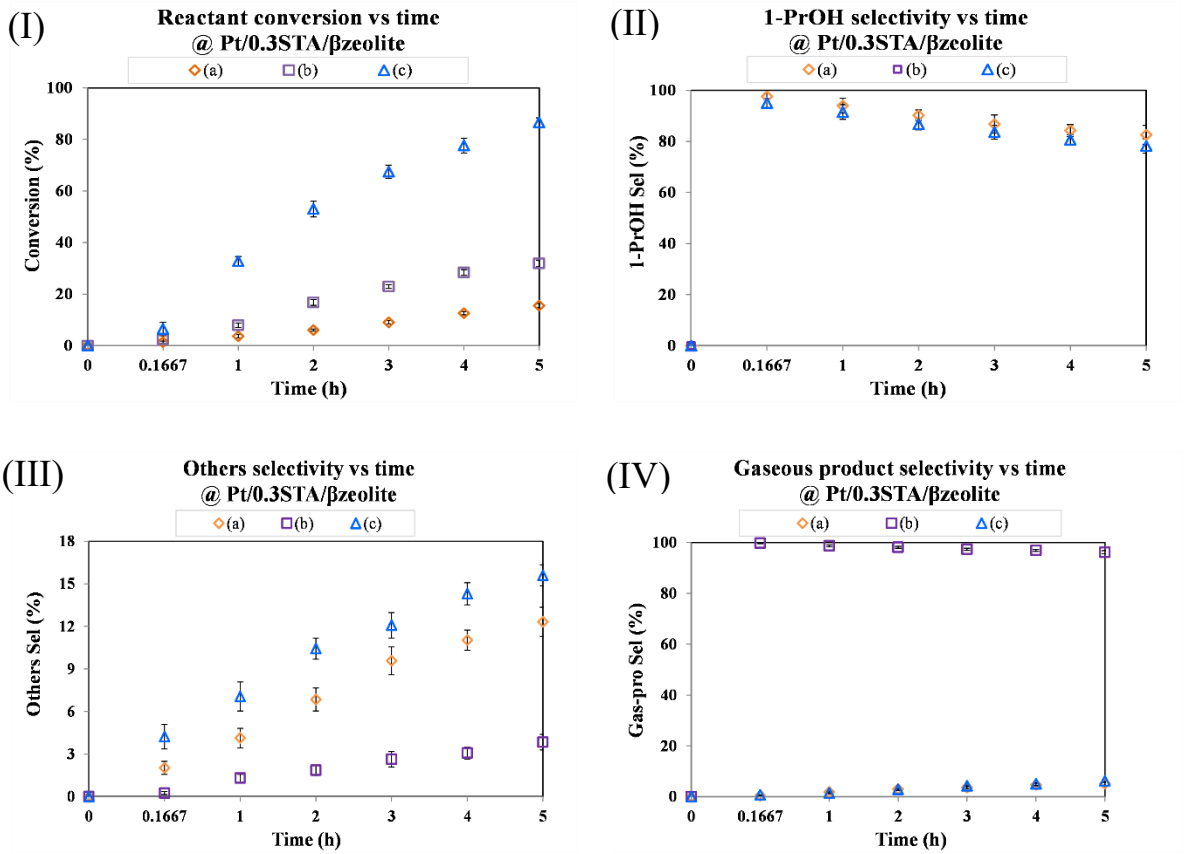

Figure 5.9. 1,3-PDO, 1,2-PDO, and 1-PrOH hydrogenolysis profiles: (a)- 1,3-PDO, (b)- 1-PrOH, (c)- 1,2-PDO

The result shows that the observed conversion of 1,2-PDO over Pt-0.3STA/β-zeolite (see Figure 5.9 (I)) catalyst was the highest (86.61 ± 1.78%), followed by conversion of 1-PrOH (31.91 ± 1.26%), and finally the conversion of 1,3-PDO as 15.52 ± 0.71%, after 5 h of reaction. These experiments were conducted to check the stability of glycerol hydrogenolysis products in the reaction environment. The conversion of 1,2-PDO was nearly 6 times the conversion of 1,3-PDO. Furthermore, the conversion of 1-PrOH was 2 times the conversion of 1,3-PDO, which means 1,3-PDO is more stable compared to 1,2-PDO and 1-PrOH in the reaction

environment. Here, the key product from both PDO hydrogenolysis was 1-PrOH (see Figure 5.9 (II)) with selectivity as 82.56 ± 3.70% from 1,3-PDO and 78.23 ± 2.81% from 1,2-PDO after 5 h of reaction. Thus, it is clear that 1-PrOH largely comes from the 1,2-PDO, in line with the previous report [190]. Furthermore, the selectivity of others (see Figure 5.9 (III)) was also the highest in the case of 1,2-PDO as 15.58 ± 1.43%, followed by 12.32 ± 1.29% from 1,3-PDO, and 3.84 ± 0.14% from 1-PrOH after 5 h of reaction. In the case of 1-PrOH hydrogenolysis, the major products were gaseous (see Figure 5.9 (IV)) propane with selectivity 96.16 ± 0.86% after 5 h of reaction. These results confirm that the gaseous products originate by and large from the hydrogenolysis of 1-PrOH.

b) Hydrogenolysis using Pt-0.7STA/β-zeolite catalyst

A Similar study was performed over Pt-0.7STA/β-zeolite catalyst under otherwise similar conditions. Figure 5.10 (I) represents reactant conversion vs. time, Figure 5.10 (II) represents 1-PrOH selectivity vs. time, Figure 5.10 (III) shows others selectivity vs. time, and Figure 5.10 (IV) shows the gaseous product selectivity vs. time.

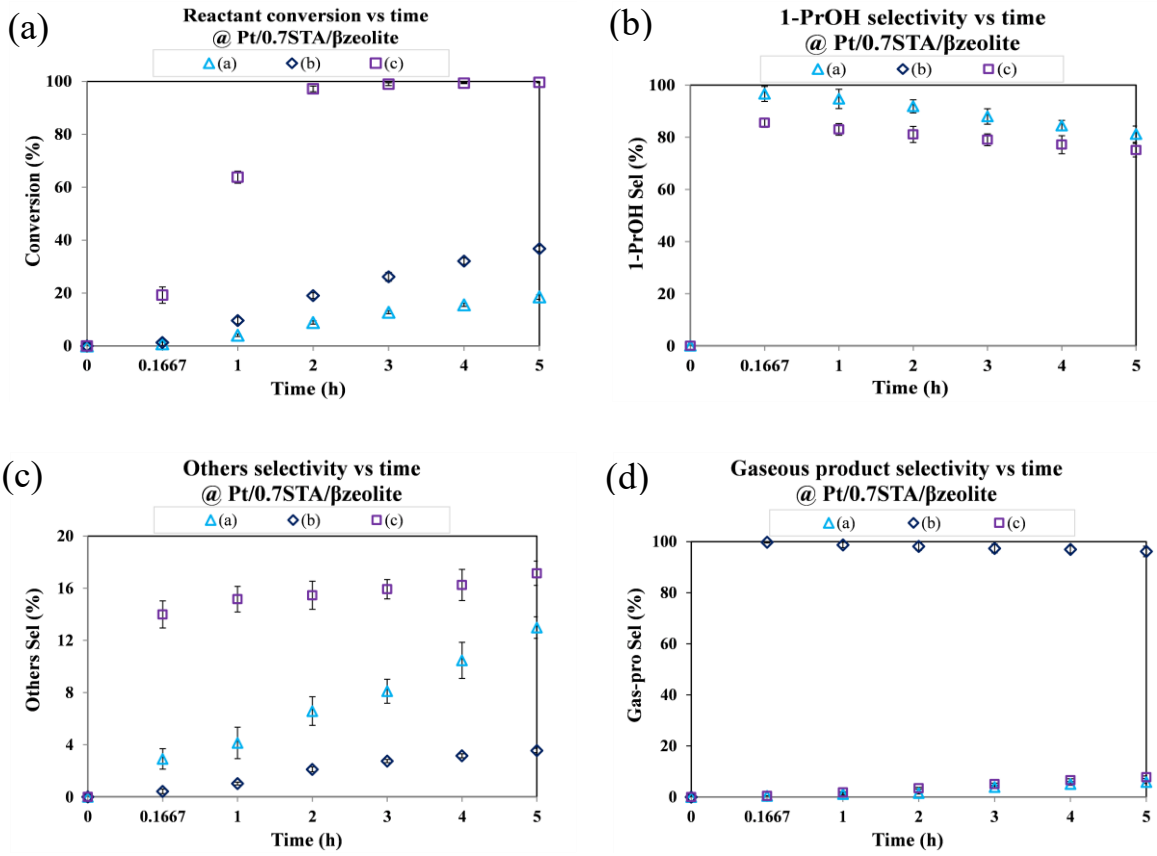

Figure 5.10. 1,3-PDO, 1,2-PDO, and 1-PrOH hydrogenolysis profiles: (a)- 1,3-PDO, (b)- 1-PrOH, (c)- 1,2-PDO.

The result shows that the conversion of 1,2-PDO reached more than 97% in just 2 h of reaction over Pt-0.7STA/β-zeolite (see Figure 5.10 (I)). The conversion of 1-PrOH and 1,3-PDO was 36.78 ± 1.01% and 18.5 ± 0.87%, respectively, after 5 h of reaction. The highest conversion of 1,2-PDO over Pt-0.7STA/β-zeolite catalyst was attributed to its highest Brønsted acidity. Moreover, it also confirms that the rates of 1,2-PDO hydrogenolysis are higher over Pt-0.7STA/β-zeolite catalysts compared to Pt-0.3STA/β-zeolite catalysts. Furthermore, these results prove that 1,3-PDO is more stable compared to 1,2-PDO and 1-PrOH in the reaction conditions. Both the PDOs converted to 1-PrOH (see Figure 5.10 (II)) with selectivity higher than 75%. The yield of 1-PrOH was highest via the 1,2-PDO route, which confirms 1-PrOH was largely produced via 1,2-PDO hydrogenolysis. The formation of others (see Figure 5.10 (III)) via 1,2-PDO hydrogenolysis was highest and the formation of gaseous product (see Figure 5.10 (IV)) via 1-PrOH hydrogenolysis was highest after 5 h of reaction. The results over Pt-0.7STA/β-zeolite catalyst followed the similar trend which was observed over Pt-0.3STA/β-zeolite catalyst except that the reactant conversion was higher over former catalyst.

From the foregoing discussion, it is clear that the two catalysts *viz.* Pt-0.3STA/β-zeolite and Pt-0.7STA/β-zeolite show a better performance in terms of 1,3-PDO yield or selectivity from glycerol compared to catalysts formulated with other HPAs. Attributed to their higher concentration of Brønsted acid sites, good Pt particle dispersion, small Pt crystal size, strong electronic interaction between Pt and STA species, and hydrogen spillover, etc. (see chapter 4). These catalysts can be subjected to study the effect of reaction parameters such as temperature, pressure, initial glycerol concentration, catalyst loading in reaction, platinum loading in catalyst, and effect of reaction time. This study will help in carrying out the reaction at those conditions, which will further improve the yield of 1,3-PDO from glycerol over these catalysts. The next chapter will show the results obtained during a parametric study carried out using these catalysts.

5.1.6 Mechanism of glycerol hydrogenolysis over Pt-HPA/β-zeolite catalyst

After carefully observing the effect of catalyst type and reaction conditions on hydrogenolysis of glycerol, PDOs, and 1-PrOH, a probable reaction pathway may be derived as shown in Figure 5.11 and Figure 5.12. Figure 5.11 shows the complete reaction mechanism involving all possible products of glycerol hydrogenolysis, while Figure 5.12 shows the detailed steps involved in the 1,3-PDO synthesis mechanism from glycerol. The previous reports claim that the formation of PDOs proceeds *via* glycerol dehydration to either hydroxyacetone (acetol) or

3-hydroxypropanal (3-HyPA) over acid catalyst followed by their respective hydrogenation to 1,2-PDO or 1,3-PDO by hydrogen atom concerted on metal sites [98].

The reaction proceeds *via* adsorption of glycerol molecule on the surface of HPA/β-zeolite (see Figure 5.12 or route 1 of Figure 5.11), thereby forming an alkoxide species [111]. At the same time, H_2 molecule splits into concerted H atoms upon adsorption over the surface of Pt metal. The hydroxyl (–OH) group of glycerol binds with the proton (H^+) (oxygen lone pair binds with proton) donated from Brønsted acid sites of either STA or β-zeolite (in the case of Pt/β-zeolite) catalyst surface. As this bonding (H^+ and –OH group) is not affected by steric hindrance, H^+ can bind with either terminal or central –OH group of glycerol to generate 1° or 2° carbocation respectively after dehydration which releases H_3O^+ (hydronium) species. In general, 2° carbocation are more stable compared to the 1° carbocation. Moreover, 3-hydroxypropionaldehyde (3-HPA) which proceeds *via* 2° carbocation, is kinetically more favorable than hydroxyacetone or acetol, which forms via 1° carbocation [198]. Therefore, the reaction progresses through protonation of 2° –OH group followed by its dehydration to produce propene 1,3-diol (route 1 of Figure 5.11). This diol undergoes keto-enol tautomerization due to instability and forms a stable 3-HPA. It is important to note that 3-HPA is thermodynamically less stable than acetol [198]. Hence its quick hydrogenation to 1,3-PDO is indeed important to avoid its further dehydration to acrylaldehyde or acrolein, which may hydrogenate to 1-PrOH (blue color path in route 1 of Figure 5.11). The hydrogenation step proceeds *via* the transfer of H atoms from Pt surface to the adsorbed 3-HPA molecule and thereby producing 1,3-PDO. The formed 1,3-PDO may release from the catalyst surface by acid hydrolysis, and the catalyst site will be available for the other molecule. Lastly, the proton sites of STA or β-zeolite surface will be regenerated by the interaction of H_3O^+ ions with its conjugate base [45]. Therefore, in our case, Pt/β-zeolite catalyst produced less 1,3-PDO, and catalyst Pt/0.3STA/β-zeolite produced more owing to their respective Brønsted acidic sites (See Table 4.2).

Contrastingly, the 1,2-PDO formation occurs via Lewis acid sites. The terminal or middle –OH group of glycerol can share their lone pair of electrons with the Lewis acid sites by coordination bond. This coordination is affected by steric hindrance and therefore, the terminal –OH group of glycerol can more easily coordinate with the Lewis acid sites than the middle –OH group. Hence, the terminal –OH group of glycerol gets dehydrated by Lewis acid sites, producing propene 1,2-diol on dehydration (route 2 of Figure 5.11). Due to instability, this diol may undergo keto-enol tautomerization and form a stable molecule hydroxyacetone (acetol).

The acetol upon hydrogenation yields 1,2-PDO *via* transfer of H atoms from the surface of metallic Pt. The formed 1,2-PDO can be released from the catalyst surface by acid hydrolysis. The catalyst site will be available for the other molecule to interact. Finally, the Lewis acid sites of STA or β-zeolite surface gets regenerated by thermal dehydration of their hydrated forms [45].

Furthermore, PDOs and 1-PrOH hydrogenolysis results revealed that both the PDOs could further transform to 1-PrOH, ethanol, methanol, or some gaseous products (mostly 1-PrOH), etc. in extreme hydrogenolysis reaction. The reaction mechanism in Figure 5.11 reveals the possible pathway for the formation of such products.

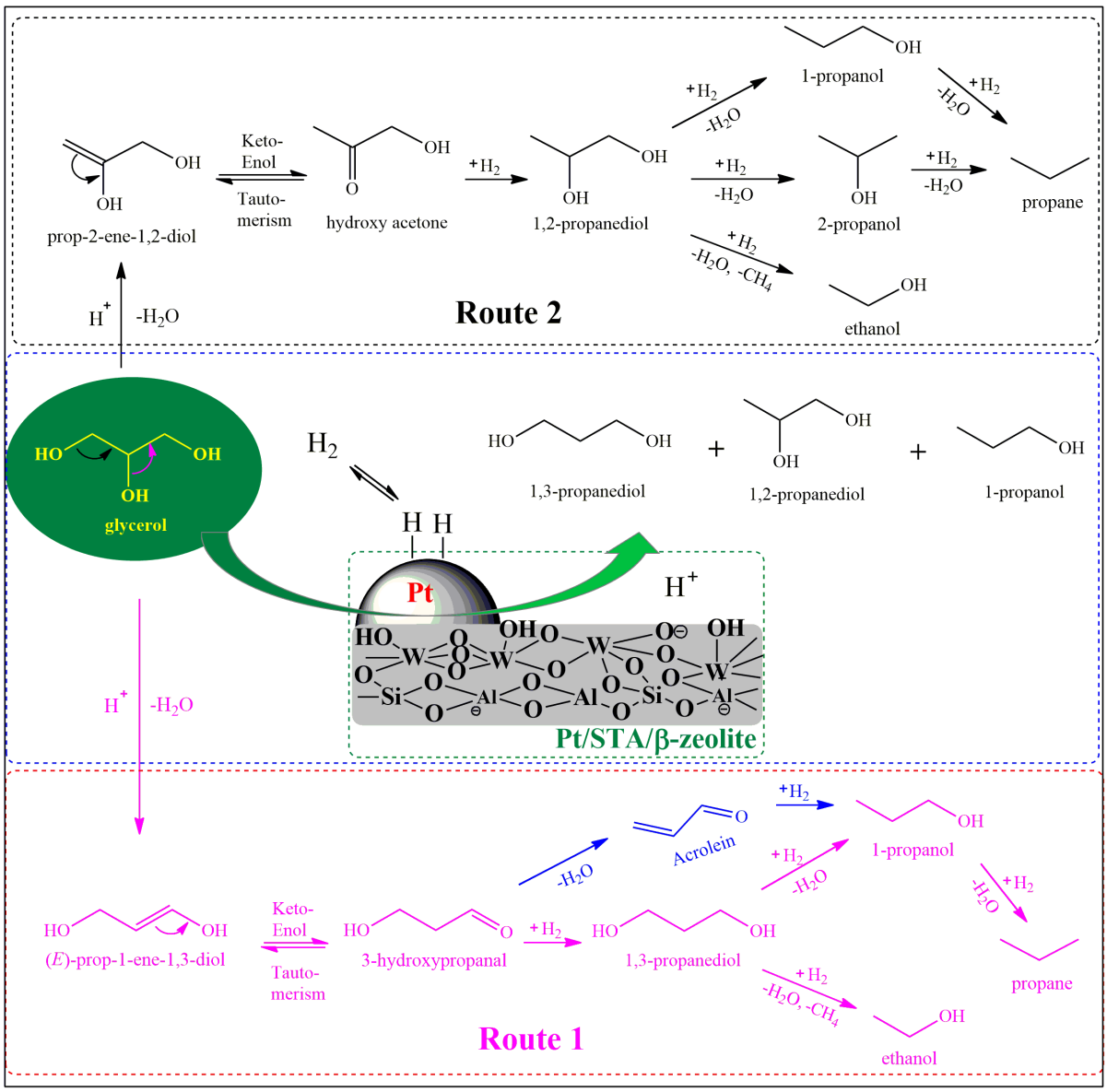

Figure 5.11. Complete reaction mechanism of glycerol hydrogenolysis over Pt-HPA/β-zeolite

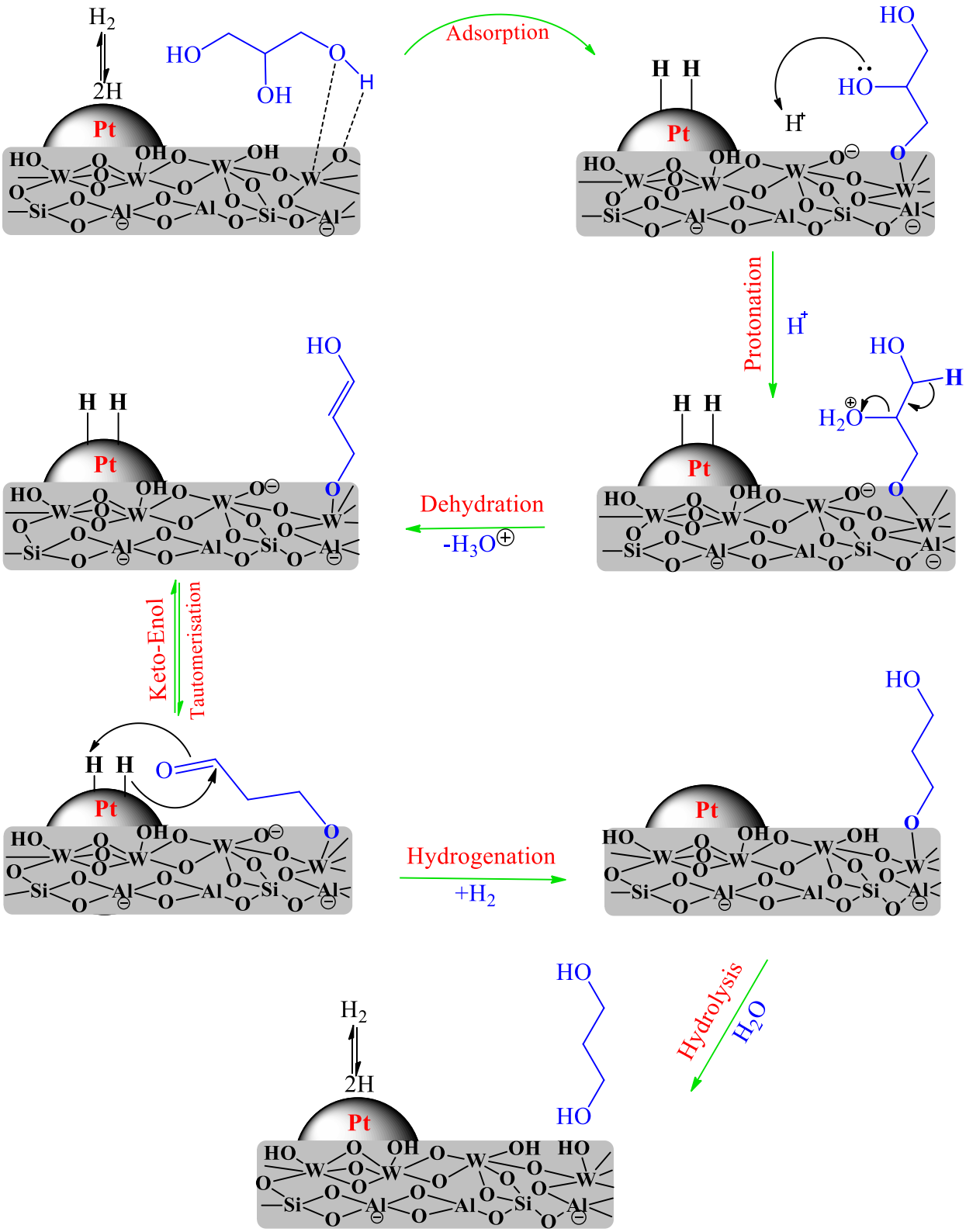

Figure 5.12. The detailed reaction mechanism on the transformation of glycerol to 1,3-PDO over Pt-HPA/β-zeolite

5.1.7 Comparison of observed glycerol hydrogenolysis results with reported results

Table 5.1 compares the Pt/xSTA/β-zeolite (x=0.3 or 0.7) catalytic performance with those reported in the literature for glycerol hydrogenolysis reaction. It is found that the selective transformation of glycerol to 1,3-PDO via hydrogenolysis is still difficult and challenging. A relatively high 1,3-PDO can be obtained by means of severe reaction conditions such as a high reaction temperature, a high H_2 pressure, and a long residence/batch time, etc.

Table 5.1. Comparison of Pt/xSTA/β-zeolite catalytic performance with those reported in literature

Entry	Catalyst	T [°C]	P [bar]	Batch time	X (%)	$S_{1,3\text{-PDO}}$ [%]	$Y_{1,3\text{-PDO}}$ [%]	Reference
1	Pt/m-WO_3	180	55	12 h	18	39.2	7.1	[86]
2	Pt/WOx	140	10	12 h	59.8	36.3	21.7	[87]
3	Pt/Nb-WOx	160	50	12 h	40.3	27.5	11.1	[90]
4	Pt/Al_2O_3+HSiW	200	40	18 h	49	28	13.7	[85]
5	Pt-HSiW/mAl_2O_3	200	40	15 h	60.5	33.3	20.1	[95]
6	Pt-WOx/SiO_2	210	--	75 h	42.6	25.8	11	[100]
7	Pt/WO_3/TiO_2/SiO_2	180	55	12 h	15.3	50.5	7.7	[105]
8	Pt/WO_3/ZrO_2	170	80	18 h	85.8	28.2	24.2	[73]
9	Pt/WO_3/ZrO_2	170	55	12 h	31.6	34.9	11	[61]
10	Pt/WO_3/ZrO_2	180	80	50 h	77.7	21.9	23.1	[107]
11	Pt/WOx/Al_2O_3	220	45	24 h	60.3	31.2	18.8	[111]
12	Pt/WOx/Al_2O_3	200	45	16 h	80.3	38.5	30.9	[113]
13	Pt-WOx/SiO_2-Al_2O_3	210	--	50 h	53	24.3	12.8	[104]
14	Pt-WOx/SAPO-34	210	60	50 h	48	18.8	9	[103]
15	Pt/15WOx/H-ZSM-5	200	25	16 h	17.3	20.6	3.6	[115]
16	Pt/0.3STA/β-zeolite	220	50	5 h	27.8	35.0	9.7	This work
17	Pt/0.7STA/β-zeolite	220	50	5 h	30.4	42.0	12.8	This work

Generally, a high glycerol conversion means a sacrifice of the 1,3-PDO selectivity. Moreover, the higher batch time required for the reaction represents its slower nature (rates). However, almost all of the studies reported the higher batch times as high as 75 h and as low as 12 h.

The Pt/WO_3/TiO_2/SiO_2 catalyst showed the highest 1,3-PDO selectivity of 50.5%. However, the glycerol conversion was only 15.3% even after 12 h of reaction. 1,3-PDO selectivity over our (Pt/xSTA/β-zeolite) catalytic systems (35 – 42%) is comparable to most of the catalytic

systems reported in Table 5.1. In the case of 1,3-PDO yield, we have observed a moderate yield of 1,3-PDO within 5 h of reaction. The longer reaction time (> 5 h) in our case has increased the glycerol conversion, but the 1,3-PDO selectivity was decreased due to its over hydrogenolysis. The glycerol hydrogenolysis study over WOx promoted zeolites (entry 14 and 15) also shows the superior performance of Pt/xSTA/β-zeolite catalyst compared to others.

5.1.8 Tabulated glycerol hydrogenolysis reaction results over all synthesized catalysts

Table 5.2. Glycerol hydrogenolysis reaction results over different catalysts (synthesized)

Entry	Catalyst	Gly. Conver. (%)	Selectivity (%)				Yield (%)
			1,3-PDO	1,2-PDO	1-PrOH	Others	1,3-PDO
1	β-Zeolite	8.7	0.0	15.0	12.9	63.8	0
2	0.3STA/β-Zeolite	3.8	0.0	0.0	17.2	73.8	0
3	Pt/β-Zeolite	15.1	5.0	34.8	35.5	16.8	0.8
4	Pt/0.07STA/β-Zeolite	17.6	17.0	14.1	44.1	18.5	3.0
5	Pt/0.1STA/β-Zeolite	18.3	18.0	10.4	48.1	16.2	3.3
6	Pt/0.2STA/β-Zeolite	22.7	20.3	8.2	47.2	18.5	4.6
7	Pt/0.3STA/β-Zeolite	24.9	31.0	10.4	37.1	15.5	7.7
8	Pt/0.4STA/β-Zeolite	29.3	22.0	13.0	41.0	17.6	6.5
9	Pt/0.5STA/β-Zeolite	35.1	21.0	12.2	40.0	20.5	7.4
10	Pt/0.6STA/β-Zeolite	34.1	20.2	15.5	38.1	18.2	6.9
11	Pt/0.7STA/β-Zeolite	26.8	38.8	8.1	35.1	13.8	10.4
12	Pt/0.8STA/β-Zeolite	24.8	29.2	13.0	35.1	14.9	7.2
13	Pt/1.0STA/β-Zeolite	20.1	23.2	15.1	38.1	16.3	4.7
14	Pt/1.5STA/β-Zeolite	14.9	22.4	16.6	38.6	15.0	3.3
15	Pt/2.3STA/β-Zeolite	12.5	20.6	18.0	39.1	15.9	2.6
16	Pt/4.0STA/β-Zeolite	13.6	22.2	14.0	40.2	17.0	3.0
17	Pt/9.0STA/β-Zeolite	16.4	21.6	15.1	37.2	16.4	3.6
18	Pt/STA	19.9	23.6	14.9	37.4	14.8	4.7
19	Pt/0.3PTA/β-Zeolite	26.9	24.1	9.4	40.1	18.9	6.5
20	Pt/0.3PMA/β-Zeolite	19.9	14.5	19.9	41.7	17.2	2.9
21	Pt/0.7PTA/β-Zeolite	29.2	28.5	11.4	37.6	17.0	8.3
22	Pt/0.7PMA/β-Zeolite	21.1	16.0	12.4	45.8	19.8	3.4

Reaction condition: 80 ml aqueous solution of 5 wt% glycerol in 100 ml autoclave, 2 g of catalyst, stirring at 800 rpm, 220 ^{o}C, 40 bar H_2, 5 h.

Table 5.2 compares the catalytic performance of all synthesized catalysts for hydrogenolysis of glycerol reaction. The result shows that the addition of STA to Pt/β-zeolite catalyst improves

the glycerol conversion. The glycerol conversion was increased up to 0.5 STA to β-zeolite ratio. Further addition of STA resulted in decreased glycerol conversion due to a decrease in total acidity. Moreover, 1,3-PDO was not formed over β-zeolite or STA/β-zeolite, but Pt/β-zeolite showed some selectivity for 1,3-PDO, which was further improved after the addition of STA to it.

The addition of STA to Pt/β-zeolite catalyst increased the 1,3-PDO selectivity up to 0.3 STA to β-zeolite ratio. Beyond this loading, the 1,3-PDO selectivity was decreased. However, the Pt/0.7STA/β-zeolite catalyst showed the highest 1,3-PDO selectivity due to its highest Brønsted to Lewis acidity ratio in the entire series of synthesized catalysts.

Additionally, we have also studied the glycerol hydrogenolysis over Pt/β-zeolite catalyst supported by other heteropolyacids (phosphotungstic, phosphomolybdic acid). The result shows that the catalyst containing phosphomolybdic acid has performed poorer than phosphotungstic acid-containing catalysts (see entries 19 to 22).

Lastly, the highest yield of 1,3-PDO was observed over Pt/0.7STA/β-Zeolite catalyst (10.4%) followed by Pt/0.7PTA/β-Zeolite catalyst (8.3%) and Pt/0.3STA/β-Zeolite catalyst (7.7%).

5.2 Conclusion

The glycerol hydrogenolysis over different synthesized catalysts showed the potential of STA as a promotor to Pt-β-zeolites (Si/Al=300) to increase glycerol conversion and 1,3-PDO selectivity. The catalyst β-zeolite has shown some activity towards glycerol; however, the product of interest (1,3-PDO) was not formed. Adding Pt to β-zeolite catalyst has shown some selectivity towards 1,3-PDO, and the addition of STA further improved this. This confirms that Pt and STA are both important in a catalyst for glycerol transformation to 1,3-PDO. The addition of STA increased the total acidity of the β-zeolite catalyst, which helped in improving glycerol conversion. The glycerol conversion was increased from 15.06% to 37.58% in 5 h with an increase in STA to β-zeolite ratio from 0 to 0.5. Further increase in STA to β-zeolite ratio from 0.6 to 2.33 showed the decrease in glycerol conversion from 34.14% to 12.46%. The total acidity correlation with glycerol conversion showed a direct relationship. The glycerol conversion increased with an increase in total acidity and decreased with a decrease in the catalyst's total acidity. At STA to β-zeolite ratio 4.0 or higher, the glycerol conversion again increased despite a decrease in total acidity due to an increase in $HxWO_3$ species, which acts

as a Brønsted acid site. The catalyst Pt–0.7STA/β-zeolite with tungsten surface density 3.6 atoms nm^{-2} offered the highest 1,3-PDO selectivity up to 38.8% in 5 h, and the catalyst Pt–0.3STA/β-zeolite with tungsten surface density 1.6 atoms nm^{-2} has offered the second-highest 1,3-PDO selectivity up to 31.04% in 5 h. The 1,3-PDO selectivity was found to improve at least 7 times and its productivity increased 14 times (over Pt–0.7STA/β-zeolite) compared to Pt/β-zeolite, which is due to the large concentration of Brønsted acid sites of $H_{0.53}WO_3$ species with appropriate acid amounts, strong electronic interaction between Pt and STA species, and hydrogen spillover. The reusability study revealed that the catalysts were reusable even after the 4^{th} run and has given nearly comparable results to the fresh catalyst.

The correlation between Brønsted acidity and 1,3-PDO yield also confirms that the Brønsted acid sites do favor the formation of 1,3-PDO. Concurrently, the highest yield of 1,2-PDO was obtained over a catalyst with no STA (Pt/β-zeolite). This may be attributed to a large concentration of Lewis acid sites, the absence of strong acid sites, and a lower amount of total acidic sites. The TOF results revealed that the catalyst Pt/β-zeolite showed the highest value for TOF despite the low Pt dispersion compared to STA promoted catalysts. However, the STA promoted catalysts offered the higher 1,3-PDO selectivity and productivity compared to the Pt/β-zeolite catalyst.

The catalytic performance of heteropolyacids (HPAs) modified Pt/β-zeolite catalysts revealed that STA containing catalyst showed the highest 1,3-PDO selectivity compared to other catalysts. Attributed to its high thermal stability and large Brønsted acidity compared to PTA and PMA containing catalysts. The hydrogenolysis of other substrates showed that 1,3-PDO is more stable in the reaction environment compared to 1,2-PDO or 1-PrOH. It implies that compounds like 2-PrOH, ethanol, methanol, or part of 1-PrOH, etc., would have formed mainly *via* 1,2-PDO. Additionally, the results also indicate that part of 1-PrOH would have directly formed via acrolein due to its appearance since the start of the reaction. Finally, a possible reaction mechanism was proposed after carefully observing the trends in the formation of reaction products and the independent studies on the hydrogenolysis of respective products.

Chapter 6:
EFFECT OF REACTION PARAMETER/CONDITION ON THE KINETICS

The performance evaluation of STA (HPA) promoted catalysts in Chapter 5 revealed that the two catalysts *viz.* Pt-0.3STA/β-zeolite and Pt-0.7STA/β-zeolite have shown the highest selectivity for 1,3-PDO from glycerol. This chapter presents the results of studies on the effect of reaction parameters such as temperature, pressure, initial glycerol concentration, catalyst loading in reaction, platinum loading in catalyst, and effect of reaction time.

6.1 Summary results of parametric study over Pt-0.3STA/β-zeolite catalyst

The details of the parametric study conducted over Pt-0.3STA/β-zeolite catalyst is provided in the following sections (see section 6.3). Here, the results are summarized in Table 6.1. The effect of the parameters was studied, taking the conditions of row 2 as the base case – reaction time (rows 1-3), temperature (rows 2,4, and 5), glycerol concentration (rows 2 and 6), hydrogen pressure (rows 2,7, and 8), catalyst loading (rows 2, 9, and 10) and Pt loading in the catalyst (rows 2, 11, and 12). The results in Table 6.1 show that the batch reaction time has a significant impact on the product distribution. At the longer reaction times, the glycerol conversion was found to increase together with increase in the selectivity of 1-PrOH, others and gaseous products, but the selectivity of propanediols was decreased. This is attributed to the over hydrogenolysis of PDOs. It is thus necessary to also restrict the reaction time to typically less than or equal to 5 hrs under the conditions of interest (see rows 1-3).

Table 6.1. Reaction parameter study for glycerol hydrogenolysis reaction over Pt-0.3STA/β-zeolite (quantitative)

Reaction/catalyst Parameters	Initial reaction rates	Reactant conversion	Product selectivities					Carbon Balance
	(mol g_{cat}^{-1} h^{-1})	Glycerol	1,3-PDO	1,2-PDO	1-PrOH	Others	gases	($C_{measured}$ / $C_{reacted}$) *100
220 °C, 40 bar H_2, **10 min**, 2 g of 5 wt% Pt cat, 5 wt% gly aqueous solution	1.86E-05	1.3	37.1	21.3	38.3	3.3	0.1	99.9
220 °C, 40 bar H_2, **5 h**, 2 g of 5 wt% Pt cat, 5 wt% gly aqueous solution	1.86E-05	24.9	31.0	10.4	37.1	15.5	6.0	94.0
220 °C, 40 bar H_2, **16 h**, 2 g of 5 wt% Pt cat, 5 wt% gly aqueous solution	1.86E-05	60.0	25.7	6.5	35.8	14.3	17.7	82.3
200 °C, 40 bar H_2, 5 h, 2 g of 5 wt% Pt cat, 5 wt% gly aqueous solution	8.80E-06	12.5	34.2	14.5	33.8	12.4	5.1	94.9
240 °C, 40 bar H_2, 5 h, 2 g of 5 wt% Pt cat, 5 wt% gly aqueous solution	2.34E-05	32.2	9.0	4.1	23.7	26.9	36.3	63.7
220 °C, 40 bar H_2, 5 h, 2 g of 5 wt% Pt cat, **30 wt% gly aqueous solution**	2.74E-05	34.8	21.9	7.9	33.0	23.0	14.2	85.8
220 °C, **10 bar H_2**, 5 h, 2 g of 5 wt% Pt cat, 5 wt% gly aqueous solution	1.30E-05	16.6	14.4	26.9	36.4	16.7	5.6	94.4
220 °C, **50 bar H_2**, 5 h, 2 g of 5 wt% Pt cat, 5 wt% gly aqueous solution	2.00E-05	27.8	35.0	9.1	32.7	15.0	8.2	91.8
220 °C, 40 bar H_2, 5 h, **1 g of 5 wt% Pt cat**, 5 wt% gly aqueous solution	1.14E-05	15.2	20.7	16.7	36.1	21.1	5.3	94.7
220 °C, 40 bar H_2, 5 h, **3 g of 5 wt% Pt cat**, 5 wt% gly aqueous solution	2.20E-05	30.4	21.5	8.2	40.0	18.5	11.8	88.2
220 °C, 40 bar H_2, 5 h, **2 g of 2.5 wt% Pt cat**, 5 wt% gly aqueous solution	1.10E-05	16.7	20.6	17.0	39.2	16.0	7.2	92.8
220 °C, 40 bar H_2, 5 h, **2 g of 10 wt% Pt cat**, 5 wt% gly aqueous solution	2.18E-05	27.4	25.6	9.3	39.1	16.9	9.1	90.9

The increase in reaction temperature beyond 220 ºC, while it increases the rate of glycerol conversion, is undesirable from a 1,3-PDO selectivity point of view. The increase in temperature results in the formation of degradation and gaseous products with their combined selectivity > 63%. On the contrary, a decrease in reaction temperature adversely affects glycerol conversion rate but the 1,3-PDO selectivity increases. Hence, the desired temperature range is 200–220 ºC (see rows 2,4, and 5).

Another important parameter is the concentration of glycerol in the aqueous phase. We found that an increase in glycerol concentration increases the reaction rate but at the cost of higher formation of "others" and gaseous products. A glycerol concentration of 5% w/w in water was found to be optimal (see rows 2 and 6). The detailed reaction kinetics will throw more light on this aspect and would help one to optimize the concentration for industrial exploitation of the reaction.

An increase in reaction (hydrogen) pressure was advantageous for both glycerol conversion rates and 1,3-PDO selectivity. The conversion was increased to 27.8% and 1,3-PDO selectivity to 35% when the pressure was raised from 40 to 50 bar H_2 under otherwise similar conditions (see rows 2,7, and 8). Thereby reducing the formation of 1,2-PDO and 1-PrOH. Further increases in reaction pressure may also be helpful but were not explored in this study due to equipment limitations. Contrary, a decrease in hydrogen pressure to 10 bar reduced the glycerol conversion to 16.6% and 1,3-PDO selectivity to 14.4%. Followed by a considerable increase in 1,2-PDO selectivity under otherwise similar conditions (see rows 2,7, and 8).

An increase in catalyst loading resulted in an increased glycerol conversion rate, but again, 1,3-PDO selectivity decreased considerably. The increase in the catalyst amount in the reaction mixture resulted in a notable increase in 1-PrOH and gaseous products due to the over-hydrogenolysis of PDOs. Conversely, decreasing the catalyst loading resulted in lesser glycerol conversion rates, and 1,3-PDO selectivity also decreased significantly. Therefore, a catalyst loading of 2 g seems optimal to obtain the best yield towards 1,3 PDO (see rows 2, 9, and 10).

We also found an optimum in the platinum loading on the catalyst for a given total catalyst loading in the mixture. At higher Pt loading, the formation of 1-PrOH and gaseous products were enhanced with higher glycerol conversion rates, while at lower Pt loading, 1,2-PDO formation was promoted with reduced glycerol conversion rates (see rows 2, 11, and 12). Therefore, platinum loading of 5 wt% in a catalyst was found to be ideal in order to get maximum yield towards 1,3-PDO.

6.2 Summary results of parametric study over Pt-0.7STA/β-zeolite catalyst

Table 6.2 summarizes the results of the effect of parameters on glycerol hydrogenolysis reaction using Pt-0.7STA/β-zeolite catalyst. The detailed parametric study results observed are discussed in the following section (see section 6.3). The results over Pt-0.7STA/β-zeolite catalyst show nearly a similar trend as we have observed over Pt-0.3STA/β-zeolite catalyst (See Table 6.1). The effect of the following parameters was studied, taking the conditions of row 2 as the base case – reaction time (rows 1-3), glycerol concentration (rows 2 and 4), hydrogen pressure (rows 2, 5, and 6), temperature (rows 2, 7, and 8), Pt loading in the catalyst (rows 2, 9, and 10), and catalyst loading (rows 2, 11, and 12).

The parametric study results show that the batch reaction time has a significant impact on glycerol conversion and product distribution. At the longer reaction times, the glycerol conversion was found to increase to 63.5%, but the selectivity to others and gases has increased and the selectivity to propanediols was decreased. This is attributed to the over hydrogenolysis of PDOs. On the other hand, at the lower reaction times, the 1,3-PDO selectivity was increased to 44.7%, but the glycerol conversion was found to decrease to 1.3%. It is thus necessary to restrict the reaction time to typically less than or equal to 5 hrs under the conditions of interest (see rows 1-3).

The effect of glycerol concentration in the reaction mixture showed that the increase in glycerol concentration increases the rate of reaction. We found that an increase in glycerol concentration to 30% w/w increases the rate of reaction roughly by 41% but at the cost of higher formation of “others” and “gaseous products.” The higher glycerol concentration adversely affects the 1,3-PDO selectivity. Therefore, a glycerol concentration of 5% w/w in water was found to be optimal (see rows 2 and 4).

Table 6.2: - Summarized results from a parametric study of glycerol hydrogenolysis reaction over Pt-0.7STA/β-zeolite catalyst

Reaction/catalyst Parameters	Initial reaction rate	Reactant conversion	Product selectivities					Carbon Balance
	(mol g_{cat}^{-1} h^{-1})	Glycerol	1,3-PDO	1,2-PDO	1-PrOH	Others	gaseous	($C_{measured}$/ $C_{reacted}$) *100

220 °C, 40 bar H_2, **10 min**, 2 g of 5 wt% Pt cat, 5 wt% gly aqueous solution	1.95E-05	1.3	44.7	12.8	35.7	5.8	0.9	99.1
220 °C, 40 bar H_2, **5 h**, 2 g of 5 wt% Pt cat, 5 wt% gly aqueous solution	1.95E-05	26.8	38.8	8.1	35.1	13.8	4.3	95.7
220 °C, 40 bar H_2, **16 h**, 2 g of 5 wt% Pt cat, 5 wt% gly aqueous solution	1.95E-05	63.5	31.1	4.6	34.7	16.2	13.4	86.6
220 °C, 40 bar H_2, 5 h, 2 g of 5 wt% Pt cat, **30 wt% gly aqueous solution**	3.01E-05	37.7	29.4	6.7	27.1	19.0	17.8	82.2
220 °C, **10 bar H_2**, 5 h, 2 g of 5 wt% Pt cat, 5 wt% gly aqueous solution	1.13E-05	18.5	12.3	30.8	36.1	15.7	5.1	94.9
220 °C, **50 bar H_2**, 5 h, 2 g of 5 wt% Pt cat, 5 wt% gly aqueous solution	2.01E-05	30.4	42.0	7.9	27.0	15.1	8.0	92.0
200 °C, 40 bar H_2, 5 h, 2 g of 5 wt% Pt cat, 5 wt% gly aqueous solution	1.14E-05	17.8	41.7	10.1	33.3	11.9	3.0	97.0
240 °C, 40 bar H_2, 5 h, 2 g of 5 wt% Pt cat, 5 wt% gly aqueous solution	2.73E-05	33.9	8.2	3.5	22.2	24.6	41.4	58.6
220 °C, 40 bar H_2, 5 h, **2 g of 2.5 wt% Pt cat**, 5 wt% gly aqueous solution	1.18E-05	17.2	22.7	16.9	36.2	18.0	6.2	93.8
220 °C, 40 bar H_2, 5 h, **2 g of 10 wt% Pt cat**, 5 wt% gly aqueous solution	2.13E-05	30.3	25.4	7.1	40.2	18.9	8.4	91.6
220 °C, 40 bar H_2, 5 h, **1 g of 5 wt% Pt cat**, 5 wt% gly aqueous solution	1.27E-05	18.1	23.0	18.6	38.1	17.2	3.1	96.9
220 °C, 40 bar H_2, 5 h, **3 g of 5 wt% Pt cat**, 5 wt% gly aqueous solution	2.78E-05	32.3	29.1	5.9	41.1	15.8	8.1	91.9

An increase in initial reaction (hydrogen) pressure was found to be beneficial for both 1,3-PDO selectivity and glycerol hydrogenolysis rates. The glycerol conversion was increased to 30.4% and 1,3-PDO selectivity was increased to 42.0% when the pressure was raised from 40 to 50 bar H_2 under otherwise similar conditions. Thereby reducing the formation of 1,2-PDO and 1-PrOH. Further increases in reaction pressure may also be helpful but were not explored in this study due to apparatus limitations. On the contrary decrease in reaction pressure to 10 bar has

reduced the glycerol conversion to 18.5% and 1,3-PDO selectivity to 12.3%, resulting in an increase in selectivity of 1,2-PDO to 30.8% and 1-PrOH to 36.1%. Hence, for higher 1,3-PDO selectivity, the H_2 pressure of 40 bar or higher is recommended (see rows 2, 5, and 6).

The temperature effects revealed that an increase in reaction temperature above 220 ^oC increases the rate of glycerol hydrogenolysis, but it is undesirable from a 1,3-PDO selectivity point of view. The temperature of 240 ^oC increased the glycerol conversion to 33.9%, but the 1,3-PDO selectivity was only 8.2%. The higher temperature results in the formation of degradation and gaseous products via over-hydrogenolysis with their combined selectivity > 66%. Whereas the decrease in reaction temperature adversely affects glycerol hydrogenolysis rate but the 1,3-PDO selectivity increases. At 200 ^oC the 1,3-PDO selectivity was 41.7% with 17.8% glycerol conversion. Hence, the desired temperature range appears to be 200–220 ^oC (see rows 2, 7, and 8).

An increase in the platinum amount over a catalyst for a given total catalyst loading in the reaction mixture resulted in an increased glycerol hydrogenolysis rate. However, the 1,3-PDO selectivity decreased considerably, for 10 wt% Pt loading 1,3-PDO selectivity was 25.4% with 30.3% glycerol conversion. At higher Pt loading, the formation of 1-PrOH, others, and gaseous products were enhanced with higher glycerol hydrogenolysis rates, while at lower Pt loading, 1,2-PDO formation was promoted with reduced glycerol conversion rates. For 2.5 wt% Pt loading 1,3-PDO selectivity was 22.7% with 17.2% glycerol conversion (see rows 2, 9, and 10).

In the case of catalyst loading in a reaction mixture, we have found that an increase in catalyst loading increases the glycerol hydrogenolysis rates, but again, 1,3-PDO selectivity decreased considerably. The increase in the catalyst amount in the reaction mixture resulted in a notable increase in 1-PrOH and gaseous products due to the over-hydrogenolysis of PDOs. At higher catalyst loading, the conversion of glycerol was 32.3% with 29.1% 1,3-PDO selectivity. Conversely, decreasing the catalyst loading resulted in lesser glycerol hydrogenolysis rates, and 1,3-PDO selectivity also decreased significantly. At lower catalyst loading, the conversion of glycerol was 18.1% with 23.0% 1,3-PDO selectivity. Therefore, a catalyst loading of 2 g seems optimal to obtain the best yield towards 1,3 PDO (see rows 2, 11, and 12).

The following section shows the detailed study on the effect of reaction/catalyst parameter on glycerol hydrogenolysis reaction over Pt-0.3STA/β-zeolite and Pt-0.7STA/β-zeolite catalysts.

6.3 Detailed parametric study over Pt-0.3STA/β-zeolite and Pt-0.7STA/β-zeolite catalysts

6.3.1 Effect of reaction temperature on glycerol hydrogenolysis over Pt-0.3STA/β-zeolite and Pt-0.7STA/β-zeolite catalysts

In the literature, a wide range of temperatures ranging from 110 ºC [199] to 315 ºC [128] has been tried for glycerol conversion. The experiments were performed at temperatures varying from 140–240 ºC, to determine the effective temperature for glycerol hydrogenolysis over STA-promoted catalysts with an initial hydrogen pressure of 40 bar and reaction time of 5 h. The glycerol hydrogenolysis reaction was not even initiated at 140, 150, 160, 170, 180, and 190 ºC over both catalysts. Hence, the reaction was studied at a temperature of 200 ºC and higher. The results over Pt-0.3STA/β-zeolite and Pt-0.7STA/β-zeolite catalysts are given in Figure 6.1 and Figure 6.2, respectively. Here, each figure represents the effect of temperature on (I) glycerol conversion, (II) 1,3-PDO selectivity, (III) 1,2-PDO selectivity, (IV) 1-PrOH selectivity, (V) other selectivity, and (VI) gaseous products selectivity vs. time/conversion. Additionally, (a), (b), (c), and (d) in each figure show the results of the reaction study at 200 ºC, 210 ºC, 220 ºC, and 240 ºC respectively.

The glycerol hydrogenolysis results over both the catalysts show that the glycerol conversion increases with an increase in reaction temperature. In the case of Pt-0.3STA/β-zeolite catalyst, the glycerol conversion was 12.51% at 200 ºC; it was increased to 18.19% at 210 ºC, then again to 24.88% at 220 ºC, and finally, it was 32.19% at 240 ºC (See Figure 6.1 (I)). While in the case of Pt-0.7STA/β-zeolite catalyst, the glycerol conversion was 17.81% at 200 ºC, it was increased to 21.96% at 210 ºC, then again to 26.76% at 220 ºC, and finally, it was 33.88% at 240 ºC (See Figure 6.2 (I)). It can be observed that temperature has favorable effects on glycerol conversion, as shown in previous reports [105,117,118].

The selectivity of 1,3-PDO decreased with an increase in reaction temperature. After 5 h of reaction, the selectivity to 1,3-PDO over Pt-0.3STA/β-zeolite catalyst was 34.25% at 200 ºC, which was reduced to 33.02% at 210 ºC, then to 31.04% at 220 ºC, and lastly to 9.02% at 240 ºC (See Figure 6.1 (II)). The 1,3-PDO selectivity over Pt-0.7STA/β-zeolite catalyst was 41.72% at 200 ºC, which was reduced to 40.48% at 210 ºC, then to 38.81% at 220 ºC, and to 8.2% at 240 ºC (See Figure 6.2 (II)). Literature also shows that temperature has an adverse

effect on 1,3-PDO selectivity [92,105,117]. 1,2-PDO selectivity over Pt-0.3STA/β-zeolite catalyst after 5 h of reaction was 14.50% at 200 °C, which was reduced to 12.98% at 210 °C, 10.37% at 220 °C and lastly to 4.15% at 240 °C (See Figure 6.1 (III)).

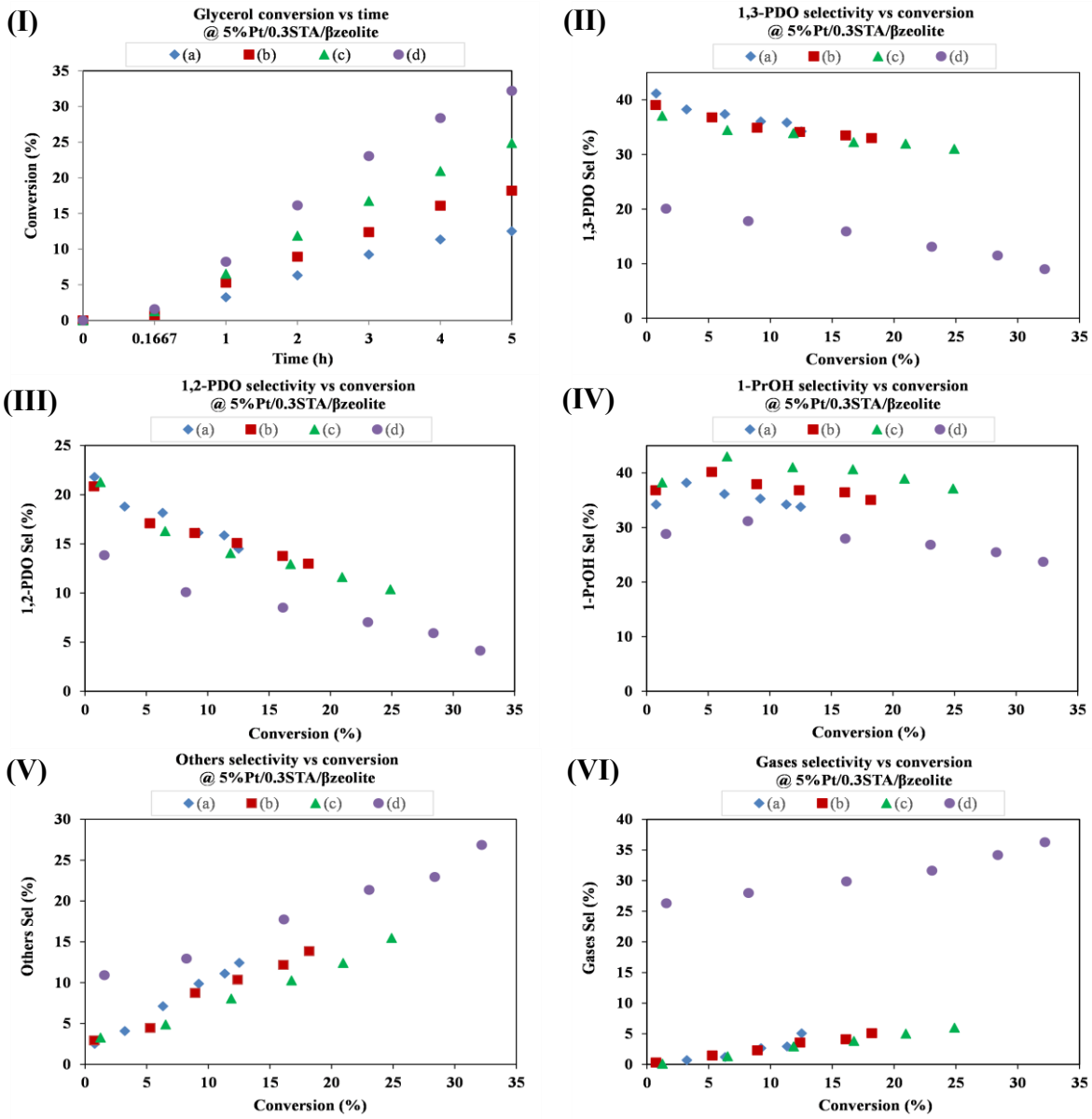

Figure 6.1. Effect of reaction temperature on: (I) glycerol conversion, (II) 1,3-PDO selectivity, (III) 1,2-PDO selectivity, (IV) 1-PrOH selectivity, (V) others selectivity, (VI) gaseous products selectivity vs. time/conversion over Pt-0.3STA/β-zeolite. Here, (a) 200 °C, (b) 210 °C, (c) 210 °C, (d) 240 °C.

Additionally, the selectivity of 1,2-PDO over Pt-0.7STA/β-zeolite catalyst after 5 h of reaction was 10.10% at 200 °C, which was reduced to 9.17% at 210 °C, then to 8.07% at 220 °C and to 3.48% at 240 °C (See Figure 6.2 (III)). Zhu et al. [117] found that the 1,2-PDO selectivity decreases monotonically with an increase in temperature due to its over hydrogenolysis at higher temperatures [117]. The selectivity to 1-PrOH after 5 h over Pt-0.3STA/β-zeolite

catalyst was 33.76% at 200 °C, it was increased to 35.05% at 210 °C, then to 37.13% at 220 °C, and then it was decreased to 23.71% at 240 °C (See Figure 6.1 (IV)). While over Pt-0.7STA/β-zeolite catalyst, it was 33.27% at 200 °C, 34.02% at 210 °C, 35.07% at 220 °C, and lastly, it was decreased to 22.25% at 240 °C (See Figure 6.2 (IV)).

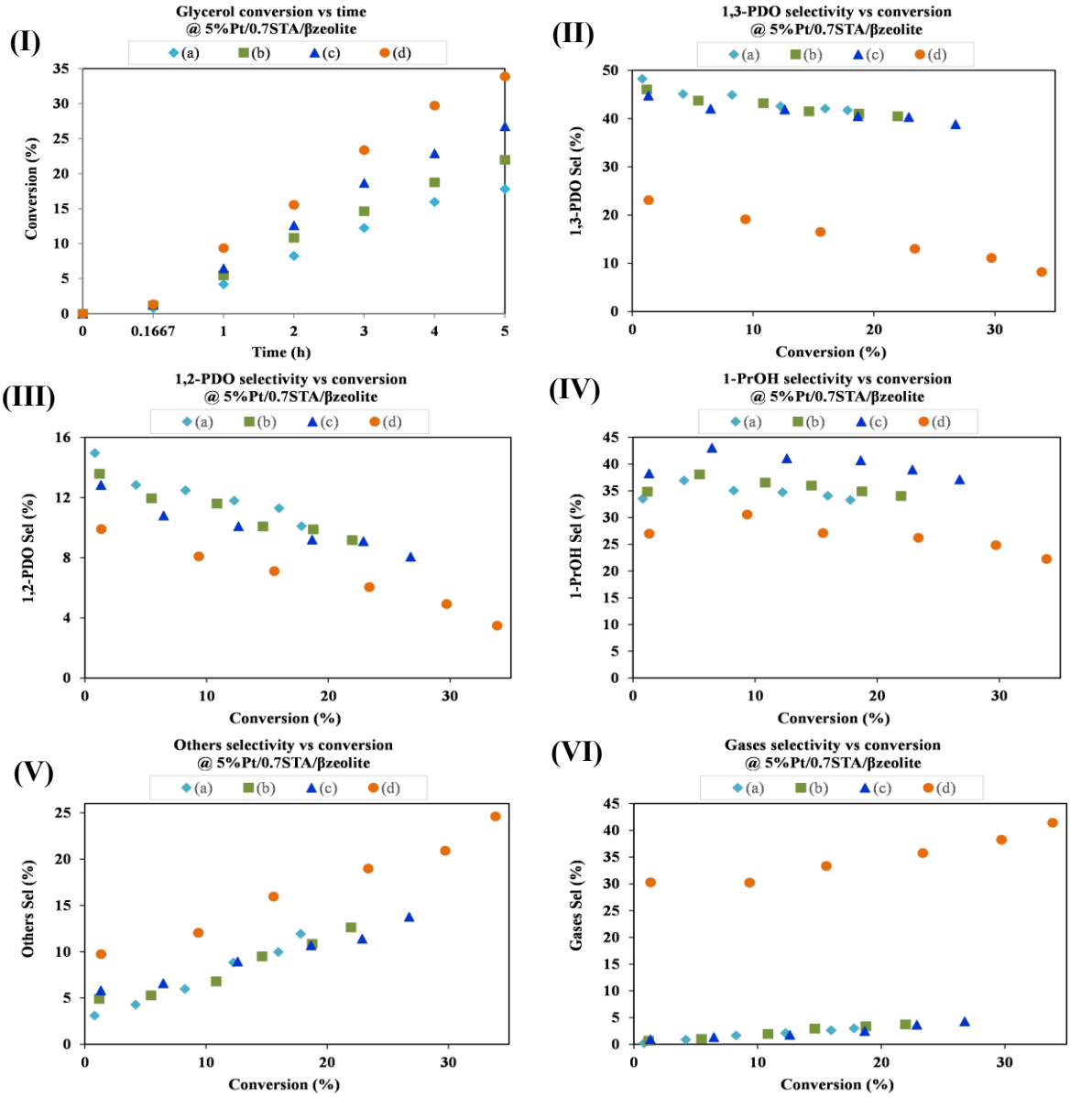

Figure 6.2. Effect of reaction temperature on: (I) glycerol conversion, (II) 1,3-PDO selectivity, (III) 1,2-PDO selectivity, (IV) 1-PrOH selectivity, (V) others selectivity, (VI) gaseous products selectivity vs. time/conversion over Pt-0.7STA/β-zeolite. Here, (a) 200 °C, (b) 210 °C, (c) 210 °C, (d) 240 °C.

At 240 °C, the selectivity for 1-PrOH was decreased because of its conversion into degradation and gaseous products. The increase in temperature shows an increase in 1-PrOH selectivity except for 240 °C. The results are in line with the reported results [105,117,118]. Regarding the other liquid products (others) selectivities, it increased slightly with an increase in reaction

temperature from 200 to 220 ºC and increased considerably at a temperature of 240 ºC. Others selectivity after 5 h of reaction over Pt-0.3STA/β-zeolite catalyst was 12.43% at 200 ºC, which was increased to 13.86% at 210 ºC, then to 15.47% at 220 ºC, and 26.86% at 240 ºC (See Figure 6.1 (V)). Whereas the catalyst Pt-0.7STA/β-zeolite showed others selectivity as 11.93% at 200 ºC, it was increased to 12.62% at 210 ºC, then to 13.77% at 220 ºC, and finally to 24.63% at 240 ºC (See Figure 6.2 (V)).

Finally, the gaseous products selectivity after 5 h of reaction over Pt-0.3STA/β-zeolite catalyst was 5.07% at 200 ºC, which was 5.09% at 210 ºC, then 5.99% at 220 ºC, and it was 36.27% at 240 ºC (See Figure 6.1 (VI)). Its selectivity over Pt-0.7STA/β-zeolite catalyst was 2.97% at 200 ºC, then 3.71% at 210 ºC and 4.28% at 220 ºC it was 41.43% at 240 ºC (See Figure 6.2 (VI)). The gaseous product selectivity was slightly increased when the temperature was raised from 200 to 220 ºC. However, it increased to a great extent when the temperature was further raised from 220 to 240 ºC.

The increase in the selectivities for others and gaseous products were attributed to the fact that the higher temperature facilitated the C–C bond cleavage, leading to the formation of lower alcohols like ethanol, methanol, propane, ethane, etc. [136]. Accordingly, lowering the reaction temperature favors the propanediols (PDOs) selectivity, which may be due to the lower conversion of the substrate as well as the reduced over-hydrogenolysis of PDOs. Furthermore, the elevated temperature has also produced gaseous products like propane, ethane, methane, etc. Their combined selectivity obtained through mass/carbon balance has varied between 5-10% for a temperature up to 220 ºC. However, a reaction temperature of 240 °C has increased both the degradation products such as ethanol, methanol and gaseous products; their combined selectivity was > 63%. Hence, further investigation was performed at 220 ºC as the reaction temperature. Amada and coworkers [63] have observed similar results for activity and 1,3-PDO selectivity over Ir–ReOx/SiO_2 catalyst. They reported that lower glycerol hydrogenolysis temperature is beneficial to produce 1,3-PDO with higher selectivity. However, the activity of the reaction is lower. Huang et al. [96] have reported that the temperature above 230 ºC for glycerol hydrogenolysis over Cu-$H_4SiW_{12}O_{40}/SiO_2$ catalyst has resulted in a significant increase of degradation products selectivities such as ethyl glycol, ethanol, and methane, etc.

6.3.2 Effect of initial hydrogen pressure on glycerol hydrogenolysis over Pt-0.3STA/β-zeolite and Pt-0.7STA/β-zeolite catalysts

Experiments were performed to study the effect of initial hydrogen (H_2) pressure on the glycerol hydrogenolysis reaction over best-performing catalysts. The results over Pt-0.3STA/β-zeolite and Pt-0.7STA/β-zeolite catalysts are given in Figure 6.3 and Figure 6.4, respectively. The experiments were carried out at three different H_2 pressures, namely 10 bar, 40 bar, and 50 bar. Figure 6.3 and Figure 6.4 show the effect of initial H_2 pressure on (I) glycerol conversion, (II) 1,3-PDO selectivity, (III) 1,2-PDO selectivity, (IV) 1-PrOH selectivity, (V) others selectivity, and (VI) gaseous products selectivity vs. time/conversion. Here, (a), (b), and (c) in each figure stands for the reaction studied at 10 bar, 40 bar, and 50 bar, respectively.

The result shows that the increase in initial H_2 pressure favors the glycerol conversion. After 5 h of reaction over Pt-0.3STA/β-zeolite catalyst, the glycerol conversion was 16.58% at 10 bar, increased to 24.88% at 40 bar, and further increased to 27.83% at 50 bar H_2 pressure (See Figure 6.3 (I)). On the other hand, the conversion over Pt-0.7STA/β-zeolite catalyst was 18.52% at 10 bar, 26.76% at 40 bar, and 30.4% at 50 bar H_2 pressure (See Figure 6.4 (I)). This is attributed to the higher concentration of protons and hydride ions which are formed from the heterolytic dissociation of H_2 molecule over the hydrogenation metal at higher H_2 pressures. The protons and hydride ions are involved in the activation of glycerol molecules [199]. Similar effects were also reported in the literature [105,113,117,118,200].

The increase in pressure has a positive impact on the 1,3-PDO selectivity. It increased significantly with increased hydrogen pressure from 10 to 40 bar and increased slightly at 50 bar. The 1,3-PDO selectivity after 5 h of reaction over Pt-0.3STA/β-zeolite catalyst was 14.39% at 10 bar, which was increased to 31.04% at 40 bar. Moreover, it has further increased to 35.03% at 50 bar (See Figure 6.3 (II)). Whereas, trends in selectivity over Pt-0.7STA/β-zeolite catalyst was 12.28% at 10 bar, 38.81% at 40 bar, and 41.97% at 50 bar initial H_2 pressure (See Figure 6.4 (II)). The increase in 1,3-PDO selectivity with an increase in H_2 pressure is attributed to the increased amount of active hydrogen species, which increased the hydrogenation of 3-hydroxypropanal to 1,3-PDO.

Trends in 1,2-PDO selectivity revealed that the increase in initial H_2 pressure had decreased the 1,2-PDO selectivity considerably. 1,2-PDO selectivity after 5 h over Pt-0.3STA/β-zeolite catalyst was 26.88% at 10 bar, which was reduced to 10.37% at 40 bar and then remains nearly constant as 9.1% at 50 bar H_2 (See Figure 6.3 (III)). Whereas 1,2-PDO selectivity over Pt-

0.7STA/β-zeolite catalyst was 30.8% at 10 bar, it was 8.07% at 40 bar and 7.94% at 50 bar H_2 (See Figure 6.4 (III)). Zhu et al. [92] reported that an increase in initial hydrogen pressure increases the selectivity for 1,3-PDO while the selectivity for 1,2-PDO was decreased gradually with an increase in pressure except at higher H_2 pressure. Our results are in agreement with theirs. Additionally, Huang et al. [96] reported that the positive impact of initial H_2 pressure on 1,3-PDO selectivity is partly due to the thermodynamic limitation of acetol and 3-hydroxypropanal hydrogenation.

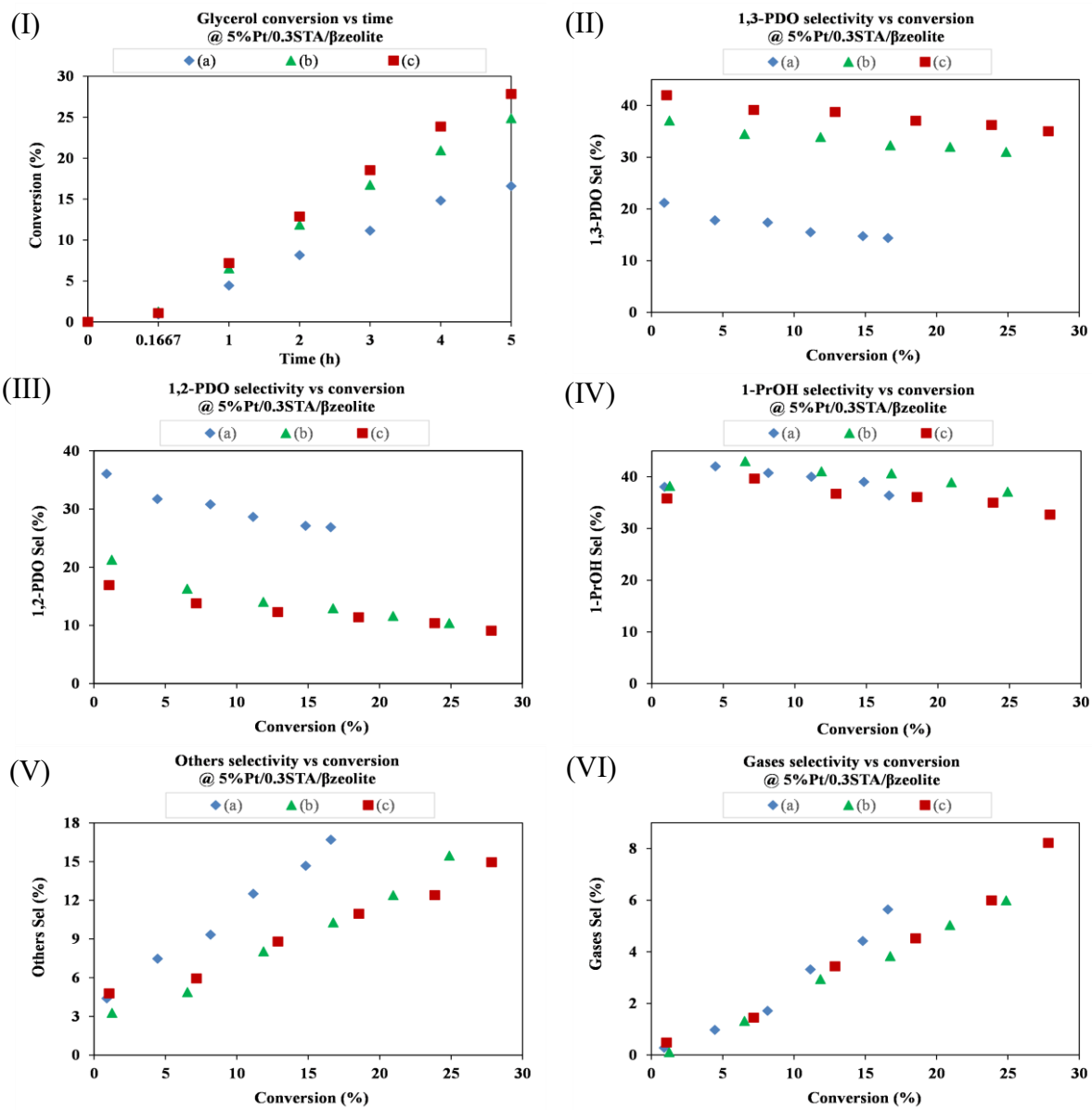

Figure 6.3. Effect of initial hydrogen (H_2) pressure on: (I) glycerol conversion, (II) 1,3-PDO selectivity, (III) 1,2-PDO selectivity, (IV) 1-PrOH selectivity, (V) others selectivity, (VI) gaseous products selectivity vs. time/conversion over Pt-0.3STA/β-zeolite, where (a) 10 bar, (b) 40 bar, (c) 50 bar.

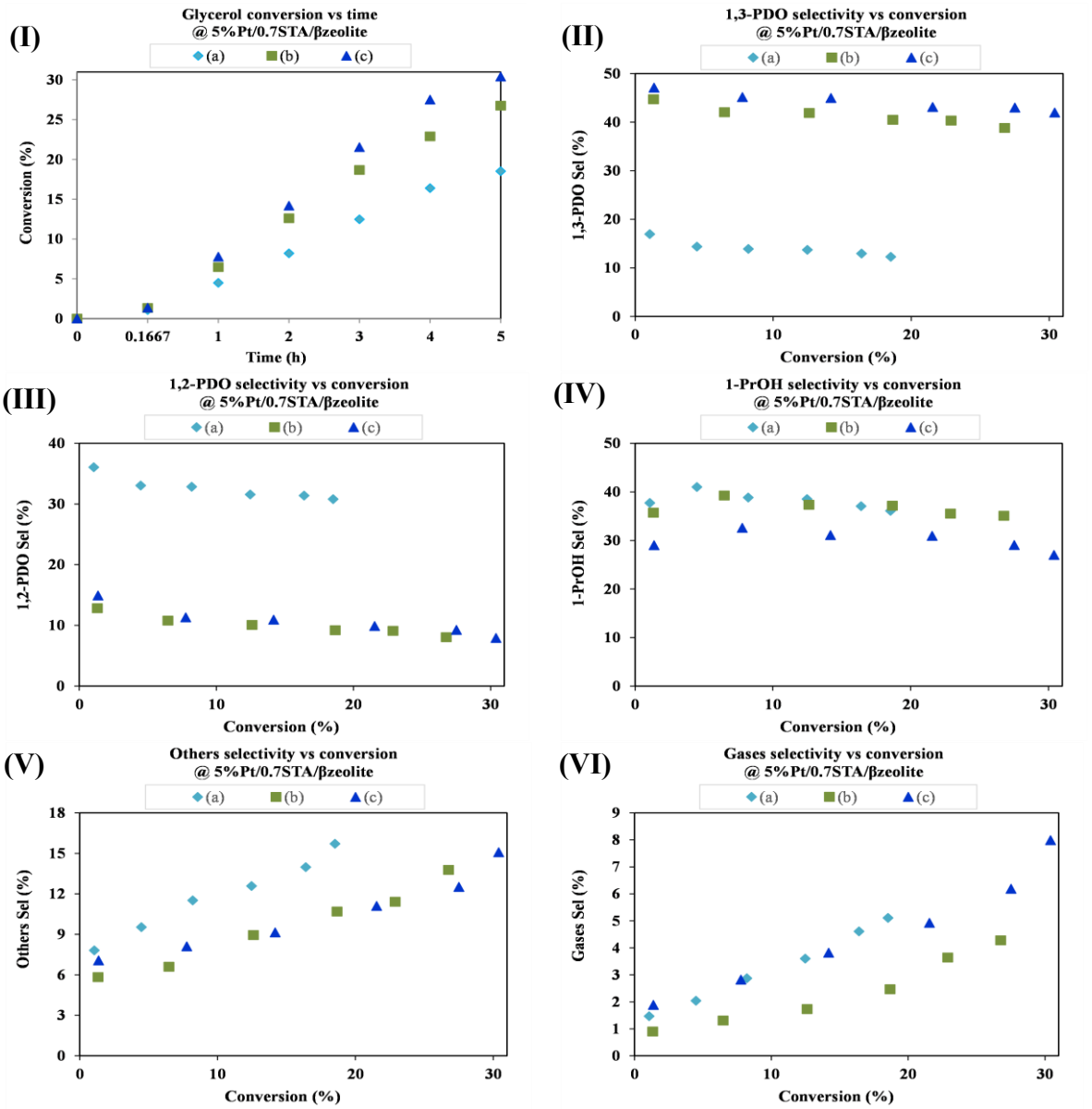

Figure 6.4. Effect of initial hydrogen (H_2) pressure on: (I) glycerol conversion, (II) 1,3-PDO selectivity (III) 1,2-PDO selectivity, (IV) 1-PrOH selectivity, (V) others selectivity, (VI) gaseous products selectivity vs. time/conversion over Pt-0.7STA/β-zeolite, where (a) is 10 bar, (b) is 40 bar, (c) is 50 bar.

The 1-PrOH selectivity was nearly constant with an increase in pressure over both the catalysts and decreased slightly at higher pressure. Gong et al. [105] and Zhu et al. [92] have reported similar results; however, they haven't stressed on the decrease in the selectivity of 1-PrOH. The obtained 1-PrOH selectivity after 5 h over Pt-0.3STA/β-zeolite catalyst was 36.39% at 10 bar. It was 37.13% at 40 bar, while it was decreased to 32.7% at 50 bar (See Figure 6.3 (IV)). While, 1-PrOH selectivity over Pt-0.7STA/β-zeolite catalyst was 36.1% at 10 bar, 35.07% at 40 bar, and it was 27.02% at 50 bar (See Figure 6.3 (IV)). The decrease in the selectivity of 1-

PrOH was due to increased selectivity of 1,3-PDO at higher pressures which will eventually reduce the overall selectivity of all the other products.

Selectivity for other liquid products (others) didn't show a significant change with an increase in pressure. The others selectivity after 5 h over Pt-0.3STA/β-zeolite catalyst was 16.71% at 10 bar, 15.47% at 40 bar, and 14.96% at 50 bar (See Figure 6.3 (V)). Others selectivity over Pt-0.7STA/β-zeolite catalyst was 15.71% at 10 bar, 13.77% at 40 bar, and 15.07% at 50 bar (See Figure 6.4 (V)). Lastly, regarding the gaseous products selectivities, it was also nearly constant with pressure except for 50 bar where it was slightly increased. After 5 h over Pt-0.3STA/β-zeolite catalyst, the gaseous products selectivity was 5.64% at 10 bar, 5.99% at 40 bar, and 8.22% at 50 bar (See Figure 6.3 (VI)). Its selectivity over Pt-0.7STA/β-zeolite catalyst was 5.11% at 10 bar, 4.28% at 40 bar, and 7.99% at 50 bar (See Figure 6.4 (VI)). These results suggest that the effect of initial H_2 pressure on the selectivities of others and gaseous products over both catalysts was very small or negligible.

6.3.3 Effect of Platinum (Pt) loading on glycerol hydrogenolysis over Pt-0.3STA/β-zeolite and Pt-0.7STA/β-zeolite catalysts

The experiments were performed to study the effect of platinum loading on the glycerol hydrogenolysis reaction over Pt-0.3STA/β-zeolite and Pt-0.7STA/β-zeolite catalysts. The experiments were performed with three different platinum loadings, *viz.* 2.5 wt%, 5 wt%, and 10 wt% at standard reaction conditions. Figure 6.5 and Figure 6.6 illustrates the glycerol hydrogenolysis results obtained with different platinum content in the catalysts on (I) glycerol conversion, (II) 1,3-PDO selectivity, (III) 1,2-PDO selectivity, (IV) 1-PrOH selectivity, (V) others selectivity, (VI) gaseous products selectivity vs. time/conversion. Here, (a), (b), and (c) stands for the reaction studied with catalysts containing 2.5 wt% Pt, 5 wt% Pt, and 10 wt% Pt, respectively.

The result shows that the increase in the platinum loading has gradually increased the glycerol conversion, the glycerol conversion after 5 h of reaction over Pt-0.3STA/β-zeolite catalyst was 16.73% with 2.5 wt% Pt, it was increased to 24.88% with 5 wt% Pt, and finally, it was increased to 27.38% with 10 wt% Pt (See Figure 6.5 (I)). The glycerol conversion over Pt-0.7STA/β-zeolite catalyst was 17.23% with 2.5 wt% Pt. It was 26.76% with 5 wt% Pt and 30.3% with 10 wt% Pt (See Figure 6.6 (I)). The increase in Pt loading from 2.5 to 5 wt% showed a positive impact on selectivity of 1,3-PDO, but further increase in Pt loading reduced its selectivity. The

1,3-PDO selectivity after 5 h of reaction over Pt-0.3STA/β-zeolite catalyst was 20.60% with 2.5 wt% Pt, which increased to 31.04% with 5 wt% Pt, and then reduced to 25.63% with 10 wt% Pt (See Figure 6.5 (II)). 1,3-PDO selectivity over Pt-0.7STA/β-zeolite catalyst was 22.73% with 2.5 wt% Pt, which increased to 38.81% with 5 wt% Pt, and it was 25.41% with 10 wt% Pt (See Figure 6.6 (II)).

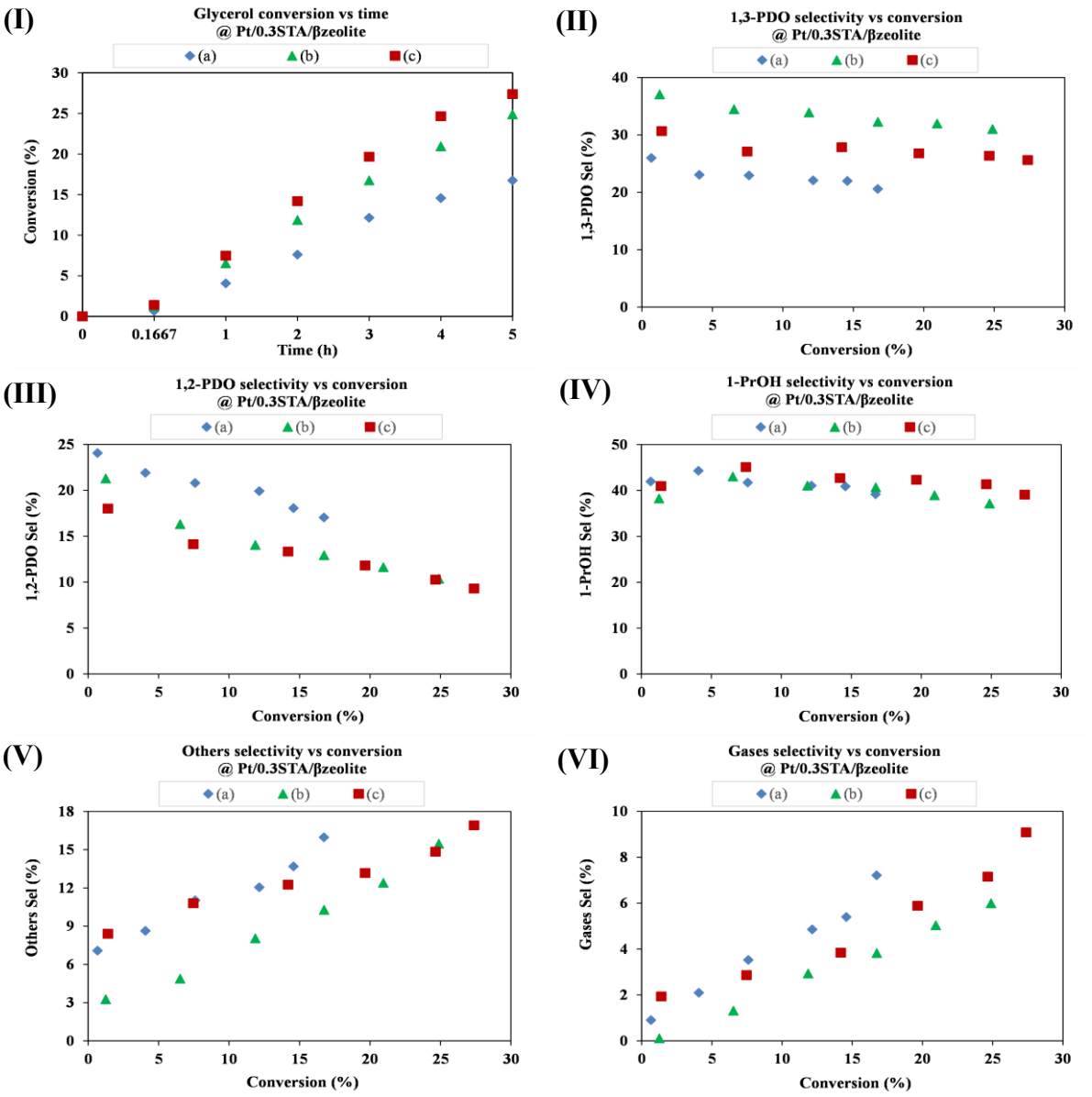

Figure 6.5. Effect of catalyst platinum loading on: (I) glycerol conversion, (II) 1,3-PDO selectivity, (III) 1,2-PDO selectivity, (IV) 1-PrOH selectivity, (V) others selectivity, (VI) gaseous products selectivity vs. time/conversion over Pt-0.3STA/β-zeolite. (a) – 2.5 wt%, (b) – 5 wt%, (c) – 10 wt%.

The selectivity of 1,2-PDO showed continuous fall with the increase in Pt loading. The 1,2-PDO selectivity after 5 h of reaction over Pt-0.3STA/β-zeolite catalyst was 17.05% with 2.5 wt% Pt, which was reduced to 10.37% with 5 wt% Pt, and then it was 9.3% at 10 wt% Pt (See

Figure 6.5 (III)). While 1,2-PDO selectivity over Pt-0.7STA/β- zeolite catalyst was 16.95% with 2.5 wt% Pt, it was 8.07% with 5 wt% Pt, and it was 7.09% with 10 wt% Pt (See Figure 6.6 (III)).

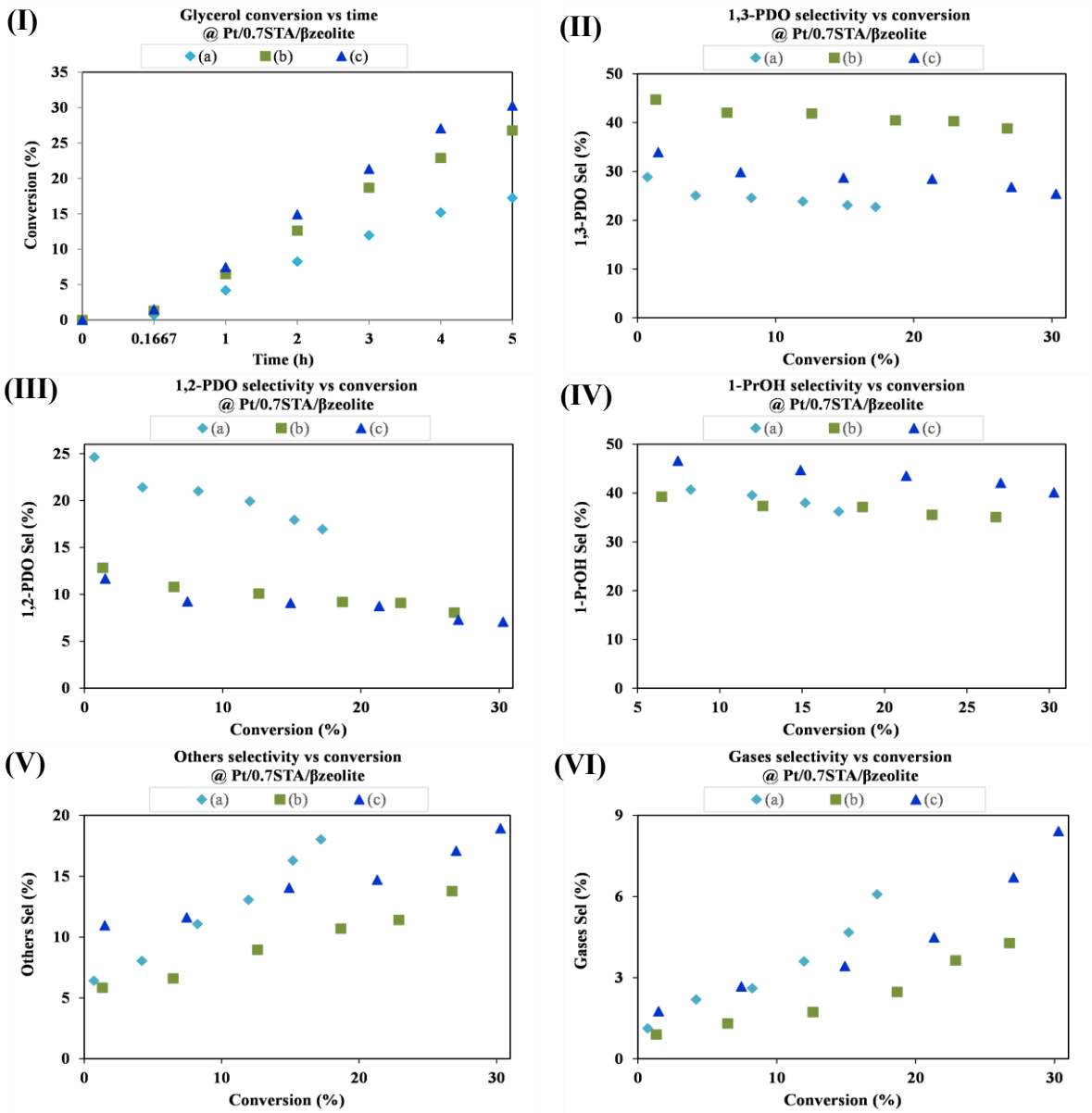

Figure 6.6. Effect of catalyst platinum loading on: (I) glycerol conversion, (II) 1,3-PDO selectivity, (III) 1,2-PDO selectivity, (IV) 1-PrOH selectivity, (V) others selectivity, (VI) gaseous products selectivity vs. time/conversion over Pt-0.7STA/β-zeolite. (a) – 2.5 wt%, (b) – 5 wt%, (c) – 10 wt%.

The selectivity for 1-PrOH over Pt-0.3STA/β-zeolite catalyst remained almost constant at 2.5 and 10 wt% loadings while it was decreased slightly at 5 wt% Pt content in the catalysts. The 1-PrOH selectivity after 5 h over Pt-0.3STA/β-zeolite catalyst was 39.16% with 2.5 wt% Pt, which was increased to 37.13% with 5 wt% Pt and then it was increased to 39.06% with 10wt% Pt (See Figure 6.5 (IV)). On the other hand, selectivity of 1-PrOH over Pt-0.7STA/β-zeolite

catalyst slightly decreased at 5 wt% Pt content and then again increased at 10 wt% content. 1-PrOH selectivity over Pt-0.7STA/β-zeolite catalyst was 36.21% with 2.5 wt% Pt, 35.1% with 5 wt% Pt, and 40.16% with 10 wt% Pt (See Figure 6.6 (IV)). The selectivity of others over Pt-0.3STA/β-zeolite catalyst slightly decreased at 5 wt% Pt loading while it was increased at 10 wt% Pt loading. After 5 h of reaction over Pt-0.3STA/β-zeolite catalyst, the selectivity of others was 15.97% with 2.5 wt% Pt, 15.47% with 5 wt% Pt 16.92% with 10 wt% Pt (See Figure 6.5 (V)). The selectivity of others over Pt-0.7STA/β-zeolite catalyst was nearly constant at 2.5 and 10 wt% Pt content while it was decreased at 5 wt% Pt content in the catalyst. The selectivity of others over Pt-0.7STA/β-zeolite catalyst was 18.03% with 2.5 wt% Pt, 13.77% with 5 wt% Pt, and 18.93% with 10 wt% Pt (See Figure 6.6 (V)). The increase in selectivity of others is attributed to the over hydrogenolysis of PDOs.

Lastly, the selectivity of gaseous products was slightly reduced with an increase in Pt loading from 2.5 to 5 wt%. However, it was again increased when the Pt loading was 10 wt% over both the catalysts. After 5 h of reaction over Pt-0.3STA/β-zeolite catalyst, the selectivity of gaseous products was 7.21% with 2.5 wt% Pt, 5.99% with 5 wt% Pt 9.09% with 10 wt% Pt (See Figure 6.5 (VI)). The selectivity of gaseous products over Pt-0.7STA/β-zeolite catalyst was 6.18% with 2.5 wt% Pt, 4.28% with 5 wt% Pt, and 8.43% with 10 wt% Pt (See Figure 6.5 (VI)).

Qin and coworkers [199] reported an increase in Pt content in the catalyst had increased the hydrogen uptake. It was reported by Chen et al. [201] and Triwahyono et al. [171] that the amount of protons and hydride species formed over hydrogenation metal from the dissociation of H_2 molecule increases with the increase in hydrogen uptakes. These excessive protons and hydride ions act as the active sites for glycerol dehydration or hydrogenolysis, and the glycerol conversion increases with an increase in Pt loading. However, the surplus of protons and hydride species might increase the successive hydrogenolysis of PDOs to propanols or degradation products, which ultimately reduces the selectivity towards 1,3-PDO and 1,2-PDO.

6.3.4 Effect of catalyst amount on glycerol hydrogenolysis over Pt-0.3STA/β-zeolite and Pt-0.7STA/β-zeolite catalysts

Experiments were performed to study the effect of catalyst loading/amount on the glycerol hydrogenolysis reaction over Pt-0.3STA/β-zeolite and Pt-0.7STA/β-zeolite catalysts. The experiments were performed with three different catalyst loadings such that the ratio of catalyst to glycerol was 0.25, 0.5, and 0.75. The experiments were carried out at the standard reaction

conditions. Figure 6.7 and Figure 6.8 revealed the glycerol hydrogenolysis reaction results observed at different catalyst loadings. Each figure shows the effect of catalyst amount on: (I) glycerol conversion, (II) 1,3-PDO selectivity, (III) 1,2-PDO selectivity, (IV) 1-PrOH selectivity, (V) others selectivity, (VI) gaseous products selectivity vs. time/conversion. Moreover, (a), (b), and (c) stands for the reaction studied at catalyst to glycerol (C/G) ratio as 0.25, 0.5, and 0.75, respectively.

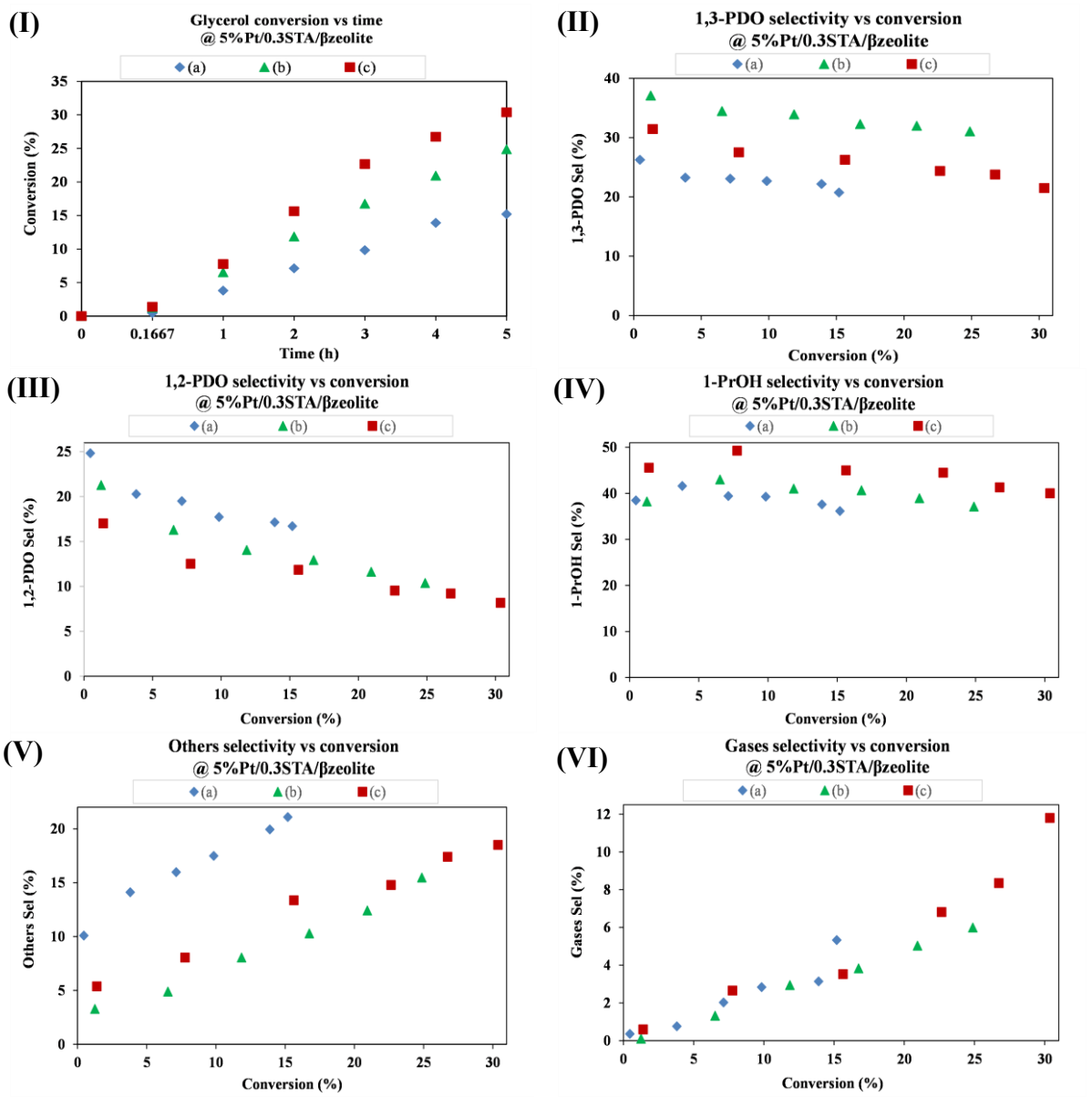

Figure 6.7. Effect of catalyst amount in reaction on: (I) glycerol conversion, (II) 1,3-PDO selectivity, (III) 1,2-PDO selectivity, (IV) 1-PrOH selectivity, (V) others selectivity, (VI) gaseous products selectivity vs. time/conversion over Pt-0.3STA/β-zeolite. Here, catalyst to glycerol ratio: (a) 0.25, (b) 0.5, (c) 0.75.

The results show that the increase in the catalyst loading increases the glycerol conversion rate. Glycerol conversion after 5 h of reaction over Pt-0.3STA/β-zeolite catalyst was 15.19% at 0.25 catalyst to glycerol ratio, it was increased to 24.88% at 0.5 C/G ratio, and it was further increased to 30.37% at 0.75 C/G ratio (See Figure 6.7 (I)). The glycerol conversion over Pt-0.7STA/β-zeolite catalyst was 18.07% at 0.25 C/G ratio, it was increased to with 26.76% at 0.5 C/G ratio, and it was further increased to 32.28% at 0.75 C/G ratio (See Figure 6.8 (I)). The 1,3-PDO selectivity increased with an increase in catalyst to glycerol ratio from 0.25 to 0.5. However, further increase in catalyst loading has decreased the 1,3-PDO selectivity over both the catalysts. The initial increase in catalyst loading has positively impacted 1,3-PDO selectivity, but the higher catalyst amount has reduced the 1,3-PDO selectivity, probably due to its over hydrogenolysis.

The 1,3-PDO selectivity after 5 h of reaction for Pt-0.3STA/β-zeolite catalyst was 20.73% with 0.25 catalyst to glycerol ratio, which was increased to 31.04% with 0.5 C/G ratio followed by a decrease to 21.50% with 0.75 C/G ratio (See Figure 6.7 (II)). In the case of Pt-0.7STA/β-zeolite catalyst 1,3-PDO selectivity was 23.01% at 0.25 C/G ratio, 38.81% at 0.5 C/G ratio and 29.11% at 0.75 C/G ratio (See Figure 6.8 (II)). The selectivity of 1,2-PDO showed a continuous decrease with an increase in catalyst to glycerol ratio in the reaction mixture, probably due to its instability (See Section 5.1.5) which makes its over-hydrogenolysis easy. The 1,2-PDO selectivity after 5 h of reaction over Pt-0.3STA/β-zeolite catalyst was 16.7% at 0.25 catalyst to glycerol ratio, which was reduced to 10.37% at 0.5 C/G ratio and then further decreases to 8.17% at 0.75 C/G ratio (See Figure 6.7 (III)). 1,2-PDO selectivity over Pt-0.7STA/β-zeolite catalyst was 18.57% with 0.25 C/G ratio, then 8.07% with 0.5 C/G ratio and 5.87% with 0.75 C/G ratio (See Figure 6.8 (III)).

The 1-PrOH selectivity was increased continuously with an increase in catalyst to glycerol ratio in the reaction over Pt-0.3STA/β-zeolite catalyst. However, it was first decreased and then increased over Pt-0.7STA/β-zeolite catalyst with an increase in catalyst to glycerol ratio. The 1-PrOH selectivity after 5 h of reaction over Pt-0.3STA/β-zeolite catalyst was 36.15% with a 0.25 catalyst to glycerol ratio, which was increased to 37.13% at 0.5 C/G ratio, then it was further increased to 40.03% at 0.75 C/G ratio (See Figure 6.7 (IV)). It is attributed to the over hydrogenolysis of propanediols which largely end up in making 1-PrOH, others or gases. 1-PrOH selectivity after 5 h over Pt-0.7STA/β-zeolite catalyst was 38.07% at 0.25 catalyst to glycerol ratio, which reduced to 35.07% at 0.5 C/G ratio, then it increased to 41.06% at 0.75 C/G ratio (See Figure 6.8 (IV)). The catalyst Pt-0.7STA/β-zeolite possesses the highest amount

of Brønsted acid sites, and a sufficient amount of catalyst will enhance the 1,3-PDO selectivity. However, the catalyst's excess amount will lead to over hydrogenolysis of 1,3-PDO despite its higher stability (See Section 5.1.5). The others selectivities were reduced with an increased catalyst to glycerol ratio from 0.25 to 0.5 and then again increased at 0.75 C/G ratio over both the catalysts. After 5 h of reaction over Pt-0.3STA/β-zeolite catalyst, the selectivity for others was 21.09% with a 0.25 catalyst to glycerol ratio, which reduced to 15.47% at 0.5 C/G ratio then it was further increased to 18.5% at 0.75 C/G ratio (See Figure 6.7 (V)). Others selectivity in the case of Pt-0.7STA/β-zeolite catalyst was 17.23% at 0.25 C/G ratio, 13.77% at 0.5 C/G ratio, and 15.81% at 0.75 C/G ratio (See Figure 6.8 (V)).

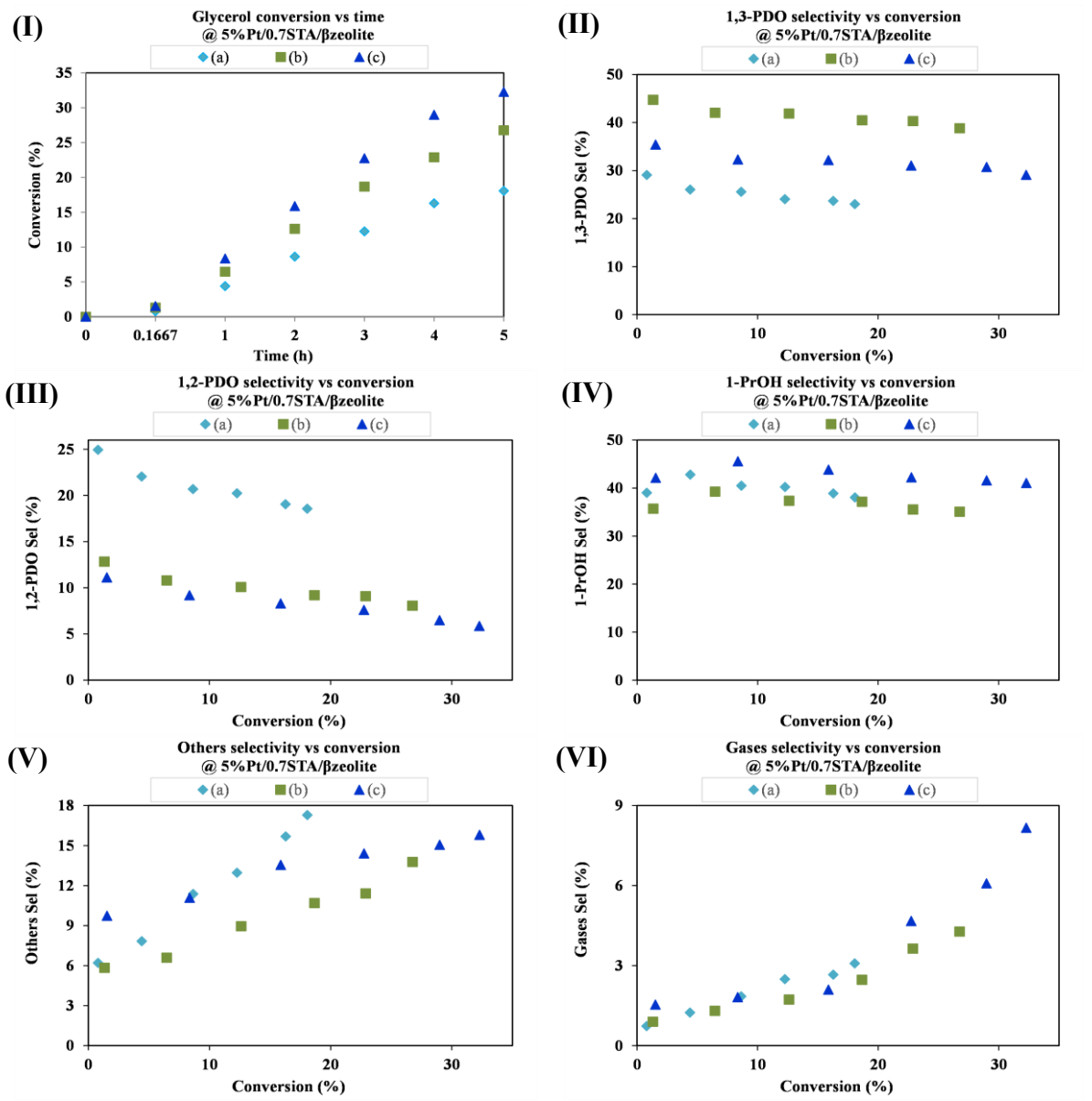

Figure 6.8. Effect of catalyst amount in reaction on: (I) glycerol conversion, (II) 1,3-PDO selectivity, (III) 1,2-PDO selectivity, (IV) 1-PrOH selectivity, (V) others selectivity, (VI) gaseous products selectivity vs. time/conversion over Pt-0.7STA/β-zeolite. Here, catalyst to glycerol ratio: (a) 0.25, (b) 0.5, (c) 0.75.

The gaseous products selectivity showed an increasing trend with an increase in catalyst to glycerol ratio over both the catalysts. Though the increase was small when the C/G ratio was changed from 0.25 to 0.5, but at 0.75 C/G ratio the increase was more than double compared to its selectivity over the 0.25 C/G ratio. After 5 h of reaction over Pt-0.3STA/β-zeolite catalyst, the selectivity for gaseous products was 5.33% at a 0.25 catalyst to glycerol ratio. It increased to 5.99% at a 0.5 C/G ratio; then it was further increased to 11.80% at a 0.75 C/G ratio (See Figure 6.7 (VI)). The gaseous products selectivity over Pt-0.7STA/β-zeolite catalyst was 3.08% at 0.25 C/G ratio, 4.28% at 0.5 C/G ratio, and 8.14% at 0.75 C/G ratio (See Figure 6.8 (VI)). The increase of the catalyst amount in a reaction mixture increases the number of hydrogenation metal sites and the acidic sites simultaneously. The metal sites will produce a greater number of protons and hydride species by dissociating the H_2 molecule heterolytically. The higher catalyst loading increases the number of acid sites, more number of acidic sites will dehydrate the more number of glycerol molecules. This will increase the number of glycerol molecules reacted, and therefore the glycerol conversion increases. However, the excess number of protons and hydride species will increase the successive hydrogenolysis of propanediols, and their selectivity will go down. Zhu et al. [117] reported that the increase in catalyst amount increases the selectivity of 1-PrOH and 2-PrOH at the cost of propanediols. Our results are in agreement with their results.

6.3.5 Effect of glycerol concentration on glycerol hydrogenolysis over Pt-0.3STA/β-zeolite and Pt-0.7STA/β-zeolite catalysts

The effect of initial glycerol concentration on the hydrogenolysis of glycerol was studied at the standard reaction conditions over both catalysts. The glycerol concentration was varied as 5%, 10%, 20%, and 30%. Here, the amount of glycerol and water (solvent) was adjusted to make the particular concentration of glycerol. Figure 6.9 and Figure 6.10 represent the effect of initial glycerol concentration on (I) glycerol conversion, (II) 1,3-PDO selectivity, (III) 1,2-PDO selectivity, (IV) 1-PrOH selectivity, (V) others selectivity, (VI) gaseous products selectivity vs. time/conversion. Additionally, (a), (b), (c), and (d) stands for the reaction studied at glycerol concentration of 5 wt%, 10 wt%, 20 wt%, and 30 wt% respectively.

The results show that an increase in glycerol concentration has a positive impact on glycerol conversion. The glycerol conversion was increased with an increase in initial glycerol concentration. The glycerol conversion after 5 h of reaction over Pt-0.3STA/β-zeolite catalyst was 24.88%, 27.91%, 30.84, and 34.82% and their respective glycerol concentrations was 5%,

10%, 20%, and 30% (See Figure 6.9 (I)). While the glycerol conversion over Pt-0.7STA/β-zeolite catalyst was 26.76% at 5 wt% glycerol concentration, 30.53% at 10 wt% concentration, 33.90% at 20 wt% concentration, and 37.67% at 30 wt% concentration (See Figure 6.10 (I)).

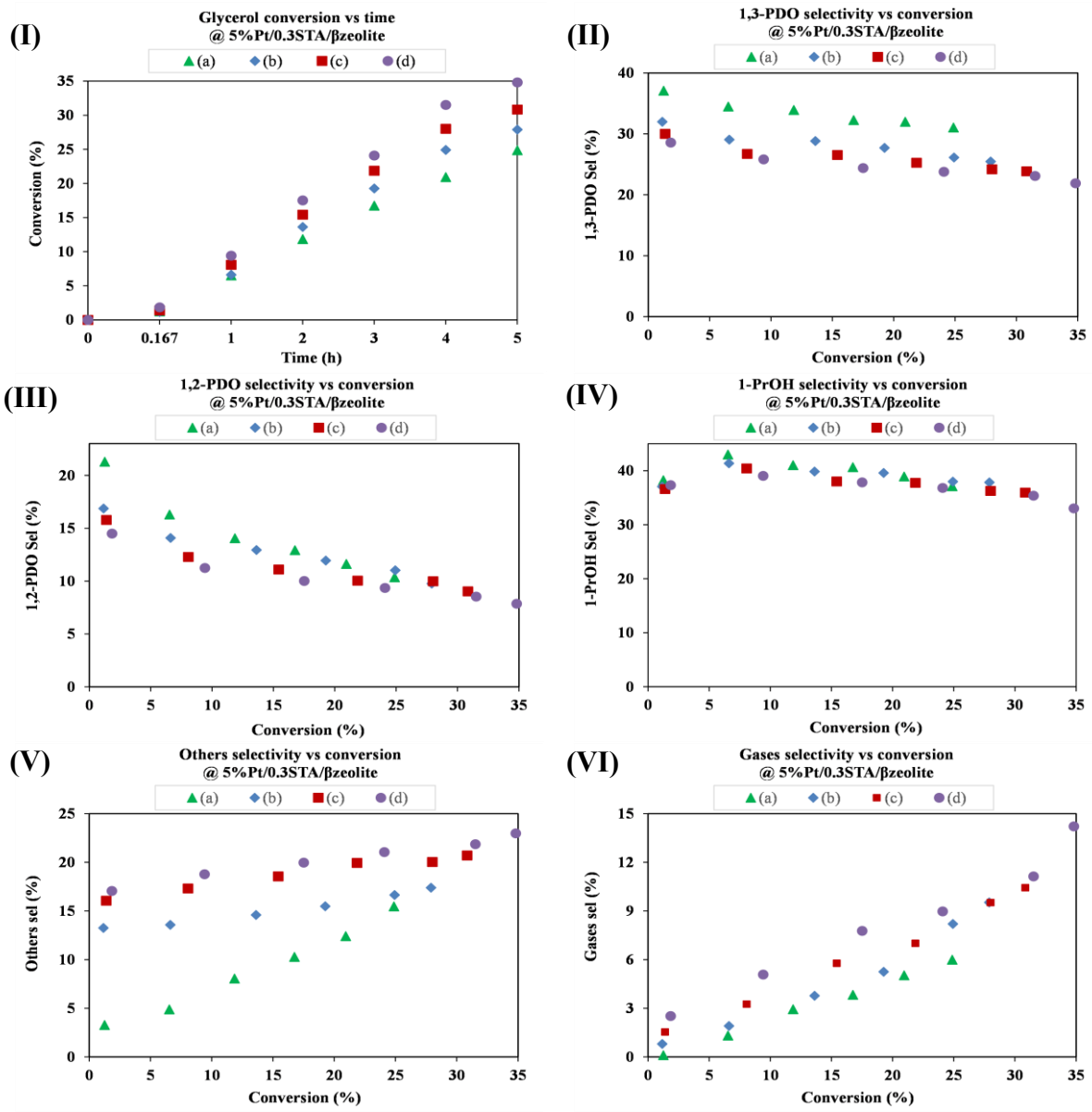

Figure 6.9. Effect of initial glycerol concentration on: (I) glycerol conversion, (II) 1,3-PDO selectivity, (III) 1,2-PDO selectivity, (IV) 1-PrOH selectivity, (V) others selectivity, (VI) gaseous products selectivity vs. time/conversion over Pt-0.3STA/β-zeolite. Here, (a) – 5 wt% glycerol, (b) – 10 wt% glycerol, (c) – 20 wt% glycerol, (d) – 30 wt% glycerol.

The selectivities of propanediols (PDOs) and 1-PrOH showed a gradual decrease with an increase in glycerol concentration. However, the selectivities for others and gaseous products showed an increase with the increase in glycerol concentration.

The 1,3-PDO selectivity after 5 h of reaction over Pt-0.3STA/β-zeolite catalyst was 31.04% at 5 wt% glycerol concentration, which was 25.47% at 10 wt% concentration, 23.86% at 20 wt% concentration, and lastly, it was 21.89% at 30 wt% concentration (See Figure 6.9 (II)). The selectivity of 1,3-PDO over Pt-0.7STA/β-zeolite catalyst was 38.81% at 5 wt% glycerol concentration. It was 34.92% at 10 wt% concentration, it was 33.72% at 20 wt% concentration, and 29.36% at 30 wt% concentration (See Figure 6.10 (II)).

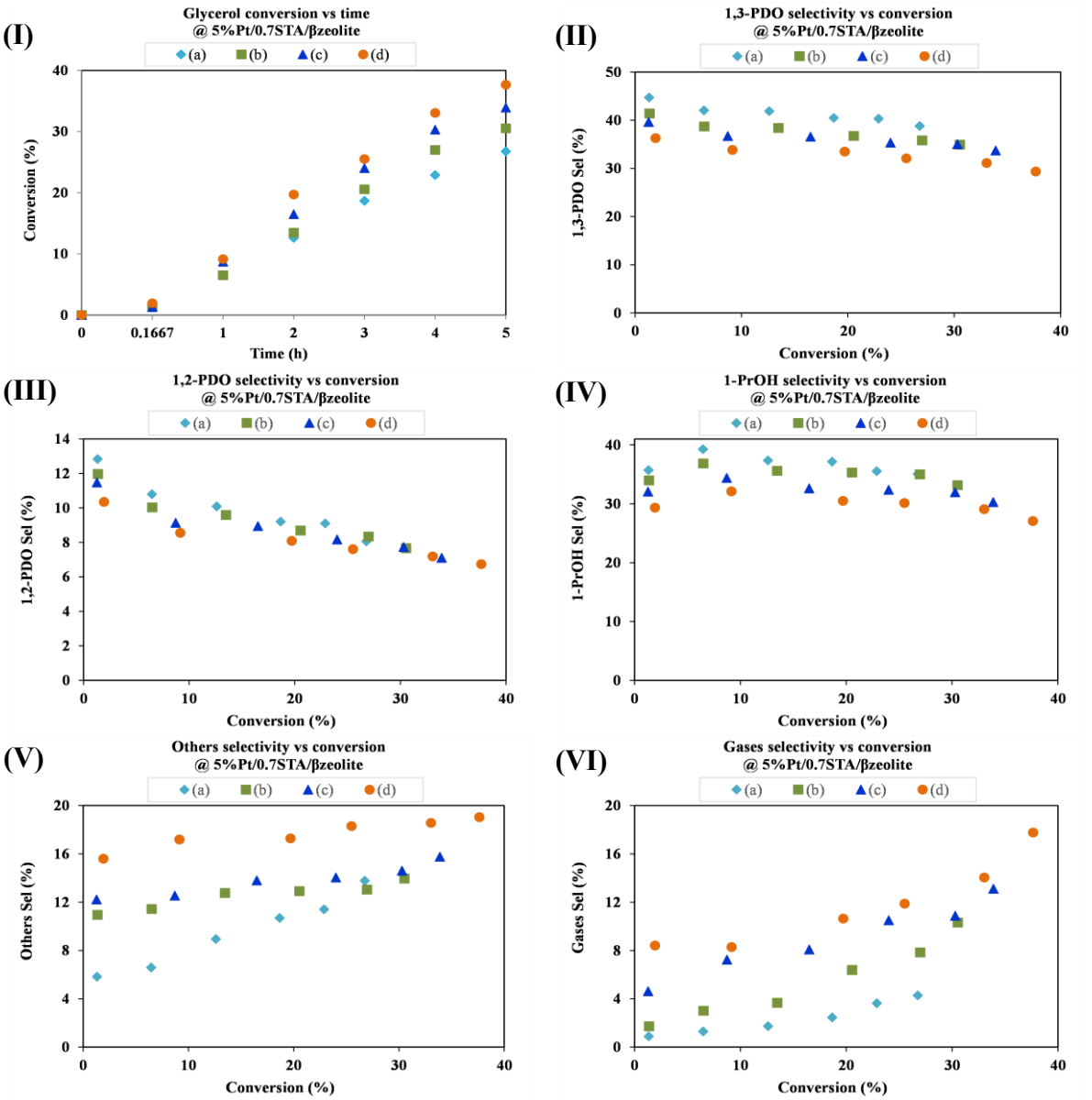

Figure 6.10. Effect of initial glycerol concentration on: (I) glycerol conversion, (II) 1,3-PDO selectivity, (III) 1,2-PDO selectivity, (IV) 1-PrOH selectivity, (V) others selectivity, (VI) gaseous products selectivity vs. time/conversion over Pt-0.7STA/β-zeolite. Here, (a) – 5 wt% glycerol, (b) – 10 wt% glycerol, (c) – 20 wt% glycerol, (d) – 30 wt% glycerol.

The selectivity of 1,2-PDO after 5 h of reaction over Pt-0.3STA/β-zeolite catalyst was 10.37% at 5 wt% glycerol concentration, which was 9.76% at 10 wt% concentration, 9.03% at 20 wt% concentration, and 7.86% at 30 wt% glycerol concentration (See Figure 6.9 (III)). While 1,2-PDO selectivity over Pt-0.7STA/β-zeolite catalyst was 8.07% at 5 wt% glycerol concentration, 7.66% at 10 wt% concentration, 7.11% at 20 wt% concentration, and 6.74% at 30 wt% concentration (See Figure 6.10 (III)).

The selectivity of 1-PrOH after 5 h over Pt-0.3STA/β-zeolite catalyst was 37.13% at 5 wt% glycerol concentration, which was slightly increased to 37.84% at 10 wt% glycerol concentration and then decreased to 35.96% at 20 wt% concentration and finally to 33.05% (5 h) at 30 wt% concentration (See Figure 6.9 (IV)). The selectivity of 1-PrOH over Pt-0.7STA/β-zeolite catalyst was 35.07% at 5 wt% glycerol concentration, 33.15% at 10 wt% glycerol concentration, 30.29% at 20 wt% concentration and 27.08% at 30 wt% concentration (See Figure 6.10 (IV)).

The selectivity of other liquid products (others) was increased continuously with an increase in glycerol concentration. After 5 h of reaction over Pt-0.3STA/β-zeolite catalyst, the selectivity of others was 15.47% at 5 wt% glycerol concentration, 17.39% at 10 wt% concentration, 20.70% at 20 wt% concentration and 22.99% at 30 wt% concentration (See Figure 6.9 (V)). The selectivity of others over Pt-0.7STA/β-zeolite catalyst was 13.77% at 5 wt% glycerol concentration, 13.95% at 10 wt% concentration 15.76% at 20 wt% concentration, and 19.04% at 30 wt% concentration (See Figure 6.10 (V)). Similar trends were observed in the selectivity of gaseous products. It was also increased with an increase in glycerol concentration over both the catalysts. After 5 h of reaction over Pt-0.3STA/β-zeolite catalyst, the selectivity of gaseous products was 5.99% at 5 wt% glycerol concentration, 9.53% at 10 wt% concentration, 10.44% at 20 wt% concentration and lastly 14.22% at 30 wt% concentration (See Figure 6.9 (VI)). The selectivity of gaseous products over Pt-0.7STA/β-zeolite catalyst was 4.28% at 5 wt% glycerol concentration. It was 10.31% at 10 wt% concentration, 13.11% at 20 wt% concentration, and lastly 17.77% at 30 wt% concentration (See Figure 6.10 (VI)).

The decrease in the selectivity of propanediols and increase in the selectivities of other products was attributed to the over hydrogenolysis of propanediols. Nearly similar results for glycerol hydrogenolysis at higher concentrations were reported in the literature over the Pt/WOx/Al_2O_3 catalyst [113]. Amada et al. [63] have reported that the glycerol conversion over Ir–ReO_x/SiO_2 catalyst has increased with an increase in glycerol concentration up to 20%, and it became

saturated after 20% glycerol concentration. However, their results show an increase in glycerol conversion at 67% concentration.

6.3.6 Glycerol hydrogenolysis products after 16 h of reaction

The products of glycerol hydrogenolysis over different catalysts after 16 h of reaction are reported in Table 6.3. Here, the catalyst Pt-0.7STA/β-zeolite (highlighted in Table 6.3) has shown the highest 1,3-PDO selectivity followed by Pt-0.3STA/β-zeolite among all the catalysts even after 16 h of reaction. The larger times of reaction increase the over-hydrogenolysis of propanediols. However, the higher stability of 1,3-PDO compared to 1,2-PDO makes the 1,3-PDO hydrogenolysis difficult, and therefore its selectivity was higher than 1,2-PDO. The over-hydrogenolysis products mainly include 1-PrOH, others, and gaseous products.

Table 6.3. Glycerol conversion and product selectivities after 16 h of reaction

Catalyst	Glycerol conversion (%)	Selectivity				
		1,3-PDO (%)	1,2-PDO (%)	1-PrOH (%)	Others (%)	gaseous (%)
Pt/β-Zeolite	28.86	2.68	27.10	32.57	17.11	20.53
Pt/0.07STA/β-Zeolite	43.05	15.25	10.60	38.59	16.93	18.62
Pt/0.1STA/β-Zeolite	48.76	17.53	6.58	42.15	13.02	20.72
Pt/0.2STA/β-Zeolite	57.96	18.49	5.94	37.67	15.96	21.94
Pt/0.3STA/β-Zeolite	60.01	25.72	6.51	35.81	14.30	17.66
Pt/0.4STA/β-Zeolite	64.94	16.35	6.53	35.22	19.52	22.38
Pt/0.5STA/β-Zeolite	65.20	12.70	4.67	39.07	17.58	25.98
Pt/0.6STA/β-Zeolite	64.73	17.28	7.29	36.24	18.97	20.22
Pt/0.7STA/β-Zeolite	63.50	31.07	4.62	34.73	16.20	13.38
Pt/0.8STA/β-Zeolite	49.89	20.87	6.58	38.26	17.28	17.01
Pt/1.0STA/β-Zeolite	46.18	12.32	5.47	41.53	14.23	26.45

6.4 Conclusion

The parametric study on glycerol hydrogenolysis over Pt-0.3STA/β-zeolite and Pt-0.7STA/β-zeolite catalysts revealed that a temperature higher than 220 ^{o}C leads to the degradation products to more than 60%. Low hydrogen pressures (10 bar H_2) favor the formation of 1,2-PDO, while higher pressure (40 bar H_2) favors the formation of 1,3-PDO. The optimum platinum loading in a catalyst comes out to be 5 wt%, lower Pt amount increases 1,2-PDO formation, and higher Pt amount increases 1,3-PDO over-hydrogenolysis. Similar results were observed over catalyst loading. The 2.5 wt% of catalyst loading in a 5 wt% glycerol solution or 0.5 catalysts to glycerol ratio was found to be optimum. The glycerol concentration higher than 5 wt% increases the formation of degradation products and reduces the selectivity of 1,3-PDO. The reaction time higher than 5 h also increases the formation of degradation products like others and gases.

This study concludes that the best catalyst is 5%Pt-0.7STA/β-zeolite, and the best reaction conditions are 200 ^{o}C, 50 bar H_2, and 5 h reaction time, which offers 30.4% glycerol conversion, 44% 1,3-PDO selectivity, 7.9 % 1,2-PDO selectivity, and 28% 1-PrOH selectivity. The other good catalyst is 5%Pt-0.3STA/β-zeolite, and the best reaction conditions for this catalyst are 200 ^{o}C, 50 bar H_2, and 5 h reaction time which offers 27.8% glycerol conversion, 35% 1,3-PDO selectivity, 10.1% 1,2-PDO selectivity, and 33.4% 1-PrOH selectivity.

Chapter 7: KINETIC MODELING

7.1 Introduction

Studies related to the kinetics of glycerol hydrogenolysis over heterogeneous catalysts seem to be limited in the literature, though this reaction has gained research interest in the past 20 years. The first kinetic analysis on glycerol hydrogenolysis was published by Lahr and Shanks in 2003 [202]. The same authors published another study in 2005; a kinetic model was developed to study the effect of sulfur and temperature on hydrogenolysis of glycerol to glycols *viz.* propylene glycol (1,2-PDO) and ethylene glycol [203]. Lahr and Shanks developed a Langmuir–Hinshelwood-type model on a commercial Ru/C catalyst in both the articles. They Described the reaction steps and showed the significance of competitive adsorption occurring between the 1,2-PDO, ethylene glycol, and glycerol on the Ru/C surface. However, this model does not include all the reactions.

Xi et al. [204] proposed a kinetic model for glycerol conversion over Co–Pd–Re/C catalyst. The proposed mechanism was based on dehydrogenation–dehydration–hydrogenation in a trickle-bed reactor. However, the estimated kinetic parameters from this study seem unreliable due to mass and heat transfer limitations [205]. Zhou et al. [206] reported glycerol hydrogenolysis kinetics in a tubular fixed-bed reactor over a Cu–ZnO–Al_2O_3 catalyst. The authors proposed a Langmuir–Hinshelwood kinetic model based on a two-step dehydration–hydrogenation mechanism that considers the competitive adsorption 1,2-PDO acetol and glycerol. Torres et al. [207] studied the kinetics of glycerol hydrogenolysis in a batch reactor over a bimetallic Ru–Re/C catalyst. The authors considered a complex reaction network of liquid and gas products formed, as in the presence of this catalyst, the maximum selectivity of the desired 1,2-PDO is limited to 36.6%.

Literature also reports a few other kinetic models for glycerol hydrogenolysis [208–211]. However, none of them includes all the reactions. They essentially talk about glycerol hydrogenolysis to 1,2-PDO and ethylene glycol. The glycerol hydrogenolysis to lactic acid was also reported [212]. However, the kinetic model on the conversion of glycerol to 1,3-PDO and its further transformation to 1-PrOH is least talked about. According to our knowledge, we have only come across two studies in which conversion of glycerol to 1,3-PDO has been

incorporated. Rajkhowa et al. [213] studied the kinetics of liquid-phase glycerol hydrogenolysis over a stable, commercial Cu-based catalyst in a fixed bed tubular reactor. They have developed a comprehensive kinetic model considering the formation of main products and the side products over supported Cu catalyst. As Cu is non-noble metal, it is less selective towards the formation of 1,3-PDO. The amount of 1,3-PDO in this study was significantly less, and therefore, the focus of this study was mainly on 1,2-PDO. Moreover, the authors have not incorporated the formation of 1-PrOH from 1,3-PDO in their model. Vasiliadou and Lemonidou [4] authored the other study, which included the formation of 1,3-PDO from glycerol. The authors considered a dehydration–hydrogenation type reaction mechanism for aqueous-phase glycerol hydrogenolysis over Cu/SiO_2 catalyst. Here, though the catalyst was 95% selective towards the 1,2-PDO, the authors have developed the model considering 1,3-PDO as one of the key products. The authors proposed a simple power-law model for the formation of propanediols from glycerol. However, no other reactions were included in this model; only the conversion of glycerol to propanediols is explored.

To the best of our knowledge, a kinetic model for glycerol hydrogenolysis over a catalyst containing a noble metal like Pt is not available in the literature. Moreover, most of the models focus on converting glycerol to 1,2-PDO and do not consider the formation of other products. A kinetic model considering the key products such as 1,3-PDO, 1,2-PDO, and 1-PrOH is missing in the literature. Therefore, in the present work, we attempt to investigate glycerol hydrogenolysis kinetics in the liquid phase in the presence of a Pt-0.3STA/β-zeolite catalyst. The model is working well for both the catalysts Pt-0.3STA/β-zeolite and Pt-0.7STA/β-zeolite. In this report, we are presenting work on the Pt-0.3STA/β-zeolite catalyst.

Based on our findings, we have already proposed a possible reaction mechanism in Chapter 5. Based on this reaction mechanism, we model the kinetic pathways and estimate the parameters in the present chapter. The kinetic model We have developed in this work considers all of the reactions occurring during glycerol hydrogenolysis over Pt-0.3STA/β-zeolite catalyst.

Before the kinetic analysis, all the possible mass and heat transfer limitations were considered so as to eliminate the influence of transport phenomena.

7.2 Kinetic modeling

Reliable quantitative kinetic data in a 3 phase (gas, liquid, and solid) system like glycerol hydrogenolysis is only possible if the absence of mass and heat transfer limitations is ensured. These limitations comprise external and internal mass transfer of H_2 from the gas to liquid and then to the catalyst active sites. In this process, H_2 gas has to diffuse through the gas phase to the gas-liquid interphase and then to the bulk liquid. Dissolved H_2 and reactant (glycerol or propanediol etc.) from the bulk liquid transfer to the external catalyst surface through the solid-liquid diffusion film and then through the pores to the active sites where the reaction takes place. Additionally, Heat transfer limitations may also be present in this type of system. However, we have conducted the reaction isothermally, ensuring the absence of heat transfer limitations. In the case of glycerol hydrogenolysis, though the reaction is exothermic (ΔH_{rxn} = –103 kJ/mol), the heat transfer limitations are unlikely because of the small particle size of the catalysts.

7.2.1 Validation of absence mass transport limitations

The absence of external mass transfer limitations (H_2 transfer to the bulk liquid and reactant transport to catalyst surface) is typically ensured by optimizing the stirring speed for a given catalyst loading. It should be noted that the gas phase mass transfer resistance can be neglected as the gas phase largely consist of H_2 (owing to the low vapor pressure of the solution and low concentration of gas products). Hence, the gas-liquid interface is instantly saturated with H_2. In this study, the stirring speed of the reaction was chosen as 800 rpm based on the experimental data. The reaction tests with agitation speed between 500 and 1000 rpm showed no significant changes in the initial reaction rate (see Figure A.4 in Appendix-A). Lahr and Shanks [203] reported that above 500 rpm, there was no change in the glycerol hydrogenolysis catalytic performance over Ru-based catalysts. While Hichri et al. [214] showed that an increase in the stirring speed beyond 800 rpm did not affect the reaction rate during the liquid phase hydrogenation of o-cresol over Ni/SiO_2 catalyst. Based on the above, it can be ensured that the influence of external diffusion resistances can be neglected. Also, the variation of the catalyst to glycerol ratio (Figure 7.1) between 0.25 to 0.75 clearly shows a linear relation with the reaction rate proving the absence of external mass transfer limitations.

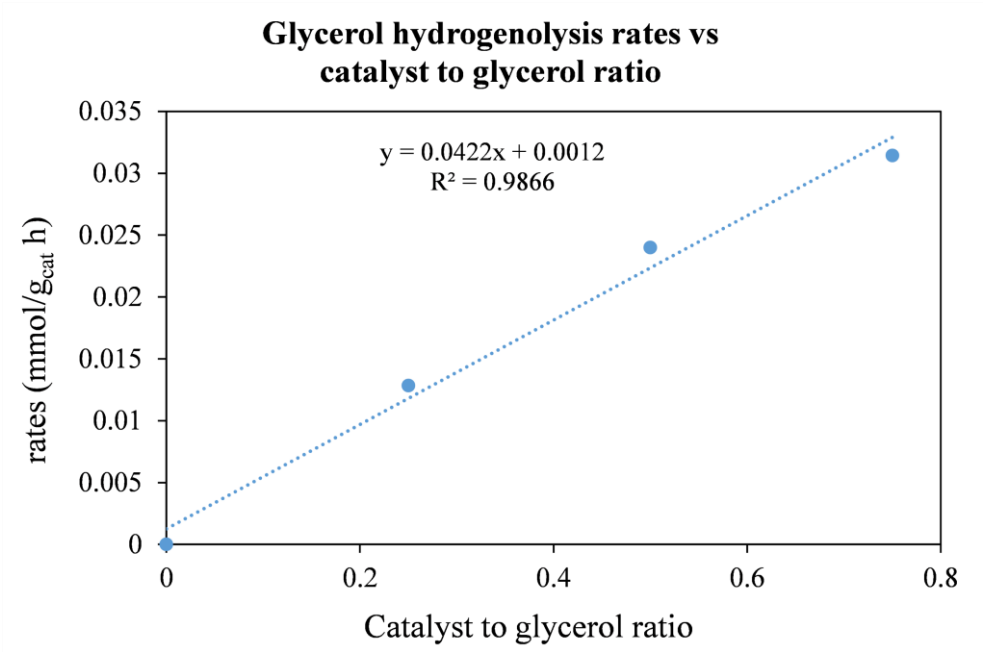

Figure 7.1. Effect of catalyst to glycerol ratio on the initial rate of glycerol hydrogenolysis, T = 220 °C, 40 bar H_2.

Regarding the internal particle diffusion, the catalyst is in powder form (typically less than 50 μm) in this study which generally ensures insignificant internal diffusion resistance, based on the cited studies [215,216]. Moreover, the estimated value of Weisz–Prater criterion for our system was $C_{WP} << 1$ (see Appendix-A), this confirms that there are no diffusion limitations. Consequently, no concentration gradient exists within the pellet.

It should be noted that the pore size distribution of the Pt-0.3STA/β-zeolite catalyst follows a monomodal pattern (see Figure 4.1 (III)), thus ensuring the absence of a rate change that can be present if a bimodal distribution exists [217].

Based on the kinetic experiments and reaction mechanism reported in Chapter 5, the kinetic pathway shown in Figure 7.2 is proposed for glycerol hydrogenolysis to various products.

From the experimental observation, it was found that 1-PrOH formation occurs from the very early stages of the reaction, which suggests the presence of a direct route for the synthesis of 1-PrOH from glycerol apart from PDOs hydrogenolysis. The possible route through which 1-PrOH forms directly from glycerol is dehydration to acrolein, followed by hydrogenation to 1-PrOH. Further, from the critical analysis of the experimental data (Chapter 5 and 6), we found that at any given time, the selectivity of acrolein (selectivity of 3 to 4% at any conversion in "lumped in others") was very less compared to the selectivity of 1-PrOH 40 to 50%.

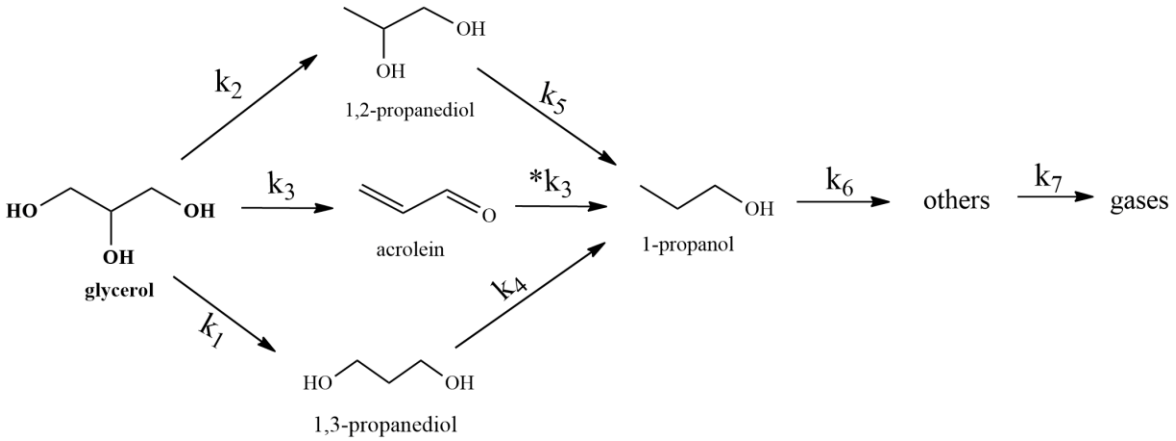

Figure 7.2. Proposed kinetic pathways of glycerol hydrogenolysis for kinetic modeling

This indicates that 1-PrOH may form via acrolein in a fast step. Literature also reports high acrolein hydrogenation rates over Pt-WO_3 catalytic system [218]. From the reported results and our observed results, we estimate that the difference in TOFs of glycerol hydrogenolysis and acrolein hydrogenation to be between 300 to 1000 times. Hence, we believe that, as soon as acrolein forms, it converts to 1-PrOH in the prevailing conditions.

In the case of 1-PrOH formation from glycerol via acrolein, the dehydration step seems more rate-controlling than the hydrogenation step, i.e., $*k_3 >> k_3$. Therefore, we have combined the dehydration of glycerol to acrolein and its hydrogenation to 1-PrOH steps in the conversion of glycerol to 1-PrOH step (see Figure 7.3) and considered the latter as a rate-controlling step in the kinetic model.

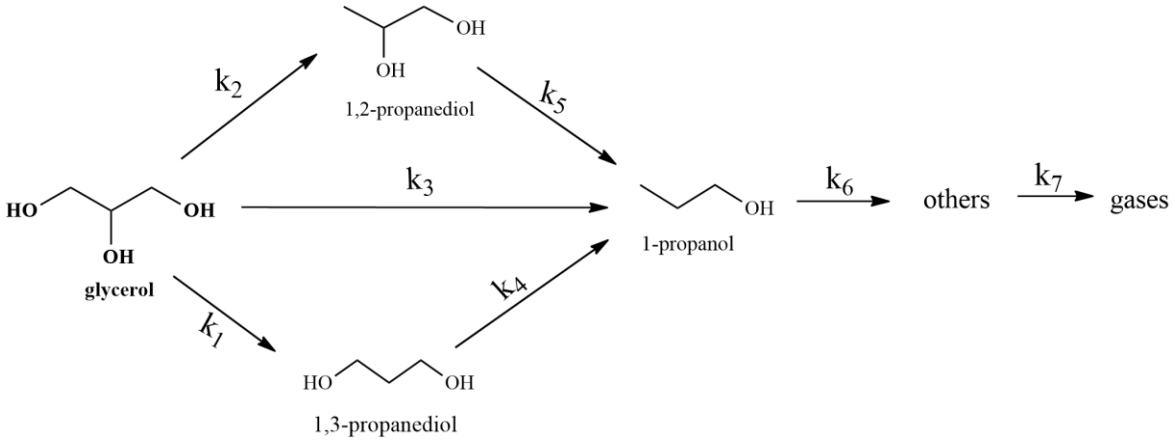

Figure 7.3. Updated kinetic pathways of glycerol hydrogenolysis for kinetic modeling

Based on the updated kinetic pathways (Figure 7.3), the model equations were written assuming 1st order kinetics for all reaction steps since the hydrogen partial pressure is constant through the run. It is expected that the parameters will have a dependence on hydrogen pressure.

7.2.2 Kinetic equations

The reactions are:

$C_3H_8O_3 + H_2 \longrightarrow C_3H_8O_2 + H_2O$ Rxn-1

$\boldsymbol{C_{gly}}$ $\boldsymbol{C_{1,3-PDO}}$

$C_3H_8O_3 + H_2 \longrightarrow C_3H_8O_2 + H_2O$ Rxn-2

$\boldsymbol{C_{gly}}$ $\boldsymbol{C_{1,2-PDO}}$

$C_3H_8O_3 + 2H_2 \longrightarrow C_3H_8O + 2H_2O$ Rxn-3

$\boldsymbol{C_{gly}}$ $\boldsymbol{C_{1-PrOH}}$

$C_3H_8O_2 + H_2 \longrightarrow C_3H_8O + H_2O$ Rxn-4

$\boldsymbol{C_{1,3-PDO}}$ $\boldsymbol{C_{1-PrOH}}$

$C_3H_8O_2 + H_2 \longrightarrow C_3H_8O + H_2O$ Rxn-5

$\boldsymbol{C_{1,2-PDO}}$ $\boldsymbol{C_{1-PrOH}}$

$C_3H_8O + H_2 \longrightarrow others + H_2O$ Rxn-6

$\boldsymbol{C_{1-PrOH}}$ $\boldsymbol{C_{others}}$

$others + H_2 \longrightarrow \text{gases} + H_2O$ Rxn-7

$\boldsymbol{C_{others}}$ $\boldsymbol{C_{gases}}$

The model equations for batch reaction studies under isothermal conditions and constant partial pressure of H_2 are written as follows:

$$\frac{dC_{gly}}{dt} = r_{glycerol} = -k_1C_{gly} - k_2C_{gly} - k_3C_{gly} \qquad \textbf{Eq 7.1}$$

$$\frac{dC_{1,3-PDO}}{dt} = r_{1,3-PDO} = k_1 C_{gly} - k_4 C_{1,3-PDO} \quad \textbf{Eq 7.2}$$

$$\frac{dC_{1,2-PDO}}{dt} = r_{1,2-PDO} = k_2 C_{gly} - k_5 C_{1,2-PDO} \quad \textbf{Eq 7.3}$$

$$\frac{dC_{1-PrOH}}{dt} = r_{1-PrOH} = k_4 C_{1,3-PDO} + k_5 C_{1,2-PDO} + k_3 C_{gly} - k_6 C_{1-PrOH} \quad \textbf{Eq 7.4}$$

$$\frac{dC_{others}}{dt} = r_{others} = k_6 C_{1-PrOH} - k_7 C_{others} \quad \textbf{Eq 7.5}$$

$$\frac{dC_{gases}}{dt} = r_{gases} = k_7 C_{others} \quad \textbf{Eq 7.6}$$

7.2.3 Methodology of parameter estimation

As already mentioned in chapter 5 and 6, the selectivities of all the liquid products were measured using GC analysis, while the selectivity of gases was estimated using mass/carbon balance.

The differential equations were simultaneously solved for the given initial conditions to obtain the concentration profiles with time using MATLAB *ode45*. The calculated concentration profiles as functions of time were then compared with the experimental data. The best-fit kinetic parameters were determined by a minimization of the weighted sum of squares of relative error, defined as:

$$Error = \sum \left(\frac{Y_{EXP,ij} - Y_{EST,ij}}{Y_{EXP,ij}} \right)^2 \quad \textbf{Eq 7.7}$$

using the non-linear fitting subroutine *lsqnonlin* in MATLAB. Here, $Y_{EXP,ij}$ is the concentration of the component j in the i^{th} experimental point, $Y_{EST,ij}$ is the corresponding concentration as

estimated by the model. We have also used *nlparci* subroutine in MATLAB to determine the confidence interval (CI) at 95% confidence in rate constants (k_i).

Based on the model equations and methodology discussed above, we shall discuss the effect of reaction conditions (temperature and hydrogen pressure) on the estimated kinetic rate parameters in the subsequent subsections.

7.3 Results and Discussion

7.3.1 Effect of hydrogen pressure on kinetic parameters

The effect of hydrogen pressure on glycerol hydrogenolysis over a Pt-0.3STA/β-zeolite catalyst is already studied experimentally, and the data is given in chapter 6 (see section 6.2.2). Here, estimation of reaction parameters was carried out using the same experimental data.

This section discusses the effect of hydrogen pressure on product yield and conversion rates. Therefore, maintaining the other operating conditions (temperature, catalyst loading, reaction time, etc.) constant. Here, an attempt is made to estimate the kinetic model parameters for each reaction carried at different hydrogen pressure, *viz.* 10, 40 & 50 bar. The model parameters are calculated using the methodology described in section 7.2.3.

It must be noted that the concentration of gases ($\mathbf{C_{gases}}$) was calculated from the carbon balance of the experimental data. Theoretically, it was calculated by solving the differential equation with the known rate parameters. Moreover, all the reactions were considered first order with respect to the substrate concentration.

Initially, parameter estimation was carried out using guess values for all the unknown parameters of ki (k_1 to k_7). After optimization, we got the values of "k" (see Table 7.1) for all three pressures. The program was written such that the evaluated parameter set of each run can be used as the initial guess for new runs and estimations. Further, different sets of initial values were tried, and based on the value of the objective function at the minimum, the final values of rate constants for each reaction were chosen. The observed results are tabulated in Table 7.1.

Table 7.1 Values of rate constant after solving and optimizing the kinetic model at three different hydrogen pressures

Rate constants (min^{-1})	Pressure (bar)		
	10	**40**	**50**
k_1	1.10E-04	3.62E-04	4.78E-04
k_2	2.23E-04	1.63E-04	1.68E-04
k_3	3.12E-04	4.61E-04	4.74E-04
k_4	1.04E-03	1.16E-03	1.34E-03
k_5	1.87E-03	3.00E-03	3.25E-03
k_6	3.45E-03	3.53E-03	4.09E-03
k_7	3.23E-03	3.82E-03	4.86E-03

It is observed that the rate parameters (ki) for all reactions (i.e., glycerol to 1,3-PDO, glycerol to 1-PrOH, 1,3-PDO to 1-PrOH, 1,2-PDO to 1-PrOH, 1-PrOH to others, and others to gases formation) increased with an increase in hydrogen pressure except for glycerol to 1,2-PDO. The simulated results showed good agreement with experimental results (see Figure 7.4).

Figure 7.4 (I) to (IV) shows the concentration versus time plot for predicted/simulated and experimental values for glycerol concentration and its hydrogenolysis products. Figure 7.4 shows the excellent agreement between experimental and simulated data. The results show that the concentration of 1,3-PDO (key product) increased with an increase in pressure.

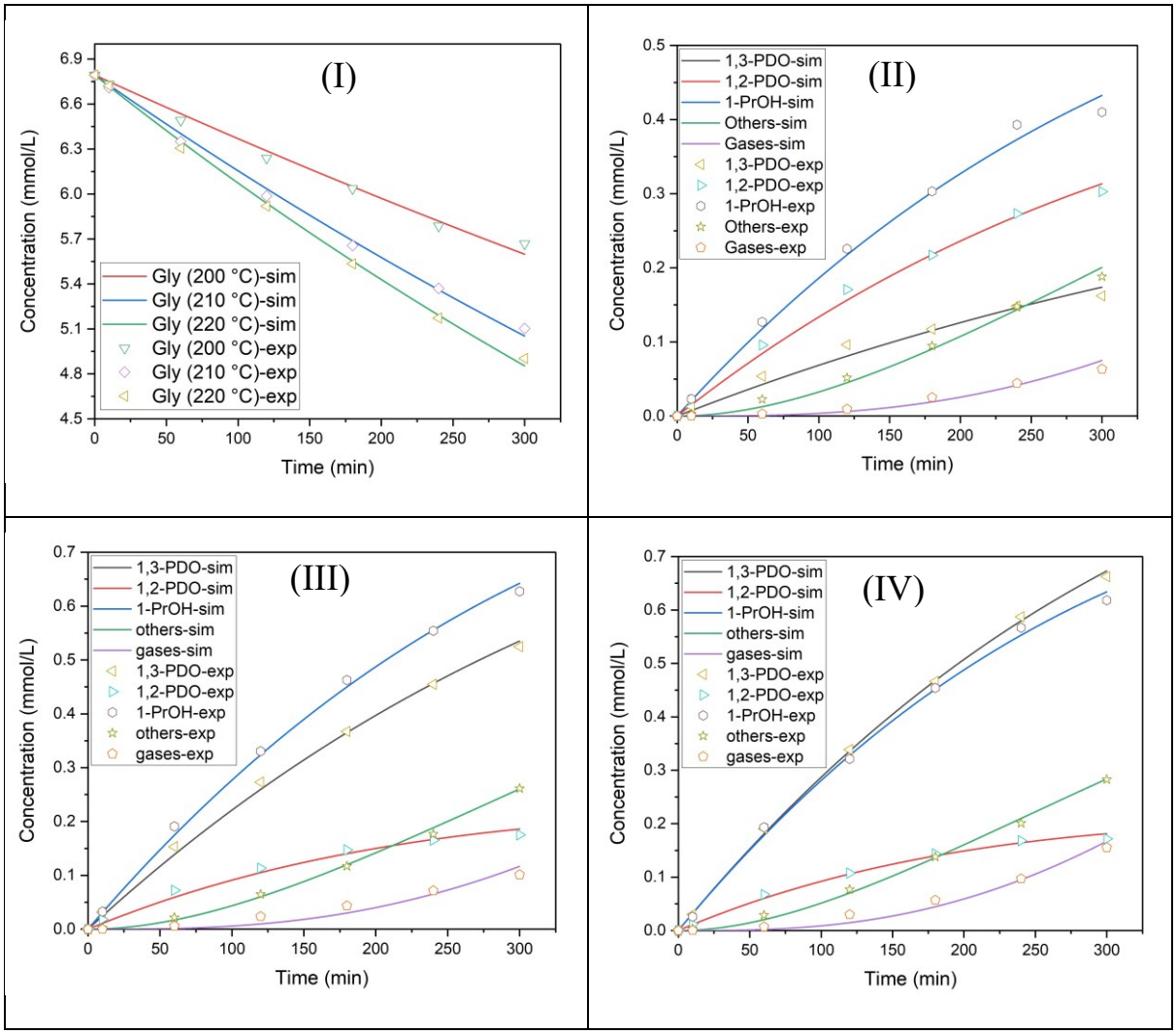

Figure 7.4. Concentration versus time (C/t) profiles for (I) glycerol at different pressures, (II) products at 10 bar, (III) products at 40 bar, (IV) products at 50 bar. Here, experimental data are shown by markers (dot) & simulated data are shown by lines. Reaction conditions: 80 mL of a 5 wt% glycerol solution, 2 g Pt-0.3STA/β-zeolite catalyst, reaction temperature = 220 °C, 5 h of reaction time, stirring speed = 800 RPM.

The increase in pressure increased the glycerol hydrogenolysis rates. At the same time, the conversion of glycerol to 1,3-PDO (k_1) increased continuously with an increase in pressure. In contrast, 1,2-PDO (k_2) formation decreased with an increase in pressure from 10 to 40 bar but slightly increased with further pressure. It was reported that glycerol hydrogenolysis, 1,3-PDO formation increases with an increase in pressure. However, the formation of acetol reduces with an increase in pressure but its rate of hydrogenation increases with an increase in pressure [205]. Therefore, a small rise in the 1,2-PDO formation rate (k_2) was observed between 40 to 50 bar pressures. The overall formation rate of 1-PrOH i.e., $k_3 + k_4 + k_5$ (via glycerol (k_3), 1,3-PDO (k_4) or 1,2-PDO (k_5)) increases with increase in pressure. The formation of others (k_6) and gases (k_7) also increased with an increase in pressure.

The confidence interval (CI) values for rate parameters with 95% confidence at different pressures were also estimated. The values for 40 bar were given in Table 7.3 as values at 220 ^{o}C (as most of the reactions were conducted at this temperature); CI values (lower bound and upper bound) for other pressure are given in the appendix (Table A.4 and A.5 in Appendix-A).

The correlation coefficients (R^2) values for each component at different hydrogen pressures and the different reaction temperature is tabulated in Table 7.2.

Here, the correlation coefficients (R^2) values for all the components at different hydrogen pressures showed values higher than 0.98 except for gases that show a low value as 0.93. As the gases are determined from carbon balance, small discrepancies in experimental and predicted data are anticipated.

Table 7.2. Correlation coefficients (R^2) values for all the components fitted using optimized model parameters for reaction under three different hydrogen pressures.

R^2 values	10 bar	40 bar	50 bar
Glycerol (Gly)	0.99	0.99	0.99
1,3-propanediol (1,3-PDO)	0.98	0.99	0.99
1,2-propanediol (1,2-PDO)	0.99	0.98	0.99
1-propanol (1-PrOH)	0.99	0.99	0.99
others	0.99	0.99	0.99
gases	0.95	0.93	0.97

All other components showed a good correlation between simulated values and experimental values.

7.3.2 Arrhenius dependence study

The effect of temperature on glycerol hydrogenolysis over a Pt-0.3STA/β-zeolite catalyst is already reported in chapter 6 (see section 6.2.1). Here, estimation of reaction parameters was carried out using the same experimental data.

This study aims to estimate the activation energy of the reactions using Arrhenius temperature dependence. Therefore, maintaining the other operating conditions (H_2 pressure, catalyst loading, reaction time, etc.) constant. The reactions were conducted at three different

temperatures *viz.* 200, 210 and 220 ºC (i.e., 473, 483 and 493 K). The rate parameters for each set of data were estimated according to the methodology given in section 7.2.3.

Even for this case, the evaluated parameter set of each run was used as the initial guess for new runs and estimations. Further, various sets of initial values were tried and based on the value of the objective function at the minimum, the final values of rate constants for each reaction were chosen. Based on the obtained values of rate constants at different temperatures from the regression of the kinetic model, the temperature dependence of each rate constant (in accordance with the Arrhenius equation) was determined by plotting the ln (ki) vs. 1/T.

$$k = k_0 \times exp\left(\frac{-E}{RT}\right) \qquad \textbf{Eq 7.8}$$

E is the activation energy of reactions, k is the rate constant at temperature T, and k_0 is the pre-exponential factor.

Table 7.3. Values of rate constant after solving and optimizing the kinetic model at three different temperatures.

Rate constants (min^{-1})	**Temperature ˚C**			**Δk values with 95% confidence interval**
	200	**210**	**220**	**k ± Δk @ 220 ºC**
k_1	1.86E-04	2.71E-04	3.62E-04	3.62E-04 ± 4.17E-05
k_2	9.32E-05	1.32E-04	1.63E-04	1.63E-04 ± 5.59E-05
k_3	1.78E-04	3.00E-04	4.61E-04	4.61E-04 ± 5.84E-05
k_4	1.17E-03	1.12E-03	1.16E-03	1.16E-03 ± 9.71E-04
k_5	2.32E-03	2.55E-03	3.00E-03	3.00E-03 ± 2.91E-03
k_6	3.31E-03	3.42E-03	3.53E-03	3.53E-03 ± 3.15E-04
k_7	3.56E-03	3.67E-03	3.82E-03	3.82E-03 ± 9.77E-04

Initially, all the unknown parameters were estimated using guess values for ki (k_1 to k_7). After optimization, we got the values of "k" (see Table 7.3) for all the three temperatures which were used in activation energy estimations. The values of 95 % confidence intervals in rate constants are reported for temperature 220 °C, as most of the reactions were conducted at this temperature. The values for Δk (variation in rate constants) are reported in Table 7.3). The confidence intervals on the parameters seem satisfactory for all of the rate constants except for k_5, where the estimated lower bound value was negative (see Table A.3 in Appendix-A). This was therefore set to zero and the value for Δk was estimated.

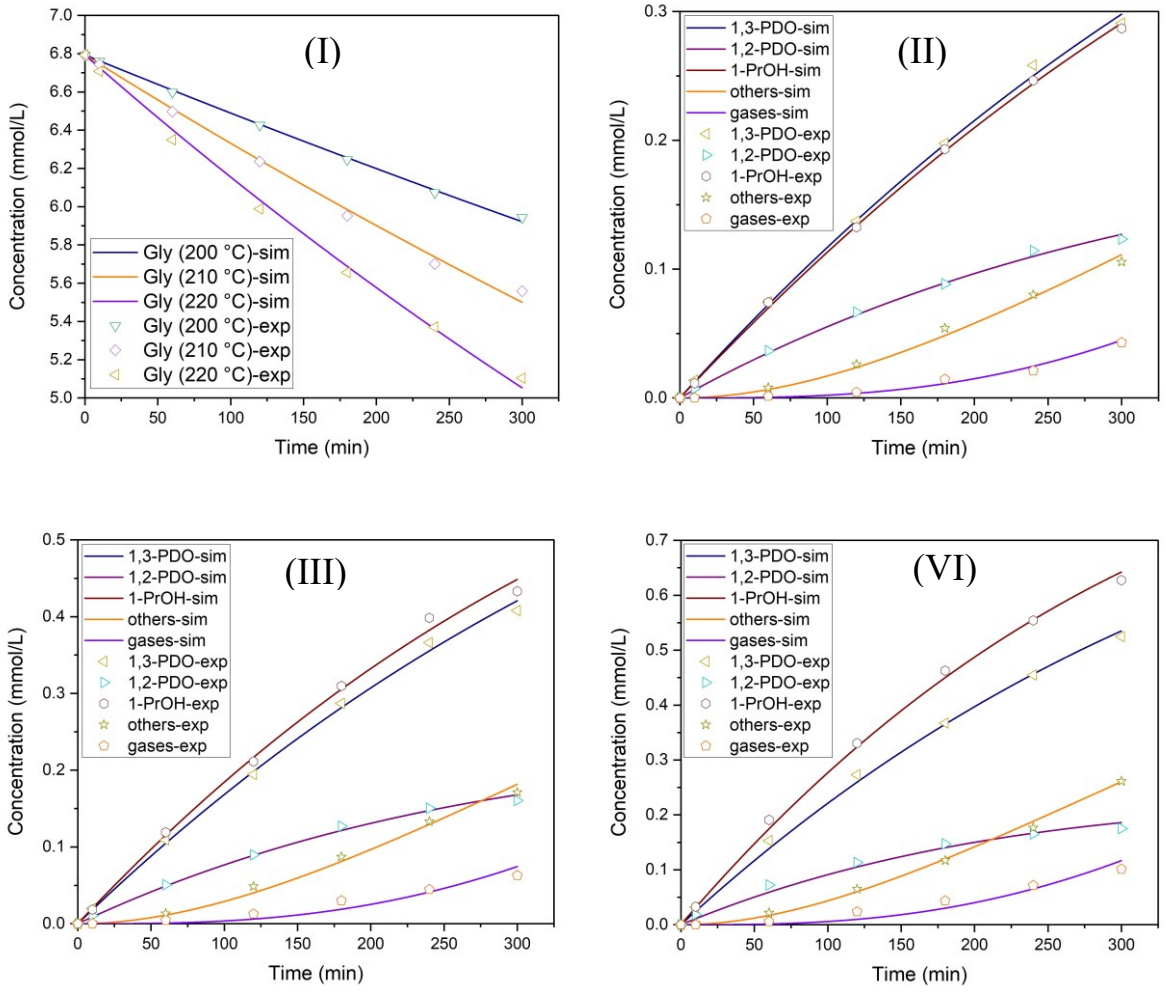

Figure 7.5. Concentration versus time (C/t) profiles for (I) glycerol at different temperatures, (II) products at 200 °C, (III) products at 210 °C, (IV) products at 220 °C. Here, experimental data are shown by markers (dot) & simulated data are shown by lines. Reaction conditions: 80 mL of a 5 wt% glycerol solution, 2 g Pt-0.3STA/β-zeolite catalyst, H_2 pressure = 40 bar, 5 h of reaction time, stirring speed = 800 RPM.

Based on the estimated kinetic parameters after the optimization process, as discussed in the methodology section for each set of temperature (200, 210, and 220 °C), concentration versus time profiles (C/t profile) was generated (see) by solving a differential equation, putting the known parameters. Figure 7.5 (I) to (IV) shows the comparison of C/t profiles for glycerol and products at different temperatures obtained from simulation with the experimentally observed. It is seen that both the results (simulated and experimental) show a good agreement. Though the concentration of gases was estimated from the carbon balance, its estimated values fit well with the simulated values for all the temperatures.

The correlation coefficient (R^2) values for each component at different reaction temperatures estimated from the model are given in Table 7.4.

Table 7.4. Correlation coefficients (R^2) values for all the components fitted using optimized model parameters for reaction under three different temperatures.

R^2 values	200 °C	210 °C	220 °C
Glycerol (Gly)	0.99	0.99	0.99
1,3-propanediol (1,3-PDO)	0.99	0.99	0.99
1,2-propanediol (1,2-PDO)	0.99	0.99	0.98
1-propanol (1-PrOH)	0.99	0.99	0.99
others	0.99	0.99	0.99
gases	0.98	0.91	0.93

The correlation coefficient (R^2) values for all the components showed a similar trend as observed over different pressure. The values of R^2 for all the components are higher than 0.98 except for gases that show a low value as 0.91. However, they all offer a good correlation between predicted values by model and experimental values. In the case of gases, their concentration was estimated by carbon balance. Hence a small amount of error in gaseous product concentrations is expected.

The mechanism of glycerol hydrogenolysis is very complex; here, we have just presented a simplified version of it assuming pseudo-first-order kinetics. Our presented kinetic modeling for Pt-0.3STA/β-zeolite catalyzed reaction shows good agreement of experimental and simulated data.

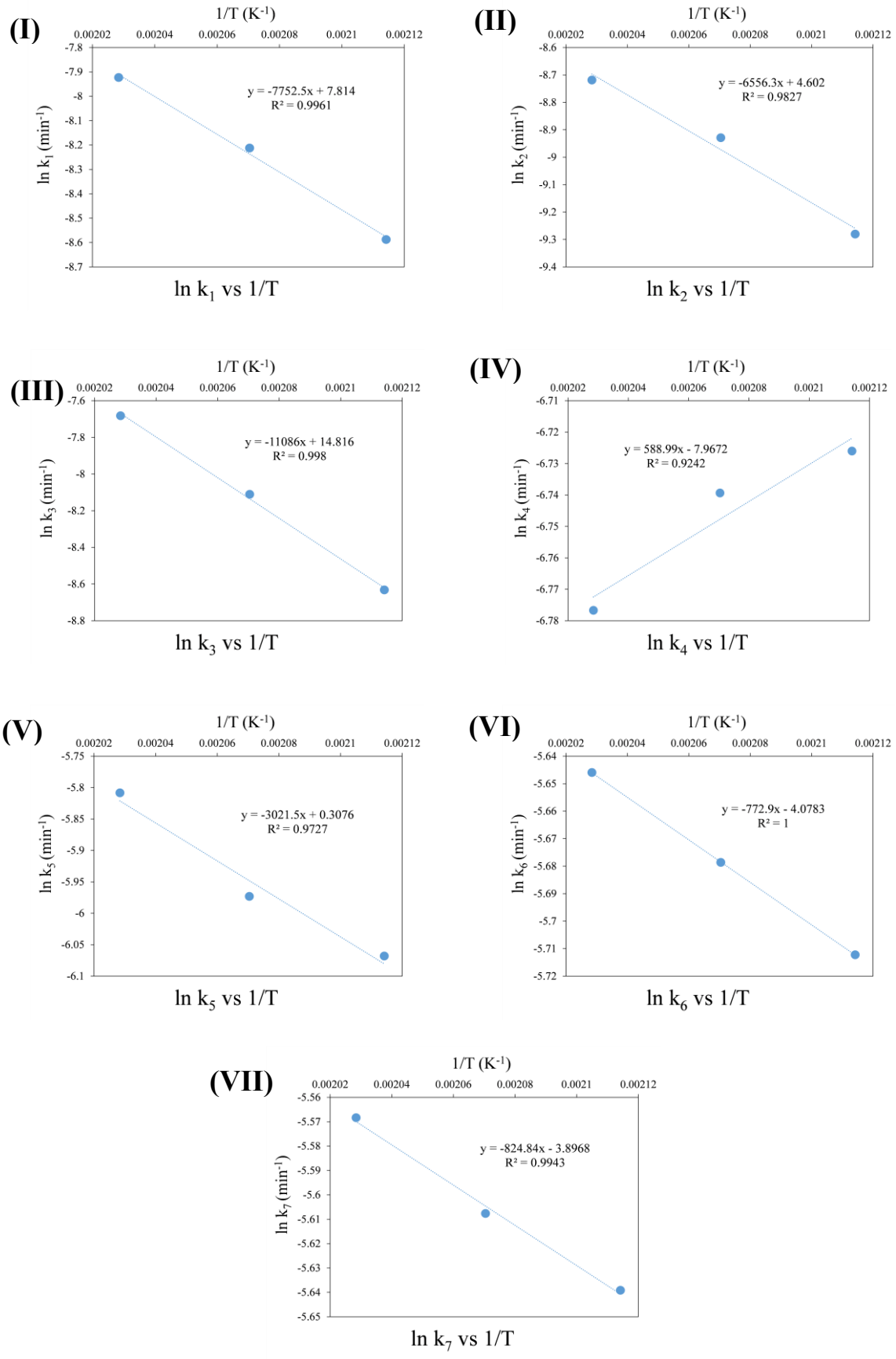

Figure 7.6. Arrhenius plot for rate constants

The Arrhenius plots for rate constants are given in Figure 7.6 (I) to (VII), and the calculated activation energies (E) based on the obtained kinetic parameters at different temperatures are tabulated in Table 7.5.

Table 7.5. Results of parameter estimation (for Pt-0.3STA/β-zeolite catalyzed reaction)

Parameters [k]	Parameters [k_0 (min^{-1})]	Activation energy [E in kJ/mol]	Correlation Coefficient [R^2-value]
k_1(min^{-1})	2475.01	64.45	0.99
k_2 (min^{-1})	99.68	54.51	0.98
k_3 (min^{-1})	272.1×10^4	92.17	0.99
k_4 (min^{-1})	3.47×10^{-4}	negligible	0.93
k_5 (min^{-1})	1.36	25.12	0.97
k_6 (min^{-1})	0.0169	6.43	1
k_7 (min^{-1})	0.0203	6.86	0.99

The primary product of the glycerol hydrogenolysis reaction over Pt-0.3STA/β-zeolite catalyst is 1,3-PDO, 1,2-PDO, and 1-PrOH. The activation energy for the reaction glycerol to 1,3-PDO was 64.45 kJ/mol, whereas it was 54.51 kJ/mol for reaction glycerol to 1,2-PDO. The activation energies of these two parallel reaction routes show the selective formation of the 1,2-PDO at lower temperatures. The results are in agreement with the reported experimental results [205,213]. The activation energy for reaction glycerol to 1-PrOH was 92.17 kJ/mol. The results show that the synthesis of 1,3-PDO requires moderate temperature, while higher temperatures

will increase the formation of 1-PrOH from glycerol. Therefore, at 200 ºC reaction temperature, the selectivity of 1,3-PDO is higher than 1-PrOH (see Figure 7.5 (II)). Whereas reaction temperatures 210 or 220 ºC reduced the selectivity of 1,3-PDO and increased the selectivity of 1-PrOH (see Figure 7.5 (III) & (IV)).

The activation energy for the reaction route 1,3-PDO to 1-PrOH is negligible. In this case, the value of the rate constant is nearly equal. Moreover, variation in k_4 value (manually putting the average value of k_4 in the model equations) in the model doesn't affect the overall fitting of experimental data, indicating that the rate constant k_4 is insensitive to the temperature. The values of activation energies and frequency factors for other reaction routes (k_5 or k_6 or k_7) are small compared to key products (1,3-PDO, 1,2-PDO, and 1-PrOH) activation energies and frequency factors. Therefore, the concentration of others and gases is also small in all cases. On the other hand, the activation energy for 1,3-PDO to 1-PrOH (E_4) is lower than 1,2-PDO to 1-PrOH (E_5). However, experimental evidence revealed that 1,3-PDO is more stable than 1,2-PDO (see section 5.1.5), which means ideally E_4 should have been more than E_5 to make 1,3-PDO more stable. Since we have assumed a simplified model without considering catalyst site reactions (adsorption or desorption), however, by developing a more complex model like the Langmuir Hinshelwood type, these kinds of discrepancies can be removed. This can be a part of future work.

7.4 Conclusions

The kinetics of the zeolite-supported bifunctional (Pt-0.3STA/β-zeolite) catalyzed glycerol hydrogenolysis reaction were studied in this work. Experiments were conducted to determine the dependence of product selectivities on hydrogen pressure and reaction temperature. Experiments show that 1-PrOH formation occurs from the start of the reaction, showing that it forms directly from glycerol via acrolein apart from propanediols. Perhaps, as a result, we observe significant yields of 1-PrOH even at the very early stages of reaction. A simpler form of reaction pathway was proposed from the critical analysis of concentration-time plots of all the products.

Detailed experimentation under kinetically controlled conditions and the effect of operating variables (temperature and hydrogen pressure) showed that the rates of glycerol consumption and product formation are strongly affected by experimental conditions. A kinetic model is

formulated based on the proposed reaction pathways assuming the first-order kinetics for all the products. Comparison of the model predicted data with experimental data shows an excellent agreement supporting that the assumed mechanism for forming all the components via glycerol hydrogenolysis over Pt-0.3STA/β-zeolite catalyst is accurate.

The observed result showed that the glycerol consumption rate is strongly dependent (first-order) on the reaction temperature and hydrogen pressure. The 1,3-PDO formation rates are also showed strong dependence on H_2 pressure (first-order), while higher temperatures seem unfavorable for 1,3-PDO synthesis. Based on the results, optimum pressure values are selected for Arrhenius temperature dependence studies in the kinetic regime. We have obtained the activation energies for all the participating reactions. Furthermore, the influence of other reaction pressure on kinetic parameters is also reported in this study. The favorable conditions for 1,3-PDO synthesis from glycerol seem to be higher pressure (50 bar or higher) and low temperature (200 ^{o}C) from the concentration versus time plot.

Such kind of studies on kinetic analysis and modeling helps the researchers in the field to explore the possibility of tuning the reaction conditions to enhance the selectivity towards the desired product(s).

Chapter 8:
NEW APPROACHES: Conversion of glycerol to 1,3-PDO via protection of terminal hydroxyl groups

8.1 Introduction

From the glycerol hydrogenolysis study in chapters 5, 6, and 7, it is clear that converting glycerol to 1,3-PDO is challenging and leads to many products via hydrogenolysis. This is largely attributed to the reactivity of terminal hydroxyl (–OH) groups of glycerol. They are more reactive compared to the middle –OH group due to steric hindrance. To overcome this issue, we have proposed a new route through which 1,3-PDO can be formed with higher selectivity. A similar process has been reported by Wang et al. [26]. However, they used more steps to produce 1,3-PDO, and that made the overall process expensive. We attempted 1,3-PDO synthesis with lesser steps; the observed results will be discussed in the coming sections. The glycerol's terminal hydroxyl (–OH) groups can be protected by reacting glycerol with aldehydes or acids etc. The reaction of glycerol with aldehydes produces 5 or 6-membered glycerol acetals, which can be used as a substrate to make 1,3-PDO. Moreover, glycerol acetals also have industrial importance.

Glycerol acetals can also be used in disinfectants, flavors, and surfactants [219,220]. Moreover, acetals are also used in food products, pharmaceuticals, solvents for cosmetic and medical products, and fragrances [221,222]. The most important application of acetal is found as a suitable oxygenated additive for fuels [223]. The reaction of glycerol with benzaldehyde effectively produces green cyclic acetals such as 2-phenyl-1,3-dioxolane-4-methanol or 2-phenyl-1,3-dioxane-5-ol (five or six-ring atoms), which has shown the importance as intermediates in the synthesis of dihydroxyacetone or 1,3-PDO [224]. Therefore, in this work,

we attempt to synthesize cyclic acetals from glycerol followed by their separation and tried their conversion to 1,3-PDO.

8.2 Process Concept

The new glycerol conversion approach is illustrated in Figure 8.1. In this process, the conversion of glycerol to 1,3-PDO was carried out either in 3 steps or 2 steps, namely acetalization, dehydration, and hydrogenation. In acetalization reaction, the terminal –OH groups of glycerol are protected. This protection of terminal –OH groups of glycerol will leave the formed compound (acetal) with only one (middle) –OH group. The dehydration (step 2) followed by hydrogenation (step 3) of acetal or in-situ hydrogenolysis of acetal (step 2 and 3 combined) may result in 1,3-PDO, and that's how the 1,3-PDO selectivity can be improved.

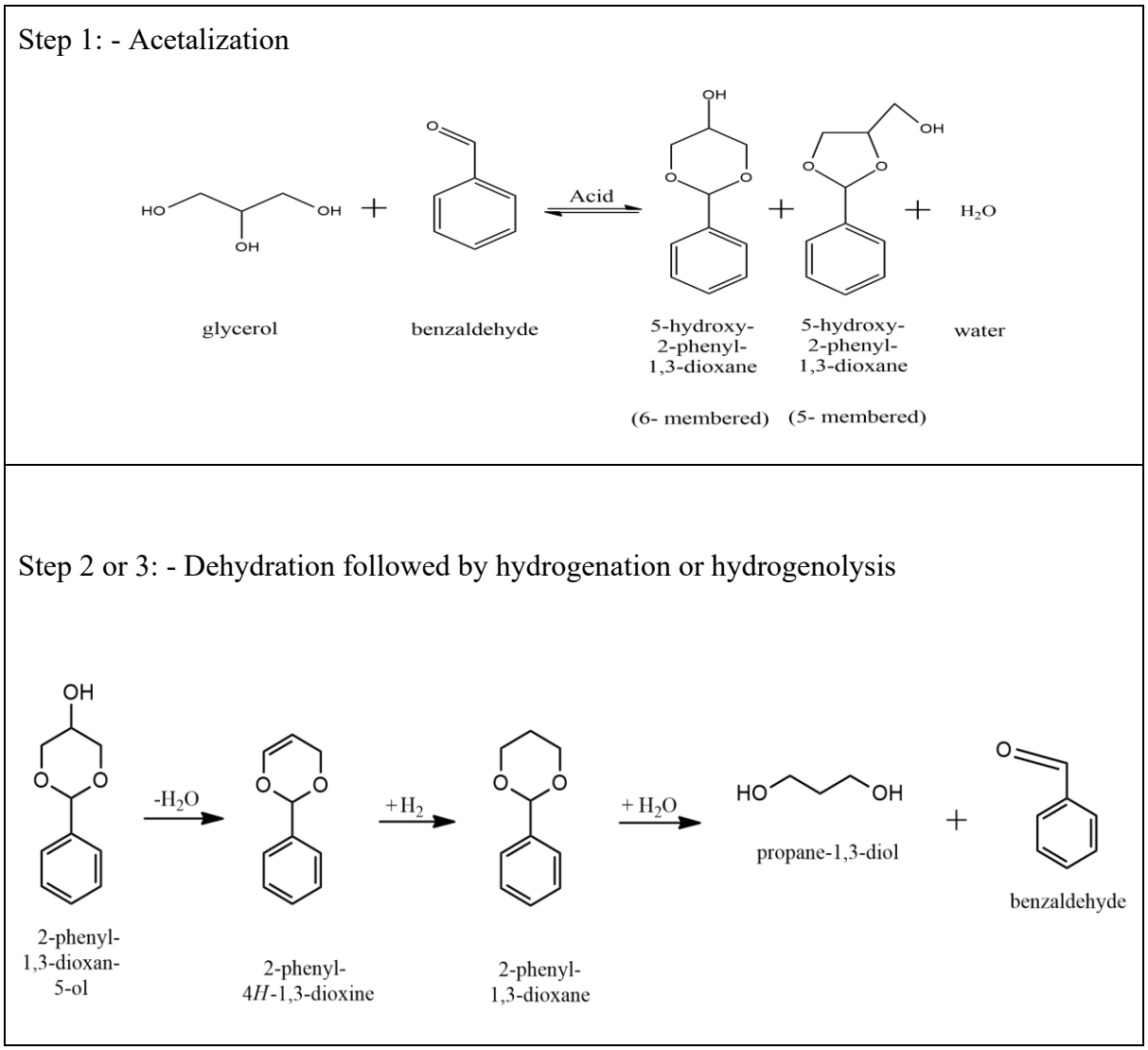

Figure 8.1. Representation of the new approach to glycerol conversion with benzaldehyde.

Figure 8.1 shows the proposed approach for selective synthesis of 1,3-PDO from glycerol. In step 1, acetalization of glycerol with benzaldehyde is carried out. In step 2, the formed 6-membered acetals are dehydrated to 2-phenyl-4H-1,3-dioxine. In step 3, the formed compound of step 2 will be hydrogenated to 2-phenyl-1,3-dioxane, then acid hydrolysis will release 1,3-PDO and benzaldehyde. Steps 2 and 3 can also be carried out in a single vessel (in-situ) via hydrogenolysis. In the study described in this chapter, we have synthesized the acetals from glycerol and tried hydrogenolysis of acetal. We speculated the hydrogenolysis of acetals would improve the selectivity of 1,3-PDO. The observed results will be discussed in the coming sections.

If the acetalization was carried out using formaldehyde, then the process of 1,3-PDO synthesis would have been like Figure 8.2.

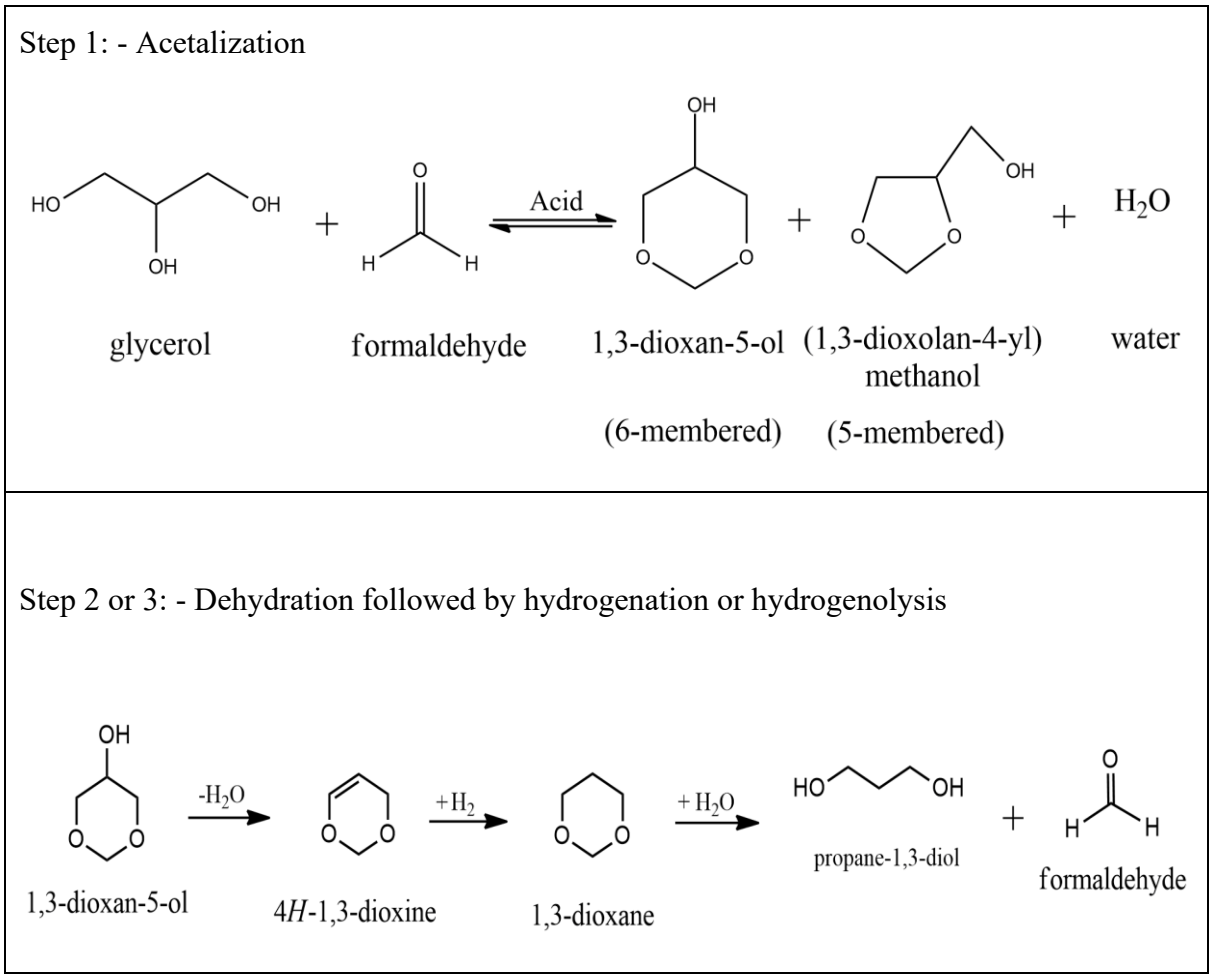

Figure 8.2. Representation of the new approach to glycerol conversion with formaldehyde

8.3 Experimental

8.3.1 Materials and Methods

Merck Ltd. India supplied glycerol (≥99.5%), benzaldehyde (≥98.5%), and paraformaldehyde (95%). These chemicals were used as a reactant during acetalization reaction. Ethylene glycol (99.5%) supplied by Merck Ltd. India was used as a GC standard. The benzene (≥99.5%), toluene (≥99.5%), xylene (≥99.5%) were used as the reaction solvent, and they were purchased from Merck Ltd. India. Sulfuric acid (≥98%), phosphoric acid (85%), or p-toluenesulfonic acid (≥99%) was used as a homogeneous catalyst; these chemicals were purchased from Merck Ltd. India. The commercially available cation exchange resin Amberlyst 15, also used as a (heterogeneous) catalyst, was obtained from Rohm and Haas Pvt. Ltd. India. It was washed with distilled water, isopropyl alcohol (IPA), diluted hydrochloric acid, and distilled water before its use. It was then dried at 70 ^{o}C under vacuum for 10 hrs. The β-zeolite was obtained from zeolyst international USA and used as a heterogeneous catalyst. It was calcined at 500 ^{o}C for 5 hrs before its use.

8.3.2 Product Analysis

A similar analysis procedure to the one reported in chapter 3 was adopted for analyzing the products observed during acetalization and hydrogenolysis. Here, ethylene glycol was used as a GC standard. The identified compounds are glycerol, benzaldehyde, 5-hydroxy-2-phenyl-1,3-dioxane (6-membered benzylidene acetal), and 4-hydroxy-methyl-2-phenyl-1,3-dioxolane (5-membered benzylidene acetal), 1,3-dioxane-5-ol (6-membered acetal), 1,3-Dioxolane-4-methanol (5-membered acetal). Additionally, a few other compounds like benzyl alcohol, benzoic acid, and methyl-2-hydroxy-3-phenylpropanoate (non-cyclic acetal confirmed by GC-MS) were also observed.

8.3.3 Experimental Setup

The acetalization reaction was performed in a round bottom flask with the Dean-Stark receiver, as shown in Figure 8.2 A. A cylindrical glass reactor with an overhead stirrer shown in Figure 8.2 B was used to obtain the reaction's kinetics.

The experimental setup consisted of a 250 ml capacity round bottom Dean-Stark reactor/ apparatus or a cylindrical reactor. The cylindrical reactor was used to generate the kinetic data because the cylindrical reactor ensures the uniform flow distribution and uniform mass transfer resistance. A condenser was used for a reaction carried out in a Dean-Stark apparatus. The magnetic needle was used to stir the reaction mixtures in the Dean-Stark apparatus, and the overhead stirrer was used to stir the reaction mixtures in a cylindrical reactor. In the case of the Dean-Stark apparatus, the stirring speed was controlled by a controlling knob inbuilt in the magnetic stirrer with a heating plate. An external thermostat controlled the stirring speed in the cylindrical reactor with an accuracy of ± 5 rpm. According to the given setpoint, the reaction temperature was controlled by an external thermostat in both reactors. The thermostat is capable of handling the reaction temperature with an accuracy of ± 0.05 ^{o}C.

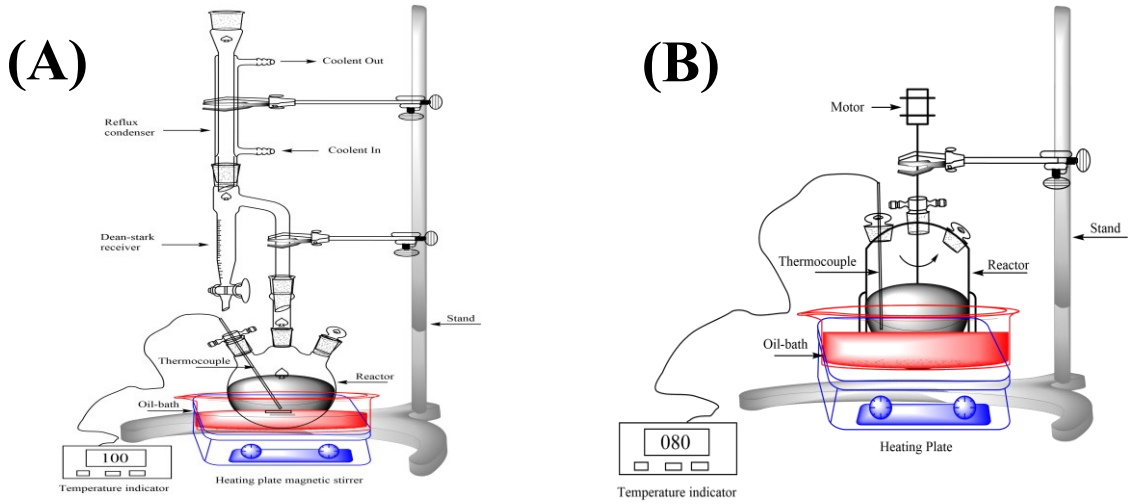

Figure 8.3. (A) Dean-Stark apparatus and (B) cylindrical reactor

In a typical experiment, the reactor was charged with a mixture of glycerol and aldehyde, and a known amount of catalyst was added to the reactor. The desired reaction temperature was given as a set point. When the temperature reached close to a setpoint, the reaction mixture was stirred slowly (50 rpm) to avoid temperature overshoots. We have not observed any noticeable changes in reactant concentration (samples analyzed in GC) at this stirring speed. Once the reaction mixture temperature stabilizes at the setpoint, the stirring speed is increased to the desired value (400 or 600 or 800 rpm). This time (after nearly 10 minutes of stabilization time) was considered as the "zero-reaction" time for the reaction. The samples were collected periodically from the sampling port using a sampling needle, ensuring no loss of catalyst from the reactor., the samples were cooled down immediately to avoid any vapor loss. The samples were then analyzed in a GC.

The conversion of glycerol and selectivity of products were calculated using equations provided in chapter 3.

8.3.4 Acetalization in Dean-Stark Apparatus

To protect the terminal –OH groups of glycerol, an acetalization reaction was performed using benzaldehyde or formaldehyde. The products observed from the acetalization of glycerol with benzaldehyde are 5 and 6-membered benzylidene acetals 4-hydroxymethyl-2-phenyl-1,3-dioxolane (5-membered benzylidene acetal) and 5-hydroxy-2-phenyl-1,3-dioxane (6 membered benzylidene acetal), while the products observed from the acetalization of glycerol with formaldehyde were a mixture of 1,3-dioxan-5-ol (6-membered acetal) and 1,3-dioxolane-4-methanol (5-membered acetal).

The acetalization of glycerol with benzaldehyde was conducted with benzene as a solvent in the Dean-Stark apparatus, as shown in Figure 8.2 A. In a typical experiment, 20 g of glycerol, 24 g of benzaldehyde (ca. 4% excess on a mole basis), and 100 mL of benzene, together with 5 wt% of Amberlyst 15 or 1 g of PTSA or a few drops of H_2SO_4 catalyst, were placed in the reaction flask. The reaction was initiated once the desired temperature (boiling state) was reached. The progress of the reaction was monitored by the volume of the water collected in the dean-stark receiver. The benzene solvent was boiled off from the reaction mixture after the completion of the reaction. The reaction mixture is left only with products and excess benzaldehyde. The analysis of the final reaction mixture was performed by GC. The isolation of the 6-membered benzylidene acetal from the reaction mixture was accomplished by crystallizing it using a 1:1 benzene-pet ether solution using a procedure given by Hill et al.[225].

A similar reaction was conducted using paraformaldehyde with the same amount of benzene. The product of this reaction contains a mixture of 5 and 6 membered acetals (see Figure 8.2), which could not be separated by distillation due to their close boiling points.

The synthesis of 1,3-PDO from acetal requires a 6-membered compound, while a 5-membered compound can lead to 1,2-PDO. As the product of interest is 1,3-PDO, therefore we have used 6-membered benzylidene acetal to perform the further study.

8.3.5 Acetalization in Cylindrical Reactor

Kinetics of glycerol acetalization with benzaldehyde was performed in a 250 mL capacity cylindrical reactor shown in Figure 8.2 B as the cylindrical reactor ensures the uniform flow distribution inside the reactor. The measured quantities of glycerol, benzaldehyde, and catalyst (Amberlyst-15) were added to the reactor. The procedure given in section 8.2.3 was adopted for carrying out reactions. Several experiments were carried out to study the effect of different parameters, including temperature, catalyst loading, stirring speed, and mole ratio, on the reaction's kinetics.

8.3.6 Dehydration and hydrogenolysis of benzylidene acetal

The dehydration reaction of isolated 6-membered benzylidene acetal was performed in a Dean-Stark apparatus. In a typical experiment, 10-15 g of acetal, with 100 mL of solvent (benzene, toluene, or xylene) together with the desired amount of catalyst (H_2SO_4, H_3PO_4, PTSA, Amberlyst 15, or β-zeolite) were placed in the reaction flask. The reaction was initiated after the reaction mixture started boiling, and the reaction progress was monitored by the water collection in the Dean-Stark receiver. The reaction was stopped after 4 h, and the final reaction mixture was analyzed in GC.

The hydrogenolysis of isolated 6-membered benzylidene acetal was performed in a 100 ml capacity autoclave. The autoclave was operated using a similar procedure described in chapter 3 (see section 3.3). In a typical experiment, the reactor was charged with 10-15 g of acetal, 3.0 g of synthesized catalyst (4 wt% of the reaction mixture), and 60 g of solvent (methanol or dioxane). The reaction mixture was analyzed in a GC.

8.4 Results and discussion

8.4.1 Acetalization of glycerol with aldehydes

Acetalization of glycerol with benzaldehyde or formaldehyde protects its 1^o and 3^o –OH group of glycerol. The acetalization reaction is a reversible reaction that tends towards equilibrium, but it can be driven to completion by removing one of the products from the reaction (water). Therefore, the Dean-Stark apparatus was used as a reactor to remove the water from the reaction continuously. Furthermore, the reaction is non-selective because it forms both the 5-

membered and 6-membered benzylidene acetals. These acetals are in equilibrium with each other during the reaction. It was reported that the selectivity of the 6-membered compound could be improved by recycling the 5-membered compound from the previous batch [26,226].

Here, the reaction of glycerol with benzaldehyde over Amberlyst 15 or PTSA or H_2SO_4 catalyst has given the 100% glycerol conversion with 46.8% yield of 5 membered benzylidene acetal and 37.7% yield of 6 membered benzylidene acetal measured using GC peaks. The other products (high boilers) were also observed during acetalization, like benzyl alcohol or methyl 2-hydroxy-3-phenylpropanoate (see Figure 8.4). These products were also observed by Yamamoto et al. [224]. The product mixture was separated using the crystallization technique. After purification, the final yield of 6 membered benzylidene acetal was 22%. The results are in line with the reported results [26,227].

Similarly, the reaction of glycerol with formaldehyde over H_2SO_4 or PTSA or Amberlyst 15 catalyst also given the 100% glycerol conversion. The yield of 5 membered acetals was 51.3%, and that of 6 membered acetals was 47.4% measured using GC. Few unknown products were also observed during the reaction, which was also observed by others [228]. The solvent was boiled off using distillation and the products were isolated. The product was a mixture of 5 and 6-membered acetal. Their further separation was not possible due to close boiling points. Similar results were also reported in the literature [224,228].

8.4.2 Acetalization kinetics

The effect of different parameters like temperature, stirring speed, catalyst loading, and mole ratio on the glycerol conversion was studied in a glass reactor. The observed results during these experiments are discussed in the following section.

a) Effect of speed of agitation

The effect of external mass transfer on the reaction between glycerol and benzaldehyde was studied by performing experiments with different stirring speeds such as 400, 600, and 800 rpm in a cylindrical reactor (Figure 8.3 B). The observed glycerol conversion results are given in Figure 8.5 (I). The results showed only a small change in the conversion of glycerol when the stirring speed was increased from 400 to 800 rpm. Hence, for all of the other experiments, the reaction stirring speed was kept at 800 rpm to obtain intrinsic kinetics that is free from external mass transfer limitations.

b) Effect of catalyst loading

The effect of catalyst amount/loading on the acetalization reaction between glycerol and benzaldehyde was performed and the observed results were given in Figure 8.5 (II). As expected, the conversion of glycerol has increased with an increase in catalyst loading. The observed glycerol conversion at different catalyst loading (in wt%) was 23.9% at 0 wt% (without catalyst), 33.85 at 2.5 wt%, 57.8% at 5 wt%, and 65.1% at 10 wt%. The rate of increase in glycerol conversion with catalyst loading from 2.5 to 5 wt% was higher, but further increase in catalyst loading has slightly increased the rate of glycerol conversion (see Figure 8.5 (II)). The selectivity of 6-membered acetal was slightly increased with an increase in catalyst loading from 0 to 5 wt%. Its selectivity after 2 h of reaction was 41.3% at 0 wt% loading, 43.3% at 2.5 wt% loading, and 45.7% at 5 wt% loading. At higher catalyst loading, its selectivity was decreased to 42.6% at 10 wt% loadings. In the case of 5-membered acetal selectivity, it was slightly decreased with an increase in catalyst loading from 0 to 10 wt%, its selectivity was 51.3% at 0 wt% loading, 49.7% at 2.5 wt% loading, and 48.2% at 5 wt% loading, and 47.6% at 10 wt% loading.

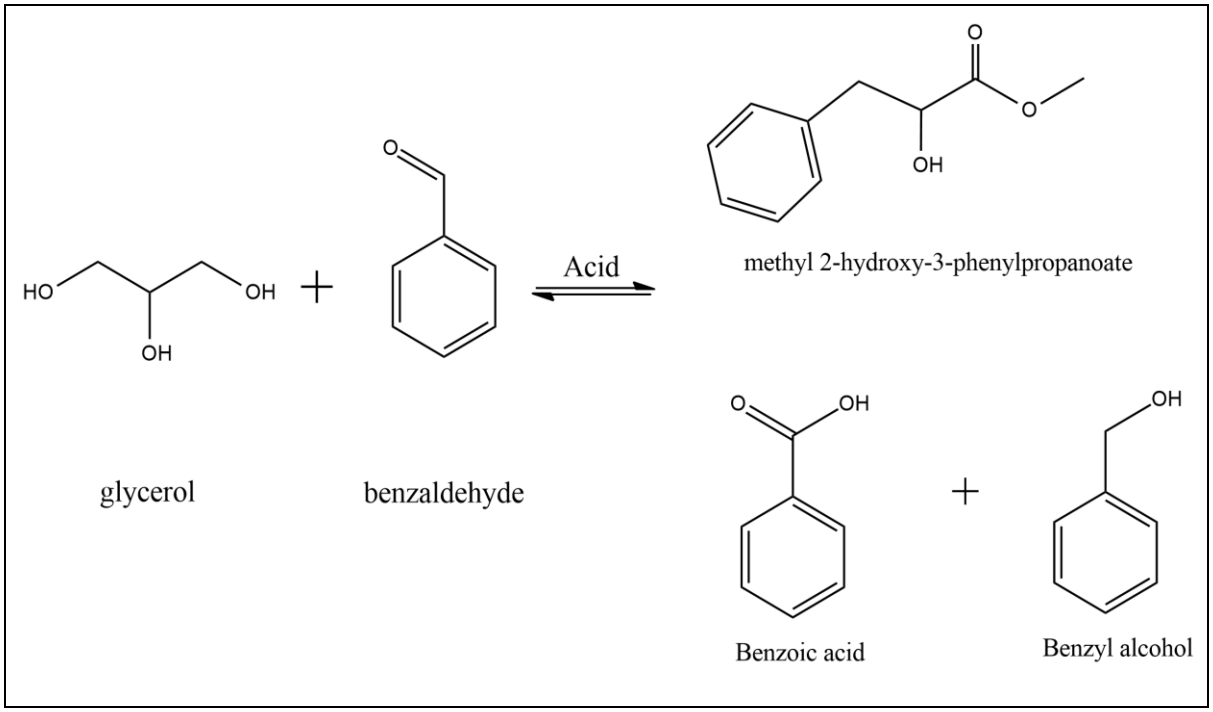

Figure 8.4. Side-products observed during the acetalization of glycerol with benzaldehyde

Figure 8.4 shows side products formed during acetalization of glycerol with benzaldehyde. The benzaldehyde and benzyl alcohol were observed at higher ratios of benzaldehyde and higher catalyst loadings. In contrast, the formation of methyl-2-hydroxy-3-phenylpropanoate (non-cyclic acetal) was observed at higher temperatures and higher catalyst loading.

c) Effect of reaction temperature

The effect of temperature on the reaction between glycerol and benzaldehyde was performed over the temperature range between 60–90 °C using 1:1 mole ratio of reactants. The increase in reaction temperature has increased the overall reaction rate (see Figure 8.5 (I)). The conversion of glycerol was increased from 33.7% to 64.3% after 120 min when the temperature was raised from 60–90 °C. Though 90 °C has given the highest conversion, however, at this temperature, the formation of side products (shown in Figure 8.4) has increased. The selectivity of 6-membered acetal was slightly increased up to 80 °C; however, it was reduced at 90 °C. After 2 h of reaction, its selectivity was 44.1% at 60 °C, 44.8% at 70 °C, 45.7% at 80 °C, and 40.4% at 90 °C. Selectivity of 5-membered acetal was slightly decreased with an increase in temperature. Its selectivity was 51.5% at 60 °C, 49.7 at 70 °C, 48.2% at 80 °C, and 47.7% at 90 °C.

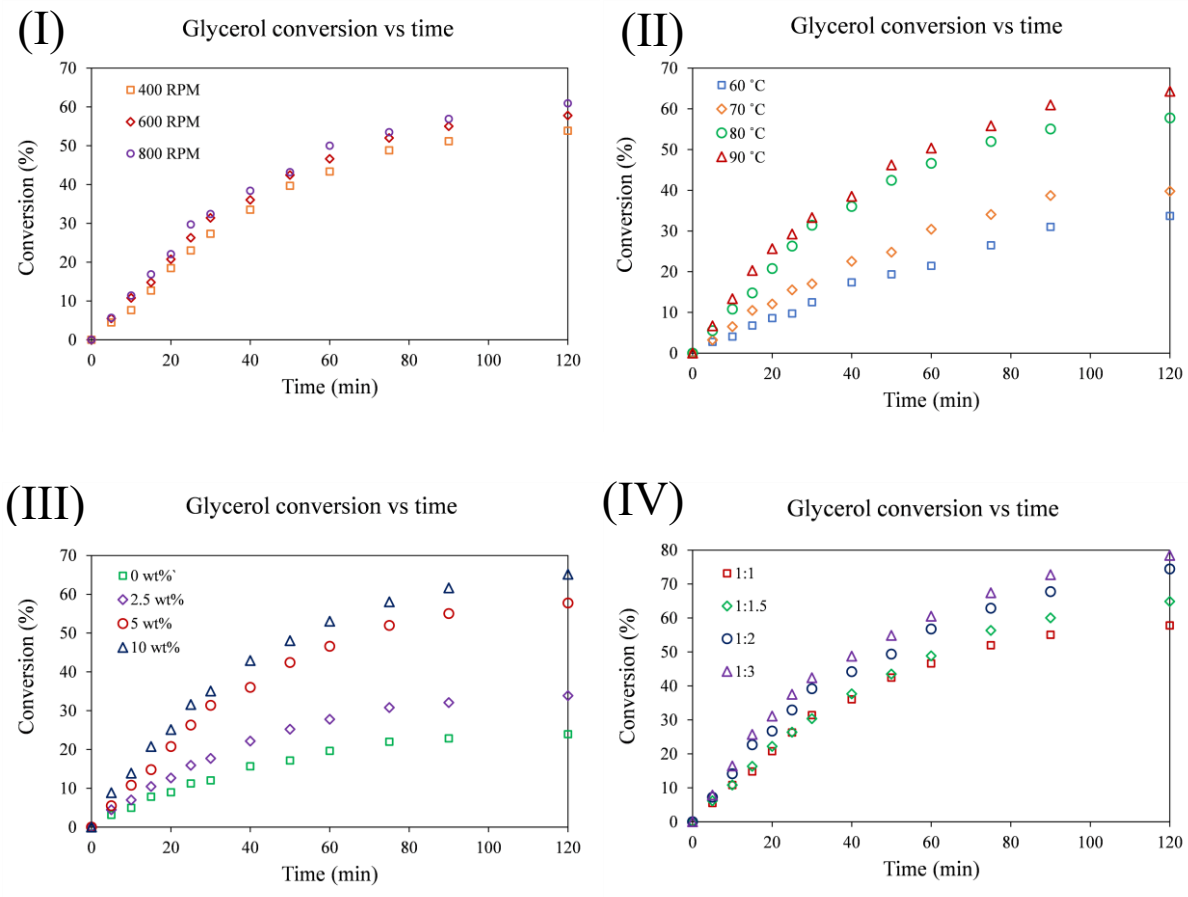

Figure 8.5. Concentration vs. time profiles for acetalization of glycerol with benzaldehyde: - (I) Effect of RPM, (II) Effect of catalyst loading, (III) Effect of reaction temperature, (IV) Effect of reactant mole ratio

Hence, the optimum temperature with higher glycerol conversion seems 80 ºC. Literature reports similar behavior for an increase in glycerol conversion with the increase in reaction temperature [229–231].

d) Effect of reactant mole ratio

The effect of change in an initial mole ratio of glycerol to benzaldehyde (benzaldehyde was varied) on acetalization reaction was studied at 80 ºC. The results show an increase in glycerol conversion with an increase in benzaldehyde amount. The glycerol to benzaldehyde ratio was varied as 1:1, 1:1.5, 1:2, and 1:3. The respective rise in glycerol conversion was 57.8, 64.9, 74.4, and 78.4, respectively. It is worth noting that, increase in glycerol to benzaldehyde ratio from 1:1 to 1:3 has increased the formation of other products from 6.1% to 15%, respectively. The selectivity of 6-membered acetal after 2 h of reaction was 45.7% with 1:1 ratio, 44.1% at 1:1.5 ratio, 43.4% at 1:2 ratio, and 40.1% at 1:3 ratio. Selectivity of 5-membered acetal was 48.2% at 1:1 ratio, 47.3% at 1:1.5 ratio, 46.8% at 1:2 ratio, and 45.2% at 1:3 ratio.

The catalyst re-usability was also performed with 1:1 reactant molar ratio, 5 wt% Amberlyst 15 catalyst, 80 ºC. The catalyst has not lost its activity even after 5th repetition, indicating the clean reaction with zero catalyst deactivation.

e) Dehydration of benzylidene acetal

The dehydration of formed acetal was carried out in dean-stark apparatus with benzene, toluene or xylene solvents. Different solvents were used to increase the boiling point of the reaction mixture. The toluene-water system boils at temperatures higher than 85 ºC and the water-xylene system boils at a temperature higher than 95 ºC. The use of heterogeneous catalysts like Amberlyst 15, β-zeolite has not even initiated the reaction. After 4 h, the final product of the reaction was benzylidene acetal only. Similar results were observed over homogeneous catalysts like PTSA, H_3PO_4 except for H_2SO_4. Few drops of H_2SO_4 have initiated the reaction. However, the product of the reaction is a polymerized black mass. The reaction was also carried out without solvent even at low temperatures -5 ºC; however, the reaction results are the same. Hence, we conclude that the acetalization of glycerol with benzaldehyde is easy. Still, the dehydration of formed acetal is very difficult because the compound's hydroxyl (–OH) group is a weak leaving group. Therefore, Wang et al. [26] replaced the –OH group of benzylidene acetal with a better leaving tosyloxyl group (tosyl chloride) and synthesized 1,3-PDO. The cost of tosyl chloride makes this process non-friendly to the industry.

As dehydration of benzylidene acetal seems complicated, we tried its hydrogenolysis over Pt-0.7STA/β-zeolite catalyst. The observed results will be discussed in the following section.

f) Hydrogenolysis of benzylidene acetal

The hydrogenolysis of formed acetal was carried out in 100 ml capacity high-pressure autoclave at 50 bar H_2 pressure. The acetal was dissolved in 50 ml of solvent, either methanol or 1,4-dioxane. The reaction was carried out at 150 ^oC. After 5 h, the conversion of benzylidene acetal was 86.4%. However, the product of hydrogenolysis was benzaldehyde and glycerol. That means the hydrogenolysis has resulted in the ring-opening of acetals. Chia et al. [232] studied the hydrogenolysis of cyclic ethers with –OH group over Rh-ReOx/C catalyst and found the formation of straight-chain molecules after ring-opening (cyclic compound). Similar results for hydrogenolysis of cyclic ethers with –OH group over Ir–ReOx/SiO_2 catalyst were also reported by Chen et al. [233]. In our case, the hydrogenolysis of cyclic acetal with –OH group resulted in the formation of glycerol and benzaldehyde after ring-opening.

To overcome this issue, one may synthesize a catalyst that will only be active for the –OH group, then 1,3-PDO can be formed from direct hydrogenolysis of benzylidene acetal.

8.5 Conclusion

A new approach for the transformation of glycerol to 1,3-PDO selectively is proposed and a few exploratory studies were carried out. The idea is to synthesize 6-membered glycerol acetals and selectively remove the 2^o –OH group from the formed acetal. H_2SO_4 only initiated the dehydration of acetal, but it has formed the polymeric compounds. The hydrogenolysis of acetal over Pt-0.7STA/β-zeolite catalyst has resulted in ring-opening. The formation of 1,3-PDO did not occur through the proposed route, but the formed acetals can be used for other applications.

The effect of reaction temperature, catalyst loading, and glycerol to benzaldehyde mole ratio positively impacted glycerol conversion during acetalization of glycerol. However, higher catalyst loading, higher temperature, or high mole ratio favored the formation of undesired compounds. The best operating condition for the synthesis of benzylidene acetal over Amberlyst 45 was a 1:1 mole ratio, 80 ^oC temperature, 5 wt% catalyst, and 800 rpm.

Chapter 9:
CONCLUSION & FUTURE SCOPE

9.1 Conclusion

Increasing biodiesel production as a fossil fuel alternative to fulfill the increasing energy demands has increased the availability of glycerol in the chemical market at cheaper rates. Glycerol is being viewed increasingly as a 'building block' chemical [234]. Hydrogenolysis is one of the major routes to derive 1,3-PDO, a commercially important chemical from glycerol. The 1,3-PDO is an essential reactant in synthesizing poly-trimethylene terephthalate (a biodegradable polymer). However, the conversion of glycerol to 1,3-PDO has a complex mechanism; it is challenging to direct it to the desired product (1,3-PDO). But, intrusions at the level of reaction mechanism (through the application of selective catalysts) and at the level of reaction conditions (through reaction engineering) are possibilities that suggest themselves in this context.

The present work was proposed to investigate the aqueous phase hydrogenolysis of glycerol with molecular hydrogen in a slurry reactor. This thesis broadly covers the micro (catalysis) and macro (engineering) aspects of glycerol hydrogenolysis. The study has explored the usage of Pt-STA on the β-zeolite supported bifunctional catalyst for the glycerol hydrogenolysis reaction.

Based on these studies, the following conclusion can be drawn from the thesis:

9.1.1 Hydrogenolysis of glycerol with Pt-STA/β-zeolite catalysts

Hydrogenolysis of glycerol has been performed with the use of the Pt-STA/β-zeolite catalyst. The use of high SiO_2 to Al_2O_3 ratio β-zeolite as catalyst support for glycerol hydrogenolysis is tried for the first time. This work demonstrates the potential of STA as a promotor to Pt-β-zeolites catalyst in terms of tuning its acidic properties, electronic structure, metal dispersion, hydrogen spillover, and thereby achieving a higher selectivity towards 1,3-PDO. β-zeolite mostly acts as a support, but it has shown some activity towards glycerol; however, the 1,3-

PDO formation was not observed on it. Adding Pt to β-zeolite catalyst has shown some selectivity towards 1,3-PDO, and the addition of STA further improved this. This confirms that all three elements are equally important in a catalyst for glycerol transformation to 1,3-PDO.

The increase in STA to β-zeolite ratio from 0 to 0.5 resulted in an increase in the total acidity of the catalyst. As a result, the glycerol conversion increases from 15.06% to 37.58% in 5 h of reaction. The further increase in STA to β-zeolite ratio (>0.5) results in a decrease in the total acidity of the catalyst, and the glycerol conversion reduced 34.14% to 20.05% under otherwise similar conditions. This suggests a correlation between the glycerol conversion activity of the catalyst and its total acidity.

The catalyst characterization study provided more insights into the catalyst structure and mechanism of action. It showed how STA is beneficial in increasing preferentially the Brønsted acidity required for enhancing the 1,3-PDO selectively. The XRD data showed the existence of tungsten bronze phase ($H_{0.53}WO_3$) and crystalline m-WO_3 at a higher STA to β-zeolite ratio. The Py-FTIR and Py/2,6-dTBPy-TGA results showed the presence of the highest Brønsted acidity over Pt–0.7STA/β-zeolite catalyst followed by Pt–0.3STA/β-zeolite catalyst. Therefore, these catalysts have given the highest 1,3-PDO selectivity as 38.8% and 31.04% respectively in 5 h of reaction compared to other catalysts. The correlation between Brønsted acidity and 1,3-PDO yield also confirms that the Brønsted acid sites favor the formation of 1,3-PDO by removing the secondary –OH group of glycerol.

The CO-chemisorption results showed an improvement in Pt dispersion with the incorporation of STA in the catalyst. H_2-TPR result revealed the strong interaction between metal and support. XPS analysis confirms the presence of W^{5+} species over a catalyst surface, which formed after the hydrogen spillover from Pt to STA surface. TEM images revealed the presence of well-dispersed 2 to 4 nm Pt particles.

The 1,3-PDO selectivity was found to improve at least 7 times, and its productivity increased 14 times compared to Pt/β-zeolite catalyst. It is attributed to the large concentration of Brønsted acid sites of $H_{0.53}WO_3$ species with appropriate acid amounts, strong electronic interaction between Pt and STA species, and hydrogen spillover.

The reusability study revealed that the catalyst was reusable even after the 4^{th} run and has given nearly comparable results to the fresh catalyst.

The study on the effect of operating parameters on glycerol hydrogenolysis reaction revealed that high temperatures (>220 ºC), long reaction times (>5 h), and low pressures (< 40 bar) were

found to be undesirable from the 1,3 PDO selectivity point of view. The optimum Pt loading was found to be 5 wt%. Hence, the best catalyst found to be 5%Pt-0.7STA/β-zeolite and best reaction conditions are 200 ^{o}C, 50 bar H_2 pressure, and 5 h reaction time which offers 30.4% glycerol conversion, 44% 1,3-PDO selectivity, 7.9 % 1,2-propanediol (1,2-PDO) selectivity, and 28% 1-propanol (1-PrOH) selectivity.

9.1.2 Kinetic Modeling and Simulation

The concluding part of the thesis is dedicated to the kinetic modeling and simulation of the experimental reaction data. The kinetics of the Pt-0.3STA/β-zeolite catalyzed glycerol hydrogenolysis was studied in detail, and a kinetic model was proposed based on the reaction mechanism for the intrinsic kinetic regime. The model incorporates the rate of change of concentration in all the reactants and products during glycerol hydrogenolysis, the rates of the different reactions in the proposed mechanism is assumed to be of first-order in the respective reactant concentrations, the order with respect to hydrogen being subsumed in the rate constant since the data were obtained at constant hydrogen pressure. The model was able to explain the observed trends in the experimental data. The values of the rate constants and activation energies were evaluated as per the Arrhenius plot. The activation energy for 1-PrOH was higher while it was lower for 1,3-PDO, which shows lower temperature favors 1,3-PDO formation. Hydrogen pressure seems to affect both rate and selectivity of the reaction, and it is found to be favorable for 1,3-PDO synthesis.

This thesis can conclude that the bifunctional catalyst containing Pt-STA seems to be a promising catalyst for the hydrogenolysis of glycerol to 1,3-PDO.

The main contributions of the work are coming out to be the synthesis of a new series of catalysts for glycerol hydrogenolysis to 1,3-PDO. Furthermore, we have discussed mechanistic investigations through extensive characterization and performance studies, leading to an understanding of the precise role of the various constituents of the catalyst and hence to an optimized formulation of the catalyst. Additionally, detailed kinetic studies on one of the most promising catalysts in the series synthesized and a kinetic model over the temperature range of 200 to 220 ^{o}C and pressure range of 10 to 50 bar H_2 is given.

9.1.3 New approach for 1,3-PDO synthesis

A new way is proposed to improve the 1,3-PDO selectivity from glycerol by protecting terminal hydroxyl groups of glycerol, converting the sec-OH group by hydrogenolysis, and then de-derivatizing the product to obtain 1,3PDO. Unfortunately, the proposed path has not worked out due to the ring-opening of formed cyclic acetals in acidic conditions. However, synthesis of benzylidene acetal was performed, which is an important raw material in synthesizing value-added products like dihydroxyacetone.

Preliminary investigations into an improved process for 1,3-PDO through chemical derivatization of the terminal –OH groups of glycerol before hydrogenolysis, leading to an identification of the challenges in this approach.

9.2 Future Work

9.2.1 Catalysts

SiO_2 seems to be a dominant species in high SiO_2 to Al_2O_3 ratio β-zeolite catalyst. In this work, we have demonstrated the effect of STA addition on the performance of Pt-STA/β-zeolite catalyst. The addition of STA has improved the performance of the Pt/β-zeolite catalyst due to better interaction between Pt-STA species. However, literature also reports the better interaction between Ir-ReOx (iridium and rhenium oxide) supported on SiO_2 [235] catalysts. The Ir-ReOx/SiO_2 catalyst has shown the higher selectivity for 1,3-PDO during glycerol hydrogenolysis [65]. Therefore, it will be interesting to study the effect of β-zeolite supported Ir-ReOx catalysts on glycerol hydrogenolysis due to β-zeolite's high SiO_2 content.

Moreover, the difference in surface areas of β-zeolite and SiO_2 is roughly 4 to 5 times. The high surface area of β-zeolite will help incorporate more ReOx species up to sub-monolayer coverage compared to SiO_2, which is ultimately beneficial for 1,3-PDO synthesis from glycerol. Additionally, the effect of Ir-ReOx incorporation on SiO_2 has already been studied extensively. However, work on Ir-ReOx incorporation on β-zeolite has not been explored. Therefore, it will be worth investigating the promoting effect of ReOx on β-zeolite for glycerol hydrogenolysis.

9.2.2 Reaction Engineering studies

There is no clear understanding of the effect of contacting conditions on the selectivity to different products in the glycerol hydrogenolysis. As we have batch kinetics at hand, it will be interesting to study a continuous process pilot scale using the present catalyst. Moreover, experimental and modeling studies on the fixed-bed reactor (which allows continuous operation) will be helpful to understand the reactor engineering aspects of glycerol hydrogenolysis. Additionally, the effect of operating conditions in a continuous process is worth exploring. Because glycerol hydrogenolysis reaction is complex and the isothermal strategy may not be optimal for 1,3-PDO synthesis. Hence the effect of operating conditions will throw more light on this. The kinetic model will also provide guidance in arriving at an optimal temperature profile.

The kinetic studies performed using a batch autoclave (Chapter 7) show that the reaction follows first-order kinetics under the given reaction conditions. Hence, from these results, we can anticipate that a continuous fixed bed reactor (packed bed reactor) will give better glycerol conversion and improve the selectivity to 1,3-PDO. This is because, as we have already shown, glycerol's reaction to 1,3-PDO is faster than 1,3-PDO to 1-PrOH (Chapter 7). Hence, we can exploit the conditions in our favor, reducing the over-hydrogenolysis and improving the 1,3-PDO selectivity. Moreover, though the residence time is large (5 h batch time), in a fixed bed reactor, efforts can be made to reduce them by manipulating catalyst loading or feed flowrate, etc. While in the case of CSTR, the residence time will be even larger, making CSTR unsuitable for this reaction. Therefore, fixed bed reactor seems suitable for this reaction.

Appendix-A

Calibration curve for the key product(s) and reactant of glycerol hydrogenolysis

Calibration curves for all the hydrogenolysis liquid products and glycerol were prepared. Figure A.1 shows the calibration curve for a few key products.

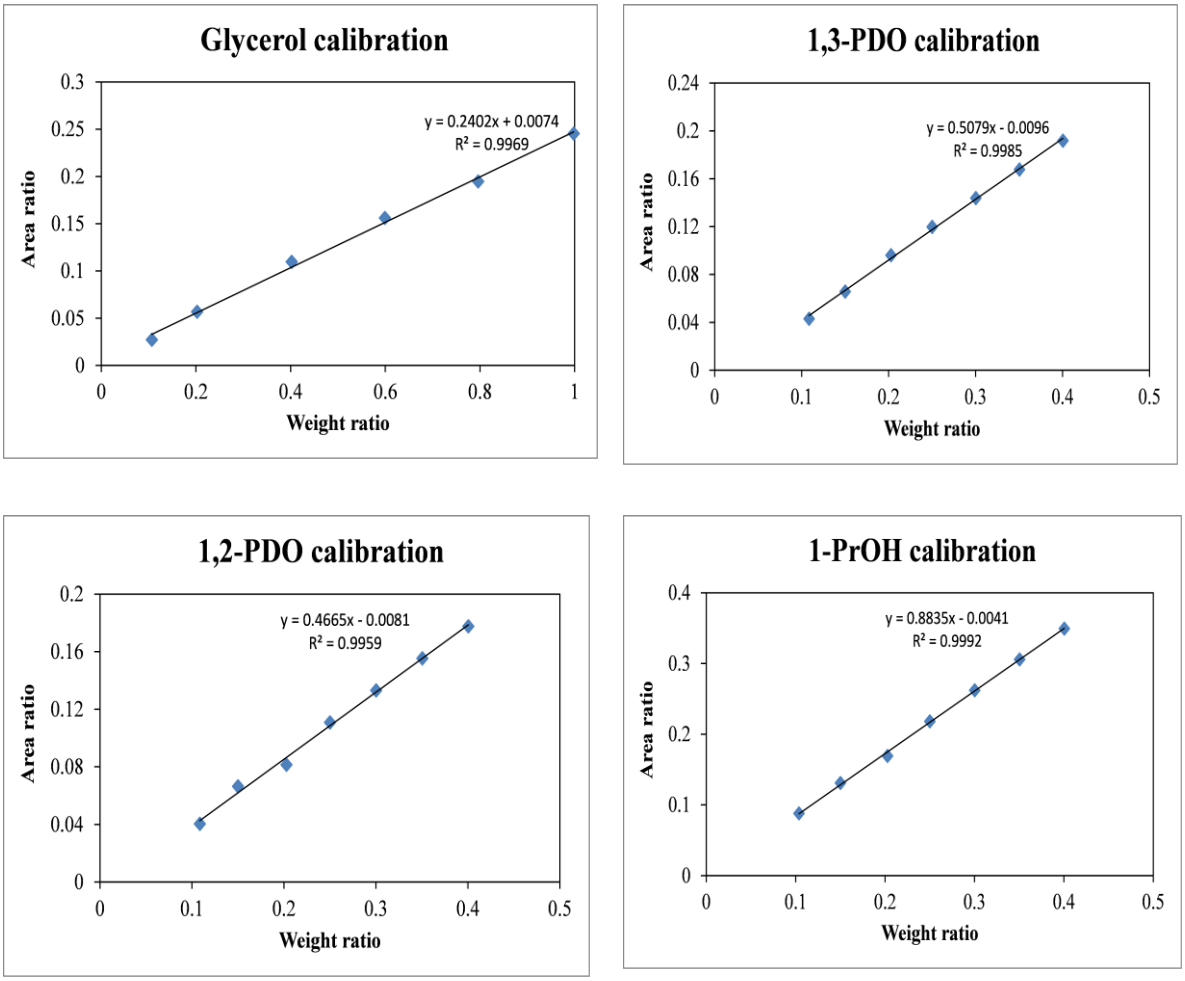

Figure A.1. Calibration curve for key product(s) and reactant of glycerol hydrogenolysis

The formula for determining the monolayer coverage and tungsten surface density

$\text{Monolayer coverage} = [\%WO_3 \text{ actual x } N_a \text{ x } 0{,}58 \times 10^{-18}]/[231{,}85 \text{ x } \%\text{HUSY x } BET_{HUSY}]$	Eq A.1
$\delta = \frac{\frac{wt\%W}{100}}{\frac{M_W}{}} \times 6.023 \times 10^{23} \Big/ \text{S.A.} \times 10^{18}$	Eq A.2

Where wt% W, M_W, and S.A. are the content of W in the sample (wt %), the molar weight of W (183.84 g/mol), and the specific surface area of the sample (m^2/g), respectively. In this equation, W surface density (δ) is thus expressed as W/nm^2 based on the weight of sample.

Correlation between the Lewis acid sites and 1,2-PDO yield using Py-FTIR

According to the literature, 1,2-PDO preferentially forms over the Lewis acid sites from glycerol dehydration to acetol followed by hydrogenation at metal sites to 1,2-PDO [93,196]. Hence, we attempted to correlate 1,2-PDO yield obtained over each catalyst with their Lewis acid sites measured using the Py-FTIR technique (See Figure A.3 for correlation using TGA technique) as shown in Figure A.2. It can be seen that the correlation is not so good. It is mainly attributed to the instability of 1,2-PDO in the reaction environment [93]. Similar results were also reported by Zhu et al. [114]. Moreover, Pt/β-zeolite catalyst has only given the highest yield of 1,2-PDO, which is certainly due to the presence of a large number of Lewis acid sites. However, it also contained a less total number of acid sites which will help 1,2-PDO to remain stable and not let it over-hydrogenolyse to 1-PrOH or other products.

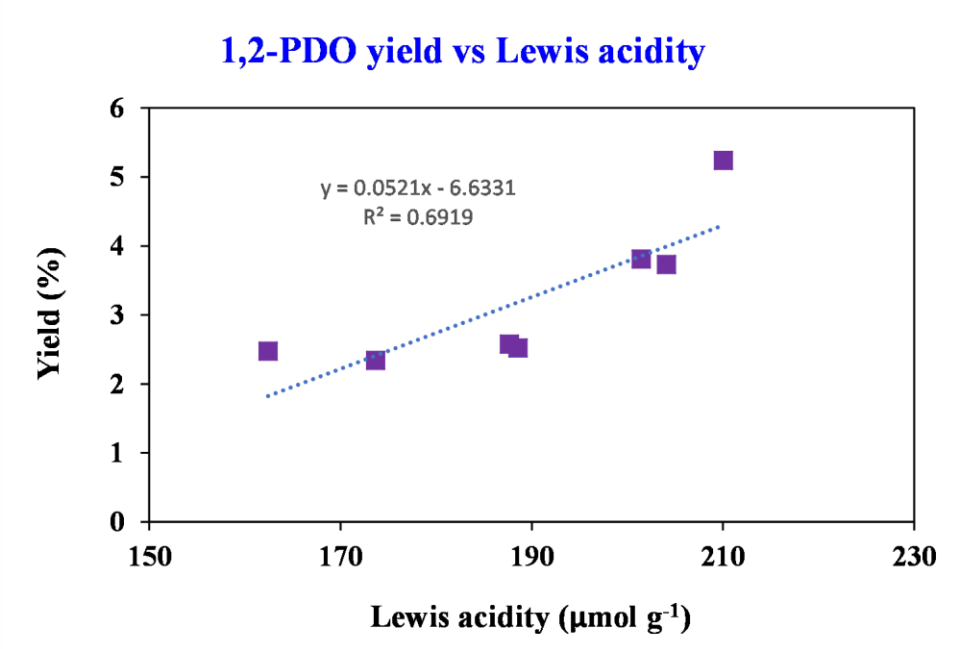

Figure A.2. Correlation between 1,2-PDO yield and Lewis acidity using Py-FTIR

Correlation between the acid sites and product yield using TGA

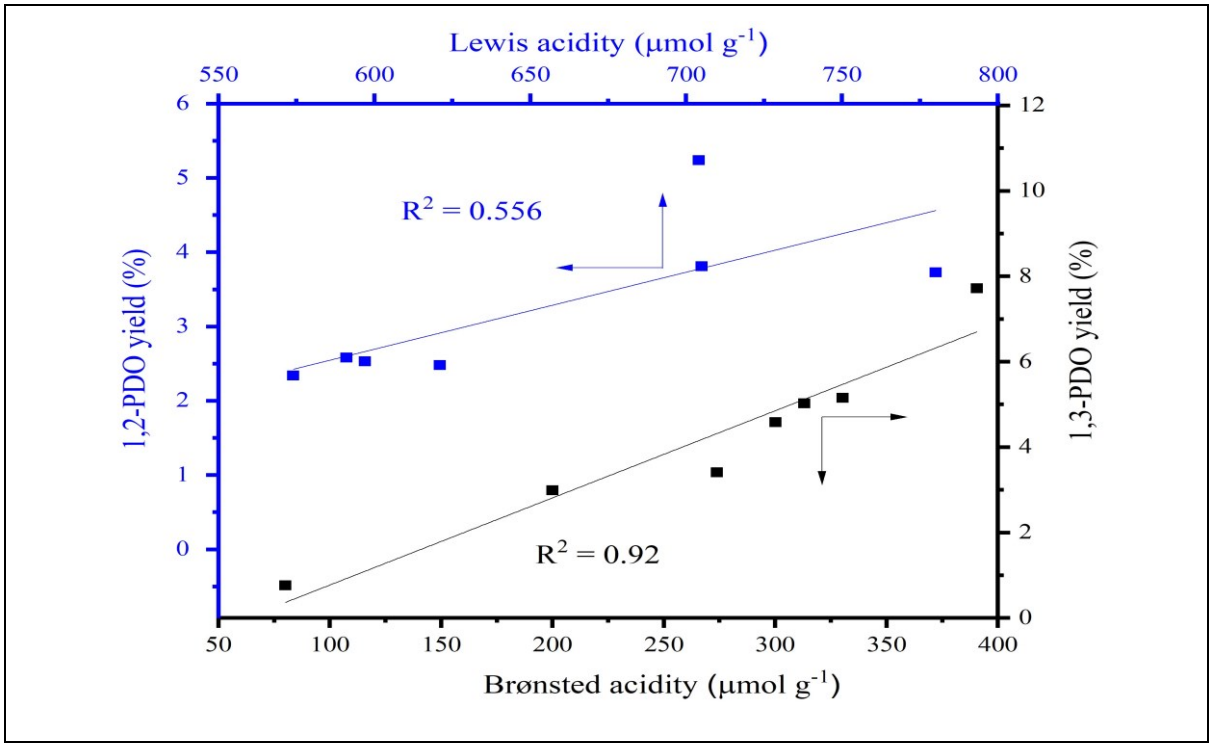

Figure A.3. Correlation between the product yield and amount of acid sites measured using TGA

Figure A.3 shows the relationship between the product yield (1,2-PDO and 1,3-PDO) and the amount of acid sites measured using the TGA technique. The result shows that the relationship between Brønsted acid sites and 1,3-PDO yield looks good. However, the relationship between 1,2-PDO yield and Lewis acidity is not that good. The results from Py-FTIR and TGA study have given nearly equal correlation.

Effect of speed of agitation during glycerol hydrogenolysis

The effect of external mass transfer on glycerol hydrogenolysis reaction was studied by varying the stirring speeds such as 500, 800, and 1000 rpm in an autoclave reactor over Pt-0.3STA/β-zeolite catalyst. The observed glycerol conversion results are given in Figure A.4 (I). The results showed only a small change in glycerol conversion when the stirring speed was increased from 500 to 1000 rpm.

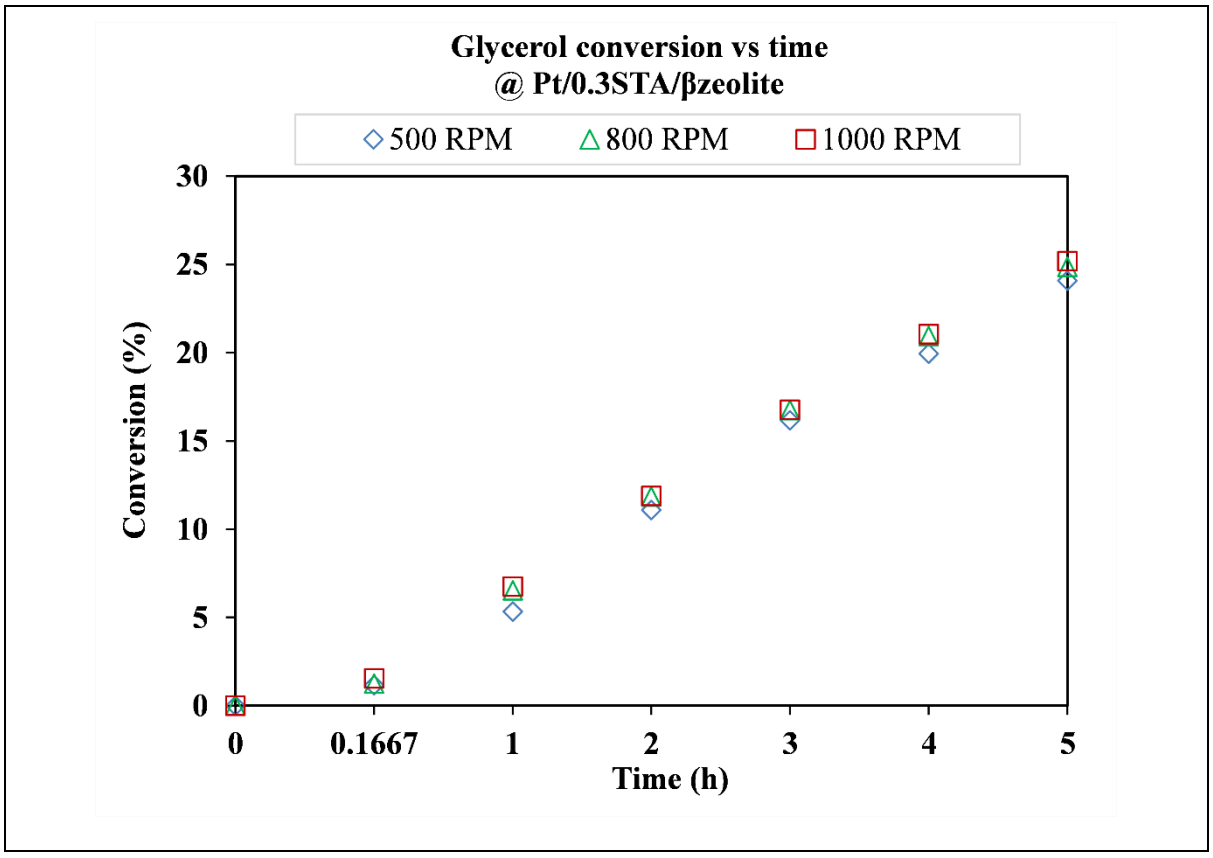

Figure A.4. Glycerol conversion vs. time profiles for glycerol hydrogenolysis at different RPM.

Internal Mass-Transport Resistance: Weisz-Prater Criterion

The effect of internal mass-transfer resistance (effect of pore-diffusion) for catalysts understudy has been investigated by calculating the W-P criterion given by Weisz and Prater (1954). The porous heterogeneous catalyst contains the active sites well distributed within their structure. The reactant molecule has to travel from the catalyst surface to the active site inside the porous network. In the case of glycerol hydrogenolysis, hydrogen has to pass from the gas phase to glycerol; and then to the catalyst surface and the pores for reaction. Here hydrogen acts as a limiting reagent. Therefore, $\Phi_{WP,i}$ have to be evaluated for hydrogen, which is given as,

$$\Phi_{WP,i} = \frac{r^{eff} . r_P^2}{C_{i,s} . D_{i,mix}^{eff}} < 0.3$$

$\Phi_{WP,i}$ (C_{WP}): dimensionless Weisz−Prater parameter;

r^{eff}: effective (observed) rate per volume of the catalyst in mol/ L.min

r^P : radius of the catalyst particle in m;

$C_{i,s,}$: concentration of *i* (H_2) at the surface of the particle in mol/L; and

$D^{eff}_{i,mix}$: effective diffusivity of *i* in the mixture in m^2/min

The value of effective (observed) rate per volume of the catalyst in mol/ L.min = 5.3587E-07 mol/ L.min.

Radius of the catalyst particle in m = 25 μm = 25E-06 m.

concentration of *i* (H_2) at the surface of the particle in mol/L = 5.43E-04 mol/L at 25 ºC.

Tortuosity (τ) = 2 to 15.

Porosity = 0.1 (assumed to be less porous)

$D^{eff}_{i,mix}$ = 2.25E-06 at τ = 2 and 3.00E-07 at τ = 15.

The value of C_{WP} was 1.27815E-07 for τ = 2 and 9.59E-07 for τ = 15.

The values are less than 1, which confirms that there are no diffusion limitations. The reaction is very slow, and thus rate is kinetically controlled.

Among all the experiments conducted, the highest rate value is taken for estimation of the Weisz−Prater criterion. The Weisz−Prater criterion's value was found to be very much less than 1. Hence for the rest of the experiments also the reaction rate is definitely controlled by intrinsic kinetics.

Confidence interval (CI) values for rate parameters with 95% confidence at different temperatures

Table A.1. Values of CI bound for 200 °C

rate constants (min^{-1})	Rate constant values		
	Lower bound	Upper bound	Actual
k_1	1.72E-04	2.00E-04	1.86E-04
k_2	7.52E-05	1.06E-04	9.32E-05
k_3	1.63E-04	1.95E-04	1.78E-04
k_4	5.66E-04	1.81E-03	1.17E-03
k_5	6.86E-04	3.66E-03	2.32E-03
k_6	3.06E-03	3.52E-03	3.31E-03
k_7	2.80E-03	4.22E-03	3.56E-03

Table A.2. Values of CI bound for 210 °C

rate constants (min^{-1})	Rate constant values		
	Lower bound	Upper bound	Actual
k_1	2.26E-04	3.03E-04	2.71E-04
k_2	7.99E-05	1.65E-04	1.32E-04
k_3	2.65E-04	3.48E-04	3.00E-04
k_4	0.00	2.15E-03	1.12E-03
k_5	0.00	4.86E-03	2.55E-03
k_6	2.99E-03	3.79E-03	3.42E-03
k_7	2.39E-03	4.65E-03	3.67E-03

Table A. 3. Values of CI bound for 220 °C

rate constants (min^{-1})	Rate constant values		
	Lower bound	Upper bound	Actual
k_1	3.22E-04	4.05E-04	3.62E-04
k_2	9.55E-05	2.07E-04	1.63E-04
k_3	4.14E-04	5.31E-04	4.61E-04
k_4	1.89E-04	2.13E-03	1.16E-03
k_5	-1.07E-03	5.81E-03	3.00E-03
k_6	3.12E-03	3.75E-03	3.53E-03
k_7	2.87E-03	4.82E-03	3.82E-03

Confidence interval (CI) values for rate parameters with 95% confidence at different pressures

Table A. 4. Values of CI bound for 10 bar H_2

rate constants (min^{-1})	Rate constant values		
	Lower bound	Upper bound	Actual
k_1	4.52E-05	1.33E-04	1.10E-04
k_2	1.69E-04	2.65E-04	2.23E-04
k_3	2.69E-04	3.72E-04	3.12E-04
k_4	-3.12E-03	2.28E-03	1.04E-03
k_5	-5.87E-05	3.63E-03	1.87E-03
k_6	3.17E-03	4.25E-03	3.45E-03
k_7	1.81E-03	4.52E-03	3.23E-03

Table A.5. Values of CI bound for at 50 bar H_2

rate constants (min^{-1})	Rate constant values		
	Lower bound	Upper bound	Actual
k_1	4.38E-04	5.15E-04	4.78E-04
k_2	1.14E-04	2.10E-04	1.68E-04
k_3	4.35E-04	5.32E-04	4.74E-04
k_4	6.41E-04	2.03E-03	1.34E-03
k_5	4.38E-04	5.44E-03	3.25E-03
k_6	3.80E-03	4.36E-03	4.09E-03
k_7	4.09E-03	5.55E-03	4.86E-03

Summary results of parametric study over Pt-0.3STA/β-zeolite catalyst

The details of the parametric study conducted over Pt-0.3STA/β-zeolite catalyst is provided in the section 6.2. Here, Table A.6 shows the summarized qualitative results. The results show that an increase in reaction temperature to greater than 220 ºC increases the rate of glycerol conversion but is undesirable from a 1,3-PDO selectivity point of view. The increase in temperature results in the formation of degradation and gaseous products with their combined selectivity > 63%. On the contrary, a decrease in reaction temperature adversely affects glycerol conversion. Hence, a compromise temperature range of 200–220 ºC seems to be optimal.

An increase in reaction (hydrogen) pressure was advantageous for both glycerol conversion and 1,3-PDO selectivity. The conversion increased by 12% and 1,3-PDO selectivity increased by 13% when the pressure was raised from 40 to 50 bar H_2 under otherwise similar conditions, thereby reducing the formation of 1,2-PDO and 1-PrOH.

Table A.6. Reaction parameter study for glycerol hydrogenolysis reaction over Pt-0.3STA/β-zeolite (qualitative)

Reaction/catalyst Parameters	Reactant conversion	Product selectivities				
	Glycerol	1,3-PDO	1,2-PDO	1-PrOH	Others	gaseous
Increase in reaction temperature (240 ºC)	✓✓	××	××	××	✓✓	✓✓
decrease in reaction temperature (200 ºC)	××	✓	✓	×	×	≈
Increase in reaction pressure (50 bar)	✓	✓	×	×	≈	≈
decrease in reaction pressure (10 bar)	××	××	✓✓	≈	≈	≈
Increase in glycerol concentration (30 wt%)	✓✓	××	×	×	✓✓	✓✓
Increase in catalyst amount (3 g)	✓✓	××	×	✓	✓	✓✓

decrease in catalyst amount (1 g)	✗✗	✗✗	✓✓	≈	✓✓	≈
Increase in platinum loading (10 wt%)	✓	✗✗	≈	✓	≈	✓
decrease in platinum loading (2.5 wt%)	✗✗	✗✗	✓✓	≈	✓	≈
Increase in reaction time (16 h)	✓✓	✗✗	✗✗	✓	✓	✓✓
decrease in reaction time (10 min)	✗✗	✓✓	✓✓	✗	✗✗	✗✗

✓ — increase in selectivity or conversion by ≤ 5% ✗ — decrease in selectivity or conversion by ≤ 5%
✓✓ — increase in selectivity or conversion by > 5% ✗✗ — decrease in selectivity or conversion by > 5%
≈ — increase in selectivity or conversion by ≥ 1.2%

Further increases in reaction pressure may also be helpful but were not explored in this study due to safety limitations. The decrease in hydrogen pressure to 10 bar resulted in decreased glycerol conversion, 1,3-PDO selectivity, and an increase in the 1,2-PDO selectivity considerably.

Another critical parameter is the concentration of glycerol in the aqueous phase. We found that an increase in glycerol concentration increases the rate of reaction, but at the cost of higher formation of others and gaseous products. A glycerol concentration of 5% w/w in water was found to be optimal.

The increase in the catalyst loading resulted in increased glycerol conversion, but 1,3-PDO selectivity decreased considerably. The increase in the catalyst amount in the reaction mixture resulted in a notable increase in 1-PrOH and gaseous products due to the over-hydrogenolysis of PDOs. Conversely, decreasing the catalyst loading resulted in lesser glycerol conversion, and 1,3-PDO selectivity also decreased significantly. Therefore, a catalyst loading of 2 g seems optimal to obtain the best yield towards 1,3 PDO.

We also found an optimum in the platinum loading on the catalyst for a given total catalyst loading in the mixture. At higher Pt loading, the formation of 1-PrOH and gaseous products were enhanced, while at lower Pt loading, 1,2-PDO formation was promoted. The batch reaction time also has a significant impact on the product distribution. At a longer reaction

time, the conversion was found to increase at the cost of forming 1-PrOH and other products. This is attributed to the over hydrogenolysis of PDOs. It is thus necessary to also restrict the reaction time to typically less than or equal to 5 hrs under the conditions of interest.

Summary results of parametric study over Pt-0.7STA/β-zeolite catalyst

Figure A.5 (bar chart) summarizes the results of the effect of parameter on glycerol hydrogenolysis using Pt-0.7STA/β-zeolite catalyst. The bar chart depicts the effect of reaction conditions/parameters on product selectivity or glycerol conversion. In this figure, the central bar (bar no 6) represents the results observed over standard reaction conditions *viz.* 220 ^{o}C, 40 bar H_2, 5 h, 2 g of 5 wt% Pt catalyst, and 80 ml of 5 wt% glycerol solution. Its left-hand and right-hand sides show the effect of decrease and increase in reaction parameters over product selectivity or glycerol conversion. The glycerol conversion roughly decreased with a decrease in parameter and increased with an increase in parameter. In this section, we will briefly describe the effects of parameters on glycerol conversion and product selectivities. A detailed parametric study on glycerol hydrogenolysis over Pt-0.7STA/β-zeolite catalyst is provided in the following section 6.2 (Chapter 6).

The results over Pt-0.7STA/β-zeolite catalyst show nearly a similar trend as we have observed over Pt-0.3STA/β-zeolite catalyst (See Table A.6). Here, the results show that an increase in reaction temperature increased the glycerol conversion. However, it has an adverse effect on 1,3-PDO selectivity. The temperature of 240 ^{o}C increased the glycerol conversion to 33.9%, but reduced the 1,3-PDO selectivity to 8.2%. Moreover, this temperature resulted in the formation of degradation and gaseous products with their combined selectivity > 66%. On the contrary, a decrease in reaction temperature adversely affects the glycerol conversion but helps in improving the 1,3-PDO selectivity. Hence, the desired temperature range is 200–220 ^{o}C.

An increase in reaction (hydrogen) pressure was advantageous for both glycerol conversion and 1,3-PDO selectivity. The conversion was increased to 30.4% and 1,3-PDO selectivity to 42.0% when the pressure was raised from 40 to 50 bar H_2 under otherwise similar conditions. Thereby reducing the formation of 1,2-PDO and 1-PrOH. Due to safety limitations, we have not explored the effect of a further increase in pressure. Contrarily, the decrease in reaction pressure to 10 bar has reduced the glycerol conversion to 18.5% and 1,3-PDO selectivity to 12.3%, resulting in an increase in selectivity of 1,2-PDO to 30.8% and 1-PrOH to 36.1%. Hence, for higher 1,3-PDO selectivity, H_2 pressure of 40 bar or higher is recommended.

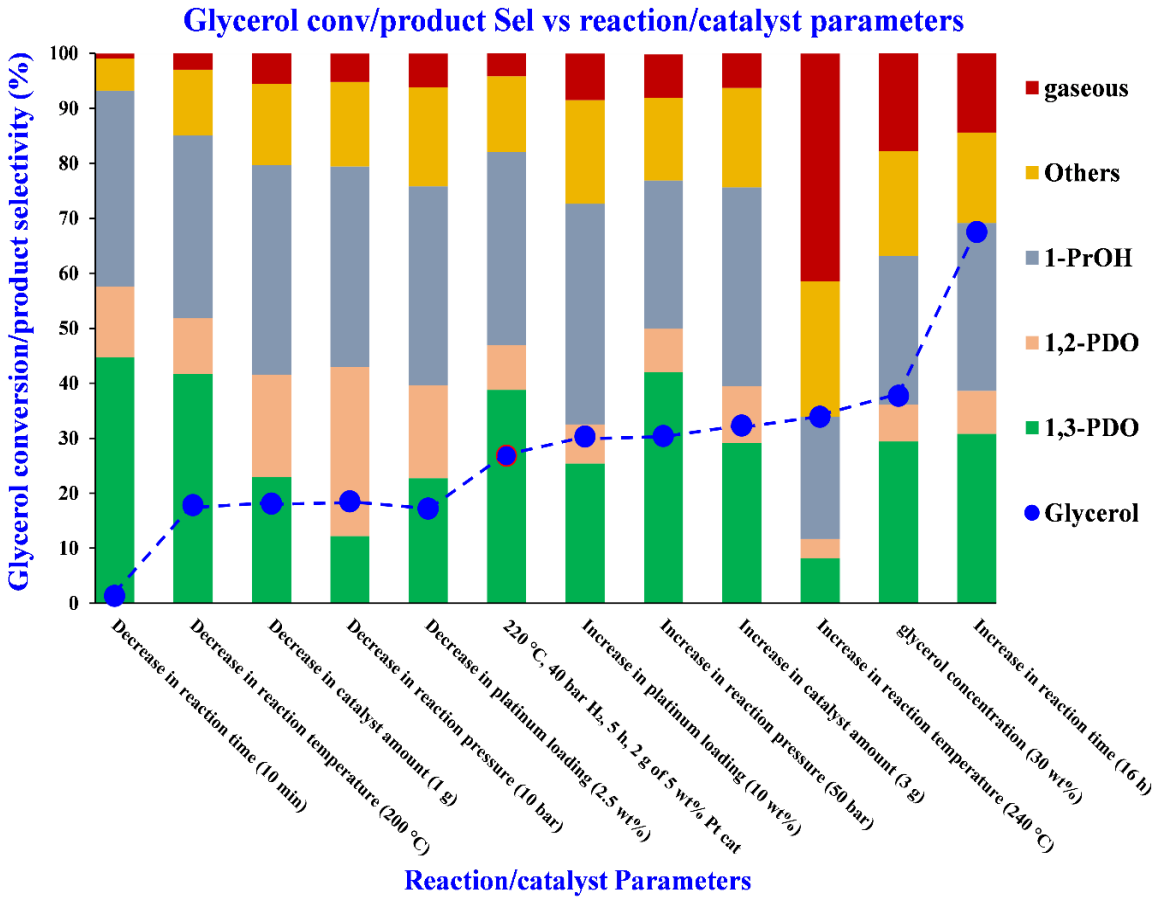

Figure A.5. Bar chart representing the effect of reaction or catalyst parameters on glycerol conversion and product selectivities.

The effect of initial glycerol concentration in the reaction mixture shows that an increase in glycerol concentration increases the rate of reaction at the cost of formation of the degradation (others) and gaseous products. The increase in glycerol initial concentration from 5 to 30 wt% increased the conversion from 26.8% to 37.7%, others from 13.8% to 19%, and gaseous products from 4.3% to 17.8%. A glycerol concentration of 5% w/w in water was found to be optimal.

The effect of an increase in catalyst loading shows that an increase or decrease in catalyst loading resulted in increasing or decreasing the glycerol conversion. However, the 1,3-PDO selectivity was decreased to 29.1% and 23.0%, with an increase or decrease in catalyst loading. Hence, a catalyst loading of 5 wt% seems optimal to obtain the best yield towards 1,3 PDO.

The effect of the platinum amount in a catalyst revealed that an increase in platinum amount resulted in increased glycerol conversion to 30.3%. Its decrease has decreased the glycerol conversion to 17.2%. At higher Pt loading, the formation of 1-PrOH, others, and gaseous

products was enhanced. While at lower Pt loadings, 1,2-PDO formation was doubled along with a slight increase in selectivities of 1-PrOH, others, and gaseous products.

The batch reaction time showed a significant impact on glycerol conversion and product selectivities. At a longer reaction time, glycerol conversion was found to increase with increase in the formation of gaseous products increasing from 4.3 (after 5 h) to 13.4% (after 16 h). This is attributed to the over hydrogenolysis of PDOs and others. Hence, it is essential to restrict the reaction time to typically less than or equal to 5 hrs under the conditions of interest.

The following section shows the detailed study on the effect of reaction/catalyst parameter on glycerol hydrogenolysis reaction over Pt-0.3STA/β-zeolite and Pt-0.7STA/β-zeolite catalysts.

Economic analysis

Here, we have made an attempt to perform some economic calculations which certainly needs an optimization. However, one can take it as a basic and perform the detailed techno-economic analysis.

Basis: - Synthesis of 1,3-propanediol using 30 wt% aqueous glycerol solutions with 5%Pt/0.7STA/β-zeolite catalyst.

Glycerol concentration = 30 wt%

Reaction temperature = 220 °C

Reaction pressure = 50 bar hydrogen (H_2)

Glycerol conversion after 5 h of reaction = 37.7%

Catalyst required = 2.5 wt% of reaction mixture

The main product of the reaction is 1,3-propanediol and 1,2-propanediol.

Market price of 1,3-propanediol in Rs per kg = 200 Rs/kg (Source: - Market Prospecting and Assessment of the Economic Potential of Glycerol from Biodiesel)

Market price of glycerol in Rs per kg = 12.8 Rs/kg (Source: - Market Prospecting and Assessment of the Economic Potential of Glycerol from Biodiesel)

Market price of 1,2-propanediol in Rs per kg = 90 Rs/kg (Source: - Chemical Weekly)

Market price of hydrogen (H_2) in Rs per kg = 50 Rs/kg (Source: - Sunlight gas Pvt Ltd, India)

Catalyst cost = 1,13,701.1173 Rs/kg (Source: - Indiamart)

Catalyst life = 150 h (30 times recyclable) (Assumed)

Assumed glycerol processing rate in kg per h = 4040 kg/h

Solvent (water) processing rate in kg per h = 9437 kg/h

Amount of H_2 consumed in kg per h = 57.1 kg/h

Catalyst required in kg per h (2.5 wt% of reaction mixture) = 0.025 x (4040 + 9437) kg/h

= 337 kg/h.

Catalyst is usable for up to 150 h, then to maintain its activity, 0.5% of the catalyst's total cost is required **(Assumed)**. This make-up cost (0.5% of total catalyst cost) is considered the working capital or raw material cost.

Table A.7. Product stream composition from the reactor

Product stream	**Product selectivity (fraction)**	**Product formed mole/h**	**Product formed kg/h**
Water (solvent)	--	--	9436.7105
Water (formed)	--	29.31	527.653
Unreacted Glycerol	--	--	2516.880
1,3-propanediol (Target product)	0.294	4.869	370.017
1,2-Propanediol (Target product)	0.067	1.110	84.324
1-PrOH	0.271	4.488	269.266
Ethanol	0.047	0.775	35.670
Methanol	0.094	1.561	49.967
Acetone	0.022	0.370	21.446
2-Propanol	0.027	0.440	26.384
Gases	0.178	2.948	129.698
Total (Product formed)	1.000	16.560	986.771
Total (Stream mass)			13468.014

The separable products from Table A.7 are 1,3-propanediol and 1,2-propanediol. Rest of the products have a boiling point of less than 100 °C and a few of them form an azeotrope with water (like ethanol-water or 1-propanol-water) which makes the distillation of these products

difficult. Therefore, the targeted products from the Table 1 are 1,3-propanediol and 1,2-propanediol.

Now,

1,3-propanediol produced per h = 370 kg/h.

1,2-propanediol produced per h = 84 kg/h.

Revenue generated after selling 370 kg/h of 1,3-propanediol =

= 370 x 200 = 74000 Rs/h.

Revenue generated after selling 84 kg/h of 1,2-propanediol =

= 84 x 90 = 7560 Rs/h.

Total revenue generated from both the products = 81560 Rs/h.

Raw material cost includes the cost of glycerol consumed, cost of hydrogen consumption, and cost of catalyst required per h.

Cost of glycerol consumption per h = 19500.8 Rs/h.

Cost of H_2 consumption per h = 2855 Rs/h.

Cost of catalyst consumption per h =

Total cost of Raw material consumption per h = 19500.8 + 2855

Total Raw material cost (without catalyst) in Rs per h = 19500.8 + 2855 = 22355.8 Rs/h.

Total Raw material cost (with catalyst) in Rs per h = 22355.8 + 337 x 113701 x 0.005

= 2,13,942 Rs/h

The process seems industrially feasible without the catalyst. However, even with the use of 0.5% catalyst make-up cost (in raw material), the given process seems unfeasible industrially.

Furthermore, while with the yields obtained in the work and the given raw material and product prices, the route shows a promising economic potential, one may need to work on process simulation and optimization to work out the minimum energy consumption. The separation of 1,2-propanediol and 1,3-propanediol is challenging. Our preliminary analysis indicates that the major cost may come from energy required in downstream processing. Hence, for detailed techno-economic analysis, one may need to work on this aspect carefully.

In the following section we have made an attempt to estimate the energy cost **using Aspen simulation**. These costs need further fine-tuning (optimization) to come up with a final techno-economic analysis.

Basis: - Here, a biodiesel plant of capacity 200 kiloton per year was assumed which produces 20 kiloton of glycerol per year. The following section shows the performed calculations.

Table A.8. Plant details for 200 kilotons of biodiesel produced per year (glycerol produced 20 kilotons per year)

On weight Basis			
Attributes	**Capacity/ values**	**Unit**	**Source**
Biodiesel Plant Capacity per year	200	kilotons	Assumed
Glycerol produced per year	20	kilotons	Calculated
Plant operation	330	days	Assumed
Plant life	10	years	Assumed
Plant daily operation	24	24	Assumed
Number of batches	3	--	--
Downtime	3	h	--
Reaction time	5	h	--
Plant charges [Fixed capital investment (FCI)]	--	Rs	--
Depreciation method	Straight line	--	(Green and Perry, 2008)
Depreciation Period	10	years	Assumed
Salvage value	10 % of FCI	%	--
Income tax	25	%	www.incometaxindia.gov.in
Discount rate	10	%	Arora et al., 2018
Inflation rate	4	%	Arora et al., 2018
Glycerol produced per day	60.606	tons	--
Glycerol process rate kg/h	4040.4	kg/h	--
Stream flowrate with 30 wt% glycerol kg/h	13468.0135	kg/h	--

Separation flow sheet: -

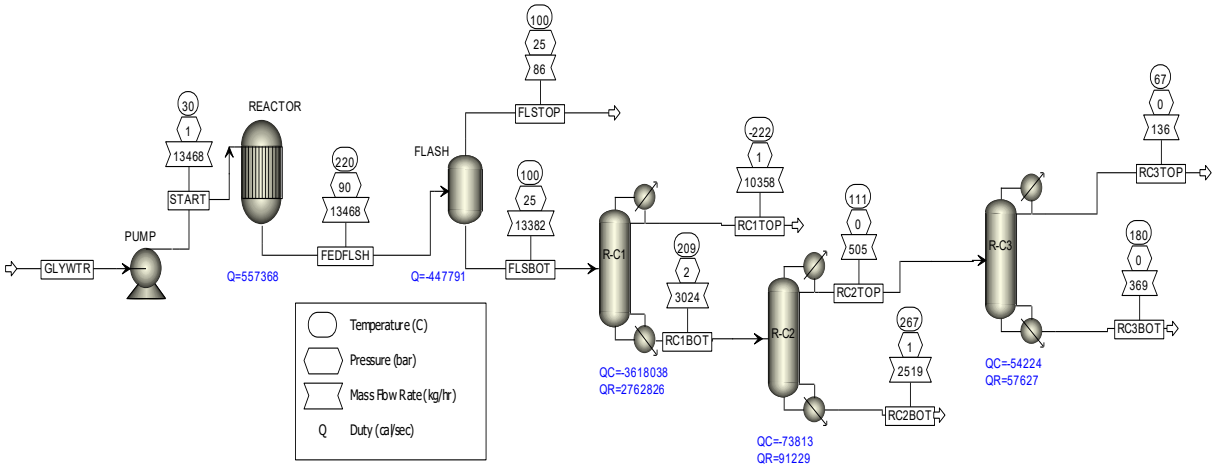

Figure A.6. A rough process flow sheet of the 1,3-propanediol production route

Table A.9. Stream composition from each equipment

Products	Unit	Feed to flash column	Flash Bottom	Flash Top	RC-1 Bottom	RC-1 Top	RC-2 Bottom	RC-2 Top	RC-3 Bottom	RC-2 Top
Total Mass Flows	kg/h	13468.10	13382.17	85.93	3024.37	10357.80	2519.3	505.07	368.70	136.37
Ethanol	kg/h	49.96	49.60	0.36	0.00	49.60	0.00	0.00	0.00	0.00
Methanol	kg/h	35.67	35.50	0.17	0.00	35.50	0.00	0.00	0.00	0.00
Acetone	kg/h	21.50	21.34	0.16	0.00	21.34	0.00	0.00	0.00	0.00
1-propanol	kg/h	269.30	268.65	0.65	0.67	267.99	0.00	0.67	0.00	0.67
Iso-propanol	kg/h	26.40	26.29	0.11	0.00	26.29	0.00	0.00	0.00	0.00
1,2-propanediol	kg/h	84.30	84.29	0.01	84.29	0.00	0.00	84.29	1.81	82.48
1,3-propanediol	kg/h	370.00	369.99	0.01	369.99	0.00	2.40	367.59	366.89	0.69
glycerol	kg/h	2516.89	2516.89	0.00	2516.89	0.00	2516.9	0.00	0.00	0.00
water	kg/h	9907.28	9886.41	20.87	52.52	9833.89	0.00	52.52	0.00	52.52
hydrogen	kg/h	57.10	0.00	57.10	0.00	0.00	0.00	0.00	0.00	0.00
propane	kg/h	129.70	123.19	6.51	0.00	123.19	0.00	0.00	0.00	0.00

1,3-propanediol produced = 369 kg/h with 99.4% purity.

Raw material cost (without catalyst) and revenue generated from selling the product: -

Revenue generated after selling 369 kg/h of 1,3-propanediol =

= 369 x 200 = **73800 Rs/h.**

Revenue generated after selling 82.5 kg/h of 1,2-propanediol =

= 82.5 x 90 = **7425 Rs/h.**

Raw material cost

Cost of glycerol + cost of hydrogen consumed per h = **22356 Rs/h.**

Energy cost required to purify 1,3-propanediol per h: -

Figure A.6 shows the process of 1,3-propanediol production from glycerol. In this process, the heat energy needs to be supplied to the reactor, distillation columns 1, 2, and 3. Moreover, the heat needs to be removed from the flash column, distillation columns 1, 2, and 3.

Industrially,

Medium pressure steam for heating costs = 2 Rs/kg

And Cooling water costs = 0.25 (25 paise) Rs/kg

Cost of heating: -

Amount of heat required for a **reactor** to reach temperature of 220 °C = 557368 cal/sec

Amount of steam required to heat the **reactor** to 220 °C = 2992.3 kg/h

Cost of steam required to heat the **reactor** to 220 °C = 5984.3 Rs/h

Amount of heat required in a **RadFrac column 1** = 2762826 cal/sec

Amount of steam required in **RadFrac column 1** reboiler = 14870.4 kg/h

Cost of steam required to heat the **RadFrac column 1** reboiler = 29470.7 Rs/h

Amount of heat required in a **RadFrac column 2** = 91229 cal/sec

Amount of steam required in **RadFrac column 2** reboiler = 496.3 kg/h

Cost of steam required to heat the **RadFrac column 2** reboiler = 992.5 Rs/h

Amount of heat required in a **RadFrac column 3** = 57627 cal/sec

Amount of steam required in **RadFrac column 3** reboiler = 310.6 kg/h

Cost of steam required to heat the **RadFrac column 3** reboiler = 621.2 Rs/h

The **total** cost of **heating** energy required (from flow sheet) = 37338.9 Rs/h

Cost of cooling: -

Amount of cooling required for a **flash column** = 447791 cal/sec

Amount of cooling water required in a **flash column** = 85747.2 kg/h

Cost of cooling water required in a **flash column** = 21436.8 Rs/h

Amount of cooling required in a condenser of **RadFrac column 1** = 3618038 cal/sec

Amount of cooling water required in a condenser of **RadFrac column 1** = 692815.8 kg/h

Cost of cooling water required in a condenser of **RadFrac column 1** = 173203.9 Rs/h

Amount of cooling required in a condenser of **RadFrac column 2** = 73813 cal/sec

Amount of cooling water required in a condenser of **RadFrac column 2** = 14134.4 kg/h

Cost of cooling water required in a condenser of **RadFrac column 2** = 3533.6 Rs/h

Amount of cooling required in a condenser of **RadFrac column 3** = 54224 cal/sec

Amount of cooling water required in a condenser of **RadFrac column 3** = 10383.3 kg/h

Cost of cooling water required in a condenser of **RadFrac column 3** = 2595.83 Rs/h

The **total** cost of **cooling** water required (from flow sheet) = 200770.2 Rs/h

Now,

Profit/loss gained per h = 73800 – 22356 – 38331.5 – 200770.2 = - 1,87,657.7 Rs/h (without catalyst).

The analysis shows that the energy cost for separation is coming to be very large probably due to distillation and cooling of huge amount of water. This cost analysis needs the further optimization. The distillation (RadFrac) column 1 shows a distillate temperature of -222 °C, in practice we may not required to cool the distillate of column 1 to -222 °C. However, there will be some cost associated for cooling the distillate from column 1. One needs to optimize it in order to come up with a final techno-economic analysis. Here, we have just made an attempt to check what would be the rough estimate for energy requirements.

The result concludes that without even considering the cost of catalyst (which is expensive), the given process of 1,3-propanediol synthesis seems industrially unfeasible. The higher 1,3-propanediol yield and higher glycerol concentration (less quantity of water) probably make this process industrially feasible.

References

[1] D. Singh, D. Sharma, S.L. Soni, S. Sharma, P. Kumar Sharma, A. Jhalani, A review on feedstocks, production processes, and yield for different generations of biodiesel, Fuel. 262 (2020) 116553. https://doi.org/10.1016/j.fuel.2019.116553.

[2] I.B. Banković-Ilić, O.S. Stamenković, V.B. Veljković, Biodiesel production from non-edible plant oils, Renew. Sustain. Energy Rev. 16 (2012) 3621–3647. https://doi.org/10.1016/j.rser.2012.03.002.

[3] CIA Fact Book, No Title, 2016.

[4] S. Machado Corrêa, G. Arbilla, Carbonyl emissions in diesel and biodiesel exhaust, Atmos. Environ. 42 (2008) 769–775. https://doi.org/10.1016/j.atmosenv.2007.09.073.

[5] J. Chang, D.Y.C. Leung, C.Z. Wu, Z.H. Yuan, A review on the energy production, consumption, and prospect of renewable energy in China, Renew. Sustain. Energy Rev. 7 (2003) 453–468. https://doi.org/10.1016/S1364-0321(03)00065-0.

[6] U.K. Mirza, N. Ahmad, T. Majeed, An overview of biomass energy utilization in Pakistan, Renew. Sustain. Energy Rev. 12 (2008) 1988–1996. https://doi.org/10.1016/j.rser.2007.04.001.

[7] OECD/IEA, Key World Energy Statistics 2016, International Energy Agency, Peris, Int. Energy Agency, Peris. (2016) 1–77. http://www.indiaenvironmentportal.org.in/files/file/EnergyStatistics2016.pdf http://www.iea.org/statistics/statisticssearch/.

[8] M.N. Nabi, M.M. Rahman, M.S. Akhter, Biodiesel from cotton seed oil and its effect on engine performance and exhaust emissions, Appl. Therm. Eng. 29 (2009) 2265–2270. https://doi.org/10.1016/j.applthermaleng.2008.11.009.

[9] M. Kouzu, J.S. Hidaka, Transesterification of vegetable oil into biodiesel catalyzed by CaO: A review, Fuel. 93 (2012) 1–12. https://doi.org/10.1016/j.fuel.2011.09.015.

[10] O.S. Stamenković, A. V. Veličković, V.B. Veljković, The production of biodiesel from vegetable oils by ethanolysis: Current state and perspectives, Fuel. 90 (2011) 3141–3155. https://doi.org/10.1016/j.fuel.2011.06.049.

[11] A. Demirbas, Progress and recent trends in biodiesel fuels, Energy Convers. Manag. 50 (2009) 14–34. https://doi.org/10.1016/j.enconman.2008.09.001.

[12] A.K. Azad, M.M.K. Khan, T. Ahasan, S.F. Ahmed, Energy Scenario: Production, Consumption and Prospect of Renewable Energy in Australia, J. Power Energy Eng. 02 (2014) 19–25. https://doi.org/10.4236/jpee.2014.24004.

[13] C. Biofuels, Recensione: OECD-FAO Agricultural Outlook 2008-2017, Econ. Dirit. Agroaliment. (2018) 191–206. https://doi.org//10.1787/agr-outl-data-en.

[14] A.H. Hazimah, T.L. Ooi, A. Salmiah, Recovery of Glycerol and Diglycerol From Glycerol Pitch Recovery of Glycerol and Diglycerol From Glycerol Pitch, J. Oil Palm Res. 15 (2003) 1–5.

[15] M. Pagliaro, R. Ciriminna, H. Kimura, M. Rossi, C. Della Pina, Recent advances in the conversion of bioglycerol into value-added products, Eur. J. Lipid Sci. Technol. 111 (2009) 788–799. https://doi.org/10.1002/ejlt.200800210.

[16] M. Ayoub, A.Z. Abdullah, Critical review on the current scenario and significance of crude glycerol resulting from biodiesel industry towards more sustainable renewable energy industry, Renew. Sustain. Energy Rev. 16 (2012) 2671–2686. https://doi.org/10.1016/j.rser.2012.01.054.

[17] L. Wang, W. Du, D. Liu, L. Li, N. Dai, Lipase-catalyzed biodiesel production from soybean oil deodorizer distillate with absorbent present in tert-butanol system, J. Mol. Catal. B Enzym. 43 (2006) 29–32. https://doi.org/10.1016/j.molcatb.2006.03.005.

[18] P. Kenkel, R. Holcomb, Proceedings of a conference Feasibility of On-Farm or Small Scale Oilseed Processing and Biodiesel Production Background, (2008). https://ageconsearch.umn.edu/bitstream/48710/2/Feasibility of On-Farm or Small Scale.pdf.

[19] D. Baldwin, 2018 Glycerine Structural Shift, (2018) 1–42.

[20] F. Yang, M. a Hanna, R. Sun, Value-added uses for crude glycerol--a byproduct of biodiesel production, Biotechnol. Biofuels. 5 (2012) 13. https://doi.org/10.1186/1754-6834-5-13.

[21] C.S.S. Lee, M.K.K. Aroua, W.M. a. W.M.A.W. Daud, P. Cognet, Y. Pérès-Lucchese, P.-L.L. Fabre, O. Reynes, L. Latapie, A review: Conversion of bioglycerol into 1,3-propanediol via biological and chemical method, Renew. Sustain. Energy Rev. 42

(2015) 235–244. https://doi.org/10.1016/j.rser.2014.10.033.

[22] Z. Yuan, L. Wang, J. Wang, S. Xia, P. Chen, Z. Hou, X. Zheng, Hydrogenolysis of glycerol over homogenously dispersed copper on solid base catalysts, Appl. Catal. B Environ. 101 (2011) 431–440. https://doi.org/10.1016/j.apcatb.2010.10.013.

[23] C.J.A. Mota, B.P. Pinto, A.L. de Lima, Glycerol: A Versatile Renewable Feedstock for the Chemical Industry, Springer International Publishing, 2017. https://doi.org/10.1007/978-3-319-59375-3.

[24] S. Huang, S. Liu, Q. Zhu, X. Zhu, W. Xin, H. Liu, Z. Feng, C. Li, S. Xie, Q. Wang, L. Xu, The effect of calcination time on the activity of WO_3/Al_2O_3/HY catalysts for the metathesis reaction between ethene and 2-butene, Appl. Catal. A Gen. 323 (2007) 94–103. https://doi.org/10.1016/j.apcata.2007.02.004.

[25] B. News, 16 Januar 2015 1,3-Propanediol (PDO) Market by Applications (PTT, Polyurethane, Cosmetic, Personal Care & Home Cleaning & Others) & Geography – Global Market Trends & Forecasts to 2021, (n.d.).

[26] K. Wang, M.C. Hawley, S.J. DeAthos, Conversion of glycerol to 1,3-propanediol via selective dehydroxylation, Ind. Eng. Chem. Res. 42 (2003) 2913–2923. https://doi.org/10.1021/ie020754h.

[27] G.A. Kraus, Synthetic methods for the preparation of 1,3-propanediol, Clean - Soil, Air, Water. 36 (2008) 648–651. https://doi.org/10.1002/clen.200800084.

[28] J. V. Kurian, A new polymer platform for the future - Sorona® from corn derived 1,3-propanediol, J. Polym. Environ. 13 (2005) 159–167. https://doi.org/10.1007/s10924-005-2947-7.

[29] Grand View Research Inc. http://www.grandviewresearch.com/industry-analysis/3d-bioprinting-market, Mark. Res. Rep. Report ID: (2016) 110.

[30] Marketsandmarkets 1,3-Propanediol (PDO) Market worth $870 million by 2024 https://www.marketsandmarkets.com/PressReleases/1-3-propanediol-pdo.asp, (n.d.).

[31] M. Pagliaro, R. Ciriminna, H. Kimura, M. Rossi, C. Della Pina, From glycerol to value-added products, Angew. Chemie - Int. Ed. 46 (2007) 4434–4440. https://doi.org/10.1002/anie.200604694.

[32] R. Dobson, V. Gray, K. Rumbold, Microbial utilization of crude glycerol for the

production of value-added products, J. Ind. Microbiol. Biotechnol. 39 (2012) 217–226. https://doi.org/10.1007/s10295-011-1038-0.

[33] X. Chen, D.J. Zhang, W.T. Qi, S.J. Gao, Z.L. Xiu, P. Xu, Microbial fed-batch production of 1,3-propanediol by Klebsiella pneumoniae under micro-aerobic conditions, Appl. Microbiol. Biotechnol. 63 (2003) 143–146. https://doi.org/10.1007/s00253-003-1369-5.

[34] G. Yang, J. Tian, J. Li, Fermentation of 1,3-propanediol by a lactate deficient mutant of Klebsiella oxytoca under microaerobic conditions, Appl. Microbiol. Biotechnol. 73 (2007) 1017–1024. https://doi.org/10.1007/s00253-006-0563-7.

[35] H.J. Liu, D.J. Zhang, Y.H. Xu, Y. Mu, Y.Q. Sun, Z.L. Xiu, Microbial production of 1,3-propanediol from glycerol by Klebsiella pneumoniae under micro-aerobic conditions up to a pilot scale, Biotechnol. Lett. 29 (2007) 1281–1285. https://doi.org/10.1007/s10529-007-9398-2.

[36] Y. Zhang, Y. Li, C. Du, M. Liu, Z. Cao, Inactivation of aldehyde dehydrogenase: A key factor for engineering 1,3-propanediol production by Klebsiella pneumoniae, Metab. Eng. 8 (2006) 578–586. https://doi.org/10.1016/j.ymben.2006.05.008.

[37] Y.Z. Xu, N.N. Guo, Z.M. Zheng, X.J. Ou, H.J. Liu, D.H. Liu, Metabolism in 1,3-propanediol fed-batch fermentation by a D-lactate deficient mutant of Klebsiella pneumoniae, Biotechnol. Bioeng. 104 (2009) 965–972. https://doi.org/10.1002/bit.22455.

[38] C.H.H.C. Zhou, J.N. Beltramini, Y.-X. Fan, G.Q.M. Lu, Chemoselective catalytic conversion of glycerol as a biorenewable source to valuable commodity chemicals., Chem. Soc. Rev. 37 (2008) 527–549. https://doi.org/10.1039/b707343g.

[39] I. Gandarias, J. Requies, P.L. Arias, U. Armbruster, A. Martin, Liquid-phase glycerol hydrogenolysis by formic acid over Ni-Cu/Al_2O_3 catalysts, J. Catal. 290 (2012) 79–89. https://doi.org/10.1016/j.jcat.2012.03.004.

[40] M. Akiyama, S. Sato, R. Takahashi, K. Inui, M. Yokota, Dehydration-hydrogenation of glycerol into 1,2-propanediol at ambient hydrogen pressure, Appl. Catal. A Gen. 371 (2009) 60–66. https://doi.org/10.1016/j.apcata.2009.09.029.

[41] M.R. Nimlos, S.J. Blanksby, X. Qian, M.E. Himmel, D.K. Johnson, Mechanisms of glycerol dehydration, J. Phys. Chem. A. 110 (2006) 6145–6156. https://doi.org/10.1021/jp060597q.

[42] T.M. Che, Production of propanediols., US4642394A, 1987.

[43] W. Jager, E. Drent, Hydrogenolysis of glycerol, US6080898A, 1998.

[44] M. Schlaf, P. Ghosh, P.J. Fagan, E. Hauptman, R.M. Bullock, R. Morris Bullock, Metal-catalyzed selective deoxygenation of diols to alcohols, Angew. Chemie - Int. Ed. 40 (2001) 3887–3890. https://doi.org/10.1002/1521-3773(20011015)40:20 3887::AID-ANIE38873.0.CO;2-Q.

[45] A. Alhanash, E.F. Kozhevnikova, I. V. Kozhevnikov, Gas-phase dehydration of glycerol to acrolein catalysed by caesium heteropoly salt, Appl. Catal. A Gen. 378 (2010) 11–18. https://doi.org/10.1016/j.apcata.2010.01.043.

[46] J. Chaminand, L. auren. A. Djakovitch, P. Gallezot, P. Marion, C. Pinel, C.C. Rosier, Glycerol hydrogenolysis on heterogeneous catalysts, Green Chem. 6 (2004) 359–361. https://doi.org/10.1039/b407378a.

[47] J. Oh, S. Dash, H. Lee, Selective conversion of glycerol to 1,3-propanediol using Pt-sulfated zirconia, Green Chem. 13 (2011) 2004–2007. https://doi.org/10.1039/c1gc15263g.

[48] Y. Nakagawa, Y. Shinmi, S. Koso, K. Tomishige, Direct hydrogenolysis of glycerol into 1,3-propanediol over rhenium-modified iridium catalyst, J. Catal. 272 (2010) 191–194. https://doi.org/10.1016/j.jcat.2010.04.009.

[49] S. Panyad, S. Jongpatiwut, T. Sreethawong, T. Rirksomboon, S. Osuwan, Catalytic dehydroxylation of glycerol to propylene glycol over Cu-ZnO/Al_2O_3 catalysts: Effects of catalyst preparation and deactivation, Catal. Today. 174 (2011) 59–64. https://doi.org/10.1016/j.cattod.2011.03.029.

[50] A. Kant, Y. He, A. Jawad, X. Li, F. Rezaei, J.D. Smith, A.A. Rownaghi, Hydrogenolysis of glycerol over Ni, Cu, Zn, and Zr supported on H-beta, Chem. Eng. J. 317 (2017) 1–8. https://doi.org/10.1016/j.cej.2017.02.064.

[51] Y.-W.L. and Z.-Y.Z. Long Huang, Yu-Lei Zhu, Hong-Yan Zheng, Continuous production of 1,2-propanediol by the selective hydrogenolysis of solvent-free glycerol under mild conditions, J. Chem. Technol. Biotechnol. 83 (2008) 1163–1169. https://doi.org/10.1002/jctb.

[52] O. Gómez-Jiménez-Aberasturi, J.R. Ochoa-Gómez, New approaches to producing polyols from biomass, J. Chem. Technol. Biotechnol. 92 (2017) 705–711.

https://doi.org/10.1002/jctb.5149.

[53] M.R. Nanda, Z. Yuan, W. Qin, C. (Charles) Xu, Recent advancements in catalytic conversion of glycerol into propylene glycol: A review, Catal. Rev. - Sci. Eng. 58 (2016) 309–336. https://doi.org/10.1080/01614940.2016.1166005.

[54] M. Lee, Y.K. Hwang, J.S. Chang, H.J. Chae, D.W. Hwang, Vapor-phase hydrogenolysis of glycerol to 1,2-propanediol using a chromium-free Ni-Cu-SiO_2 nanocomposite catalyst, Catal. Commun. 84 (2016) 5–10. https://doi.org/10.1016/j.catcom.2016.05.022.

[55] N. Ueda, Y. Nakagawa, K. Tomishige, Conversion of glycerol to ethylene glycol over Pt-modified Ni catalyst, Chem. Lett. 39 (2010) 506–507. https://doi.org/10.1246/cl.2010.506.

[56] R. V. Sharma, P. Kumar, A.K. Dalai, Selective hydrogenolysis of glycerol to propylene glycol by using Cu:Zn:Cr:Zr mixed metal oxides catalyst, Appl. Catal. A Gen. 477 (2014) 147–156. https://doi.org/10.1016/j.apcata.2014.03.007.

[57] M.S. Ardi, M.K. Aroua, N.A. Hashim, Progress, prospect and challenges in glycerol purification process: A review, Renew. Sustain. Energy Rev. 42 (2015) 1164–1173. https://doi.org/10.1016/j.rser.2014.10.091.

[58] S. Zhu, X. Gao, Y. Zhu, Y. Zhu, H. Zheng, Y. Li, Promoting effect of boron oxide on Cu/SiO_2 catalyst for glycerol hydrogenolysis to 1,2-propanediol, J. Catal. 303 (2013) 70–79. https://doi.org/10.1016/j.jcat.2013.03.018.

[59] Z. Huang, H. Liu, F. Cui, J. Zuo, J. Chen, C. Xia, Effects of the precipitation agents and rare earth additives on the structure and catalytic performance in glycerol hydrogenolysis of Cu/SiO_2 catalysts prepared by precipitation-gel method, Catal. Today. 234 (2014) 223–232. https://doi.org/10.1016/j.cattod.2014.02.037.

[60] S. Zhu, X. Gao, Y. Zhu, W. Fan, J. Wang, Y. Li, A highly efficient and robust Cu/SiO_2 catalyst prepared by the ammonia evaporation hydrothermal method for glycerol hydrogenolysis to 1,2-propanediol, Catal. Sci. Technol. 5 (2015) 1169–1180. https://doi.org/10.1039/c4cy01148a.

[61] L. Gong, Y. Lü, Y. Ding, R. Lin, J. Li, W. Dong, T. Wang, W. Chen, Solvent effect on selective dehydroxylation of glycerol to 1,3-propanediol over a Pt/WO_3/ZrO_2 catalyst, Cuihua Xuebao/Chinese J. Catal. 30 (2009) 1189–1191. https://doi.org/10.1016/s1872-

2067(08)60142-4.

[62] Y. Nakagawa, X. Ning, Y. Amada, K. Tomishige, Solid acid co-catalyst for the hydrogenolysis of glycerol to 1,3-propanediol over Ir-ReO_x/SiO_2, Appl. Catal. A Gen. 433–434 (2012) 128–134. https://doi.org/10.1016/j.apcata.2012.05.009.

[63] Y. Amada, Y. Shinmi, S. Koso, T. Kubota, Y. Nakagawa, K. Tomishige, Reaction mechanism of the glycerol hydrogenolysis to 1,3-propanediol over Ir-ReO_x/SiO_2 catalyst, Appl. Catal. B Environ. 105 (2011) 117–127. https://doi.org/10.1016/j.apcatb.2011.04.001.

[64] S. Koso, H. Watanabe, K. Okumura, Y. Nakagawa, K. Tomishige, Comparative study of Rh-MoO_x and Rh-ReO_x supported on SiO_2 for the hydrogenolysis of ethers and polyols, Appl. Catal. B Environ. 111–112 (2012) 27–37. https://doi.org/10.1016/j.apcatb.2011.09.015.

[65] Y. Amada, H. Watanabe, M. Tamura, Y. Nakagawa, K. Okumura, K. Tomishige, Structure of ReO_x clusters attached on the Ir metal surface in Ir-ReO_x/SiO_2 for the hydrogenolysis reaction, J. Phys. Chem. C. 116 (2012) 23503–23514. https://doi.org/10.1021/jp308527f.

[66] M. Tamura, Y. Amada, S. Liu, Z. Yuan, Y. Nakagawa, K. Tomishige, Promoting effect of Ru on Ir-ReO_x/SiO_2 catalyst in hydrogenolysis of glycerol, J. Mol. Catal. A Chem. 388–389 (2014) 177–187. https://doi.org/10.1016/j.molcata.2013.09.015.

[67] J. Feng, B. Xu, Reaction mechanisms for the heterogeneous hydrogenolysis of biomass-derived glycerol to propanediols, Prog. React. Kinet. Mech. 39 (2014) 1–15. https://doi.org/10.3184/97809059274714X13874723178485.

[68] S. Koso, Y. Nakagawa, K. Tomishige, Mechanism of the hydrogenolysis of ethers over silica-supported rhodium catalyst modified with rhenium oxide, J. Catal. 280 (2011) 221–229. https://doi.org/10.1016/j.jcat.2011.03.018.

[69] S. Koso, H. Watanabe, K. Okumura, Y. Nakagawa, K. Tomishige, Stable low-valence ReO_x cluster attached on Rh metal particles formed by hydrogen reduction and its formation mechanism, J. Phys. Chem. C. 116 (2012) 3079–3090. https://doi.org/10.1021/jp2114225.

[70] A. Shimao, S. Koso, N. Ueda, Y. Shinmi, I. Furikado, K. Tomishige, Promoting Effect of Re Addition to Rh/SiO_2 on Glycerol Hydrogenolysis, Chem. Lett. 38 (2009) 540–

541. https://doi.org/10.1246/cl.2009.540.

[71] Y. Shinmi, S. Koso, T. Kubota, Y. Nakagawa, K. Tomishige, Modification of Rh/SiO_2 catalyst for the hydrogenolysis of glycerol in water, Appl. Catal. B Environ. 94 (2010) 318–326. https://doi.org/10.1016/j.apcatb.2009.11.021.

[72] Y. Amada, S. Koso, Y. Nakagawa, K. Tomishige, Hydrogenolysis of 1,2-propanediol for the production of biopropanols from glycerol, ChemSusChem. 3 (2010) 728–736. https://doi.org/10.1002/cssc.201000040.

[73] T. Kurosaka, H. Maruyama, I. Naribayashi, Y. Sasaki, Production of 1,3-propanediol by hydrogenolysis of glycerol catalyzed by $Pt/WO_3/ZrO_2$, Catal. Commun. 9 (2008) 1360–1363. https://doi.org/10.1016/j.catcom.2007.11.034.

[74] R. Arundhathi, T. Mizugaki, T. Mitsudome, K. Jitsukawa, K. Kaneda, Highly selective hydrogenolysis of glycerol to 1,3-propanediol over a boehmite-supported platinum/tungsten catalyst, ChemSusChem. 6 (2013) 1345–1347. https://doi.org/10.1002/cssc.201300196.

[75] X. Zhao, J. Wang, M. Yang, N. Lei, L. Li, B. Hou, S. Miao, X. Pan, A. Wang, T. Zhang, Selective Hydrogenolysis of Glycerol to 1,3-Propanediol: Manipulating the Frustrated Lewis Pairs by Introducing Gold to Pt/WO_x, ChemSusChem. 10 (2017) 819–824. https://doi.org/10.1002/cssc.201601503.

[76] T. Okuhara, N. Mizuno, M. Misono, Catalytic Chemistry of Heteropoly Compounds, Adv. Catal. 41 (1996) 113–252. https://doi.org/10.1016/S0360-0564(08)60041-3.

[77] C.L. Hill, Progress and challenges in polyoxometalate-based catalysis and catalytic materials chemistry, J. Mol. Catal. A Chem. 262 (2007) 2–6. https://doi.org/10.1016/j.molcata.2006.08.042.

[78] M.T. Pope, A. Müller, Polyoxometalates: From Platonic Solids to Anti-Retroviral Activity: From Platonic Solids to Anti-Retroviral Activity, Kluwer Academic Publishers, Dordrecht, The Netherlands, 1994. https://www.google.com/search?q=dordrecht&rlz=1C1CHBF_enIN918IN918&oq=Dordrecht&aqs=chrome.0.0i355j46l2j0l3j69i60l2.896j0j7&sourceid=chrome&ie=UTF-8.

[79] I. V. Kozhevnikov, Catalysis by heteropoly acids and multicomponent polyoxometalates in liquid-phase reactions, Chem. Rev. 98 (1998) 171–198. https://doi.org/10.1021/cr960400y.

[80] L. Liu, B. Wang, Y. Du, A. Borgna, Supported $H_4SiW_{12}O_{40}/Al_2O_3$ solid acid catalysts for dehydration of glycerol to acrolein: Evolution of catalyst structure and performance with calcination temperature, Appl. Catal. A Gen. 489 (2015) 32–41. https://doi.org/10.1016/j.apcata.2014.10.017.

[81] M.H. Haider, N.F. Dummer, D. Zhang, P. Miedziak, T.E. Davies, S.H. Taylor, D.J. Willock, D.W. Knight, D. Chadwick, G.J. Hutchings, Rubidium- and caesium-doped silicotungstic acid catalysts supported on alumina for the catalytic dehydration of glycerol to acrolein, J. Catal. 286 (2012) 206–213. https://doi.org/10.1016/j.jcat.2011.11.004.

[82] H. Atia, U. Armbruster, A. Martin, Dehydration of glycerol in gas phase using heteropolyacid catalysts as active compounds, J. Catal. 258 (2008) 71–82. https://doi.org/10.1016/j.jcat.2008.05.027.

[83] A. Martin, U. Armbruster, H. Atia, Recent developments in dehydration of glycerol toward acrolein over heteropolyacids, Eur. J. Lipid Sci. Technol. 114 (2012) 10–23. https://doi.org/10.1002/ejlt.201100047.

[84] H. Atia, U. Armbruster, A. Martin, Influence of alkaline metal on performance of supported silicotungstic acid catalysts in glycerol dehydration towards acrolein, Appl. Catal. A Gen. 393 (2011) 331–339. https://doi.org/10.1016/j.apcata.2010.12.015.

[85] J. TenDam, K. Djanashvili, F. Kapteijn, U. Hanefeld, Pt/Al_2O_3 Catalyzed 1,3-Propanediol Formation from Glycerol using Tungsten Additives, ChemCatChem. 5 (2013) 497–505. https://doi.org/10.1002/cctc.201200469.

[86] L. Liu, Y. Zhang, A. Wang, T. Zhang, Mesoporous WO_3 supported Pt catalyst for hydrogenolysis of glycerol to 1,3-propanediol, Chinese J. Catal. 33 (2012) 1257–1261. https://doi.org/10.1016/S1872-2067(11)60425-7.

[87] J. Wang, X. Zhao, N. Lei, L. Li, L. Zhang, S. Xu, S. Miao, X. Pan, A. Wang, T. Zhang, Hydrogenolysis of Glycerol to 1,3-propanediol under Low Hydrogen Pressure over WO_x-Supported Single/Pseudo-Single Atom Pt Catalyst, ChemSusChem. 9 (2016) 784–790. https://doi.org/10.1002/cssc.201501506.

[88] J. Wang, N. Lei, C. Yang, Y. Su, X. Zhao, A. Wang, Effect of promoters on the selective hydrogenolysis of glycerol over Pt/W-containing catalysts, Cuihua Xuebao/Chinese J. Catal. 37 (2016) 1513–1519. https://doi.org/10.1016/S1872-2067(16)62479-8.

[89] C. Yang, F. Zhang, N. Lei, M. Yang, F. Liu, Z. Miao, Y. Sun, X. Zhao, A. Wang, Understanding the promotional effect of Au on Pt/WO_3 in hydrogenolysis of glycerol to 1,3-propanediol, Cuihua Xuebao/Chinese J. Catal. 39 (2018) 1366–1372. https://doi.org/10.1016/S1872-2067(18)63103-1.

[90] M. Yang, X. Zhao, Y. Ren, J. Wang, N. Lei, A. Wang, T. Zhang, Pt/Nb-WO_x for the chemoselective hydrogenolysis of glycerol to 1,3-propanediol: Nb dopant pacifying the over-reduction of WO_x supports, Cuihua Xuebao/Chinese J. Catal. 39 (2018) 1027–1037. https://doi.org/10.1016/S1872-2067(18)63074-8.

[91] Y. Niu, B. Zhao, Y. Liang, L. Liu, J. Dong, Promoting Role of Oxygen Deficiency on a WO_3-Supported Pt Catalyst for Glycerol Hydrogenolysis to 1,3-Propanediol, Ind. Eng. Chem. Res. 59 (2020) 7389–7397. https://doi.org/10.1021/acs.iecr.9b07067.

[92] S. Zhu, Y. Zhu, S. Hao, L. Chen, B. Zhang, Y. Li, Aqueous-phase hydrogenolysis of glycerol to 1,3-propanediol over Pt-$H4SiW_{12}O_{40}/SiO_2$, Catal. Letters. 142 (2012) 267–274. https://doi.org/10.1007/s10562-011-0757-1.

[93] S. Zhu, Y. Qiu, Y. Zhu, S. Hao, H. Zheng, Y. Li, Hydrogenolysis of glycerol to 1,3-propanediol over bifunctional catalysts containing Pt and heteropolyacids, Catal. Today. 212 (2013) 120–126. https://doi.org/10.1016/j.cattod.2012.09.011.

[94] S. Zhu, X. Gao, Y. Zhu, Y. Zhu, Applied Catalysis B : Environmental Alkaline metals modified Pt – $H_4SiW_{12}O_{40}/ZrO_2$ catalysts for the selective hydrogenolysis of glycerol to 1,3-propanediol, 141 (2013) 60–67.

[95] M. Gu, Z. Shen, L. Yang, B. Peng, W. Dong, W. Zhang, Y. Zhang, The Effect of Catalytic Structure Modification on Hydrogenolysis of Glycerol into 1,3-Propanediol over Platinum Nanoparticles and Ordered Mesoporous Alumina Assembled Catalysts, Ind. Eng. Chem. Res. 56 (2017) 13572–13581. https://doi.org/10.1021/acs.iecr.7b02899.

[96] L. Huang, Y. Zhu, H. Zheng, G. Ding, Y. Li, Direct conversion of glycerol into 1,3-propanediol over Cu-$H_4SiW_{12}O_{40}/SiO_2$ in vapor phase, Catal. Letters. 131 (2009) 312–320. https://doi.org/10.1007/s10562-009-9914-1.

[97] Y. Fan, S. Cheng, H. Wang, D. Ye, S. Xie, Y. Pei, H. Hu, W. Hua, Z.H. Li, M. Qiao, B. Zong, Nanoparticulate Pt on mesoporous SBA-15 doped with extremely low amount of W as a highly selective catalyst for glycerol hydrogenolysis to 1,3-propanediol, Green

Chem. 19 (2017) 2174–2183. https://doi.org/10.1039/c7gc00317j.

[98] S. Feng, B. Zhao, L. Liu, J. Dong, Platinum supported on WO_3 -doped aluminosilicate: A highly efficient catalyst for selective hydrogenolysis of glycerol to 1,3-propanediol, Ind. Eng. Chem. Res. 56 (2017) 11065–11074. https://doi.org/10.1021/acs.iecr.7b02951.

[99] S.S. Priya, V.P. Kumar, M.L. Kantam, S.K. Bhargava, A. Srikanth, K.V.R. Chary, High Efficiency Conversion of Glycerol to 1,3-Propanediol Using a Novel Platinum-Tungsten Catalyst Supported on SBA-15, Ind. Eng. Chem. Res. 54 (2015) 9104–9115. https://doi.org/10.1021/acs.iecr.5b01814.

[100] G. Shi, Z. Cao, J. Xu, K. Jin, Y. Bao, S. Xu, Effect of WOx Doping into Pt/SiO_2 Catalysts for Glycerol Hydrogenolysis to 1,3-Propanediol in Liquid Phase, Catal. Letters. 148 (2018) 2304–2314. https://doi.org/10.1007/s10562-018-2464-7.

[101] L. Liu, T. Asano, Y. Nakagawa, M. Tamura, K. Tomishige, One-pot synthesis of 1,3-butanediol by 1,4-anhydroerythritol hydrogenolysis over a tungsten-modified platinum on silica catalyst, Green Chem. 22 (2020) 2375–2380. https://doi.org/10.1039/d0gc00244e.

[102] W. Zhou, Y. Li, X. Wang, D. Yao, Y. Wang, S. Huang, W. Li, Y. Zhao, S. Wang, X. Ma, Insight into the nature of Brönsted acidity of Pt-(WOx)n-H model catalysts in glycerol hydrogenolysis, J. Catal. 388 (2020) 154–163. https://doi.org/10.1016/j.jcat.2020.05.019.

[103] G. Shi, J. Xu, Z. Song, Z. Cao, K. Jin, S. Xu, X. Yan, Selective hydrogenolysis of glycerol to 1,3-propanediol over Pt-WOx/SAPO-34 catalysts, Mol. Catal. 456 (2018) 22–30. https://doi.org/10.1016/j.mcat.2018.06.018.

[104] Y. Liang, G. Shi, K. Jin, Promotion Effect of Al_2O_3 on Pt–WOx/SiO_2 Catalysts for Selective Hydrogenolysis of Bioglycerol to 1,3-Propanediol in Liquid Phase, Catal. Letters. (2020). https://doi.org/10.1007/s10562-020-03140-z.

[105] L. Gong, Y. Lu, Y. Ding, R. Lin, J. Li, W. Dong, T. Wang, W. Chen, Selective hydrogenolysis of glycerol to 1,3-propanediol over a Pt/WO_3/TiO_2/SiO_2 catalyst in aqueous media, Appl. Catal. A Gen. 390 (2010) 119–126. https://doi.org/10.1016/j.apcata.2010.10.002.

[106] L.Z. Qin, M.J. Song, C.L. Chen, Aqueous-phase deoxygenation of glycerol to 1,3-

propanediol over Pt/WO_3/ZrO_2 catalysts in a fixed-bed reactor, Green Chem. 12 (2010) 1466–1472. https://doi.org/10.1039/c0gc00005a.

[107] W. Zhou, Y. Zhao, Y. Wang, S. Wang, X. Ma, Glycerol Hydrogenolysis to 1,3-Propanediol on Tungstate/Zirconia-Supported Platinum: Hydrogen Spillover Facilitated by Pt(1 1 1) Formation, ChemCatChem. 8 (2016) 3663–3671. https://doi.org/10.1002/cctc.201600981.

[108] Y. Fan, S. Cheng, H. Wang, J. Tian, S. Xie, Y. Pei, M. Qiao, B. Zong, Pt–WOx on monoclinic or tetrahedral ZrO_2: Crystal phase effect of zirconia on glycerol hydrogenolysis to 1,3-propanediol, Appl. Catal. B Environ. 217 (2017) 331–341. https://doi.org/10.1016/j.apcatb.2017.06.011.

[109] S. Zhu, X. Gao, Y. Zhu, J. Cui, H. Zheng, Y. Li, SiO_2 promoted Pt/WO_x/ZrO_2 catalysts for the selective hydrogenolysis of glycerol to 1,3-propanediol, Appl. Catal. B Environ. 158–159 (2014) 391–399. https://doi.org/10.1016/j.apcatb.2014.04.049.

[110] N. Lei, Z. Miao, F. Liu, H. Wang, X. Pan, A. Wang, T. Zhang, Understanding the deactivation behavior of Pt/WO_3/Al_2O_3 catalyst in the glycerol hydrogenolysis reaction, Chinese J. Catal. 41 (2020) 1261–1267. https://doi.org/10.1016/S1872-2067(20)63549-5.

[111] S. García-Fernández, I. Gandarias, J. Requies, M.B. Güemez, S. Bennici, A. Auroux, P.L. Arias, New approaches to the Pt/WOx/Al_2O_3 catalytic system behavior for the selective glycerol hydrogenolysis to 1,3-propanediol, J. Catal. 323 (2015) 65–75. https://doi.org/10.1016/j.jcat.2014.12.028.

[112] M. Edake, M. Dalil, M.J. Darabi Mahboub, J.L. Dubois, G.S. Patience, Catalytic glycerol hydrogenolysis to 1,3-propanediol in a gas-solid fluidized bed, RSC Adv. 7 (2017) 3853–3860. https://doi.org/10.1039/c6ra27248g.

[113] S. García-Fernández, I. Gandarias, J. Requies, F. Soulimani, P.L. Arias, B.M. Weckhuysen, The role of tungsten oxide in the selective hydrogenolysis of glycerol to 1,3-propanediol over Pt/WOx/Al_2O_3, Appl. Catal. B Environ. 204 (2017) 260–272. https://doi.org/10.1016/j.apcatb.2016.11.016.

[114] S. Zhu, X. Gao, Y. Zhu, Y. Li, Promoting effect of WOx on selective hydrogenolysis of glycerol to 1,3-propanediol over bifunctional Pt-WOx/Al_2O_3 catalysts, J. Mol. Catal. A Chem. 398 (2015) 391–398. https://doi.org/10.1016/j.molcata.2014.12.021.

[115] S. García-Fernández, I. Gandarias, Y. Tejido-Núñez, J. Requies, P.L. Arias, S. Garc, I. Gandarias, T. Çez, S. García-Fernández, I. Gandarias, Y. Tejido-Núñez, J. Requies, P.L. Arias, Influence of the Support of Bimetallic Platinum Tungstate Catalysts on 1,3-Propanediol Formation from Glycerol, ChemCatChem. 9 (2017) 4508–4519. https://doi.org/10.1002/cctc.201701067.

[116] W. Zhou, J. Luo, Y. Wang, J. Liu, Y. Zhao, S. Wang, X. Ma, WOx domain size, acid properties and mechanistic aspects of glycerol hydrogenolysis over Pt/WOx/ZrO_2, Appl. Catal. B Environ. 242 (2019) 410–421. https://doi.org/10.1016/j.apcatb.2018.10.006.

[117] S. Zhu, Y. Zhu, S. Hao, H. Zheng, T. Mo, Y. Li, One-step hydrogenolysis of glycerol to biopropanols over Pt-$H_4SiW_{12}O_{40}/ZrO_2$ catalysts, Green Chem. 14 (2012) 2607–2616. https://doi.org/10.1039/c2gc35564g.

[118] L. Qin, M. Song, C. Chen, Aqueous-phase deoxygenation of glycerol to 1 , 3-propanediol over Pt/WO_3/ZrO_2 catalysts in a fixed-bed reactor, (2010) 1466–1472. https://doi.org/10.1039/c0gc00005a.

[119] N. Suzuki, Y. Yoshikawa, M. Takahashi, M. Tamura, Process for producing product of hydrogenolysis of polyhydric alcohol, WO2007129560A1, 2007. https://patents.google.com/patent/WO2007129560A1/en.

[120] P. Uttraporn, P. Praserthdam, Effect of Calcination Temperature and Support Type of Pt/WOx/boehmite Catalyst on 1,3-propanediol Production from Hydrogenolysis of Glycerol, IOP Conf. Ser. Mater. Sci. Eng. 559 (2019). https://doi.org/10.1088/1757-899X/559/1/012012.

[121] N. Lei, X. Zhao, B. Hou, M. Yang, M. Zhou, F. Liu, A. Wang, T. Zhang, Effective Hydrogenolysis of Glycerol to 1,3-Propanediol over Metal-Acid Concerted Pt/WOx/Al_2O_3 Catalysts, ChemCatChem. 11 (2019) 3903–3912. https://doi.org/10.1002/cctc.201900689.

[122] G. Shi, Z. Cao, J. Xu, K. Jin, Y. Bao, S. Xu, Effect of WOx Doping into Pt/SiO_2 Catalysts for Glycerol Hydrogenolysis to 1,3-Propanediol in Liquid Phase, Catal. Letters. 148 (1234) 2304–2314. https://doi.org/10.1007/s10562-018-2464-7.

[123] Y. Zhang, X.C. Zhao, Y. Wang, L. Zhou, J. Zhang, J. Wang, A. Wang, T. Zhang, Mesoporous Ti-W oxide: Synthesis, characterization, and performance in selective hydrogenolysis of glycerol, J. Mater. Chem. A. 1 (2013) 3724–3732.

https://doi.org/10.1039/c3ta10217c.

[124] J. Wang, X. Zhao, N. Lei, L. Li, L. Zhang, S. Xu, S. Miao, X. Pan, A. Wang, T. Zhang, W. Jia, Z. Xiaochen, L. Nian, L. Lin, Z. Leilei, X. Shutao, M. Shu, P. Xiaoli, W. Aiqin, Z. Tao, J. Wang, X. Zhao, N. Lei, L. Li, L. Zhang, S. Xu, S. Miao, X. Pan, A. Wang, T. Zhang, Hydrogenolysis of Glycerol to 1,3-propanediol under Low Hydrogen Pressure over WOx-Supported Single/Pseudo-Single Atom Pt Catalyst, ChemSusChem. 9 (2016) 784–790. https://doi.org/10.1002/cssc.201501506.

[125] A. Corma, From microporous to mesoporous molecular sieve materials and their use in catalysis, Chem. Rev. 97 (1997) 2373–2419. https://doi.org/10.1021/cr960406n.

[126] J. García-Martínez, M. Johnson, J. Valla, K. Li, J.Y. Ying, Mesostructured zeolite y - High hydrothermal stability and superior FCC catalytic performance, Catal. Sci. Technol. 2 (2012) 987–994. https://doi.org/10.1039/c2cy00309k.

[127] M. Hartmann, Hierarchical zeolites: A proven strategy to combine shape selectivity with efficient mass transport, Angew. Chemie - Int. Ed. 43 (2004) 5880–5882. https://doi.org/10.1002/anie.200460644.

[128] Y.T. Kim, K.D. Jung, E.D. Park, A comparative study for gas-phase dehydration of glycerol over H-zeolites, Appl. Catal. A Gen. 393 (2011) 275–287. https://doi.org/10.1016/j.apcata.2010.12.007.

[129] A. Corma, G.W. Huber, L. Sauvanaud, P. O'Connor, Biomass to chemicals: Catalytic conversion of glycerol/water mixtures into acrolein, reaction network, J. Catal. 257 (2008) 163–171. https://doi.org/10.1016/j.jcat.2008.04.016.

[130] T.Q. Hoang, X. Zhu, T. Danuthai, L.L. Lobban, D.E. Resasco, R.G. Mallinson, Conversion of glycerol to alkyl-aromatics over zeolites, Energy and Fuels. 24 (2010) 3804–3809. https://doi.org/10.1021/ef100160y.

[131] S. Jin, Z. Xiao, C. Li, C.T. Williams, C. Liang, Hydrogenolysis of glycerol over HY zeolite supported Ru catalysts, J. Energy Chem. 23 (2014) 185–192. https://doi.org/10.1016/S2095-4956(14)60134-0.

[132] E. Gallegos-Suarez, A. Guerrero-Ruiz, I. Rodriguez-Ramos, A. Arcoya, Comparative study of the hydrogenolysis of glycerol over Ru-based catalysts supported on activated carbon, graphite, carbon nanotubes and KL-zeolite, Chem. Eng. J. 262 (2015) 326–333. https://doi.org/10.1016/j.cej.2014.09.121.

[133] X. Lin, Y. Lv, Y. Xi, Y. Qu, D.L. Phillips, C. Liu, Hydrogenolysis of glycerol by the combined use of zeolite and Ni/Al_2O_3 as catalysts: A route for achieving high selectivity to 1-propanol, Energy and Fuels. 28 (2014) 3345–3351. https://doi.org/10.1021/ef500147k.

[134] X. Wan, Q. Zhang, M. Zhu, Y. Zhao, Y. Liu, C. Zhou, Y. Yang, Y. Cao, Interface synergy between IrOx and H-ZSM-5 in selective C–O hydrogenolysis of glycerol toward 1,3-propanediol, J. Catal. 375 (2019) 339–350. https://doi.org/10.1016/j.jcat.2019.06.025.

[135] S.S. Priya, P. Bhanuchander, V.P. Kumar, D.K. Dumbre, S.R. Periasamy, S.K. Bhargava, M. Lakshmi Kantam, K.V.R. Chary, Platinum Supported on H-Mordenite: A Highly Efficient Catalyst for Selective Hydrogenolysis of Glycerol to 1,3-Propanediol, ACS Sustain. Chem. Eng. 4 (2016) 1212–1222. https://doi.org/10.1021/acssuschemeng.5b01272.

[136] S.S. Priya, P. Bhanuchander, V.P. Kumar, S.K. Bhargava, K.V.R. Chary, Activity and Selectivity of Platinum-Copper Bimetallic Catalysts Supported on Mordenite for Glycerol Hydrogenolysis to 1,3-Propanediol, Ind. Eng. Chem. Res. 55 (2016) 4461–4472. https://doi.org/10.1021/acs.iecr.6b00161.

[137] J. M. Thomas and W. J. Thomas, Principals and Practice of Hetrogeneous Catalysis, 1997.

[138] M.A. Vannice, Kinetics of Catalytic Reactions, first, 2005.

[139] X.B. Q Fu, F Yang, Interface-confined oxide nanostructures for catalytic oxidation reactions, Acc. Chem. Res. 46 (2013) 1692–1701.

[140] C.T. Campbell, Catalyst-support interactions: Electronic perturbations, Nat. Chem. 4 (2012) 597–598. https://doi.org/10.1038/nchem.1412.

[141] I.F. M.H. Jellinek, Advances in Catalysis, 1948.

[142] W. Swcum, Continued from, (1956) 1956.

[143] K.E. Jeong, H.D. Kim, T.W. Kim, J.W. Kim, H.J. Chae, S.Y. Jeong, C.U. Kim, Hydrogen production by aqueous phase reforming of polyols over nano- and micro-sized mesoporous carbon supported platinum catalysts, Catal. Today. 232 (2014) 151–157. https://doi.org/10.1016/j.cattod.2014.02.005.

[144] Y. Izutsu, Y. Oku, Y. Hidaka, N. Kanaya, Y. Nakajima, J. Fukuroi, K. Yoshida, Y. Sasaki, Y. Sekine, M. Matsukata, Physicochemical characterization of highly dispersed platinum and chromium on zeolite beta, J. Phys. Chem. C. 118 (2014) 10746–10753. https://doi.org/10.1021/jp500232s.

[145] G. van T. S. Amelinckx, D. van Dyck, J. van Landuyt, Handbook of Microscopy: Applications in Materials Science, Solid-State Physics and Chemistry, 1997.

[146] A.M. Venezia, X-ray photoelectron spectroscopy (XPS) for catalysts characterization, 77 (2003) 359–370.

[147] S.S. Priya, P. Bhanuchander, V.P. Kumar, D.K. Dumbre, S.R. Periasamy, S.K. Bhargava, M. Lakshmi Kantam, K.V.R. Chary, Platinum Supported on H-Mordenite: A Highly Efficient Catalyst for Selective Hydrogenolysis of Glycerol to 1,3-Propanediol, ACS Sustain. Chem. Eng. 4 (2016) 1212–1222. https://doi.org/10.1021/acssuschemeng.5b01272.

[148] L. Rodríguez-González, F. Hermes, M. Bertmer, E. Rodríguez-Castellón, A. Jiménez-López, U. Simon, The acid properties of H-ZSM-5 as studied by NH_3-TPD and 27Al-MAS-NMR spectroscopy, Appl. Catal. A Gen. 328 (2007) 174–182. https://doi.org/10.1016/j.apcata.2007.06.003.

[149] F. Ketzer, D. Celante, F. de Castilhos, Catalytic performance and ultrasonic-assisted impregnation effects on WO_3/USY zeolites in esterification of oleic acid with methyl acetate, Microporous Mesoporous Mater. 291 (2020) 109704. https://doi.org/10.1016/j.micromeso.2019.109704.

[150] A.I. Osman, J.K. Abu-Dahrieh, D.W. Rooney, S.A. Halawy, M.A. Mohamed, A. Abdelkader, Effect of precursor on the performance of alumina for the dehydration of methanol to dimethyl ether, Appl. Catal. B Environ. 127 (2012) 307–315. https://doi.org/10.1016/j.apcatb.2012.08.033.

[151] J.A. Schwarz, Temperature-Programmed Desorption and Reaction: Applications to Supported Catalysts, Catal. Rev. 25 (1983) 141–227. https://doi.org/10.1080/01614948308079666.

[152] R.J. Cvetanović, Y. Amenomiya, Catalysis Reviews : Science and Engineering A Temperature Programmed Desorption Technique for Investigation of Practical Catalysts, Catal. Rev. 6:1 (1972) 21–48. https://doi.org/10.1080/01614947208078690.

[153] J. Ryczkowski, IR spectroscopy in catalysis, Catal. Today. 68 (2001) 263–381. https://doi.org/10.1016/S0920-5861(01)00334-0.

[154] J. Lai, Z. Ma, L. Mink, L.J. Mueller, F. Zaera, Influence of peripheral groups on the physical and chemical behavior of cinchona alkaloids, J. Phys. Chem. B. 113 (2009) 11696–11701. https://doi.org/10.1021/jp906538g.

[155] J.A. de H. P.R. Griffiths, Fourier Transform Infrared Spectroscopy, 1986.

[156] J. Stöhr, NEXAFS Spectroscopy, 1992.

[157] B. Tang, W. Dai, X. Sun, G. Wu, N. Guan, M. Hunger, L. Li, Mesoporous Zr-Beta zeolites prepared by a post-synthetic strategy as a robust Lewis acid catalyst for the ring-opening aminolysis of epoxides, Green Chem. 17 (2015) 1744–1755. https://doi.org/10.1039/c4gc02116a.

[158] K.S.W. Sing, K.S.W. Sing, Provisional international union of pure and applied chemistry commission on colloid and surface chemistry subcommittee on reporting gas adsorption data, Pure Appl. Chem. 54 (1982) 2201–2218.

[159] F. Tian, Y. Wu, Q. Shen, X. Li, Y. Chen, C. Meng, Effect of Si/Al ratio on mesopore formation for zeolite beta via NaOH treatment and the catalytic performance in α-pinene isomerization and benzoylation of naphthalene, Microporous Mesoporous Mater. 173 (2013) 129–138. https://doi.org/10.1016/j.micromeso.2013.02.021.

[160] C. Thomas, Should W surface density of WOx-ZrO_2 catalysts be calculated with respect to the specific surface area of the sample or that of ZrO_2 only?, J. Phys. Chem. C. 115 (2011) 2253–2256. https://doi.org/10.1021/jp110497e.

[161] A.A. Costa, P.R.S. Braga, J.L. De MacEdo, J.A. Dias, S.C.L. Dias, Structural effects of WO3 incorporation on USY zeolite and application to free fatty acids esterification, Microporous Mesoporous Mater. 147 (2012) 142–148. https://doi.org/10.1016/j.micromeso.2011.06.008.

[162] D.G. Barton, S.L. Soled, G.D. Meitzner, G.A. Fuentes, E. Iglesia, Structural and catalytic characterization of solid acids based on zirconia modified by tungsten oxide, J. Catal. 181 (1999) 57–72. https://doi.org/10.1006/jcat.1998.2269.

[163] D.G. Barton, M. Shtein, R.D. Wilson, S.L. Soled, E. Iglesia, Structure and Electronic Properties of Solid Acids Based on Tungsten Oxide Nanostructures, J. Phys. Chem. B. 103 (1999) 630–640. https://doi.org/10.1021/jp983555d.

[164] A. Galano, G. Rodriguez-Gattorno, E. Torres-García, A combined theoretical-experimental study on the acidity of WOx-ZrO_2 systems, Phys. Chem. Chem. Phys. 10 (2008) 4181–4188. https://doi.org/10.1039/b802934b.

[165] S. Fernandez, M.L. Ostraat, J.A. Lawrence, K. Zhang, Tailoring the hierarchical architecture of beta zeolites using base leaching and pore-directing agents, Microporous Mesoporous Mater. 263 (2018) 201–209. https://doi.org/10.1016/j.micromeso.2017.12.023.

[166] C.D. Baertsch, K.T. Komala, Y.H. Chua, E. Iglesia, Genesis of Brønsted acid sites during dehydration of 2-butanol on tungsten oxide catalysts, J. Catal. 205 (2002) 44–57. https://doi.org/10.1006/jcat.2001.3426.

[167] H. Wang, W. Xin, Surface acidity of H-beta and its catalytic activity for alkylation of benzene with propylene, Catal. Letters. 76 (2001) 225–229. https://doi.org/10.1023/A:1012244526995.

[168] G. Raveendra, A. Rajasekhar, M. Srinivas, P.S. Sai Prasad, N. Lingaiah, P.S.S. Prasad, N. Lingaiah, Selective etherification of hydroxymethylfurfural to biofuel additives over Cs containing silicotungstic acid catalysts, Appl. Catal. A Gen. 520 (2016) 105–113. https://doi.org/10.1016/j.apcata.2016.04.017.

[169] S. Zhu, X. Gao, F. Dong, Y. Zhu, H. Zheng, Y. Li, Design of a highly active silver-exchanged phosphotungstic acid catalyst for glycerol esterification with acetic acid, J. Catal. 306 (2013) 155–163. https://doi.org/10.1016/j.jcat.2013.06.026.

[170] C. Emeis, Determination of integrated molar extinction coefficients for infrared absorption bands of pyridine adsorbed on solid acid catalysts, J. Catal. 141 (1993) 347–354.

[171] S. Triwahyono, T. Yamada, Hi. Hattori, IR study of acid sites on WO_3–ZrO_2 and Pt/WO3–ZrO2, Appl. Catal. A, Gen. 242 (2013) 101–109.

[172] J.W. (Eds. . G. Bergeret, P. Gallezot, in: G. Ertl, H. Knözinger, F. Schüth, Infrared spectroscopy for the characterization of surface acidity and basicity, 2008.

[173] T. Deng, H. Liu, Promoting effect of SnOx on selective conversion of cellulose to polyols over bimetallic Pt-SnOx/Al_2O_3 catalysts, Green Chem. 15 (2013) 116–124. https://doi.org/10.1039/c2gc36088h.

[174] L. Chen, Y. Zhu, H. Zheng, C. Zhang, Y. Li, Aqueous-phase hydrodeoxygenation of

propanoic acid over the Ru/ZrO_2 and $Ru-Mo/ZrO_2$ catalysts, Appl. Catal. A Gen. 411–412 (2012) 95–104. https://doi.org/10.1016/j.apcata.2011.10.026.

[175] D.J. Ostgard, L. Kustov, K.R. Poeppelmeier, W.M.H. Sachtler, Comparison of Pt/KL catalysts prepared by ion exchange or incipient wetness impregnation, J. Catal. 133 (1992) 342–357. https://doi.org/10.1016/0021-9517(92)90245-D.

[176] L.W. Ho, C.P. Hwang, J.F. Lee, I. Wang, C.T. Yeh, Reduction of platinum dispersed on dealuminated beta zeolite, J. Mol. Catal. A Chem. 136 (1998) 293–299. https://doi.org/10.1016/S1381-1169(98)00081-8.

[177] A.D. Allian, K. Takanabe, K.L. Fujdala, X. Hao, T.J. Truex, J. Cai, C. Buda, M. Neurock, E. Iglesia, Chemisorption of CO and Mechanism of CO Oxidation on Supported Platinum Nanoclusters [Erratum to document cited in CA154:392701]., J. Am. Chem. Soc. 134 (2012) 743. https://doi.org/10.1021/ja210394k.

[178] D.B. (Ed.), Handbook of X-Ray and Ultraviolet Photoelectron Spectroscopy, Heyden, London, in: 1978.

[179] T.L. Barr, Modern ESCA: The Principles and Practice of X-Ray Photoelectron Spectroscopy, in: Boca Raton : CRC Press, 1994.

[180] J.W. J.F. Watts, An Introduction to Surface Analysis by XPS and AES, in: Wiley, Chichester, 2003.

[181] A.M. Venezia, X-ray photoelectron spectroscopy (XPS) for catalysts characterization, Catal. Today. 77 (2003) 359–370. https://doi.org/10.1016/S0920-5861(02)00380-2.

[182] A.M. Alsalme, P. V. Wiper, Y.Z. Khimyak, E.F. Kozhevnikova, I. V. Kozhevnikov, Solid acid catalysts based on $H_3PW_{12}O_{40}$ heteropoly acid: Acid and catalytic properties at a gas-solid interface, J. Catal. 276 (2010) 181–189. https://doi.org/10.1016/j.jcat.2010.09.014.

[183] T. Okuhara, New catalytic functions of heteropoly compounds as solid acids, Catal. Today. 73 (2002) 167–176. https://doi.org/10.1016/S0920-5861(01)00509-0.

[184] J.G. Hernández-cortez, M. Manríquez, L. Lartundo-rojas, E. López-salinas, Study of acid – base properties of supported heteropoly acids in the reactions of secondary alcohols dehydration, 222 (2014) 32–38.

[185] L. Shen, H. Yin, A. Wang, Y. Feng, Y. Shen, Z. Wu, T. Jiang, Liquid phase dehydration

of glycerol to acrolein catalyzed by silicotungstic, phosphotungstic, and phosphomolybdic acids, Chem. Eng. J. 180 (2012) 277–283. https://doi.org/10.1016/j.cej.2011.11.058.

[186] A. V. Ivanov, E. Zausa, Y. Ben Taârit, N. Essayem, Mechanism of propene hydration over heteropolyacid catalysts, Appl. Catal. A Gen. 256 (2003) 225–242. https://doi.org/10.1016/S0926-860X(03)00403-4.

[187] A. Micek-Ilnicka, The role of water in the catalysis on solid heteropolyacids, J. Mol. Catal. A Chem. 308 (2009) 1–14. https://doi.org/10.1016/j.molcata.2009.04.003.

[188] C. Mohr, H. Hofmeister, J. Radnik, P. Claus, Identification of active sites in gold-catalyzed hydrogenation of acrolein, J. Am. Chem. Soc. 125 (2003) 1905–1911. https://doi.org/10.1021/ja027321q.

[189] J. Dam, U. Hanefeld, J. Tendam, U. Hanefeld, Renewable chemicals: Dehydroxylation of glycerol and polyols, ChemSusChem. 4 (2011) 1017–1034. https://doi.org/10.1002/cssc.201100162.

[190] L.Z. Qin, M.-J. Song, C.-L. Chen, Aqueous-phase deoxygenation of glycerol to 1,3-propanediol over $Pt/WO_3/ZrO_2$ catalysts in a fixed-bed reactor, Green Chem. 12 (2010) 1466. https://doi.org/10.1039/c0gc00005a.

[191] Z. Tai, J. Zhang, A. Wang, J. Pang, M. Zheng, T. Zhang, Catalytic conversion of cellulose to ethylene glycol over a low-cost binary catalyst of Raney Ni and tungstic acid, ChemSusChem. 6 (2013) 652–658. https://doi.org/10.1002/cssc.201200842.

[192] M. Balaraju, V. Rekha, P.S.S. Prasad, B.L.A.P. Devi, R.B.N. Prasad, N. Lingaiah, Influence of solid acids as co-catalysts on glycerol hydrogenolysis to propylene glycol over Ru/C catalysts, Appl. Catal. A Gen. 354 (2009) 82–87. https://doi.org/10.1016/j.apcata.2008.11.010.

[193] I. Gandarias, P.L. Arias, J. Requies, M.B. Güemez, J.L.G. Fierro, Hydrogenolysis of glycerol to propanediols over a Pt/ASA catalyst: The role of acid and metal sites on product selectivity and the reaction mechanism, Appl. Catal. B Environ. 97 (2010) 248–256. https://doi.org/10.1016/j.apcatb.2010.04.008.

[194] L. Liu, S. Kawakami, Y. Nakagawa, M. Tamura, K. Tomishige, Highly active iridium–rhenium catalyst condensed on silica support for hydrogenolysis of glycerol to 1,3-propanediol, Appl. Catal. B Environ. 256 (2019) 117775.

https://doi.org/10.1016/j.apcatb.2019.117775.

[195] D.C. Koningsberger, J. De Graaf, B.L. Mojet, D.E. Ramaker, J.T. Miller, The metal-support interaction in Pt/Y zeolite: Evidence for a shift in energy of metal d-valence orbitals by Pt-H shape resonance and atomic XAFS spectroscopy, Appl. Catal. A Gen. 191 (2000) 205–220. https://doi.org/10.1016/S0926-860X(99)00320-8.

[196] A. Alhanash, E.F. Kozhevnikova, I. V. Kozhevnikov, Hydrogenolysis of glycerol to propanediol over Ru: Polyoxometalate bifunctional catalyst, Catal. Letters. 120 (2008) 307–311. https://doi.org/10.1007/s10562-007-9286-3.

[197] W. Zhu, P.X. Shen, Y. Wang, F.F. Cai, G.M. Xiao, Hydrogenolysis of glycerol to propanediols over heteropolyacids promoted $AgCu/Al_2O_3$ catalysts, Chem. Pap. 71 (2017) 1645–1655. https://doi.org/10.1007/s11696-017-0160-5.

[198] E.S. Vasiliadou, A.A. Lemonidou, Glycerol transformation to value added C_3 diols: reaction mechanism, kinetic, and engineering aspects, Wiley Interdiscip. Rev. Energy Environ. 4 (2015) 486–520. https://doi.org/10.1002/wene.159.

[199] L.Z. Qin, M.J. Song, C.L. Chen, Aqueous-phase deoxygenation of glycerol to 1,3-propanediol over $Pt/WO_3/ZrO_2$ catalysts in a fixed-bed reactor, Green Chem. 12 (2010) 1466–1472. https://doi.org/10.1039/c0gc00005a.

[200] O.P.S.O. Sio, Aqueous-Phase Hydrogenolysis of Glycerol to 1 , 3-propanediol, (2012) 267–274. https://doi.org/10.1007/s10562-011-0757-1.

[201] X.R. Chen, Y.Q. Du, C.L. Chen, N.P. Xu, C.Y. Mou, Highly active and stable n-pentane isomerization catalysts without noble metal containing: Al- or Ga-promoted tungstated zirconia, Catal. Letters. 111 (2006) 187–193. https://doi.org/10.1007/s10562-006-0146-3.

[202] D.G. Lahr, B.H. Shanks, Kinetic Analysis of the Hydrogenolysis of Lower Polyhydric Alcohols: Glycerol to Glycols, Ind. Eng. Chem. Res. 42 (2003) 5467–5472. https://doi.org/10.1021/ie030468l.

[203] D.G. Lahr, B.H. Shanks, Effect of sulfur and temperature on ruthenium-catalyzed glycerol hydrogenolysis to glycols, J. Catal. 232 (2005) 386–394. https://doi.org/10.1016/j.jcat.2005.03.015.

[204] Y. Xi, J.E. Holladay, J.G. Frye, A.A. Oberg, J.E. Jackson, D.J. Miller, A kinetic and mass transfer model for glycerol hydrogenolysis in a trickle-bed reactor, Org. Process

Res. Dev. 14 (2010) 1304–1312. https://doi.org/10.1021/op900336a.

[205] E.S. Vasiliadou, A.A. Lemonidou, Kinetic study of liquid-phase glycerol hydrogenolysis over Cu/SiO_2 catalyst, Chem. Eng. J. 231 (2013) 103–112. https://doi.org/10.1016/j.cej.2013.06.096.

[206] Z. Zhou, X. Li, T. Zeng, W. Hong, Z. Cheng, W. Yuan, Kinetics of hydrogenolysis of glycerol to propylene glycol over $Cu\text{-}ZnO\text{-}Al_2O_3$ catalysts, Chinese J. Chem. Eng. 18 (2010) 384–390. https://doi.org/10.1016/S1004-9541(10)60235-2.

[207] A. Torres, D. Roy, B. Subramaniam, R. V. Chaudhari, Kinetic modeling of aqueous-phase glycerol hydrogenolysis in a batch slurry reactor, Ind. Eng. Chem. Res. 49 (2010) 10826–10835. https://doi.org/10.1021/ie100553b.

[208] A. Torres, H. Shi, B. Subramaniam, R. V. Chaudhari, Aqueous-Phase Glycerol Catalysis and Kinetics with in Situ Hydrogen Formation, ACS Sustain. Chem. Eng. 7 (2019) 11323–11333. https://doi.org/10.1021/acssuschemeng.9b00807.

[209] and R.V.C. Xin Jin, Bala Subramaniam, Kinetic Modeling of Pt/C Catalyzed Aqueous Phase Glycerol Conversion with In Situ Formed Hydrogen, AIChE J. 62 (2015) 1162–1173. https://doi.org/10.1002/aic.

[210] N.N. Pandhare, S.M. Pudi, S. Mondal, K. Pareta, M. Kumar, P. Biswas, Development of Kinetic Model for Hydrogenolysis of Glycerol over Cu/MgO Catalyst in a Slurry Reactor, Ind. Eng. Chem. Res. 57 (2018) 101–110. https://doi.org/10.1021/acs.iecr.7b03684.

[211] S. Mondal, H. Malviya, P. Biswas, Kinetic modelling for the hydrogenolysis of bio-glycerol in the presence of a highly selective $Cu\text{-}Ni\text{-}Al_2O_3$ catalyst in a slurry reactor, React. Chem. Eng. 4 (2019) 595–609. https://doi.org/10.1039/c8re00138c.

[212] S.A. Zavrazhnov, A.L. Esipovich, S.Y. Zlobin, A.S. Belousov, A. V. Vorotyntsev, Mechanism analysis and kinetic modelling of Cu NPs catalysed glycerol conversion into lactic acid, Catalysts. 9 (2019). https://doi.org/10.3390/catal9030231.

[213] T. Rajkhowa, G.B. Marin, J.W. Thybaut, A comprehensive kinetic model for Cu catalyzed liquid phase glycerol hydrogenolysis, Appl. Catal. B Environ. 205 (2017) 469–480. https://doi.org/10.1016/j.apcatb.2016.12.042.

[214] H. Hichri, A. Accary, J. Andrieu, Kinetics and slurry-type reactor modelling during catalytic hydrogenation of o-cresol on Ni/SiO_2, Chem. Eng. Process. 30 (1991) 133–

140. https://doi.org/10.1016/0255-2701(91)85002-6.

[215] V.R. Choudhary, M.G. Sane, S.S. Tambe, Kinetics of hydrogenation of o-nitrophenol to o-aminophenol on Pd/carbon catalysts in a stirred three-phase slurry reactor, Ind. Eng. Chem. Res. 37 (1998) 3879–3887. https://doi.org/10.1021/ie9800041.

[216] M. Hao, B. Yang, H. Wang, G. Liu, S. Qi, J. Yang, C. Li, J. Lv, Kinetics of liquid phase catalytic hydrogenation of dicyclopentadiene over Pd/C catalyst, J. Phys. Chem. A. 114 (2010) 3811–3817. https://doi.org/10.1021/jp9060363.

[217] U.K. Singh, M.A. Vannice, Kinetics of liquid-phase hydrogenation reactions over supported metal catalysts - A review, Appl. Catal. A Gen. 213 (2001) 1–24. https://doi.org/10.1016/S0926-860X(00)00885-1.

[218] C. Hoang-Van, O. Zegaoui, Studies of high surface area Pt/MoO_3 and Pt/WO_3 catalysts for selective hydrogenation reactions. II. Reactions of acrolein and allyl alcohol, Appl. Catal. A Gen. 164 (1997) 91–103. https://doi.org/10.1016/S0926-860X(97)00160-9.

[219] M.R. Capeletti, L. Balzano, G. De La Puente, M. Laborde, U. Sedran, Synthesis of acetal (1,1-diethoxyethane) from ethanol and acetaldehyde over acidic catalysts, Appl. Catal. A Gen. 198 (2000) 8–11. https://doi.org/10.1016/S0926-860X(99)00502-5.

[220] P.H.R. Silva, V.L.C. Gonçalves, C.J.A. Mota, Glycerol acetals as anti-freezing additives for biodiesel, Bioresour. Technol. 101 (2010) 6225–6229. https://doi.org/10.1016/j.biortech.2010.02.101.

[221] S.B. Umbarkar, T. V. Kotbagi, A. V. Biradar, R. Pasricha, J. Chanale, M.K. Dongare, A.S. Mamede, C. Lancelot, E. Payen, Acetalization of glycerol using mesoporous MoO_3/SiO_2 solid acid catalyst, J. Mol. Catal. A Chem. 310 (2009) 150–158. https://doi.org/10.1016/j.molcata.2009.06.010.

[222] S. Yang, M. Wang, Y. Liang, J. Sun, Eco-friendly one-pot synthesis of acetals and ketals by heterogeneously catalyzed liquid-solid phase reaction, Rare Met. 25 (2006) 625–629. https://doi.org/10.1016/S1001-0521(07)60003-5.

[223] I. Agirre, A. Ugarte, I. García-García, J. Requies, V.L. Barrio, M.B. Güemez, J.F. Cambra, P.L. Arias, Glycerol acetals as diesel additives: kinetic study of the reaction between formaldehyde/acetaldehyde and glycerol, First Int. Congr. Catal. Biorefineries, CatBior 2011; 2-5 October, 2011; Torremolinos, Málaga. 116 (2011) 182–188.

[224] K. Yamamoto, A.M. Kiyan, J.C. Bagio, K.A.B. Rossi, F. Delabio Berezuk, M.E.

Berezuk, Green cyclic acetals production by glycerol etherification reaction with benzaldehyde using cationic acidic resin, Green Process. Synth. 8 (2019) 183–190. https://doi.org/10.1515/gps-2018-0059.

[225] H. Hibbert, The reactions relating, 1536 (1928) 2235–2242.

[226] Z. Zheng, M. Luo, J. Yu, J. Wang, J. Ji, Novel process for 1,3-dihydroxyacetone production from glycerol. 1. Technological feasibility study and process design, Ind. Eng. Chem. Res. 51 (2012) 3715–3721. https://doi.org/10.1021/ie201710h.

[227] P. Manjunathan, V.S. Marakatti, P. Chandra, A.B. Kulal, S.B. Umbarkar, R. Ravishankar, G. V. Shanbhag, Mesoporous tin oxide: An efficient catalyst with versatile applications in acid and oxidation catalysis, Catal. Today. 309 (2018) 61–76. https://doi.org/10.1016/j.cattod.2017.10.009.

[228] L. Chen, B. Nohair, S. Kaliaguine, Glycerol acetalization with formaldehyde using water-tolerant solid acids, Appl. Catal. A Gen. 509 (2016) 143–152. https://doi.org/10.1016/j.apcata.2015.08.014.

[229] S.M. Mahajani, A.K. Kolah, M.M. Sharma, Extractive reactions with cationic exchange resins as catalysts (acetalization of aldehydes with alcohols), React. Funct. Polym. 28 (1995) 29–38. https://doi.org/10.1016/1381-5148(96)80152-0.

[230] S.P. Chopade, M.M. Sharma, Reaction of ethanol and formaldehyde: Use of versatile cation-exchange resins as catalyst in batch reactors and reactive distillation columns, React. Funct. Polym. 32 (1997) 53–65. https://doi.org/10.1016/S1381-5148(96)00069-7.

[231] V.M.T.M. Silva, A.E. Rodrigues, Synthesis of diethylacetal: Thermodynamic and kinetic studies, Chem. Eng. Sci. 56 (2001) 1255–1263. https://doi.org/10.1016/S0009-2509(00)00347-X.

[232] M. Chia, Y.J. Pagán-Torres, D. Hibbitts, Q. Tan, H.N. Pham, A.K. Datye, M. Neurock, R.J. Davis, J.A. Dumesic, Selective hydrogenolysis of polyols and cyclic ethers over bifunctional surface sites on rhodium-rhenium catalysts, J. Am. Chem. Soc. 133 (2011) 12675–12689. https://doi.org/10.1021/ja2038358.

[233] K. Chen, K. Mori, H. Watanabe, Y. Nakagawa, K. Tomishige, C-O bond hydrogenolysis of cyclic ethers with OH groups over rhenium-modified supported iridium catalysts, J. Catal. 294 (2012) 171–183. https://doi.org/10.1016/j.jcat.2012.07.015.

[234] Y. Nakagawa, K. Tomishige, Heterogeneous catalysis of the glycerol hydrogenolysis, Catal. Sci. Technol. 1 (2011) 179–190. https://doi.org/10.1039/c0cy00054j.

[235] Y. Nakagawa, M. Tamura, K. Tomishige, Catalytic materials for the hydrogenolysis of glycerol to 1,3-propanediol, J. Mater. Chem. A. 2 (2014) 6688–6702. https://doi.org/10.1039/c3ta15384c.

List of Publications

1. **Mohammad S. Khan**, Huanting Wang, Santosh J.Gharpure, Sanjay M. Mahajani, Akkihebbal K. Suresh*, "Promoting effect of silicotungstic acid (STA) on hydrogenolysis of glycerol over the bifunctional Pt–xSTA/βzeolite catalysts" (In processing).

2. **Mohammad S. Khan**, Huanting Wang, Santosh J.Gharpure, Sanjay M. Mahajani, Akkihebbal K. Suresh*, "Aqueous phase hydrogenolysis of glycerol to 1,3-propanediol over bifunctional catalysts containing Pt and heteropolyacids supported on βzeolite" (In processing).

International conferences and workshops on present work

1. **4th Indo-German Workshop Feb 2020 on** "Advances in Materials, Reactions & Separation Processes", Max Planck Institute **Berlin, Magdeburg, Germany**. Poster presented on "Promoting effect of silicotungstic acid (STA) on hydrogenolysis of glycerol to 1,3-propanediol over Pt–xSTA/β-zeolite catalysts".

2. **UK Catalysis Conference (UKCC) Jan 2021**, organized by the School of Chemistry and Chemical Engineering, **Queen's University Belfast**. ***Oral presentation on***, "Aqueous phase hydrogenolysis of glycerol to 1,3-propanediol over a bifunctional catalyst comprising heteropolyacids and Pt".

3. **13th Research Scholars' Symposium 2020,** *Department of Chemical Engineering,* ***IIT Bombay***, ***Oral presentation on***, "Aqueous phase hydrogenolysis of glycerol to 1,3-propanediol over bifunctional catalysts containing Pt and heteropolyacids supported on β-zeolite".

Acknowledgments

I want to take an opportunity to thank my supervisors, Prof. A. K. Suresh, Prof. Sanjay Mahajani, Prof. Santosh J. Gharpure (IIT Bombay), Prof. Huanting Wang (Monash University), for their interest, encouragement, and support throughout the course of this work. They have been the epitome of knowledge; the discussions, comments, and their guidance has enlightened my path of research all the way. The advice and assistance of Prof. Vinay A. Juvekar (IIT Bombay) and Associate Prof. Akshat Tanksale (Monash University) as Research Progress Committee members were of great value throughout. The help and support received from Dr. Vinay Amte and Dr. Raj Deshpande (SABIC Bengaluru) is highly appreciated.

I would like to thank the IITB-Monash Research Academy for providing the platform and opportunity to work in a unique collaboration project between IIT Bombay and Monash University. I take this opportunity to thank the Ex-CEOs of Monash Academy, Prof. Mohan Krishnamoorthy, Prof. Murali Sastry, and the current CEO of Academy, Mr. M. S. Unnikrishnan. The staff of the Academy has to be a special mention; Ms. Jayshreee T. for handing the academic paperwork, Ms. Kuheli Banerjee for bearing with all the finance issues, Ms. Beena Pillai for the wonderful trips, Ms. Nancy S. and Mr. Adrian Gertler for coordinating the Monash Visit, Mr. Rahul and Mr. Bharat for help during the arrangement of video conferences. A heartfelt thanks to all of them for making the journey smoother.

I would like to acknowledge the help from Sophisticated Analytical Instrument Facility (SAIF), IIT Bombay for (SEM, TEM, ICP-AES, and FTIR) and the Central XRD facility, MEMS Department, IIT Bombay for help with the characterization of catalysts. Thanks, Ms. Kim Phu, for help with central facilities, Chemical Engineering Department, Monash University. The discussion and help provided by Dr. Dheerendra Singh in the catalyst synthesis is commendable.

I would like to thank Mr. Maruti Patil (Nirmala Scientific Industries) for bearing with me and providing assistance as and when needed at the untimely hours for repairs and the modification in my experimental setup. Sincere thanks to Mr. Patil.

Dr. Ashish Unnarkat, Dr. Jignesh Trivedi, Dr. Bhoja Reddy, Rahul Bhatt, and Dr. Rohidas Bhoi, Dr. Junaid Shaikh were all involved in extending their hands of help during different parts in my PhD. Thanks to all of them. My other home during my Ph.D. work has been F1 Shed Reaction Engineering Lab. Thanks to all the inmates of the F1 shed, Dr. Sumit Kamal, Dr. Moiz Khan, Kapil Jayant, Sudip Das, Akash Shinde, Dr. Pankaj Verma, for making my stay memorable. Thanks to labmates in Prof. Huanting's Group and Prof. Suresh's group for all the brainstorming, help, and fun moments in the lab. Special thanks to Jainesh Jhaveri for help with modeling, simulations, discussions, and always helping me whenever required. I would also like to thanks Savita ma'am from academic section for helping me while fulfilling the academic requirements.

I am highly indebted to my family for their support and faith in me, which provided the needed motivation to move ahead. Heartfelt thanks to my brothers, Zardad, Zama, and Hajarat Khan. The words fall less to the admiration and support from them, and it's too small to thank them for being with me in every bit of my life. I also want to thank my sisters, mother, and father for their immense support in my difficult times. I dedicate this thesis to my family; without whose blessings I would not have been where I am.

Mohammad Khan (Abu)